MODELING OF ROTARY CEMENT KILNS

Submitted in partial fulfillment of the requirements
for the degree of

DOCTOR OF PHILOSOPHY

by

Kaustubh S. Mujumdar

Roll no. 03402701
Supervisor: Prof. Anurag Mehra

DEPARTMENT OF CHEMICAL ENGINEERING
INDIAN INSTITUTE OF TECHNOLOGY
BOMBAY 400 076

2008

Thesis entitled: MODELING OF ROTARY CEMENT KILNS

by KAUSTUBH S. MUJUMDAR

is approved for the degree of DOCTOR OF PHILOSOPHY

Examiners

_____

_____

_____

_____

Supervisors

_____

_____

Chairman

_____

Date _____

Place _____

INDIAN INSTITUTE OF TECHNOLOGY, BOMBAY, INDIA

CERTICATE OF COURSE WORK

This is to certify that Mr. Kaustubh S. Mujumdar was admitted to the candidacy of the Ph. D. Degree on Jan 2004, after successfully completing all the courses required or the Ph. D. Degree programme. The details of the course work done are given below.

Sr. No	Course No.	Course Name	Credits
1	CL 601	Advanced Transport Phenomena	6.0
2	CL 649	Reaction Engineering in Dispersed Phase System	6.0
3	CL 704	Seminar	4.0
4	CLs 801	Communication and Presentation Skills	4.0

I.I.T Bombay Dy. Registrar (Academic)

Date:

Abstract

Rotary cement kilns are key equipment in cement industry used for converting calcineous raw meal into cement clinkers. In this work, a combination of reaction engineering model and a CFD model was used to build adequately complete representation of practical cement kilns.

In the first part of thesis, development of reaction engineering based models for rotary cement kilns was reported. The model was formulated by coupling three models viz. model for simulating variation of bed height in the kiln, model for simulating reactions and heat transfer in the bed region and model for simulating coal combustion and heat transfer in the freeboard region of cement kilns. Melting and formation of coating within the kiln were accounted. Combustion of coal in the freeboard region was modeled by accounting devolatilization, finite rate gas phase combustion and char reaction. The simulated results were validated with the available data from 3 industrial kilns. The model was then used to understand influence of various design and operating parameters on kiln performance. Several ways of reducing energy consumption in kilns were then computationally investigated. The model was also used to propose and to assess a practical solution of using a secondary shell to reduce energy consumption in rotary cement kilns. Simulation results indicated that varying kiln operating variables viz. solid flow rate or RPM can result only in minor changes in kiln energetics. Use of secondary shell over kiln and energy recovery by passing air through the annular gap between the two, appears to be a promising way for significant energy saving. The developed model and the presented results will be useful for enhancing performance of rotary cement kilns.

Since the rotary kiln is closely coupled with associated equipments, models for pre-heater, calciner and cooler were also developed and coupled with kiln model to develop an integrated simulator for clinker manufacture in cement industry. The model for pre-heater cyclones was formulated by assuming solids and gas to be completely back mixed. The heat transfer coefficient between particle laden gas and walls cyclones was calculated using empirical correlation. The model for calciner was formulated based on Eulerian-Lagrangian approach. The coal particles and raw meal particles were considered as discrete phases and gas phase was assumed to be completely back mixed. Clinker cooler was modeled by assuming solids and gas in plug flow. The heat transfer between solids and air in clinker cooler was predicted

via empirical correlations. The simulation results using the simulator have predicted results reasonable with industrial observations.

It is important to note that because of inherent limitations of 1D framework, the developed reaction engineering model will not able to capture influence of burner design and key operating parameters like ratio of swirl or axial air etc. on performance of cement kilns. Computational fluid dynamics based models were therefore developed for rotary cement kilns on second front to achieve this. As a starting point, efforts were initiated to develop CFD models for motion of solids and heat transfer in transverse section of rotating cylinder. A systematic study of various physical parameters like diameter of solids, restitution coefficient, maximum packing limit, angle of internal friction, frictional viscosity on transverse flow revealed that frictional viscosity has the most significant impact on flow of solids in transverse plane. However, the developed models for frictional viscosity did not match the available experimental data. Use of simpler models like pseudo-homogeneous assumption for the solids phase were found to give results similar to those with much more complicated models. CFD models to predict heat transfer in partially filled rotating cylinders indicated that assuming solids as pseudo fluids with constant viscosity in the bed region was reasonable to predict temperature gradients in the bed region. Therefore the CFD model for the kiln was developed assuming solids as pseudo fluids.

The development of CFD model for rotary cement kilns was then reported. Separate CFD models were developed for the bed and the free board regions of the rotary kiln. The individual models were coupled with each other via mass and energy communication through the common boundaries. Appropriate source and sink terms were formulated to account for such mass and heat transfer communication between the bed and the freeboard regions. These models were solved iteratively using suitable under relaxation factors. The simulated results were compared with the available data from industrial kilns and were seen to capture cement kiln behavior reasonably well. The model was also used to examine influence of burner characteristics on burning zone as well as overall performance of the kiln. The developed approach, CFD model and simulation results not only are able to predict the behavior of industrial kiln reasonably but also able to predict influence of burner design and operating parameters on the kiln performance .

Overall, the developed model and presented results will be helpful in developing better understanding of clinker manufacture in cement plants.

Contents

NOTATIONS

A_{cl}	cross sectional area covered by the charge, m^2
A_{cyi}	Internal surface area of cyclone, K
A_{cyo}	External surface area of cyclone, K
A_p	Surface area of coal particle, m^2
${}^{L}A_p$	Surface area of solid particle, m^2
$\overline{a}$	Surface area per unit volume, m^2/m^3
A_{CGW}	Convection area gas to wall, m^2
A_{CGB}	Convection area from gas to bed, m^2
A_{CWB}	Conduction area from wall to bed, m^2
A_P	Particle surface area, m^2
A_{RGB}	Radiation area from gas to bed, m^2
A_{RWB}	Radiation area from wall to solids, m^2
A_0	Devolatilisation rate constant
C_C	Concentration of $CaCO_3$ particle, kg/m3
C_k	Concentration of the component in the bed, kg/m3
C_p	Specific heat of the bed, kJ/ kg K
C_T	Coating thickness, m
$C_{T,\,max}$	Maximum coating thickness, m
d_c	Inner diameter of cyclone, m
d_p	Radius of particle, m
D_e	Equivalent Diameter, m
Ecoal	Energy given by coal in the kiln, kJ/ kg clinker
E_j	Activation energy of the j^{th} reaction, kJ/ mol
E_1	Energy of activation for char combustion, J/mol
E_2	Energy of activation for calcination, J/mol
f_c	Fraction of heat given to coal particle released due to coal combustion
F_C	Coal flow rate, kg/s
$F_{p\text{-}w}$	View factor
$f_{v,\,0}$	Initial mass fraction of volatiles in coal particle
$H_{c,\,C}$	Heat of coal combustion in calciner, J/kg
$H_{c,\,K}$	Heat of coal combustion in kiln, J/kg
H_{calc}	Heat of calcination reaction in calciner, J/kg

H_i	Heat of formation of species i, J/kg
$H_{Loss, K}$	Heat losses in the kiln, J/kg
$H_{R, K}$	Heat required for clinker reactions, J/kg
h_c	Heat transfer coefficient between coal particle and gas, W/m^2K
$h_{c, c}$	Heat transfer coefficient between clinker and gas W/m^2K
$h_{c,L}$	Heat transfer coefficient between solid particle and gas, W/m^2K
h_{cyc}	Heat transfer coefficient between particle laden gas and cyclone inner wall, W/m^2 K
h	Height of solid bed, m
k_g	Thermal conductivity of air/gas, W/mK
k_r	Thermal conductivity of refractory, W/mK
k_{sh}	Thermal conductivity of shell, W/mK
$k_{s,c}$	Rate constant of char combustion, kg/m^2s kPa
k_{app}	Rate constant for pseudo homogeneous reactions, s
k_{eff}	Effective thermal conductivity of gas in freeboard region, W/m K
k_{S0}	Arrhenius factor for calcination reactions,
${}^rk_s$	Rate constant of calcination of calcium carbonate, mol/m^2s^{-1}
${}^rk^t_s$	Rate constant of calcination of calcium carbonate, mol/m^2s^{-1}
k_s	Thermal conductivity of clinker, W/mK
L	Total height of cyclone, m
L_{gcl}	Chord of the sector covered by the charge, m
Len	Length of the kiln, m
$M_{c, C}$	Mass of coal entering the calciner, kg/s
$M_{c, k}$	Mass of coal entering the kiln, kg/s
M_g	Mass of gas in cyclones, kg/s
$M_{g, K}$	Mass flow rate of secondary air entering the kiln, kg/s
$M_{g, P}$	Mass flow rate of gas entering the pre-heater, kg/s
$M_{g, S}$	Mass flow rate of secondary air entering the kiln, kg/s
$M_{g, T}$	Mass flow rate of tertiary air entering the calciner, kg/s
M_s	Mass of solids in cyclones, kg/s
M_{se}	Mass of solids entrained by gas in cyclones, kg/s
$M_{s,C}$	Mass flow rate of solids leaving the calciner, kg/s
$M_{s,K}$	Mass flow rate of clinker leaving the kiln, kg/s

$M_{s,P}$	Mass flow rate of solids entering the pre-heater, kg/s
Mw_{CaCO3}	Molecular weight of Calcium carbonate, kg/kmol
Mw_{CaO}	Molecular weight of Calcium oxide, kg/kmol
Mw_{char}	Molecular weight of carbon, kg/kmol
Mw_{CO2}	Molecular weight of Carbon dioxide, kg/kmol
Mw_{O2}	Molecular weight of oxygen, kg/kmol
Mw_{vol}	Molecular weight of volatile, kg/kmol
Mw_{w}	Molecular weight of water, kg/kmol
m_a	Mass of air in cooler, kg/s
$m_{Al2O3, i}$	Mass of total aluminum oxide in solids in calciner, kg/s
$m_{CO2, C}$	Mass of carbon-dioxide produced in calciner due to calcination, kg/s
$m_{CaCO3, i}$	Mass of total calcium carbonate in solids in calciner, kg/s
$m_{Fe2O3, i}$	Mass of total ferrous oxide in solids in calciner, kg/s
$m_{SiO2, i}$	Mass of total silicon dioxide in solids in calciner, kg/s
m_g	Mass of gas in calciner, kg
m_{gin}	Mass of air entering in calciner, kg/s
m_{gout}	Mass of air leaving calciner, kg/s
$m_{g, K}$	Mass of air leaving the kiln calciner, kg
$m_{pc, 0}$	Initial mass of coal particle, kg/s.
$m_{p, c}$	Mass of coal particle, kg.
$m_{p, cin}$	Mass of coal particle entering calciner, kg
$m_{p,cout}$	Mass of coal particle leaving calciner, kg
$m_{p, L}$	Mass of solid particle, kg
$m_{p,Lin}$	Mass of solids entering calciner, kg
$m_{p,Lout}$	Mass of solids leaving calciner, kg
m_s	Mass of solids/clinker in cooler, kg
M_W	Molecular weight, kg/ kmole
M_j	Stiochiometric coefficient of the base component
m_L	Fraction of liquid formed due to melting
${}^{c}Np$	Number of coal particles entering calciner per second
${}^{L}Np$	Number of solid particles entering calciner per second
NC	No. of components in the bed
NR	No. of reactions
P	The percentage calcination occurring inside the calciner

ΔP	Pressure drop across the cyclone, mm of H_2O
Pr	Prandtl number
p_{o2}	Partial pressure of oxygen in gas, kPa
p_{co2}	Partial pressure of carbon-dioxide in gas, kPa
p_{eq}	Equilibrium partial pressure for carbon-dioxide in gas, kPa
Pe	Peclet number for axial flow of solids
$Q^{'}$	Heat gained by the bed due to heat transfer, kJ / m^2 s
$Q^{''}$	Heat lost by gas to bed and walls, kJ/m s
Q_{CGW}	Convection gas to wall, J/s
Q_{COAT}	Heat transfer through coating, J/ s
Q_{CGB}	Convection from gas to bed, J/ s
Q_{CWB}	Conduction from wall to bed, J/ s
Q_{REF}	Heat transfer through refractory, J/s
Q_{RGB}	Radiation from gas to bed, J/s
Q_{RGW}	Heat transfer through refractory, J/s
Q_{RWB}	Radiation from wall to solids, J/s
Q_{SHELL}	Heat transfer through steel material, J/s
Q_{RAD}	Radiative heat transfer between shell and secondary shell, J/s
$Q_{CONV\text{-}SHELL}$	Convective heat transfer from shell to cooling air, J/s
$Q_{RAD\text{-}SHELL}$	Radiative heat transfer from shell to air, J/s
$Q_{CONV\text{-}SEC\text{-}SHELL}$	Convective heat transfer from secondary shell to air, J/s
$Q_{COND\text{-}SEC\text{-}SHELL}$	Conductive heat transfer in secondary shell, J/s
$Q_{RAD\text{-}SEC\text{-}SHELL}$	Radiative heat transfer from secondary shell to air, J/s
Q_{INSU}	Conductive heat transfer in insulation layer, J/s
r_i	Internal diameter of cyclone, m
r_0	External diameter of cyclone, m
r_p	Radius of solid particle, m
r_r	Internal diameter of cyclone shell, m
Re	Reynolds number
R	Internal radius of the kiln, m
R_{COMB}	combustion rate of coal per unit volume of the gas (kg/m^3 s)
R_{COMBG}	combustion rate of volatiles per unit volume of the gas (kg/m^3 s)
R_c	Non-dimensional form of radiative heat transfer coefficient.

R_i	Net Rate of formation of species i in the bed, kg/m^3 s
R_p	Particle radius, m
R_0	Initial particle radius, m
R_{SHELL}	Radius of kiln shell, m
$R_{SEC\text{-}SHELL}$	Radius of secondary shell, m
T_f	Average temperature of solids and air in cooler, K
T_g	Temperature of gas, K
$T_{g,\,in}$	Temperature of gas entering calciner, K
$T_{g,\,out}$	Temperature of gas exiting calciner, K
$T_{g,\,K}$	Temperature of gas leaving the kiln, K
$T_{g,\,S}$	Temperature of secondary air, K
$T_{g,\,T}$	Temperature of tertiary air, K
$T_{g,\,P}$	Temperature of gas leaving the pre-heater, K
T_L	Temperature of solid particle in calciner, K
$T_{iw,\,i}$	The internal wall temperature of the cyclone, K
$T_{ow,\,i}$	The external wall temperature of the cyclone, K
$T_{r,\,i}$	The temperature of interface of refractory and shell in cyclone, K
T_s	Temperature of solids/clinker in cooler, K
$T_{s,\,C}$	Temperature of solids entering the kiln, K
$T_{s,\,R}$	Temperature of solids exiting the cooler, K
T_0	Ambient air temperature, K
T_{AIR}	Temperature of air in annulus of two shells, K
T_b	Temperature of bed, K
T_C	Temperature of coal particle, K
T_{cl}	Temperature of the bed, K
T_{coat}	Temperature at which coating attains maximum thickness
T_e	Kiln external temperature, K
T_i	Steel/Refractory interface temperature, K
T_g	Temperature of gas, K
T_L	Liquidus temperature, K
T_w	Temperature of inner kiln wall, K
T_S	Solidus temperature, K
T_{SHELL}	Temperature of kiln shell, K
$T_{SEC\text{-}SHELL}$	Temperature of secondary shell, K

u_0	Inlet gas velocity in cyclone, m/s
$u_{s, x}$	Grate speed in x direction, m/s
$u_{s, y}$	Grate speed in y direction, m/s
$u_{g, x}$	Air velocity in x direction, m/s
$u_{g, y}$	Air velocity in y direction, m/s
u_c	Velocity of coal particle, m/s
u_{c0}	Initial velocity of coal particle, m/s
U_{CONV}	Convective heat transfer coefficient, W/m^2 K
V_{cl}	Velocity of the charge, m/s
V_{react}	Volume of reactor, m^3
x	Axial distance in the kiln from solid entrance, m
x_r	thickness of refractory, m
x_s	thickness of shell, m
$x_{Al2O3, C}$	Mass Fraction of aluminum oxide entering kiln
$x_{CaCO3, C}$	Mass Fraction of calcium carbonate entering kiln
$x_{CaO, C}$	Mass Fraction of calcium oxide entering kiln
$x_{Fe2O3, C}$	Mass Fraction of Ferrous oxide entering kiln
$x_{SiO2, C}$	Mass Fraction of silicon dioxide entering kiln
$y_{c, c}$	Mass fraction of char in coal particle in calciner
$y_{c, cin}$	Mass fraction of char entering in coal particle
$y_{c, cout}$	Mass fraction of char leaving in coal particle
$y_{c, K}$	Mass fraction of char in coal particle entering the calciner
$y_{v, c}$	Mass fraction of volatiles in coal particle
y_{O2}	Mass fraction of oxygen in gas
$y_{O2, in}$	Mass fraction of oxygen entering calciner in gas
$y_{O2,out}$	Mass fraction of oxygen leaving calciner in gas
y_{CO2}	Mass fraction of carbon-dioxide in gas
$y_{CO2, in}$	Mass fraction of carbon-dioxide entering calciner in gas
$y_{CO2, out}$	Mass fraction of carbon-dioxide leaving calciner in gas
y_v	Mass fraction of volatiles in gas
y_w	Mass fraction of water in gas
Y_i	Mass fractions of the i^{th} species in the bed
z	Axial distance in the kiln from burner end, m
Z_{ij}	Stiochiometric Coefficients

Greek Letters

ρ_{cl}	Bulk density of the bed, kg / m^3
ρ_b	Bulk density of solids, kg / m^3
α_g	Absorptivity of gas
β	Angle of repose, rad
γ	Kiln tilt, rad
δ	Characteristic constant for kiln burner
Γ	Angle made by solid surface at the kiln center
λ	Latent heat of melting, kJ/kg
ϕ_v	Volumetric flow of solids, m^3/s
ε_b	Emissivity of bed
ε_g	Emissivity of gas
ε_s	Solid porosity
ε_{solid}	Volume fraction of solids in the freeboard region.
ε_w	Emissivity of Kiln internal wall.
Ω	View factor for radiation.

Chemical Species

C_2S	$(2CaO.SiO_2)$
C_3S	$(3CaO.SiO_2)$
C_3A	$(3CaO.Al_2O_3)$
C_4AF	$(4CaO.Al2O_3.Fe_2O_3)$
$C_{12}A_7$	$(12CaO.7Al_2O_3)$
C_2AS	$(2CaO.Al_2O_3.SiO_2)$
CS	$(CaO.SiO_2)$
C_3S_2	$(3CaO.2SiO_2)$
CS_2	$(CaO.2SiO_2)$
CF	$(CaO.Fe_2O_3)$
C_2F	$(2CaO.\ Fe_2O_3)$

1. Introduction

Abstract

In this chapter, an introduction to rotary cement kilns is presented. The motivation for undertaking the present research is discussed. The methodology adopted is presented. The overall organization of thesis is outlined.

1.1 Introduction

The manufacture of clinker formation in cement industry has been a focus of considerable attention worldwide because of the high energy usage and high environmental impact of the process. Typically, cement clinkers are produced by burning calcineous raw meal in a high temperature environment. A schematic of a clinker manufacture is shown in Figure 1.1.

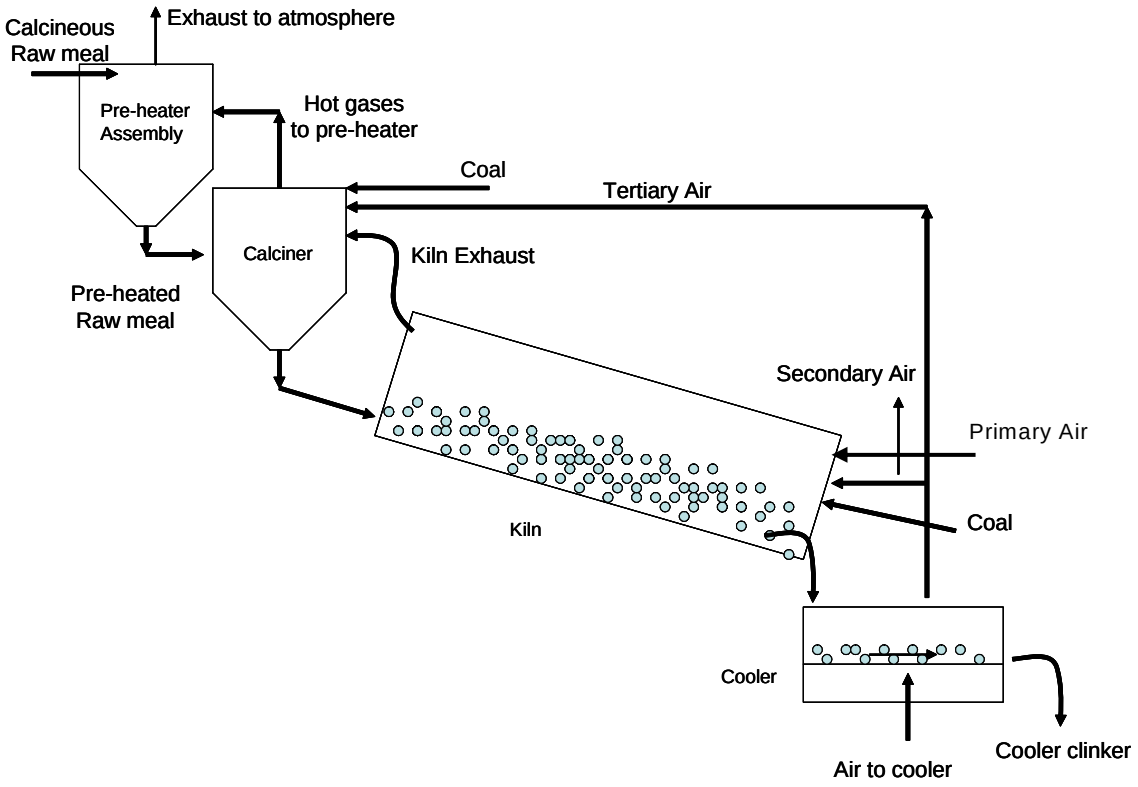

Figure 1.1: Schematic of clinker manufacture

The raw meal (consisting of predetermined quantities of $CaCO_3$, SiO_2, Al_2O_3 and Fe_2O_3) is passed sequentially through pre-heater, calciner, kiln and cooler to form cement clinkers. In pre-heater section the raw meal is preheated to calcination temperature via hot gases coming from calciner. In calciner, calcination reaction occurs. The energy required for endothermic calcination reaction is provided by combusting a suitable fuel. In most cases, coal is used to provide the required energy, especially in India. The calciner is supplied with tertiary air from the cooler and air coming out of kiln exhaust. The former is to supply sufficient O_2 for coal combustion and later to utilize the heat of kiln gases to enhance rate of heat transfer. The hot gases from calciner are sent to pre-heater assembly for preheating the solids. The partially

calcined solids from the calciner are fed to slowly to the rotary kiln. In rotary kiln remaining calcination and other clinkerization reactions occur (formation of C_2S, C_3S, C_3A, C_4AF). The energy required for endothermic clinker reactions is provided by combusting coal in the kiln. The pulverized coal along with the preheated air (secondary air) is fed to the kiln in a counter current mode with respect to solids. Part of the solids melts in the kiln. The melt formation causes an internal coating on the kiln refractories. The hot clinkers are discharged from kiln to clinker cooler and hot gases from kiln exhaust are sent to the calciner. In clinker cooler a part of energy of solids is recovered back by heat exchange with air. The air heated in the coolers is passed to the kiln and calciner as secondary and tertiary air respectively. A small part of air may be vented if required.

The ability to provide a high temperature environment, appropriate residence time for clinkinerization reactions and handle solids with large size distribution makes rotary kilns the most suitable reactor for clinker formation. Since the important reactions involved in clinker formation occur in rotary kiln, performance of rotary cement kiln controls the quality of the product and therefore the performance of the overall plant. Moreover, rotary kilns consume a major portion of total energy supplied to the entire plant and are the main sources of CO_2 emission in a cement industry. However, in spite of being a key unit and commonly practised for decades in cement industry, realistic computational models to simulate cement kilns are not readily available. A detailed understanding about cement kiln intricacies is still missing. This research work was therefore initiated towards developing comprehensive computational models to gain an understanding for rotary cement kilns and use this understanding for possible performance enhancement. In the next section of this chapter, a brief discussion about rotary cement kilns and key issues in cement kilns is presented. This discussion will provide a background of challenges involved in developing realistic computational models for rotary cement kilns. The motivation of the present research is presented subsequently. Thereafter the methodology adopted in this work is discussed followed by outline of the thesis.

1.2 Rotary Cement Kilns

Rotary kilns are commonly used in cement industry to convert calcineous raw meal to cement clinkers. Typically rotary kilns used in cement industry are very long cylinders (generally >50 m), which are slightly inclined to facilitate forward moment of the solids. The kilns are

revolved at pre-decided RPM to ensure uniform mixing of products. Schematic of a rotary cement kiln is shown in Figure 1.2.

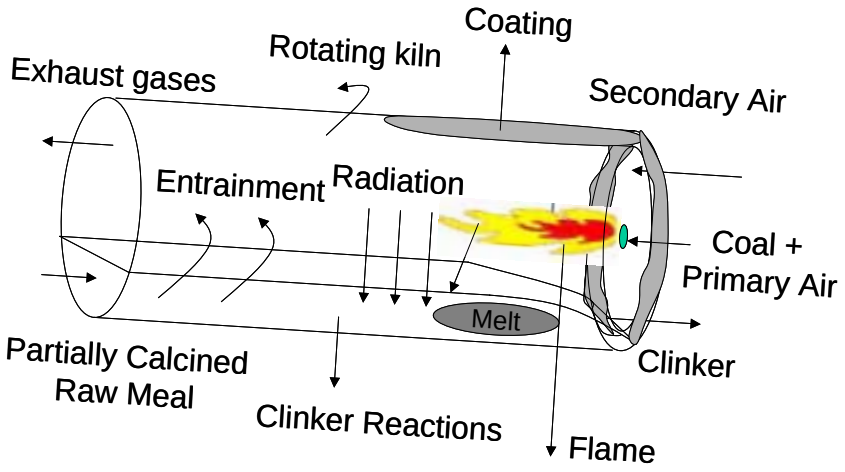

Figure 1.2: Schematic of rotary cement kiln

Partially calcined feed from calciner is fed slowly at velocity of ~ 0.05 m/s from one end. The solid charge moves in a complex manner in the kiln due to a combined translational and rotational motion. The solids in cement kilns are generally filled up to 10-15 % of fill to ensure a uniform mixing. This part forms the bed region of the kilns. In the remaining part called as freeboard region of the kiln, hot air is passed in a counter current mode with respect to solids. Primary air and fuel are supplied in appropriate quantities through burner nozzles with high velocities along with secondary air and swirling air to produce a stable flame in the freeboard region. The flame is result of several number of combustion reactions involving large number of components. The flame in the freeboard region is the direct source of heat for endothermic reactions occurring in the bed region. The heat transfer in rotary kiln occurs by various modes, which are described below

- Radiative heat transfer between hot gases and the bed.
- Radiative heat transfer between kiln refractory lining and the bed.
- Convective heat transfer between hot gases and the bed.
- Conductive heat transfer between kiln refractory lining and the bed.
- Energy losses from shell via radiation and convection.

The partially calcined raw meal, which enters the kiln, utilizes the energy given by hot gases to undergo various clinkerization reactions. In the initial part of kiln remaining calcination is

completed. This is followed by solid-solid reactions (formation of C_2S, C_3A, C_4AF). A Part of the solids melt in the kiln. One of the key reactions in clinker formation (formation of C_3S) occurs in the melt phase. The presence of melt causes a coating layer on the kiln refractories. Formation of coating is considered to be beneficial from refractory point of view. The location coating formation in the kilns govern the radiative heat losses from the shell. Counter current flow of gas entrains solid particles from bed in the free board region. Such entrainment enhances rates of radiative heat transfer by increasing effective emissivity and conductivity. Thus in a rotary cement kiln, complex turbulent flow, heat transfer and reactions occur simultaneously which involves multiple phases, vast number of species and significantly different time and length scales.

1.3 Motivation of the Present Work and Methodology Adopted

The above discussion clearly indicates the complexity of physics involved during clinker formation in cement kilns. For developing adequately accurate computational models for cement kilns it is essential to consider the flow of solids in the bed and freeboard region, clinkerization reactions in the bed region, coal combustion and gas phase combustion along with radiative heat transfer. Other than this it is also essential to develop sub-models for predicting melting of solids i.e. amount of melt formed in the burning zone, energy required for solid melting, location of coating formation, influence of solid entrainment on the heat transfer, etc. Moreover, there are numerical issues involved in cement kilns modeling as discussed in the following. The physical time scales of gas and solids in cement kilns are significantly different. The typical velocities of gas phase in the free board region is about ~10 m/s while typical velocities of solid particles in the bed region is of the order of a typically about 0.05 m/s. In addition to the time scales of the free board and bed region, actual chemical reactions occur at the scale of the particles, which is much smaller than length scale of a kiln. Therefore incorporating various phenomena occurring simultaneously in a reliable framework to predict the kiln behaviour accurately is a highly challenging task.

A detailed literature review on modeling attempts for cement kilns (as discussed in Chapter 2 later) indicates that none of the published models take into account all key factors (described above) simultaneously. The motivation of the present work was therefore to fill this gap and to develop comprehensive computational tools, which will capture most of the underlying physics in cement kilns as shown in Figure 1.3. The objective of this research work was to develop realistic computational models which consider simultaneous interaction of flow, heat

transfer and reactions occurring in cement kilns in a single framework and use these models subsequently to identify the scope of possible performance enhancement. The methodology adopted to achieve this goal is discussed in the next section.

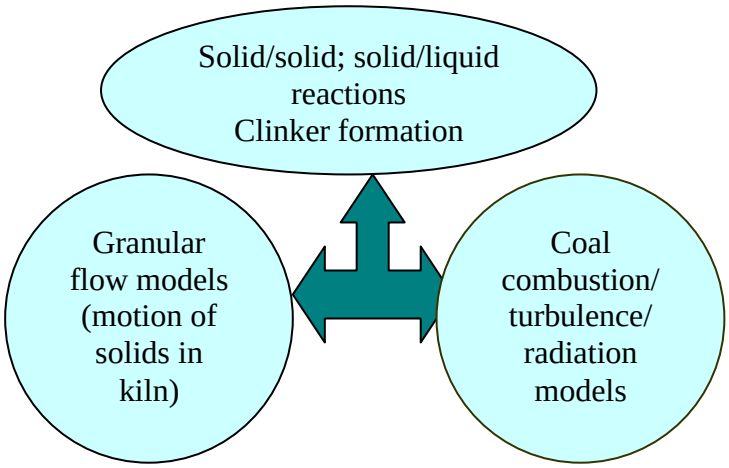

Figure 1.3: Integrated modeling approach for rotary cement kilns

Cement kilns are complex multiphase reactors where in different processes have significantly different spatio-temporal scales as explained in previous paragraph. Hence, capturing all the relevant processes in a single computational model, if not impossible, is an extremely difficult task. Therefore, computational models were developed using different approaches (reaction engineering based models and computational fluid dynamics based models), to capture relevant physics which is explained further down in this section. These models have evolved as different chapters of this thesis, which is explained further in Section 1.5 of the thesis. Nevertheless, the models developed in different chapters contribute to the model toolkit which is directed towards a single goal of developing computational models to capture behaviour of rotary cement kilns and equipments associated with it. The approach adopted here is pictographically demonstrated in Figure 1.4

The reaction engineering model was developed to gain an overall understanding of the kiln behavior. This model was formulated based on one-dimensional framework for bed and freeboard regions to allow effective simulations of overall kiln performances. Such reaction engineering models have shown to complement more detailed CFD by models providing basis for more rigorous CFD simulations of small number of promising cases (see Ranade,

V.V., 2002). The idea in developing reaction-engineering model was to develop a predictive tool for cement kilns which would require order of magnitude lower computational resources but still provide realistic simulations.

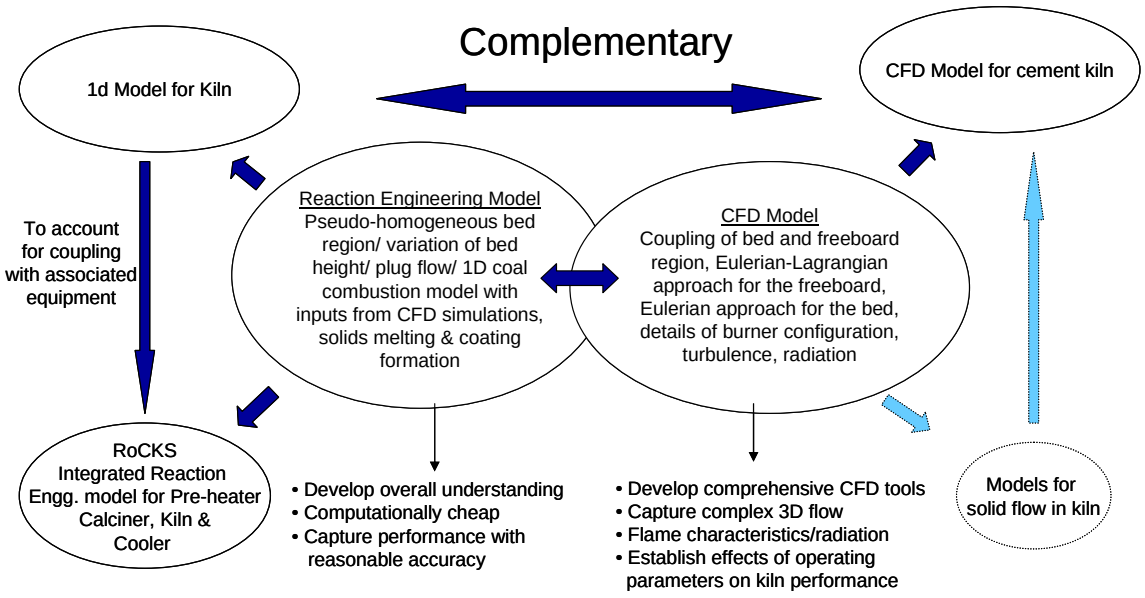

Figure 1.4: Multi-layer modeling methodology for cement kilns

It is important to note that the utilization of stand alone model for the kiln would be rather restricted since the pre-heater, calciner, kiln and cooler in clinker manufacturing are strongly coupled to each other. Therefore reaction engineering computational models were developed for pre-heater, calciner and clinker cooler. The kiln model was coupled with these models to develop an integrated simulator for cement industry. The objective of developing integrated simulator was to capture influence of key design and operating parameters on overall performance (energy consumption per unit weight of product, production rate per unit volume of kiln and so on) in clinker manufacturing.

The developed one dimensional reaction engineering model due to its inherent 1D nature will not able to capture influence of burner design and key operating parameters like ratio of swirl or axial air etc. on performance of cement kilns. Hence, it is essential to have a model, which would provide quantitative guidelines to understand effect of burner operations on the performance of cement kilns. CFD based models were therefore developed to achieve this. Initially some attempts were made to develop CFD models for simulating solids flow in transverse section of rotary kilns. The motivation of this work was to explore possibility of using these models in CFD model for the cement kiln. However, these attempts were not very

successful. The CFD model for rotary cement kiln was therefore formulated assuming solids as pseudo fluids.

1.4 Organization of Thesis

In this thesis work, computational models for rotary cement kilns and associated equipments are developed and presented. These models have evolved as different chapters of this thesis in three sections. The first section (Chapter 2) covers literature information about cement kiln modeling. Cement kiln is a complex system wherein several processes occur simultaneously. It is important to identify and adequately capture these key processes. In Chapter 2, these key processes are identified. The challenges in modeling cement kilns are clearly outlined here and status of the published models for rotary cement kilns is discussed. The remaining of thesis is organized as shown in Figure 1.5.

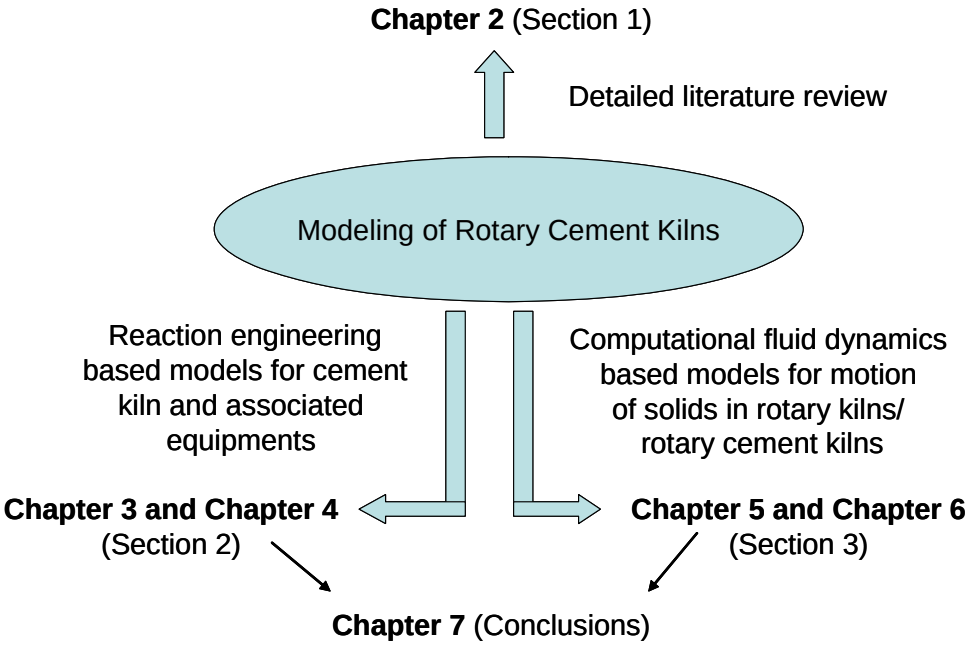

Figure 1.5: Organization of the thesis

The second section presents reaction engineering based models for rotary cement kilns and associated equipments. This section comprises Chapter 3 and Chapter 4 of the thesis. Chapter 3 presents details of reaction-engineering models developed in this work. The computational model presented in Chapter 3 was coupled with reaction engineering models developed for pre-heater, calciner and cooler to develop integrated simulator for cement

industry in Chapter 4. The FORTRAN programs implementing the solution of integrated simulator were modified to develop dynamically linked libraries (DLL) and interfaced with Visual Basic to develop a simple graphical user interface based software called RoCKS (Rotary cement kiln simulator) for cement industry. This is also discussed in Chapter 4.

In the third section of thesis (Chapter 5 and Chapter 6) computational fluid dynamics (CFD) based models developed for rotary cement kilns are presented. Chapter 5 presents CFD models developed for motion of solids and heat transfer in rotating cylinders. Chapter 6 reports development of comprehensive CFD model for rotary cement kilns. Finally the conclusions of this research are outlined in Chapter 7.

2. Key Issues in Modeling Rotary Cement Kilns

Abstract

The aim of this chapter is to identify the key issues that need to be considered while developing computational models for cement kilns. The important key issues viz. flow of solids in bed and freeboard region, height variation of bed in the kiln, reactions occurring in bed and freeboard region, melting of solids, coating formation are discussed one by one in detail in this chapter. The modeling efforts to capture these issues in published literature with their merits and limitations are discussed. The performance models for rotary cement kilns are presented.

2.1 Introduction

Various processes occurring in rotary cement kilns need to be adequately considered while developing its mathematical model. The key issues governing the performance of rotary cement kilns are shown schematically in Figure 2.1. A partially calcined raw meal enters the kiln with a certain flow rate. It is important to develop adequate models to estimate average residence time of solids and variation of bed height within the kiln as a function of solids flow rate, kiln rotational speed, tilt angle and so on. Several chemical reactions take place in the solid bed. Calcination reaction liberates carbon dioxide and reduces solids mass flow rate. Part of the solids melts in the kiln. The melt formation causes an internal coating on kiln refractories. Energy required for clinkerization reactions and melt formation is provided by the hot free board gases. Counter current flow of gas entrains solid particles in the free board region. Such entrainment enhances rates of radiative heat transfer by increasing effective emissivity and conductivity.

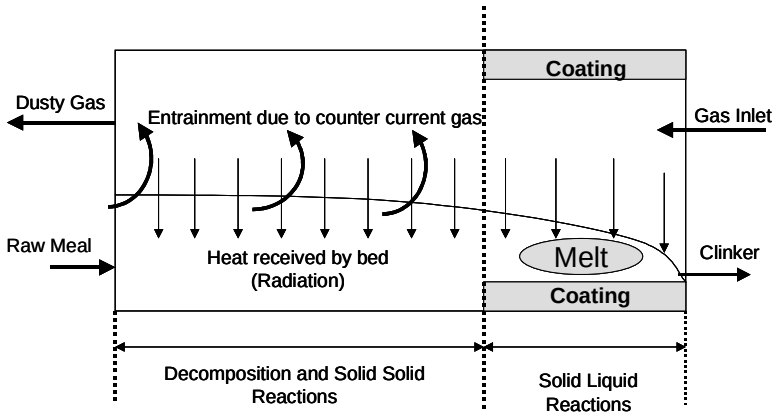

Figure 2.1: Key issues in modeling rotary cement kilns

Based on this brief description, the key processes occurring in cement kilns can broadly classified as (See Figure 2.2)

1. Flow
2. Clinkerization reactions
3. Heat transfer.

Other than these, there are few other issues like melting of solids, coating formation on kiln inner walls that occur in cement kilns during clinker formation. To develop realistic models for cement kilns it is essential include all these physical processes simultaneously. We discuss each of the issue and review the previous work related to it in following.

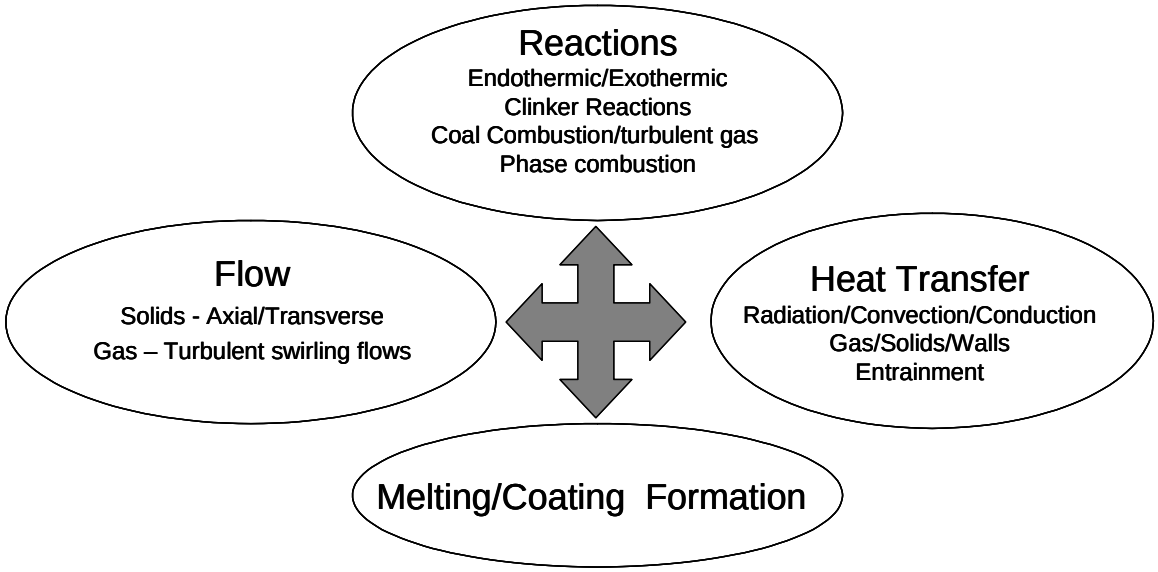

Figure 2.2: Schematic of various processes occurring in cement kilns

2.2 Flow of Solids in Rotary Cement Kilns

It is essential to accurately capture flow of solids in bed region while developing cement kiln models. Solids flow in a complicated path in cement kiln having an axial component (due to gravity) as well as radial component (due to rotation of kiln walls). It is essential to understand motion of solids in both axial and transverse direction in cement kiln to capture the residence time and mixing of solids in the kiln. We discuss about the same in this section.

2.2.1 Flow of solids in axial direction

The motion of solids in axial direction determines the solid residence time inside the kiln, which directly affects the clinker composition. Axial motion of solids in the kiln is dependent

on the mass flux of solids, speed of rotation, height of solid bed (percentage fill), particle size, angle of repose and kiln tilt. Axial velocity of solids varies along the kiln length causing variation in height of the solid bed. Though reasonable models to simulate axial velocity of solids in kiln are available, most of the models for cement kilns assume a constant bed height (and subsequently constant axial velocity) within the kiln (Spang, 1972; Mastorakos *et al.*, 1999). Assuming a constant bed height will fix the residence time of solids in the kiln for any set of operating conditions. Therefore, such models will not be able to predict the influence of key design and operating parameters of kiln on its performance and their utility will be rather restricted. It is therefore essential to use accurate models for axial motion of solids while computational model for rotary cement kilns.

Attempts of experiments and computational models for understanding motion of solids in rotating kilns in axial direction can be found in plenty (Friedman and Marshall, 1949, Saemen, 1951; Kramers and Crookewit, 1952; Perron and Bui, 1990; Spurling *et al.*, 2001). Lebas *et al. (1995)* have published experimental data of residence time, particle movement and bed depth profile in rotary kilns for a 0.6 m diameter kiln. Recently, Spurling *et al.*, (2001) have also reported height variation of solid bed in a kiln of 0.1 m diameter. The Kramer's model (Kramers and Croockewit, 1952) which relates volumetric flow rate of solids, ϕ_v, with kiln tilt (γ, radian), angle of repose (β, radian), radius of kiln (R, m), rotational speed of kiln (n) and height of solids (h) was shown to predict both the set of experimental data with reasonable accuracy as compared to other models published for rotary kilns (Lebas *et al.*, 1995). The description of Kramer's model is discussed in Chapter 3 later and is therefore not presented in this section. We have validated Kramer's model with published experimental data. The results of these simulations are shown in Figure 2.3, Figure 2.4 and Figure 2.5. Figure 2.3 and Figure 2.4 shows comparison of Kramer's model with experimental data of Lebas *et al.* (1995). It can be seen from these figures that the model is able to predict the data reasonably well for changes in kiln RPM and solid throughput to the kiln. Same results were observed with published data of Spurling *et al.* (2001) (See Figure 2.5). Hence, we have used Kramer's model for simulating bed height in this work.

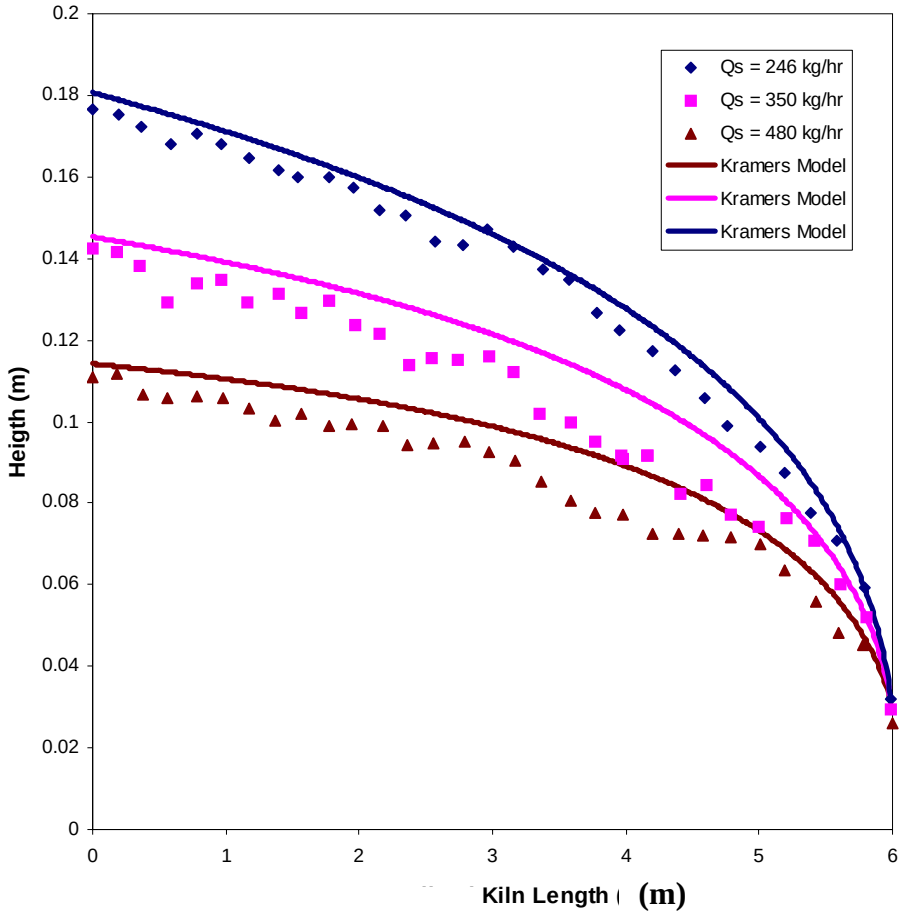

Figure 2.3: Comparison of model of Kramers and Croockewit (1952) with experimental data of Lebas *et al.* (1995) for varying flow rate

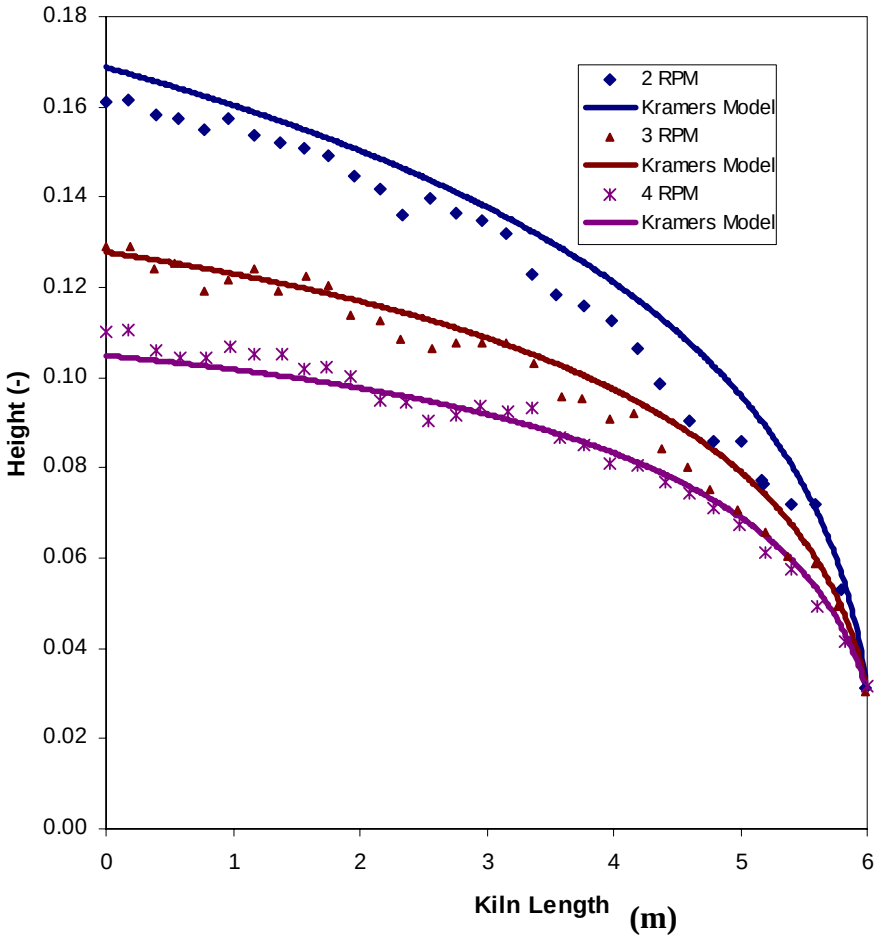

Figure 2.4: Comparison of model of Kramers and Croockewit (1952) with experimental data of Lebas *et al.* (1995) for varying rotational speed

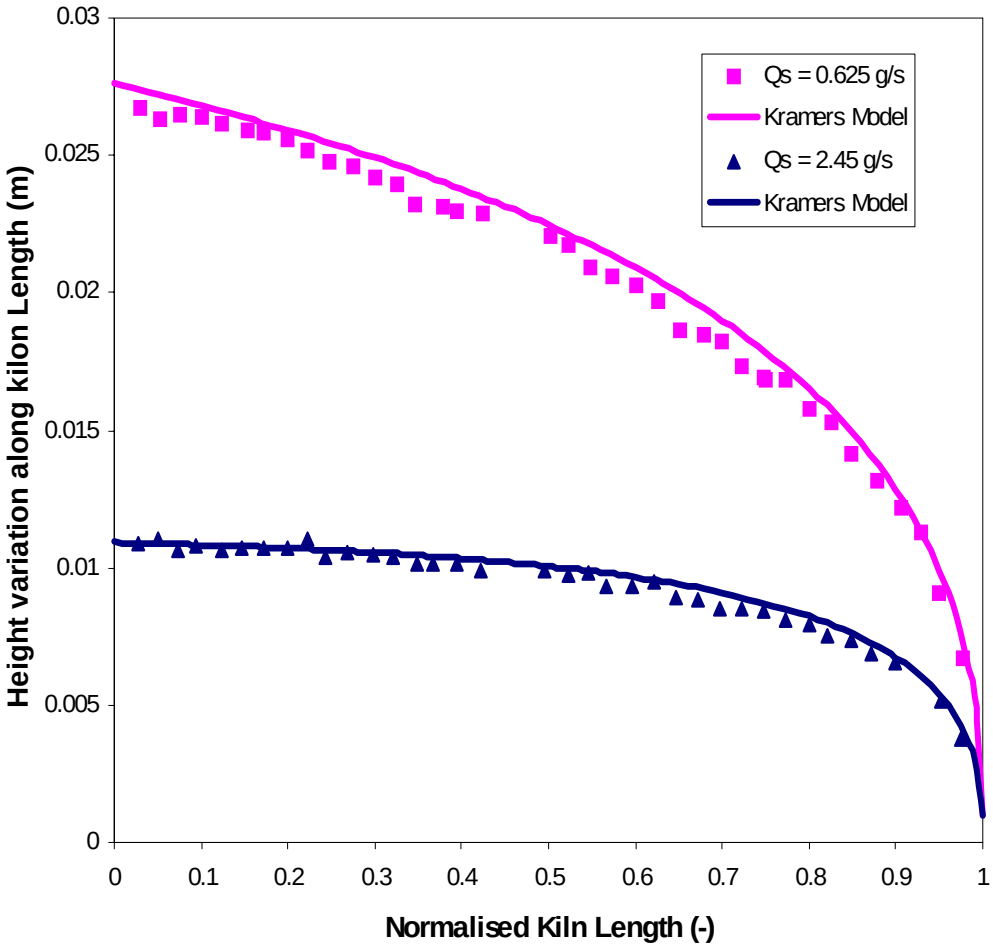

Figure 2.5: Comparison of model of Kramers and Croockewit (1952) with experimental data of Spurling *et al.* (2001) for varying flow rate

Other than motion of solids in axial direction, it is also essential to model solids mixing in axial direction. Several methods have been used to analyze mixing of solids in rotating kilns such as: 1) Finite stage transport 2) Monte Carlo simulations 3) Discrete element modeling and 4) Dispersion model (Sherritt *et al.* 2003). Axial dispersion model is the most common method of modeling axial mixing in both continuous and batch operation of rotary kilns and will be used to study axial mixing in this work. In this model, the particles are treated as continuum and the solids mixing in the axial direction is simulated using the following one-dimensional equation:

$$\frac{\partial c}{\partial t} = D_z \frac{\partial^2 C}{\partial t^2} - u_z \frac{\partial c}{\partial z} \qquad (2.1)$$

where D_z is the axial dispersion coefficient. Higher magnitude of axial dispersion coefficient indicates more mixing of solids.

Previous work on quantifying axial mixing in rotary cement kilns using axial dispersion model were reviewed in detail by Sherritt *et al.* (2003). Sherritt *et al.* (2003) has reviewed previous experiments with batch as well as continuous operation of kilns. They have analysed a total of 179 data points from the literature and proposed design correlations for slumping, rolling/cascading and cataracting bed behaviours. The following correlation was proposed by Sherritt *et al.* (2003) to estimate axial dispersion coefficient:

$$D_Z = k\left(\frac{n}{N_C}\right)^a (2R)^b d_p{}^c X^d \qquad (2.2)$$

where D_z is the axial dispersion coefficient, k is regression parameter (Range – ln k = -0.75 ± 0.53 for rolling and cascading mode). Other parameters are reported as:

a = 0.44 ± 0.14

b =1.29 ± 0.16

c =0.35 ± 0.06

d = -0.55 ± 0.16

n – rotational speed.

N_c – critical rotation speed $= \frac{60}{2\pi}\sqrt{\frac{g}{R}}$

R – radius of drum.

d_p – diameter of particle.

X – percentage fill.

We have performed several numerical experiments to get range of values of dispersion coefficients from Equation 2.2. The data obtained from an industrial kiln (R =1.7 m) was used to estimate axial dispersion coefficient for different operating conditions (percentage fill – 0.1 to 0.5; rotational speed – 1 to 6 rpm; particle size – 1 μm to 10 mm) as shown in Table 2.1, Table 2.2 and Table 2.3.

Table 2.1 Variation of axial dispersion coefficient/Peclet number with percentage fill

Percentage fill	D_Z $(m^2/s)\times10^5$	Pe $\times10^{-6}$
0.1	18.83	5.3
0.2	12.86	7.8
0.3	10.29	9.7
0.4	8.79	11.4
0.5	7.77	12.9

Table 2.2 Variation of axial dispersion coefficient/Peclet number with rotation speed

Rotational speed (rpm)	D_Z $(m^2/s)\times10^4$	Pe $\times10^{-6}$
2	1.01	10.
3	1.21	8.2
4	1.37	7.3
5	1.51	6.6
6	1.64	6.1

Table 2.3 Variation of axial dispersion coefficient/Peclet number with particle size

Particle size (m) $\times10^4$	D_Z $(m^2/s)\times10^4$	Pe $\times10^{-6}$
0.01	0.31	31.8
0.1	0.7	14.2
1.0	0.58	6.3
10.0	3.53	2.8
100.0	7.90	1.3

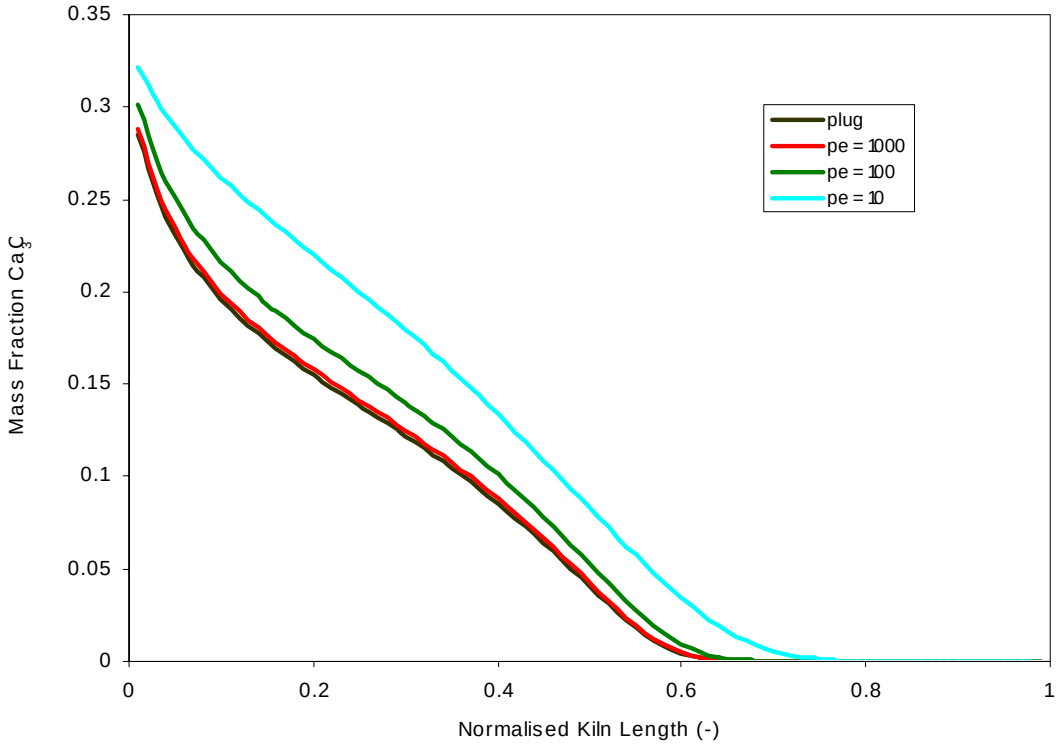

Figure 2.6 Effect of axial dispersion coefficient on the kiln performance

This study indicated that for wide range of operating conditions covered in Table 2.1 to 2.3, the values of Peclet number (u_zL/D_Z) were always greater 10^4. Thus even for a very wide spectrum of kiln operations the value of Peclet number was always over 10^4. In order to quantify influence of axial mixing on kiln performance, we have carried simulations were carried out for different values of Peclet number for a kiln wherein transverse gradients were neglected. For Peclet numbers higher than 1000, predicted results were almost indistinguishable from those obtained from considering the plug flow. Though usual Peclet numbers in the kilns are very high as discussed above, simulations were carried out at much lower values to quantify the sensitivity. The results of these are shown in Figure 2.6.

For these simulations effect of varying Peclet number on $CaCO_3$ concentration in the kiln was monitored. These simulation results indicate that solids mixing in axial direction can be safely neglected while developing computational models for cement kilns.

2.2.2 Flow of solids in transverse direction

The motion of solids in transverse direction is important from the product uniformity point of view. With increasing rotation speed six flow regimes in transverse section of rotating kilns

are identified (Heinen *et al.*, 1983). These flow regimes viz. slipping, slumping, rolling, cascading, cataracting and centrifuging are shown in Figure 2.7.

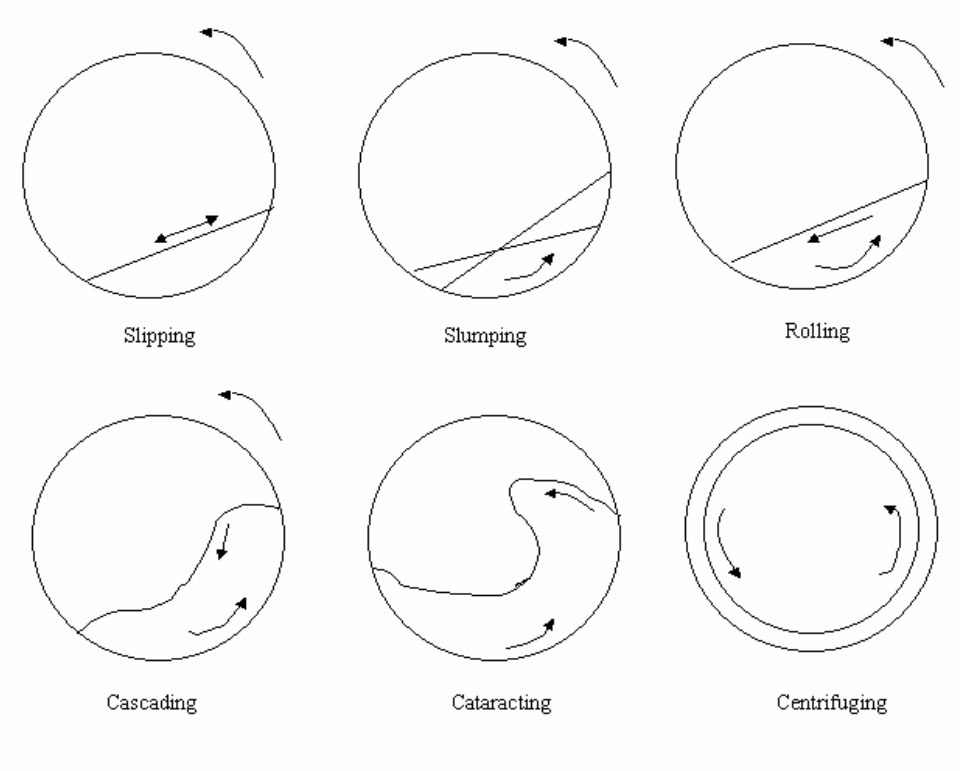

Figure 2.7 Flow regimes in transverse section

The nature of solids flow in transverse section can change significantly with particle characteristic, kiln size, rotation speed and bed fill. The surface renewal rate, which determines heat transfer, mass transfer and mixing in bed depends on the prevailing flow regime. Of all the regimes mentioned above, rolling mode offers maximum surface renewal rate with good heat transfer, mass transfer and reactions. Therefore it is the most commonly used mode in practice for cement kilns. The rolling mode is characterized by two distinct zones as shown in Figure 2.8.

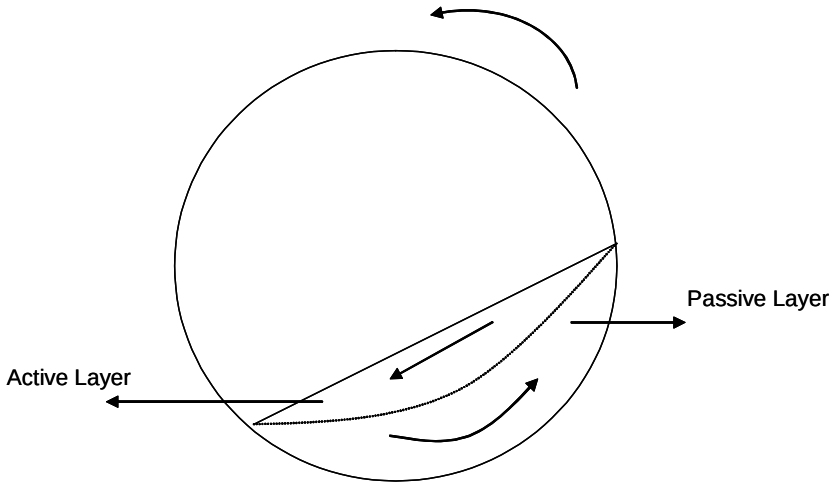

Figure 2.8: Flow of solids in rolling regime

A thinner active layer which is formed as the solids flow down the sloping upper bed surface and the much thicker passive layer (also called as plug flow region). In the passive region, the granular material moves as a rigid body and particle mixing is negligible. Particle mixing mainly occurs in the active region. The rate of such a mixing determines the surface renewal rate and hence the rates of bed-freeboard heat and mass transfer, as well as chemical reactions. This in turn influences mixing of solids in transverse section. Therefore it is essential to understand behavior of solids in transverse section of cement kilns.

Motion of solids in transverse section of rotating cylinders depends on kiln rotational speed, percentage fill and rheology of particles. The development of computational model for feed bed that includes all the above mentioned interactions is a topic of intense research itself. The constitutive equations for granular flows as yet are far from being established. The approaches for developing computational models for motion of solids in transverse section have been mainly based on Eulerial-Eulerian approach. Boateng and Barr (1996) developed a model, which employed boundary layer approach in deriving governing equations. They presented their integro-differential set of equations, which contained granular temperature term. Khakhar *et al.,* (1997) have presented an excellent work on motion and mixing of solids in transverse section of rotating drums. They have used a macroscopic balance approach to obtain velocity and layer thickness for the flow in the active layer. Ding *et al.,* (2001) developed a more sophisticated model considering a quasi-static contribution, which becomes important at low rotational speed. This term was not considered in Boateng's model. The

above-mentioned models use a polynomial function for the velocity profile in the active layer to get the solution to the integro-differential equations. This velocity profile is mostly obtained from experiments. The models assume surface of solids to be flat which is not really the case especially near the walls. Moreover, most of this work is for solids with high fill ratio's or low rotational speeds. Further, these models are restricted to the rolling mode of operating regime. Therefore, more generalized models to capture transverse flow of solids in rotating cylinders are required to be developed which may account for different particle sizes, shapes and properties at higher rotational speeds.

2.3 Clinkerization Reactions

Several solid-solid and liquid-solid reactions occur in the bed region of rotary cement kilns. The chemical reactions that occur in the kiln are described in detail by Hewlett, (1998). The most important oxides that participate in the reactions are CaO, SiO_2, Al_2O_3 and Fe_2O_3. The reactions occur in a particular sequence along the kiln length. Initially (~ 700–900 ^{0}C) calcination as well as an initial combination of alumina, ferric oxide and silica with lime takes place. Between 900 and 1200 ^{0}C belite [C_2S, i.e. (2CaO,SiO2)] is formed. Above 1350 ^{0}C, a liquid phase appears and this promotes the reaction between belite and free lime to form alite, [C3S i.e. (3CaO,SiO2)]. During the cooling stage, the molten phase forms tri-calcium aluminate [C_3A i.e. 3CaO,Al_2O_3] and a ferrite phase, [C_4AF i.e. 4CaO, Al_2O_3, Fe_2O_3]. If the cooling is slow, alite may decompose and appear as secondary belite and free lime. In the burning zone approximately 25 % of the material remains in the liquid state. At this stage the materials become ball of fused material ranging in particle size from big particles to as fine as dust (~ 50 μm – 5 mm). These materials are known as cement clinker. The parameters that control these overlapping processes are the mineralogy of the raw materials, the fineness of the raw materials, and the homogeneity of the raw mix.

Kinetics of cement clinker formation is not well understood in all details. Decomposition of solid-solid reaction between and other oxides like and solid-liquid reaction between and di-calcium silicate (formed in solid-solid reaction between CaO and are the key reactions and play most important role in the context of cement clinker formation in kiln. The main chemical reactions occurring in the kiln during clinker formation are given below:

Dissociation of $CaCO_3$ (Solid Decomposition)

$CaCO_3 \rightarrow CaO + CO_2$ $\Delta H_R = 43.74$ kcal/mol (2.3)

Combination of lime and clay (Solid-Solid Reaction)

$CaO + SiO_2 \rightarrow C2S$ $\Delta H_R = -33.24$ kcal/mol (2.4)

$3CaO + Al_2O_3 \rightarrow C3A$ $\Delta H_R = -5.8$ kcal/mol (2.5)

$4CaO+Al_2O_3 + Fe_2O_3 \rightarrow C4AF$ $\Delta H_R = -12$ kcal/mol (2.6)

Solid liquid reaction (Liquid Phase Sintering)

$CaO + C2S \rightarrow C3S$ $\Delta H_R = 0.47$ kcal/mol (2.7)

Reaction 1 (Equation 2.3, calcination reaction) is a decomposition reaction. Reactions 2, 3 and 4 (2.4, 2.5 and 2.6 respectively) are the solid-solid reactions. Reaction 5 is the solid-liquid reaction. While formation of some other compounds like $C_{12}A_7$, C_2AS, CS, C_3S_2, CS_2, CF, C_2F etc. has been reported within the kiln (Hewlett, 1998), these components are generally present in insignificant amount and are usually neglected. In general, only the major reactions taking place in clinker formation are considered for modeling rotary cement kilns (Spang, 1972, Mastorakos *et al.*, 1999). In this work therefore only five major reactions to occur during clinker formation are considered. Modeling clinkerization reactions and estimating relevant kinetics for these reactions is not a straightforward task. In this section the models available for the three major reaction mechanisms occurring in the clinker formation are described briefly.

Calcination reaction (Equation 2.3) is a decomposition reaction and has been studied extensively. The overall reaction rate is mainly controlled for the following three rate processes, 1) heat transfer (to the surface and then to the reaction zone) through the particle 2) mass transfer (both internal and external to the surface) and 3) chemical reaction at the interface of undecomposed particle and product. Relative rates of these three transport processes depend on particle size and operating conditions. Several models such as shrinking core model, grain model, uniform reaction model, nucleation and growth model and reacting particle model have been proposed for modeling decomposition of Calcium Carbonate (see for example, Ingraham and Marier, 1963; Hills, 1968; Khinast *et al.*, 1996; Irfan and Dogu, 2001; Martins, 2002). The shrinking core models were shown to be applicable to wide range of limestone species under conditions similar to that of kiln.

The solid-solid reactions occur after decomposition as described by Equation (2.3), Equation (2.4) and Equation (2.5). Modeling solid-solid reactions is not very straight forward. As a general rule, solid-solid reactions demonstrate profound multi-step characteristics. This can involve several processes with different activation energies and the mechanisms. Several attempt have been made in literature for predicting the formation kinetics of different calcium silicate, calcium aluminate and aluminoferrite phases. These phases formed due to solid solid reaction between lime and other oxides like silica, alumina and iron oxides. Many theoretical models have been derived over the past 70 years for the solid-state reaction of powders, but these models, based on various conceptualisations of the physicochemical phenomena involved, are not always successful all the way up to 100% reaction (Hao and Tanaka, 1990). The rate of the reaction of the solids depends on particle size; size distribution and previous history of the reactants themselves and these dependencies are so complex that kinetic measurements are difficult to interpret (Beretka and Brown, 1983).

The solid liquid reaction takes place mostly in the burner zone where the temperature of the charge is greater than 1350 ^{0} C. The most important and virtually the slowest step in the clinker formation is the formation of tricalcium silicate (C_3S) from uncombined lime (CaO) and dicalcium silicate (C_2S) in liquid phase (Johansen, 1973). This process is most important because C_3S is the most powerful hydraulic constituent of the cement and a low content of unreacted lime is required for a stable cement mortar. In fact the content of C_3S is the indicator of the extent of cement formation reaction. The original inhomogeneities of raw mix will result in regions of different composition which makes the CaO diffuse through the liquid reaction layer surrounded it. Assuming the unchanged contact face original radius during the reaction and applying the spherical diffusion field Johansen (1973) developed a model equation of fraction of reacted CaO in time. Using the model, the maximum size of the particle which can react fully within a given time can be estimated, as well as, for a given particle size distribution, the free content of the clinker.

Reviewing literature of clinkerization kinetics survey suggests that calcination reaction (Equation 2.3) has been studied extensively. Unlike calcination, other clinkerization (like formation of C_2S, C_3A, C_4AF and C_3S) are not extensively studied. Particle level models for these reactions are not available. Most of the previous studies are restricted to characterizing diffusion (and reactions) of CaO in silica and other oxide species. Adequate information about variation of diffusion coefficient with temperature and composition under conditions

prevailing in kiln is not available. These reactions are therefore usually modeled as pseudo-homogeneous reactions (Spang, 1972, Mastorakos *et al.*, 1999). Ignoring diffusion and particle scale processes, simple Arrhenius type expressions were used for describing overall reaction rates in this work.

2.4 Melt and Coating Formation

Another important aspect of cement kilns is the formation of melt within the kiln. In the burning zone of the kiln the solids are exposed to extremely high temperatures (of the order of 1700 K). As a result of this solids melt. Melt formation is essential for formation of C_3S. Despite this, not many of the published models for cement kilns account for formation of a melt phase in cement kilns. Mastorakos *et al.* (1999) had accounted for melting in cement kilns. However their model arbitrarily assumed a linear increase in the melt phase formation till a certain maximum melt fraction (around 30 %). The melt fraction was assumed to remain constant thereafter in the burning zone till the solids exit. The amount of melt formed depends on the bed temperature profile in the kiln. As the melt moves towards exit of the kiln it may re-solidify since the bed temperature decreases near the solids exit. However, none of the previous models account for re-solidification of the melt.

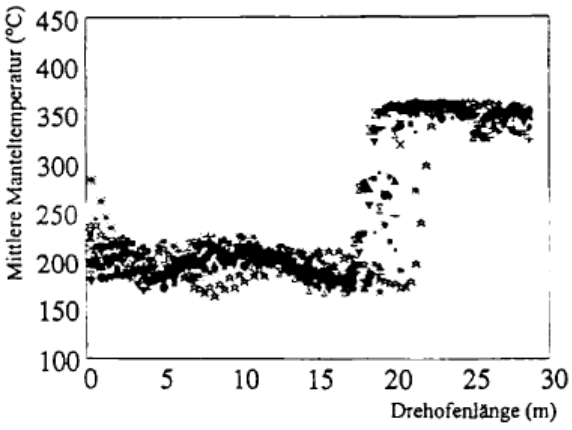

BILD 5: Versuchsdaten zur Manteltemperatur des Drehofens
FIGURE 5: Shell temperature rotary kiln experimental data
Mittlere Manteltemperatur (°C) shell mean temperature (°C)
Drehofenlänge (m) rotary kiln length (m)

Figure 2.9: Reported shell temperature measurements from Kolyfetis and Markatos, (1996) [Kiln Length: 75 m, Inner diameter: 4.35 m]

As the melt phase is formed, it forms a coating over the refractories in the remaining part of the kiln. The formation of coating is beneficial for the refractory life. The computational models for cement kilns presented earlier, either consider a uniform coating throughout the kiln (Mastorakos *et al.,* 1999) or do not consider any coating formation in kiln (Spang, 1972). Both the above assumptions are neither correct nor acceptable for realistic simulations. Coating formation starts at some distance from the solids entry after the solids melt. Such a non-uniform coating formation leads to discontinuity in kiln shell temperature with a sharp fall (~ 200 ^{o}C) in shell temperature at the point of coating formation as shown in Figure 2.9 (reproduced from Kolyfetis and Markatos, 1996). Coating formation has a direct impact on losses from kiln shell. Hence predicting accurate coating formation is essential for predicting correct figures for energy consumption.

2.5 Heat Transfer

Heat exchange between free board and solid bed needs to be captured accurately since this drives the chemical reactions in the bed. Other than heat transfer between bed and freeboard air there is heat exchange between gas and kiln walls and bed and kiln walls. Heat transfer occurs through all the three modes viz. conduction, convection and radiation. The various modes by which heat transfer takes place in kiln are shown in Figure 2.10

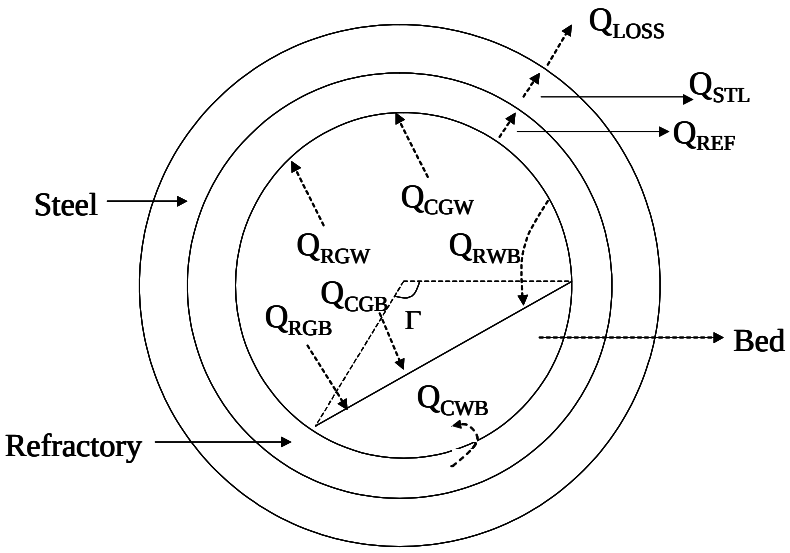

Figure 2.10: Heat transfer in rotary cement kilns

Q_{RWB} and Q_{CWB} are heat transfer rates due to radiation and conduction respectively between kiln internal wall and bed. Q_{RGB} and Q_{CGB} are heat transfer rates due to radiation and

convection between gas and bed. Q_{RGW} and Q_{CGW} are heat transfer rates due to radiation and convection between the kiln freeboard gas and internal wall. Q_{REF} and Q_{STL} are heat transfer due to conduction in refractory and steel shell respectively. Q_{LOSS} is loss of heat from steel shell by radiation and convection. Capturing the heat transfer rates accurately is also important to develop comprehensive cement kiln models. For operating conditions prevailing in cement kilns, radiation dominates the heat transfer process (Boateng and Barr, 1996; Mastorakos *et al.*, 1999; Karki *et al.*, 2000). Key parameters appearing in heat transfer models are: emissivity of gas, absorption coefficient of gas, conductivity of gas & solid. Estimation of these properties is not straightforward. Since the temperature range (minimum and maximum) in the freeboard region varies significantly, the thermal properties of gas will not be constant and a function of local temperature in the kilns. Moreover, because of the counter current flow gas flow, solids will get entrained from bed to freeboard region. The extent of solid entrainment will influence the effective emissivity as well as conductivity of gas. Hence effective thermal properties of dust-laden gas need to be estimated to model heat transfer in transverse direction accurately.

Due to extremely high temperatures encountered in the freeboard region of kiln radiation dominates the heat transfer process. Characterizing radiation energy in the freeboard region of kiln is a complex but crucial element in modeling of cement kilns. Eaton *et al.* (1999) have given a brief and nice explanation of models for characterizing radiation in pulverized coal combustors. The authors have also presented further in-depth review articles for the interested readers. A basic integro-differential equation is well developed for steady state radiative heat transfer and is given as

$$\frac{dI(s,\omega)}{ds} = -(\kappa+\sigma)I(p,\omega) + \kappa I_b + \frac{\sigma}{4\pi}\int_{4\pi} I(s,\omega)\,\Phi\,dw \qquad (2.8)$$

where I is the radiative intensity, p and ω are unit vectors in the directions of propagation, κ, and σ are the local absorption and scattering coefficients, respectively, and Φ represents a phase function used to characterize the nature of the scattering media. The term on the left side of the equation represents the gradient of intensity in the specified direction, v. The three terms on the right side of the equation represent the changes in intensity due to absorption

and out-scattering, emission and in-scattering respectively. The references describing various approaches for derivation of equation can be found in Eaton *et al.* (1999).

The accuracy of the solution, however largely depends on the accurate knowledge of radiative properties of gas. Key parameters appearing are: emissivity of gas, absorption coefficient of gas, conductivity of gas & solid. Calculation of these properties require information on temperatures, gas composition as well as particle concentration, composition, shape and size distribution. Seluck *et al.* (2002) have presented estimation of thermal properties for freeboard region of bubbling fluidized bed combustor. In this work we have used volume fraction weighted averaged values to calculate effective values of thermal properties for industrial cement kilns. However, from the present literature it seems that the data presented for predicting thermal properties of particle-laden gas is very limited.

Knowing the radiative properties of combustion gases, the radiative equation needs to be solved to quantify the radiation in the freeboard region. Since it is not possible to develop a single solution method that is applicable to wide variety of systems (Eaton *et al.,* 1999) and therefore several solution methods have been developed to solve radiation equation (equation 2.8). The different methods are evolved in varying degree of assumption considering the nature of the system, characteristic of the medium, degree of accuracy required, etc. The major approaches can be classified as (Eaton *et al.*, 1999)

- Statistical methods
- Zonal method
- Flux methods; including the discrete-ordinates approximation
- Moment methods
- Spherical harmonics approximation
- Hybrid methods.

Some of the above solution methods are also applied to estimate radiative heat transfer in rotary kilns. The standard solution techniques are also available in commercial CFD codes (Fluent 6.1.18). Multi flux radiation model is commonly used by lot of modelers. Karki *et al.* (2000) have used six flux radiation model with isotropic scattering. In six flux model radiation field is assumed to be represented by six fluxes at each point in the space. The flux in the each direction is assumed to change according to local emission, absorption and scattering. Guo *et al.* (2003), have used four heat flux radiation model. Marias (2003) have

used P-1 radiation model. Mastorakos *et al.* (1999) have used a statistical approach to estimate radiative heat transfer in cement kilns. The radiation intensity of the gas was calculated with Monte-Carlo method. Since the motivation of present work was not to study radiative heat transfer in cement kilns, standard models available in commercial codes were used to model radiation in cement kilns in this work.

2.6 Freeboard Region of Cement Kilns

Accurate modeling of freeboard region is a key in developing computational models for rotary cement kilns. The main function of the freeboard region is to supply sufficient energy to the solid bed for driving solid-solid and solid-liquid endothermic reactions for clinker formation. This energy is obtained by burning fuels like coal, natural gas, etc. Rotary kilns can be fired with different fuels. However, most of the industrial cement kilns are equipped with coal-fired burners, especially in India. Primary air and fuel are supplied in appropriate quantities through burner nozzles along with secondary air and swirling air to produce a stable flame in the freeboard region. The burner configuration, swirl air and other operating parameters influence the flame characteristics, heat transfer to the bed region and temperature profiles in the bed and the freeboard regions. The flame supplies the required energy to the solid bed for clinkerization. The heat transfer is mainly through radiative heat transfer as discussed in the previous section.

The main processes that occur in freeboard region are pictorially represented as shown in Figure 2.11. It is essential to include component models for the representation of turbulent fluid flow and heat transfer, turbulent combustion, particle reactions simultaneously to simulate freeboard region. The gaseous combustion can be either be reaction limited or mixing limited or both depending on the kiln operating conditions. The burners of cement kilns produce a complex flow. The velocity profiles of air are highly non-uniform especially near the kiln burners. It is therefore essential to capture swirling turbulent flows produce by kiln burners in the freeboard region. The burner configuration (for example, number of axial air inlets, Location of burner, proportion of swirl to axial air ratio) influences the flow and in turn flame characteristics of the freeboard region.

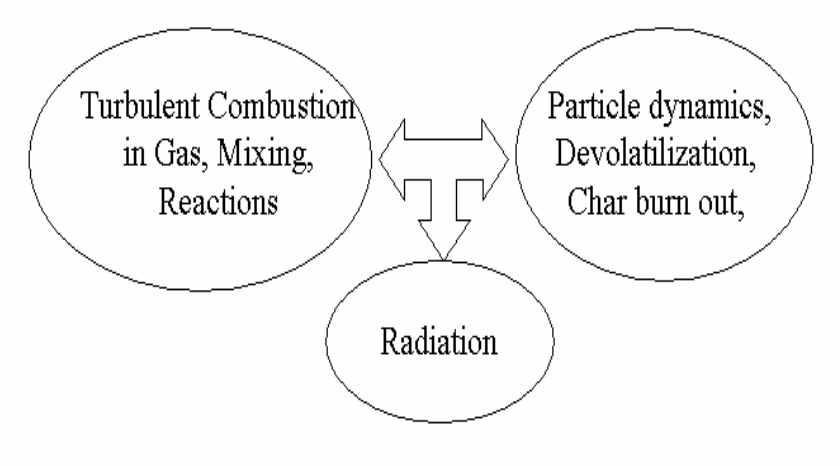

Figure 2.11 Various physico-chemical process occurring in kiln freeboard region

It is essential to properly simulate turbulent gas phase combustion and coal combustion in the freeboard region of cement kilns. Modeling non-premixed turbulent combustion processes requires an effective scheme for simultaneously modeling both mixing and reactions. Eaton *et al.* (1999) have presented in detail about modeling gas phase combustion reactions in coal combustors in their review. It is essential to calculate individual time scales or rates of mixing and reactions in freeboard region. In employing simplifying assumptions to achieve feasible solutions of turbulent gas phase combustion, three modeling approaches have been used. These approaches are classified according to two hypothetical time scales associated with chemical reactions in turbulent flow: the reaction time scale and the turbulent mixing time scale. The reaction time scale is typical time required for the species of interest to react completely. The turbulent mixing time scale is the typical time required for large scale turbulent eddies to break up and to reduce to the scale where molecular interactions can occur. In the first modeling approach, which is not expected to occur in industrial kiln, reacting species are assumed to be premixed or the turbulent mixing scale is assumed to be infinitely fast. Therefore in this case turbulent mixing can be ignored. In other modeling approach, the reaction rate is assumed to be infinitely fast and combustion is assumed to be mixing limited. In the third modeling approach, when both the rates are of same order different reaction rates are calculated and smallest rate is assumed to be the governing rate.

Other than gas phase combustion coal combustion also occurs in the freeboard region. Coal combustion is known to occur in four stages viz. 1) heat up, 2) devolatilisation of volatiles, 3)

combustion of volatiles and 4) char burnout. Heat up of coal is due to radiation and convection from surrounding gas (secondary air). Heat up leads to release of volatiles, which may burn if temperature is sufficiently high, and oxygen is available. The final stage of coal combustion is char-oxidation. Char oxidation is a relatively slow process as compared to other two steps and is a heterogeneous reaction. For char oxidation to take place oxygen has to diffuse through the pores of charcoal and then reacts with carbon to form the products. Depending upon the temperature conditions diffusion and/or chemical reaction may limit the process. It is necessary to account for different phenomena and their corresponding rates while developing the model for the free board region of cement kilns.

Several attempts of modeling these processes have been published. Modeling of heating up phase of coal particle is fairly straightforward. Modeling of coal devolatilization is also fairly well established. Most widely used approaches use correlations of volatile yield with particle temperature or define devolatilization rates using single or two step Arrehenius schemes. Modeling char combustion is however not straightforward. Char combustion is controlled by a complex coupling between transport phenomena around and within the particle. The problems associated with calculation of rate of char combustion are due to uncertainty in morphology of devolatilized coal particle, exact composition of coal and effects of ash. Computationally intensive network models, which are based on coal structural description, are not yet well established. Therefore most of the models proposed for char combustion are empirical in nature (Williams *et al.*, 2002)

2.7 Summary of Key Issues

The various physical issues which were discussed in detail in this section are summarized below.

- It is essential to simulate motion of solids/bed height in the bed region. Axial dispersion of solids can be neglected while developing computational models for rotary cement kilns.
- It is essential to account for motion of solids in transverse section. The prediction of flow in active layer/passive layer, rate of surface renewal, needs to be understood to simulate mixing/segregation in solid bed

- The melt formation in cement kilns and the re-solidification of melt near kiln exit should be considered during model development. Accurate prediction of location of coating formation is essential for proper estimation of heat losses in the kiln and shell temperatures.
- The physical properties of particle laden gas should be considered while developing models for capturing heat transfer in cement kilns. It is essential to accurately capture heat exchange specifically radiation between solids, gas and kiln walls.
- Freeboard region where turbulent fluid flow along with gas phase combustion and coal combustion occurs needs to be simulated accurately.

2.8 Performance Models for Rotary Cement Kilns

Considering the key issues (and relevant previous work) discussed above, it is not surprising that computational models are not readily available for simulating rotary cement kilns. It is evident that in order to develop a reliable computational model it is required to incorporate all the above-mentioned processes occurring in cement kilns. However, none of the published models for cement kilns have done this. This is what we aim to do in this research work. The performance models developed for cement kilns were mainly based on two approaches viz. reaction engineering based models (incorporating material and energy balance but not considering momentum balances) and CFD based models (incorporating all the three fundamental balance equations). However, the computational models published for cement kilns based on either of approaches are not very comprehensive. The lacunae of the published models are discussed below to clearly bring the need of tractable but realistic computational models for rotary cement kilns.

2.8.1. One dimensional models

Few one dimensional models were developed in about couple of decades for rotary kilns. (For example, See Watkinson and Brimacombe, 1982 and references there in). However, most of models were limited for studying heat transfer or flow in rotary kilns. Very few models (Spang, 1972) were specifically proposed for cement kilns. The published 1D models for cement kilns do not take into account simultaneously variation of bed height variation, flow, heat transfer, melting, coating formation, and reactions in the bed as well as free board (See for example, Spang, 1972; Mastorakos *et al.*, 1999). Unless this is done, it is impossible

to capture influence of design (diameter, length, tilt angle) and operating parameters (RPM) on kiln performance. Unless the kiln simulation model is able to capture influence of design and operating parameters of kiln on the kiln performance, the utility of the model will be rather restricted. None of the models for cement kilns consider melting of solids and re-solidification of melt correctly (Mastorakos *et al.*, 1999). Most of the models assume uniform coating along the kiln length (Spang, 1972; Mastorakos *et al.*, 1999). This can lead to erroneous calculation of losses from kiln shell. Thus, more comprehensive modeling framework is required to be built for rotary cement kilns.

2.8.2 CFD Models

Due to complexity of physics involved, occurrence of multiple phases with large number of reactions in bed/freeboard regions and numerical issues, very few CFD models have been published for rotary cement kilns (Kolyfetis and Markatos, 1996; Mastorakos *et al.*, 1999; Karki *et al.*, 2000). Mastorakos *et al.* (1999) developed a computational fluid dynamics (CFD) based model for cement kilns, which included combustion, radiative heat transfer, conduction in the bed/ walls and chemical reactions. The bed and freeboard models were thus treated as separate domains and coupling between them is handled explicitly. The geometry of kiln was assumed to be axisymmetric in this work and therefore the boundary conditions were applied only in an approximate manner. Moreover Mastorakos *et al.* (1999) assumed coating formation throughout the kiln length. Karki *et al.* (2000) developed a 3D CFD based model for simulating simultaneous combustion and heat transfer in cement kilns. Karki *et al.* (2000) have used an effective thermal conductivity to define degree mixing in bed region, developing a single computational model for simulating cement kilns. Different values of effective thermal conductivities at different locations in the kiln were used. However, there are no proper guidelines to choose proper effective thermal conductivity and the values used are based on experience. Moreover Karki *et al.* (2000) have focused on fluid dynamics and heat transfer and did not model clinkerization reactions. The model predictions thus gave only qualitative agreement with industrial observations reasonable for global quantities of interest. Kolyfetis and Markatos (1996) also focused on coal combustion and heat transfer in freeboard region and did not account clinker reactions. Moreover, Kolyfetis and Markatos (1996) did not consider any coating formation in their computational model.

From this literature review, it can be concluded that the computational models presented earlier for rotary cement kilns are more or less approximate and not rigorous models.

Therefore, comprehensive model for cement kilns need to be developed which will account for simultaneous flow, heat transfer and reactions occurring in rotary cement kilns. Such an attempt is made in this work which will be present in remaining part of this thesis.

3. Reaction Engineering based Model

Abstract

In this chapter, a comprehensive reaction engineering based model to simulate complex processes occurring in rotary cement kilns is presented. A modeling strategy comprising three sub-models viz. model for simulating variation of bed height in the kiln, model for simulating reactions and heat transfer in the bed region and model for simulating coal combustion and heat transfer in the freeboard region was developed. Melting and formation of coating within the kiln were accounted. Combustion of coal in the freeboard region was modeled by accounting devolatilization, finite rate gas phase combustion and char reaction. The simulated results were validated with the available data from 3 industrial kilns. The model was then used to understand influence of various design and operating parameters on kiln performance. Several ways of reducing energy consumption in kilns were then computationally investigated. The model was also used to propose and to evaluate a practical solution of using a secondary shell to reduce energy consumption in rotary cement kilns. Simulation results indicate that varying kiln operating variables viz. solid flow rate or RPM can result only in small changes in kiln energetics. Use of secondary shell over kiln and energy recovery by passing air through the annular gap between the two, appears to be a promising way for significant energy saving. The developed model and the presented results will be useful for enhancing performance of rotary cement kilns.

Publications based on this work

- *Mujumdar, K.S., Arora, A., and Ranade, V.V. (2006), "Modeling of Rotary Cement Kilns: Applications to Reduction in Energy Consumption". Ind. Eng. Chem. Res., 45 (7), 2315 - 2330, 2006*
- *Kaustubh S. Mujumdar and Vivek V. Ranade (2006), "Simulation of Rotary Cement Kilns Using a One-dimensional Model", Chemical Engineering Research and Design, 84, 165-177*

3.1 Introduction

Rotary kilns are commonly used in cement industry to produce cement clinkers. Most of the clinkerization reactions occur in rotary kilns and therefore it governs overall performance of clinker manufacture. However, computational models are not readily available for rotary cement kilns in published literature. This can be attributed to involvement of complicated physics involved in clinker manufacture as discussed in chapter 2. However, there is an urge for developing comprehensive mathematical models for cement kilns due to their high energy requirements during clinker transformations and environmental issues coming up in recent times. Apart from aiding in developing a better understanding of complex processes in cement kilns, mathematical models can also be useful in exploring different means to reduce energy consumption in the kilns.

The energy consumption in cement kilns is attributed to several processes occurring within the kiln, namely for raising the temperature of the solids to the reaction temperature, for endothermic clinkerization reactions, for melting of solids. Apart from these, energy is lost by the kiln to environment and other connected equipment. The energy of hot solids and hot gases leaving cement kiln is recovered (at least partially) in clinker cooler and calciner/ pre heaters. The energy lost to the surroundings from kiln surface (convection and radiation) is usually not recovered and is of the order of about 15-20 % of total energy input (Engin and Ari, 2005). Therefore, every attempt should be made to reduce the losses from kiln shell (without jeopardizing the product quality) per unit weight of the product to enhance kiln energy performance.

There can be several ways for reducing net losses from kiln shell per unit weight of product. Increasing the throughput of the cement kiln might be one of them. However, in order to ensure the same quality of product, it is essential to understand behavior of kiln at different throughputs. It is desirable to have a computational tool, which allows simulation of kiln performance over a wide range of design and operating parameter space. One of the obvious ways of reducing losses from kiln shell can be use of insulation over the kiln shell. However, such insulation of a kiln shell will lead to a very high temperature of the shell wall (if the kiln internal temperature was kept the same). This is not acceptable from the mechanical integrity of the kiln shell. Engin and Ari (2005) have proposed a use of a secondary shell over a rotary cement kiln to reduce losses from the kiln (see Figure 6 of Engin and Ari (2005)). However,

this proposal leads to substantial increase in temperature of kiln wall, which is usually not acceptable. This suggestion can be made practical by recovering energy from the kiln shell without reducing the energy flux across the shell. The secondary shell and the interstitial space can be used as a heat exchanger to recover energy from kiln wall. By selecting appropriate configuration of a secondary shell and appropriate airflow rate through the interstitial space, net energy loss to the surrounding can be minimized without altering the energy flux through kiln wall. The hot air coming out of the annular space could be utilized somewhere else in the plant (for example drying fly ash or pre-heating feed/air).

In this chapter it is attempted to develop comprehensive mathematical model to simulate reactions heat transfer and flow simultaneously in a single framework. This model was further used to realize the promise of using a secondary shell or to explore design and operating parameter space to minimize energy consumption per unit weight of product. We have developed a comprehensive model comprising three sub-models viz. model for simulating variation of bed height in the kiln, model for simulating reactions and heat transfer in the bed region and model for simulating coal combustion and heat transfer in the freeboard region for simulating cement kilns. Individual sub-models were validated wherever possible. Variation of bed height, melting and formation of coating within the kiln were accounted for the first time simultaneously. Combustion of coal in the freeboard region was modeled in detail. The model was used to understand influence of various design and operating parameters on kiln performance. The simulated results were also compared with the available data from 3 industrial kilns. Several ways of reducing energy consumption in kilns were then computationally investigated.

3.2 Computational Model and Solution Methodology

In this work, separate models for bed and freeboard region of kiln were developed. These two models were solved with segregated solution approach and were coupled to each other, along with a model for bed height via mass and energy communication through common boundaries. Individual sub models are discussed in the following.

3.2.1 Model for calculating bed height in rotary kilns

Developing accurate models for axial motion of solids in rotary kilns is essential since it controls the residence time of solid particles and the variation of solid bed height within the

kiln. The bed height in rotary kilns depends on volumetric flow rate of solids, ϕ_v, kiln tilt (γ, radian), angle of repose of solids (β, radian), radius of kiln (R, m), rotational speed of kiln (n) and height of solids (h) (Spurling *et al.*, 2001; Lebas *et al.*, 1995; Kramers and Crookewit, 1951). These parameters are shown in Figure 3.

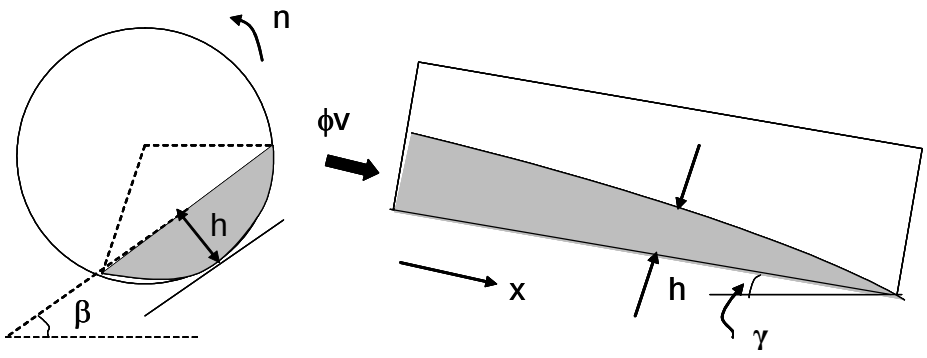

Figure 3.0: Various parameters influencing bed height in rotating kilns

In Chapter 2, it was discussed that the Kramer's model (Kramers and Croockewit, 1952) was shown to predict published experimental data with reasonable accuracy. However, it should be noted that Kramer's model does not take into account the effect of counter current gas flow on axial motion of solids. Fortunately, gas flow does not significantly affect solid hold up in kilns (Friedman and Marshall, 1949). Therefore, in this work we have used the Kramer's model for simulating axial motion of solid particle, which is given by (Kramers and Croockewit, 1952):

$$\frac{dh}{dx} = \tan\gamma\left[\frac{\tan\beta}{\sin\gamma} - \frac{3\phi_v}{4\pi nR^3}\left(\frac{2h}{R} - \frac{h^2}{R^2}\right)^{-3/2}\right] \tag{3.1}$$

From the above equation height of solids at different axial locations can be calculated. Based on the height at particular axial position, area of the clinker bed can be calculated as:

$$A_{cl} = \frac{1}{2}\times R^2 \times \Gamma - \frac{1}{2}\times L_{gcl}\times(R-h) \tag{3.2}$$

In the above equation Γ is the angle in radians made by the solids at the kiln center and L_{gcl} is the cord length of solids in the transverse section. Correspondingly area of freeboard region was calculated as:

$$A_g = A_k - A_{cl} \tag{3.3}$$

3.2.2 Bed model

It is important to consider solids mixing while developing mathematical models for simulating the cement kilns. Recently, Sherritt *et al.* (2003) have reviewed axial mixing of solids in rotary kilns and have proposed a correlation to estimate axial mixing. The correlation is valid for wide range of solid materials and kiln dimensions. This study indicated that the values of Peclet number for industrial rotary cement kilns were greater 10^4. For such a high values of Peclet number, axial mixing could be neglected as discussed in previous chapter. Therefore, the mass conservation equation for species i was written assuming a plug flow of solids as:

$$\frac{d(A_{cl}V_{cl}\rho_{cl}Yi)}{dx} = R_i A_{cl} \tag{3.4}$$

where Y_i is the species mass fraction and R_i is the rate of reaction of individual species. A_{cl} is the area of the clinker bed normal to the kiln axis, V_{cl} is the velocity of the solid bed, ρ_{cl} is bulk density of the solids. By summing the conservation equation over all the species, the overall mass conservation equation can be written as:

$$\frac{d(A_{cl}V_{cl}\rho_{cl})}{dx} = -R_{CO2}A_{cl} \tag{3.5}$$

R_{CO2} is the rate of formation of CO_2. CO_2 formed due calcination reaction in the bed region leaves the bed. Hence the solids flow rate in the kiln decreases along the kiln length. Calculation of R_{CO2} is discussed later in this section. The area of the solids bed A_{cl} was calculated by Equation (3.2). The variables Γ and L_{gcl} are functions of bed height in the kiln and can be calculated once the bed height is known. The bed height in the kiln varies along the kiln length. The variation of bed height within the kiln was modeled using Equation (3.1).

The chemical reactions occurring during clinker formation were discussed in Chapter 2 (Equation 2.3 to 2.7). The rate expressions for these reactions were calculated as:

$$R_i = \sum_{i=1}^{NC} \sum_{j=1}^{NR} \frac{Z_{ij}}{M_j} k_{0j} \exp\left(\frac{-E_j}{RT_{cl}}\right) \prod_{k=1}^{NC} C_k^{\,o(j,k)} \qquad (3.6)$$

Here, Z_{ij} are the stoichiometric coefficients, M_j is the molecular weight of the base component, k_{0j} and E_j are the Arrehenius parameters of the reactions. T_{cl} is the bed temperature, C_k is concentration of the k^{th} reactant and o (j, k) is order of j^{th} reaction with respect to k^{th} component. We have assumed the reactions to be of first order with respect to each reactant. NR is the number of reactions, which vary from 1 to 5, and NC is the number of components, which vary from 1 to 10 in the present case. The solids (particles) were assumed to be pseudo homogeneous fluids as explained in the previous section.

Selecting appropriate kinetic parameters for above reactions is important task. Critical review of published literature pointed out that there are significant differences in the kinetics reported even for relatively simple reaction like limestone calcination. The reported activation energy for calcination varies from 180-210 kJ/ mol (Irfan and Dogu, 2001) to ~ 1500 kJ/ mol (Hills, 1968). Similar level of disagreement was observed even in reported experimental data. For example, Watkinson and Brimacombe (1982) showed the initiation temperature of calcination reaction as 1100 K while Irfan and Dogu (2001) reported it as 850 K. Such disagreement in the reported data might be due to differences in the environment of calcination decomposition (air, N_2 or CO_2 containing flue gas). Several attempts have been made to model calcination kinetics. Limestone calcination was shown to be a shrinking core process (Khraisha *et al.,* 1992). Irfan and Dogu (2001) have carried out TGA experiments for wide range of limestone species. Several models like shrinking core model with mass transfer control, shrinking core model with diffusion control, shrinking core model with surface reaction controlling were compared with the measured experimental data. Shrinking core model with surface reaction controlling was reported to be the best compared to other models tested by them. Shrinking core model has also been used by various other investigators to model limestone calcination (Ingraham and Marier, 1963; Satterfield and Feakes, 1959). Hence we have used shrinking core model for limestone calcination in the present work. The reduction in radius of lime stone particle was related as:

$$\frac{dR_P}{dt} = -\frac{M_W k_{s0}}{\rho_b} e^{\frac{-E}{RT}} \qquad (3.7)$$

Where ρ_b is the bulk density of the particle, R_p is the particle diameter, M_w is the molecular weight of the particle, k_{s0} is the pre exponential factor in the Arrehenius equation and E is the activation energy.

Equation describing rate of reduction of radius of a single particle was re-written as an effective rate expression for pseudo homogeneous kinetics as:

$$-\frac{dC_c}{dt} = k_{app}\, C_C^{\,2/3}\quad e^{\frac{-E}{RT}} \tag{3.8a}$$

where

$$k_{app} = \frac{3\varepsilon_S^{1/3} k_{S0}}{R_0}\left(\frac{M_W}{\rho_B}\right)^{2/3} \tag{3.8b}$$

It can be seen that the apparent rate constant depends on the initial particle diameter and the bulk density of solids. As specified earlier, a wide discrepancy is observed in the proposed rates for calcination reaction. The large scatter in calcination kinetics was also reported by Stanmore and Gilot (2005) in their recent review on limestone calcination. It was also reported that the proposed models fit adequately their own experimental data. However, when they are applied to other results most of them fail. In absence of any reliable information on calcination kinetics, in the present work, we have compared models proposed by various investigators (see Table 3.1) with available experimental data and chosen a set of kinetics that best fits the data. The data reported in experiments of Watkinson and Brimacombe (1982) were close to actual kiln operations (bed temperature ~ 1000 to 1300 K) and was used to select appropriate calcination kinetics. The kinetic models listed in Table 3.1 were incorporated in the present model to simulate experiments of Watkinson and Brimacombe (1982). The simulated profiles of percentage calcination in calciner as a function of bed temperature (along the kiln length) for these different kinetics are shown in Figure 3.1. It can be seen from Figure 3.1 that the kinetics proposed by Rao *et al.* (1989) gives the best fit in the considered group and was therefore used in the present study.

Table 3.1: Kinetics proposed by various investigators for calcination reaction

Sr. No	Activation Energy (kJ/mol)	Pre-exponential factor (kmol/m^2 s)	Reference
1	186.9	1.020×10^8	Irfan and Dogu (2001)
2	193.6	9.670×10^7	Irfan and Dogu (2001)
3	160.0	3.650×10^7	Irfan and Dogu (2001)
4	205.8	1.070×10^8	Irfan and Dogu (2001)
5	172.2	6.050×10^7	Irfan and Dogu (2001)
6	156.2	4.190×10^7	Irfan and Dogu (2001)
7	159.1	4.090×10^7	Irfan and Dogu (2001)
8	213.3	1.430×10^8	Irfan and Dogu (2001)
9	166.0	6.700×10^3	Garcia-Labiano *et al.*(2002)
10	205.0	6.078×10^4	Borgwardt (1985)
11	169.0	1.185×10^3	Ingraham and Marier (1963)
12	154.1	2.230×10^2	Lee *et al.* (1993)
13	164.7	5.290×10^2	Lee *et al.* (1993)
14	185.0	1.180×10^3	Rao *et al.* (1989)
15	131.0	2.540×10^{-1}	Garcia-Labiano *et al.* (2002)
16	205.0	2.470×10^2	Khinast *et al.* (1996)

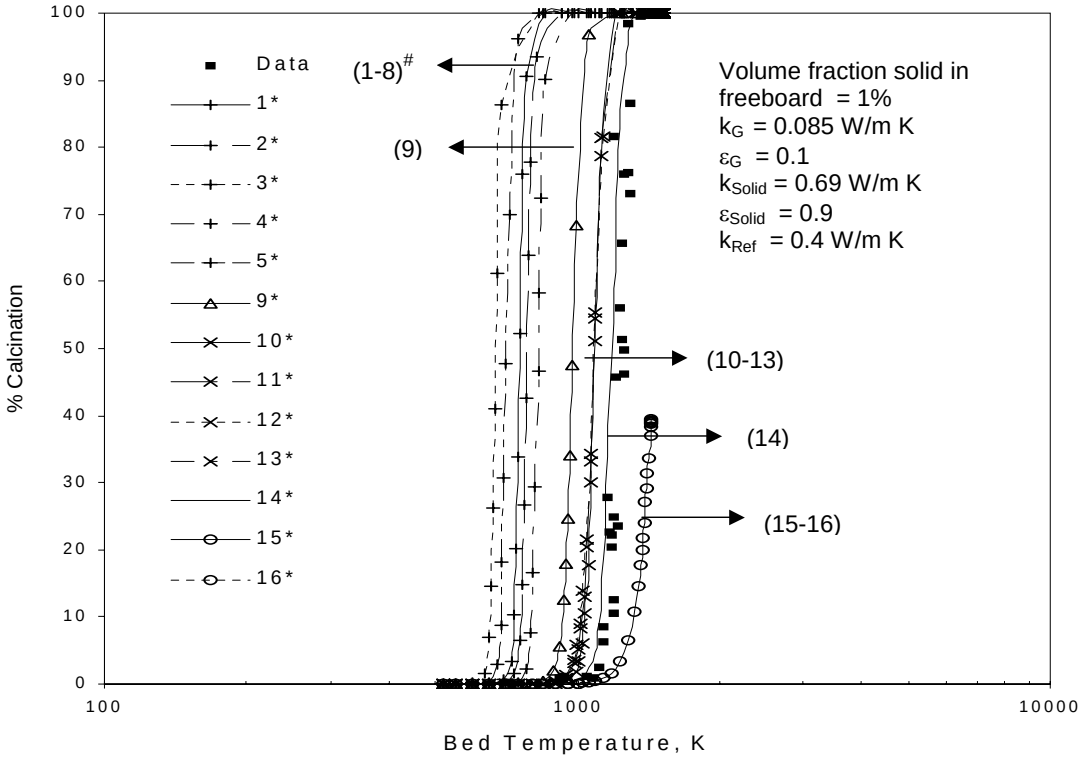

Figure 3.1: Comparison of different reaction rates on experimental data of Watkinson and Brimacombe, (1982); * Numbers in figure correspond to sequence in Table 3.1;

Only 5 curves are shown to avoid clutter, rest fall in the same range.

This set of experimental data was chosen for fitting exercise since the experimental conditions were close to actual kiln operations. Out of total 18 investigations, kinetic parameters proposed by Rao *et al.* (1989) gave the best fit and therefore used to model calcination reaction (See Table 3.1). The experimental conditions of Rao *et al.* (1989) were also close to operating conditions in kiln (Temperature in range of 953 K- 1148 K with an average grain size of ~ 10 μm). Since particle level models are not yet well established for the rest of the reactions, kinetics of these reactions were used as reported by Mastorakos *et al.* (1999) and are specified in Table 3.2.

Table 3.2: Reaction, kinetics and heat of reaction

	Reaction	k_0	E (kJ /mol)	ΔH^* (kJ/mol)
Bed				
1.	$CaCO_3 = CaO + CO_2$	1.18×10^3 (kmol/m^2-s)	185	179.4
2.	$2CaO + SiO_2 = C_2S$	1.0×10^7 (m^3/kg-s)	240	-127.6
3.	$C_2S + CaO = C_3S$	1.0×10^9 (m^3/kg-s)	420	16.0
4.	$3CaO + Al_2O_3 = C_3A$	1.0×10^8 (m^3/kg-s)	310	21.8
5.	$4CaO + Al_2O_3 + Fe_2O_4 = C_4AF$	1.0×10^8 (m^6/kg^2-s)	330	-41.3
Freeboard				
1	$CH_4 + 2O_2 = CO_2 + 2H_2O$	1.6×10^{10} (m^3/kg-s)$^+$	108$^+$	3125$^+$
2	$C + O_2 = CO_2$	1.225×10^3 (m/s)$^+$	99.77$^+$	-

$^+$ Li *et al.* (2003); * Drujic *et al.* (2005)

The chemical reactions occurring in the bed are driven by energy supplied by the free board and kiln walls. Although heat transfer occurs by all the three mechanisms, radiation is a dominant mode of heat transfer (Mastorakos *et al.,* 1999; Karki *et al.,* 2000) There was a considerable work on heat transfer in rotary kilns (Gorog *et al.,* 1981; Gorog *et al.*, 1983; Barr *et al.,* 1989). Gorog *et al.* (1983) have reported comparison of results with and without considering contributions of radiative transfer over axial distances. The relative contribution of radiative transfer over axial distances depends on axial flame temperature gradient ($\Delta T/\Delta Z$), relative flame diameter (diameter of flame/diameter of kiln) and wall refractivity. Considering the typical values of these parameters occurring in rotary cement kilns (temperature gradient of 100 K/m, relative diameter of about 0.5 and wall refractivity in the range of 0.2-0.5), it can be concluded that the maximum errors caused by neglecting radiative transfer in axial direction is less than 10%. Based on these results and considering the main

objective of this work as developing a simple yet adequately accurate model (without increasing demands on computational resources), we have neglected the contribution of radiative transfer over axial distances. The energy conservation equation was written as

$$\frac{d}{dx}(A_{cl}V_{cl}\rho_{cl}C_pT_{cl} + A_{cl}V_{cl}\rho_{cl}\lambda m_L) = (L_{gcl}Q') - (\sum_{i-1}^{NC} R_iH_i)A_{cl} - S_{CO2} \quad (3.9)$$

C_p is heat capacity of solids. The first term of the left hand side represents convective transfer of energy. The second term of left hand side represents the energy required for melting of solids. The second term in the RHS of the above equation represented energy required/ liberated during chemical reactions (H_i is the heat of formation of species i). Q′ is the heat flux received by the bed from the free board and kiln walls and L_{gcl} is the chord length of solids exposed to the freeboard region. S_{CO2} is the volumetric energy sink due to CO_2 loss from the bed. The first term in the RHS of Equation (3.9) represents the heat received by the solid bed from the freeboard gas and the hot walls. This term was evaluated as explained in the following.

Various modes by which heat transfer takes place in rotary kiln operation are shown in Figure 3.2. In Figure 3.2, region 1 represents the coating layer, region 2 represents the refractory layer and region 3 represents the kiln shell. Region 4 represents the annulus or interstitial gap between the two shells, 5 presents the secondary shell and 6 represents the insulation layer. In absence of secondary shell layers 4, 5 and 6 would not be there. Energy is transferred from freeboard to bed via radiation and convection from freeboard gas. Also there will be exchange of energy between bed and kiln inner walls via radiation and conduction. Hence, to calculate the amount of energy transferred to the bed, temperature of inner wall and freeboard gas are required. To calculate the heat losses due to radiation and convection from the kiln, the outer shell temperature is required. To calculate the temperature of inner walls, refractory, shell and secondary shell steady state heat balance across the kiln walls need to be solved. The steady state equations for heat balance across kiln walls were written as:

$$Q_{RGW} + Q_{CGW} - Q_{RWB} - Q_{CWB} = Q_{COAT} \quad (3.10)$$

$$Q_{COAT} = Q_{REF} \quad (3.11)$$

$$Q_{REF} = Q_{SHELL} \quad (3.12)$$

$$Q_{SHELL} = Q_{RAD} + Q_{CONV-SHELL} + Q_{RAD-SHELL} \quad (3.13)$$

$$Q_{RAD} = Q_{CONV-SEC-SHELL} + Q_{COND-SEC-SHELL} + Q_{RAD-SEC-SHELL} \quad (3.14)$$

$$Q_{COND-SEC-SHELL} = Q_{INSU} \quad (3.15)$$

$$Q_{INSU} = Q_{LOSSCONV} + Q_{LOSSRAD} \quad (3.16)$$

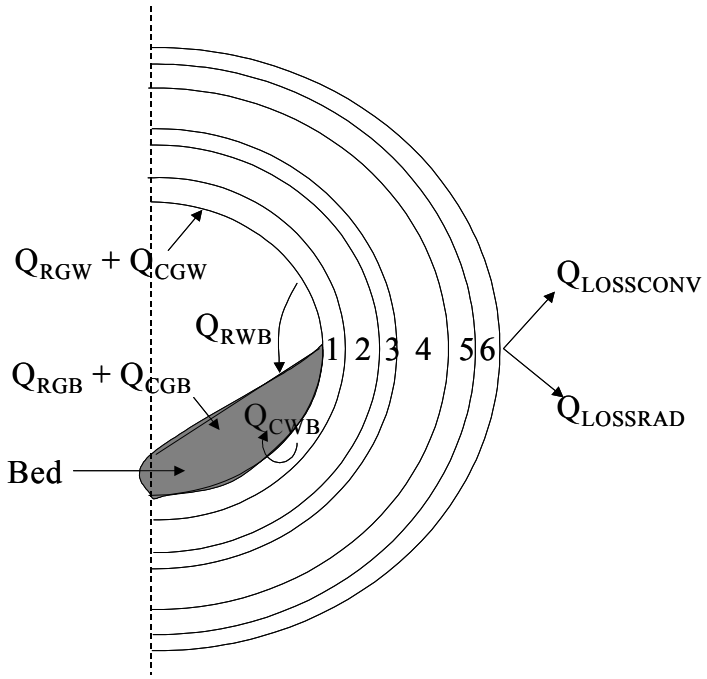

Figure 3.2: Heat transfer in transverse section of rotary kiln

In the above equations, Q_{RWB} and Q_{CWB} are heat transfer rates due to radiation and conduction respectively between the kiln internal wall and the bed. Q_{RGW} and Q_{CGW} are heat transfer rates due to radiation and convection between the freeboard and kiln internal wall. $Q_{COND-COAT}$, $Q_{COND-REF}$, Q_{SHELL}, $Q_{COND-SEC-SHELL}$ and $Q_{COND-INSU}$ are the conductive heat transfer rates in coating, refractory, kiln shell, secondary shell and insulation layers respectively. Q_{RAD} is the radiative heat transfer from kiln shell to secondary shell. $Q_{CONV-SHELL}$ and $Q_{CONV-SEC-SHELL}$ are the heat transfer rates between hot shell walls and the gaseous stream in the annulus. $Q_{LOSSCONV}$ and $Q_{LOSSRAD}$ are the losses from outer shell due to convection and radiation respectively. The calculation of individual heat transfer terms in above equations is given below

Heat transfer by radiation between gas phase & bed and gas phase & the kiln internal walls was evaluated by the equations developed by Hottel and Sarofim, (1967) valid for ε ≥ 0.8:

$$Q_{RGK} = \sigma\, A_{RKG}(\varepsilon_K + 1)\left(\frac{\varepsilon_G T_G^4 - \alpha_G T_K^G}{2}\right) \qquad \mathrm{K = B, W} \tag{3.17}$$

Q_{RGK} is the radiative heat transfer, σ is the Stefan- Boltzmann constant, A is the area of heat transfer. ε and α are the emissivity and absorptivity of the freeboard gas respectively. T_g is the temperature of the freeboard gas. Subscript B denotes solid bed and W denotes walls.

Convective heat transfer between gas phase & bed and gas phase & the kiln internal walls was evaluated as:

$$Q_{CGK} = h_{CGK} A_{CKG}(\mathrm{T_G - T_K}) \quad \mathrm{K = B, W} \tag{3.18}$$

Tscheng and Watkinson (1979) have studied the effects of convective heat transfer of kiln operating parameters like kiln rotation and kiln degree of fill in pilot plant scale. Based on their experimental data obtained for sand and limestone, they have proposed correlations for convective heat transfer coefficients for sand and limestone as:

$$h_{CGS} = 0.46\frac{k_g}{D_e}\mathrm{Re}_D^{0.535}\,\mathrm{Re}_\omega^{0.104}\,\eta^{-0.341} \tag{3.19}$$

$$h_{CGW} = 1.54\frac{k_g}{D_e}\mathrm{Re}_D^{0.575}\,\mathrm{Re}_\omega^{-0.292} \tag{3.20}$$

where k_g is the gas thermal conductivity and D_e is the hydraulic diameter of the kiln. Re_D and Re_ω are the axial and angular Reynolds number calculated as:

$$\mathrm{Re}_D = \frac{\rho_g \times u_g \times D_e}{\mu_g} \qquad \mathrm{Re}_\omega = \frac{\rho_g \times \omega \times D_e^2}{\mu_g}$$
$$D_e = \frac{0.5D \times (2\pi - \beta + \sin\beta)}{(\pi - \frac{\beta}{2} + \sin\frac{\beta}{2})} \tag{3.21}$$

It is important to note that the Reynolds numbers for commercial kilns are significantly higher as compared to experimental conditions of Tscheng and Watkinson (1979). However, there are no other systematic experimental studies reported to predict convective heat transfer

coefficients in industrial rotary kilns. Equations (3.19) and (3.20) were used to model convective heat transfer in commercial kilns and have reproduced temperature profiles for gas and solids in these kilns reasonably well (Martins *et al.,* 2000; Martins *et al.,* 2001). Therefore, Equations (3.19) and (3.20) were used to predict convective heat transfer coefficients. Fortunately, radiation dominates the overall heat transfer process and therefore possible errors associated with Equation (3.19) and (3.20) are not expected to change the simulation results significantly.

The radiative heat transfer between kiln internal walls and bed is given by:

$$Q_{RWB} = \sigma \times \mathrm{A_{RWB}} \times \varepsilon_S \times \varepsilon_W \times \Omega \times (T_W^4 - T_S^4) \tag{3.22}$$

Ω is the form factor for radiation which was calculated as:

$$\Omega = \frac{L_{gcl}}{(2\pi - \beta)R} \tag{3.23}$$

The heat transfer by conduction between the bed and the kiln internal walls was given by:

$$Q_{CWS} = h_{CWS} A_{CWS} (\mathrm{T_W} - \mathrm{T_S}) \tag{3.24}$$

h_{CWS} is the heat transfer coefficient which was evaluated using empirical correlation by Tscheng and Watkinson (1979) as:

$$h_{CGW} = 11.6 \frac{k_b}{A_{cws}} \left(\frac{\omega R^2 \Gamma}{\alpha_b} \right)^{0.3} \tag{3.25}$$

In the above expression k_b is the thermal conductivity of bed, Γ is the angle of fill of the kiln, ω is the rotational speed (rad/s) and α_b is the bed thermal diffusivity. Dhanjal *et al.* (2004) also have presented their work on wall to bed heat transfer wherein experimental results were presented by heating sand of different particle size distribution in a batch rotary kiln to bed temperatures up to 775 ^{0}C. However, Martins *et al.* (2001; 2000) have used and shown that correlations (from Equation 3.17 to Equation 3.25) work reasonably well for industrial as well as lab scale kilns and were used in this work.

Conductivity and emissivity of the freeboard gases depend on its composition and dustiness (volume fraction of solids entrained in the freeboard gases). The influence of carbon dioxide

and water vapor on emissivity was estimated from the data reported by Gorog *et al.* (1983) The thermal conductivity of the freeboard gas was assumed to be same as that of air at prevailing temperature and was calculated by the expression:

$$k_g = -7.494\times10^{-3} + 1.709\times10^{-4}T_g - 2.377\times10^{-7}T_g^{\,2} + 2.202\times10^{-10}T_g^{\,3} - 9.463\times10^{-14}T_g^{\,4} + 1.581\times10^{-17}T_g^{\,5} \quad (3.26)$$

The thermal properties of solids were available from literature and are specified in Table 3.4 Influence of entrained solids on effective emissivity and conductivity of gas was estimated as:

$$\psi_{eff} = \varepsilon_{solid}\psi_{solid} + (1-\varepsilon_{solid})\psi_{gas} \quad (3.27)$$

where ψ is the property i.e. thermal conductivity or emissivity, ε_{solid} is the solid volume fraction or dustiness of the gas. Adequate information on solid entrainment or solid volume fraction in rotating cylinders is however not readily available. Few experimental studies on solid entrainment on rotary kilns (Friedman and Marshall, 1949; Li, 1974) suggest that the volume fraction of solids in freeboard region of kiln is very small (<1 %). Therefore, for all the subsequent simulations, the value of solid volume fraction entrained in the free board region was set to 1 %. Fortunately, the predicted results (C_3S mass fraction and temperature profiles of bed and freeboard) were not found to be sensitive to the value of solid hold-up in the freeboard region up to 5 %.

Q_{RAD} is the radiative heat transfer between shell and secondary shell. Since the secondary shell is considered to be of material of low emissivity, radiation from secondary shell to kiln shell is neglected (Engin and Ari, 2005). The radiative heat transfer between of shell and secondary shell was calculated as (Engin and Ari, 2005):

$$Q_{RAD} = \frac{A_{SHELL}\sigma(T_{SHELL}^{\,4} - T_{SEC-SHELL}^{\,4})}{\frac{1}{\varepsilon_1} + \frac{1-\varepsilon_2}{\varepsilon_2}\left(\frac{R_{SHELL}}{R_{SEC-SHELL}}\right)} \quad (3.28)$$

$Q_{RAD\text{-}SHELL}$ and $Q_{RAD\text{-}SEC\text{-}SHELL}$ are the radiative heat transfer rates between hot shell walls and air in the shell annular gap and were calculated as:

$$Q_{RAD-SHELL} = \sigma \times A_{SHELL} \times \varepsilon_{SHELL} \times (T_{SHELL}^4 - T_{AIR}^4) \quad (3.29)$$

$$Q_{RAD-SEC-SHELL} = \sigma \times A_{SEC\text{-}SHELL} \times \varepsilon_{SEC-SHELL} \times (T_{SEC-SHELL}^4 - T_{AIR}^4) \quad (3.30)$$

$Q_{CONV\text{-}SHELL}$ and $Q_{CONV\text{-}SEC\text{-}SHELL}$ are the convective heat transfer rates between the hot shell walls and air passing through interstitial gap. The convective heat transfer rates are given by

$$Q_{CONV\text{-}SHELL} = U_{CONV} \times A_{SHELL} \times (T_{SHELL} - T_{AIR}) \quad (3.30a)$$

$$Q_{CONV\text{-}SEC\text{-}SHELL} = U_{CONV} \times A_{SEC\text{-}SHELL} \times (T_{SEC\text{-}SHELL} - T_{AIR}) \quad (3.30b)$$

Depending on mass of air through annulus, the heat transfer coefficient for convection for a turbulent flow (Re> 2300) was calculated as: (Quirrenbach, 1960)

$$U_{CONV} = 0.021\,(\mathrm{Re})^{0.8}(\mathrm{Pr})^{0.33}\left(\frac{d_o}{d_i}\right)^{4/5} \quad (3.30c)$$

In absence of gaseous stream through the annular space between the two cylinders the terms $Q_{CONV\text{-}SHELL}$ and $Q_{CONV\text{-}SEC\text{-}SHELL}$ would be zero.

The heat losses by convection and radiation in presence of secondary shell with insulation were calculated as:

$$Q_{CONVLOSS} = H_{CONV} \times A_{SHELL} \times (T_{INSU} - T_0) \quad (3.31a)$$

$$Q_{RADLOSS} = \sigma \times A_{SHELL} \times \varepsilon_{SHELL} \times (T_{INSU}^4 - T_0^4) \quad (3.31b)$$

In absence of secondary shell the heat losses were calculated as:

$$Q_{CONVLOSS} = H_{CONV} \times A_{SHELL} \times (T_{SHELL} - T_0) \quad (3.32a)$$

$$Q_{RADLOSS} = \sigma \times A_{SHELL} \times \varepsilon_{SHELL} \times (T_{SHELL}^4 - T_0^4) \quad (3.32b)$$

Above set of non-linear equations with appropriate boundary conditions were solved to get the temperatures of kiln walls (Equations (3.10) to (3.12) for the case without a secondary shell and Equations (3.10) to (3.16) for a case with a secondary shell). Knowing the temperature of kiln inner wall and freeboard gas, the heat flux received by the bed (Q' in Equation 9) was calculated as:

$$Q' = \frac{Q_{CWB}}{A_{CWB}} + \frac{Q_{RWB}}{A_{CWB}} + \frac{Q_{RGB}}{A_{CWB}} + \frac{Q_{CGB}}{A_{CWB}} \tag{3.33}$$

Here Q_{RGB} and Q_{CGB} are heat transfer due to radiation and convection between freeboard gas and bed respectively.

Melting of solids in the kilns was assumed to be proportional to the bed temperature in the kiln. Melting was modeled by using the following relationship between mass fraction of liquid and bed temperature:

$$m_L = max\left[0, \frac{T_{cl} - T_S}{T_L - T_S}\right] \tag{3.34}$$

where T_L and T_S are liquidus (temperature at which all mass is liquid) and solidus (temperature at which first drop of liquid forms) temperatures respectively. λ is the latent heat of melting (λ = 416 kJ/kg) (Mastorakos *et al.,* 1999). The formation of melt phase was assumed to depend only on local temperature (it was assumed to occur very fast compared to other relevant time scales). The values of T_L and T_S depend on composition of solids in the kiln and may vary within the kiln. As a first approximation, these values were assumed to be constant and were set to 1560 K and 2200 K respectively following Peray (1986).

As the part of the solids melt in the kiln, the melt forms an inner coating on the refractories. The coating formation will reduce the effective diameter of the kiln and will reduce heat losses. The change in an effective diameter of the kiln will change effective contact area between the solid bed and the free board and may affect profile of bed height within the kiln. The coating formation is an extremely complex process, which depends on flame temperature, chemical composition of kiln feed, temperature of coating and temperature of bed. The mechanism of coating formation and its interaction with design and operating parameters are not well understood. In practice, usually coating thickness is measured under cold conditions. Some of the data on maximum coating thickness available from industrial sources (listed in Table 3.2) and the values reported by Mastorakos *et al.* (1999) and Karki *et al.* (2000) indicate that the maximum coating thickness varies within the range of $0.03D_I < C_{T,max} < 0.05D_I$, where D_I is the internal diameter of the refractories. The observed differences in the predicted results (temperature profiles) with the minimum ($0.03D_I$) and

maximum ($0.05D_I$) values of $C_{T,max}$ were within 1%. Therefore, in this work, if the measured value of maximum coating thickness is available, it was used as an input data. In absence of such information, the maximum coating thickness was set to 0.04 D_I.

As mentioned earlier, coating starts forming when bed temperature exceeds solidus temperature and attains a maximum thickness after some point. In absence of any better information, in this work, we have assumed that the coating thickness varies linearly with the bed temperature up to certain limit and then remains constant thereafter. Thus the coating thickness (C_T) along the kiln length was calculated as:

$$C_T = 0.0 \qquad \text{for } T_{cl} < T_s$$

$$C_T = \left(\frac{T_{cl} - T_S}{T_{coat} - T_S} \right) C_{T,\max} \qquad \text{for } T_s < T_{cl} < T_{coat} \qquad (3.35)$$

$$C_T = C_{T,\max} \qquad \text{for } T_{cl} > T_{coat}$$

T_S is the bed solidus temperature at which bed starts melting. T_{coat} is a temperature at which coating is assumed to attain its maximum thickness, $C_{T,max}$. The value of T_{coat} was set to 1600 K. It was confirmed that changing the value of T_{coat} by 5 % had an insignificant (within 1%) effect on temperature profiles of bed and freeboard gas.

3.2.3 Freeboard model

Coal particles enter the freeboard region along with secondary air from the burner end. The pulverized coal particles enter the kiln via high velocity jets (about 50 m/s) where as superficial velocity based on kiln cross section of secondary air is within the range of 10-15 m/s. Considering the large difference in the actual velocity of coal particles and superficial gas velocity in the kiln and inertia of coal particles, it is inappropriate to assume coal particle velocity same as that of superficial velocity near the burner. Such an assumption would have significant implications for simulation of devlotalization and combustion of coal particles (Gang *et al.,* 2000, Megalos *et al.,* 2001). Away from the burner, the velocity of coal particle will eventually be more or less as the gas velocity. It is necessary to make approximations for the decaying profile of particle velocity within the one-dimensional framework of the model. In this work, the axial velocity decay of coal particles was calculated using a semi empirical equation proposed as Megalos *et al.* (2001)

$$u_c = u_{c,0}\, e^{-\delta z} \qquad (3.36)$$

where $u_{c,0}$ is the coal velocity at the nozzle entrance. Equation (3.36) was used un till the velocity of coal particles was greater than the superficial gas velocity. Once particle velocity reached the superficial gas velocity it was assumed to move with the superficial gas velocity in the kiln. It is important to note that Equation (3.36) is an empirical system specific equation. The parameter δ appearing in Equation (3.36) is a characteristic constant for a specific burner/ kiln configuration. In absence of any guidelines for determination of values of δ for kilns, in this work we had estimated the values of δ from CFD simulations of the free board region developed in Chapter 6. The particle velocities predicted by the CFD model were fitted to Equation (3.36) to obtain the value of δ. A value of 0.06 gave a reasonably good fit. Fortunately, the predicted results are not very sensitive to the value of δ (± 20 % variation in the value of δ resulted in less than 0.1 % change in the freeboard gas temperature profile along the kiln length).

The present computational model assumes coal particles to be comprised of char, volatiles and ash. Coal combustion was modeled using a shrinking core model with constant devolatilization, finite rate chemistry and char combustion. While developing the coal combustion model, it was assumed that, devolatilization proceeds with shrinking core of char, which because of relatively high porosity does not offer any resistance to gases leaving the reaction zone (Chern and Hayhurst, 2004). The coal particle first gets heated by absorbing energy from the gas. The energy is received by convection and radiation. Due to heat up the coal particle starts devolatilization. The present model assumes a constant rate devolatilization for coal combustion (Pillai, 1981). Coal devolatilization rate is given as:

$$\frac{dF_{c,vol}}{dz} = \frac{-A_0 F_{C0} m_{v0}}{u_c} \tag{3.37}$$

Here $F_{c,vol}$ is volatilization rate of coal particle (kg/s), F_{C0} is the initial coal flow rate and m_{v0} is the initial mass fraction of the volatiles in the coal. u_c is the velocity of the coal particle. A_0 (s^{-1}) is the devolatilization constant recommended as 12.0 for coal combustion. The coal particle density was assumed to decrease in proportion to the volatiles released in the gas phase (Heidenreich *et al.*, 1999). On devolatilization, in the gas phase, volatiles will react with available oxygen in the freeboard region to form CO_2 and H_2O (Guo *et al.,* 2003; Martins *et al.,* 2001). Gas phase combustion was modeled as reported by Guo *et al.* (2003) for

pulverized coal combustor. A global single step reaction of volatile fuel was assumed to take place as:

$$CH_4 + 2O_2 \rightarrow CO_2 + 2H_2O \tag{3.38}$$

The kinetics and heat of reaction for above gas phase reaction are given in Table 3.1. It should be noted that the characteristic reaction time scale at temperatures above 1500 K is less than 1 ms. Therefore, at such high temperatures, the reaction will be limited by turbulent mixing rather than reaction kinetics. For turbulent mixing limited combustion, the most commonly used model is the eddy breakup (EBU) turbulent combustion model of Magnussen and Hjertager (1976). This model compares the kinetic rate and the turbulence mixing rate and selects the lower rate for further calculations as:

$R_{combg} = \min (R_{S,\,EBU}, R_{S,\,Arr})$ where

$$R_{S,EBU} = C_R \rho \frac{k}{\varepsilon} \min(y_{F,} \frac{y_{ox}}{b}),$$
$$R_{S,Arr} = B_s \rho^2 y_F y_{OX} \exp(-\frac{E_s}{RT}) \tag{3.39}$$

y_F is the mass fraction of the fuel and y_{OX} is the mass fraction of oxygen. The values for Arrhenius kinetic constants B_S and E_S are specified in Table 3.1. C_R is a parameter of the eddy breakup (EBU) turbulent combustion model, which is usually set to 4. It can be seen that the EBU model uses ratio of turbulent kinetic energy and energy dissipation rate (k/ε) as characteristic time scale of turbulent mixing. In the present one-dimensional reaction engineering framework for modeling cement kilns, turbulent flow in the free board region is not being simulated. Therefore it is necessary to estimate the variation of (k/ε) along the kiln length. CFD simulations developed in course of this work were used to understand variation of (k/ε). The results indicated the possibility of approximating the variation by a linear profile. A simplified analysis of one-dimensional version of modeled equations of k and ε (neglecting accumulation, turbulent dispersion and approximating values of model parameters) lends some support to the linear approximation. Based on this, the variation of (k/ε) was approximated as:

$$(k/\varepsilon) = a\,(z/L) \quad [a = 1\ s] \tag{3.40}$$

where z is distance from the burner end and L is kiln length. Equation 3.40 represents system specific empirical one-dimensional version of modeled equations for k (turbulent kinetic energy) and ε (dissipation rate) along the kiln length. It can be seen that near the burner end,

time scale of turbulent mixing might be smaller than the reaction time scale (due to lower temperature and higher turbulence at the burner end). However, in the major portion of the kiln, the effective rate will be controlled by the rate of turbulent mixing.

Single step combustion reaction was assumed for char combustion in the present model (Spang, 1972):

$$C + O_2 \rightarrow CO_2 \tag{3.41}$$

For the temperature conditions and range of coal particle size (~ 50 μm) found in cement kilns, the reaction rate was written as (Smith, 1971; Young and Smith, 1989),

$$R_{comb} = \frac{M_{Coke} N_P A_P k_s C_{O_2}}{A_g u_c} \tag{3.42}$$

Where R_{comb} is the combustion rate per unit volume of the gas (kg/m^3 s), M_{coke} is the molecular weight of coke, A_P (m^2) is the surface area of each particle. k_s (m/s) is the rate constant for a first order reaction per unit surface area of the un-reacted core given in Table 3.1, u_c (m/s) is the particle velocity and A_g (m$_2$) area of freeboard region. C_{O2} is the concentration of oxygen in air. From the above equations the variation of radius along the axis of the freeboard can easily shown to be derived as:

$$\frac{dr}{dz} = \frac{1}{u_C} k_s . \frac{C_{o_2}}{C_C} \tag{3.43}$$

Where z is the distance from gas inl*et al*ong the axis and C_C is the concentration of carbon in coke. Now we present the mass and energy balance equations for discrete (coal) and continuous (gas) phase for the freeboard region.

Mass balance for discrete phase

The mass balance for discrete phase is given by

$$\frac{dF_C}{dz} = -\upsilon_{coke} R_{comb} A_g - \frac{dF_{c,vol}}{dz} \tag{3.44}$$

Where F_C is the mass flow rate of coke and ν_{coke} the stoichiometric coefficient of coke in the combustion reaction and A_g is the area of the freeboard region. The first term in the RHS of above equation represents the loss in discrete phase mass due to char reaction and the second term in the RHS of above equation represents the loss in discrete phase mass due to devolatilization of coal particles.

Energy balance for discrete phase

The energy balance for discrete phase is given as:

$$\frac{d(F_C.C_{pc}.T_C)}{dz} = \frac{N_P A_P h_c}{u_c}(T_G - T_C) + \frac{N_P \sigma \varepsilon_S A_P}{u_c}(T_G{}^4 - T_C{}^4) + f_h \Delta H_{comb} R_{comb} A_g \quad (3.45)$$

In the above equation C_{PC} is the specific heat of coal and T_C is the coal temperature. Coal was assumed to enter the kiln at 300 K. T_G is the gas temperature. ΔH_{comb} is the heat released due to coal combustion and f_h is the fraction of energy released due to coal combustion, which is absorbed by the particle. This factor was set to 0.3 following the recommendation of Boyd and Kent (1986). The first and second terms in RHS of above equations are the energy absorbed by the coal particle due to convection and radiation from the gas phase during the heat up. The heat transfer coefficient, h_c, is evaluated using the correlation of Ranz and Marshall (1952) as:

$$\frac{h_c d_p}{k_g} = 2 + 0.6(\mathrm{Re})^{0.5}(\mathrm{Pr})^{0.33} \quad (3.46)$$

Mass balance for continuous phase

The overall mass balance equation is given by:

$$\frac{dF_G}{dz} = \upsilon_i A_g R_{comb} + \frac{dF_{c,vol}}{dz} + S_G \quad (3.47)$$

Here F_G represents the mass flow of gas (kg/s). The first term in the RHS is the mass transferred to the gas phase due to combustion of coal. The second term in RHS contains the source terms for the gas phase due to devolatilization of coal particle. The final term in the above equation is mass of CO_2 coming to freeboard region due to calcination reaction in the bed region.

Mass balance of individual species can be written as

$$\frac{dF_{Gi}}{dz} = \frac{\upsilon_i A_g M_{Gi}.R_{comb}}{M_{coke}} + \frac{dF_{c,i}}{dz} + S_i \quad (3.48)$$

Where F_{Gi} is the mass flow of species i in the gas phase with a stoichiometric coefficient ν_i, molecular weight M_{Gi} and S_i is the source term. S_i accounts for species mass transfer to the freeboard region due to coal devolatilization, char combustion and CO_2 formation in the bed region due to calcination reaction.

Energy balance for the continuous phase

An energy balance for the gas phase can be written as.

$$\frac{d(F_G.C_{PG}.T_G)}{dz} = -\sum Q^{''} + \Delta H_{comb}.R_{comb}.A_g + \Delta H_{combg}.R_{combg}.A_g + S_H \qquad (3.49)$$

where F_G is the gas mass flow rate, C_{PG} is the specific heat of gas, T_G is the temperature of the gas phase, ΔH_{comb} is the heat of reaction of coke combustion per kg of coke burnt, ΔH_{combg} is the heat of reaction of gas phase reaction per kg of volatiles burnt, A_g is the freeboard area in the transverse section. $S_{H,i}$ is the heat from source/sink to freeboard region. Freeboard region will receive heat from CO_2 due to calcination in the bed region and give heat to coal particle due to convection and radiation. $\sum Q^{''}$ (W/m) is the net heat exchange between gas and kiln walls/bed. The heat transfer rate was obtained by solving heat balance across kiln walls in the transverse section as are previously explained in bed model.

Energy balance for convective air in annular gap

Along with the equation for continuous (gas) and dispersed phase (coal) convective air temperature (air in annular gap of two shells) was calculated as:

$$\frac{d(M_{AIR}C_{P,AIR}T_{AIR})}{dz} = U_{CONV}A_{SHELL}(T_{SHELL} - T_{AIR}) + \sigma\varepsilon_{SHELL}A_{SHELL}(T_{SHELL}^4 - T_{AIR}^4)$$
$$+ U_{CONV}A_{SEC-SHELL}(T_{SEC-SHELL} - T_{AIR}) + \sigma\varepsilon_{SEC-SHELL}A_{SHELL}(T_{SEC-SHELL}^4 - T_{AIR}^4) \qquad (3.50)$$

In the above equation M_{AIR} (kg/s) is the mass of air flowing in the annular gap, $C_{P,\,AIR}$ is the specific heat of the air. T_{SHELL} and $T_{SEC\text{-}SHELL}$ are the temperatures of kiln shell and secondary shell obtained by solving the heat balance in transverse section of the kiln. A_{SHELL} and $A_{SEC\text{-}SHELL}$ are corresponding areas of heat transfer. U_{CONV} is the convective heat transfer coefficient calculated by Equation (3.30c). The above set of equations for height variation, bed and freeboard are solved as described in the next section.

3.2.4 Solution methodology

In this work, all the three sub models viz. height variation model, bed model and freeboard model were solved separately. The solution procedure employed is shown in Figure 3.3. Kramer's equation (Equation 3.1) was solved initially to obtain the profile of bed height along the kiln length. Using the solution of height variation model, the freeboard model was solved by assuming a guessed temperature (linear) profile for the solid bed. The solution of the freeboard model (freeboard temperature) was used to solve the bed model to obtain the

new bed temperature profile. This bed temperature was used for solving the freeboard model. Thus, bed temperature profile was used as a boundary condition to solve the freeboard model. Similarly, freeboard temperature profile was used as a boundary condition in the bed model. The other boundary condition for freeboard and bed model was convective and radiative losses from kiln shell [in absence of secondary shell, Equation (3.32)]. For configuration with a secondary shell the boundary condition was modified to convective and radiative heat losses from insulation [Equation (3.31)]. The initial conditions to the freeboard model were mass and temperature of air exiting from the cooler. The air entering the annular space between the kiln and the secondary shell was assumed to be at 300 K. The mass and temperature of solids exiting from the calciner were used to specify the inlet conditions for the bed model. The modified Gear's method implemented in ODEPACK was used to solve the bed and freeboard model equations. The simultaneous solution of non-linear equations representing the energy balance across the cross section of the kiln (Equation 10 to Equation 16) was obtained using the Newton-Raphson method. This procedure was carried till the bed and freeboard temperature profiles along the kiln length are within ± 0.1 % on any further iteration. Typically 15-20 iterations were required for convergence.

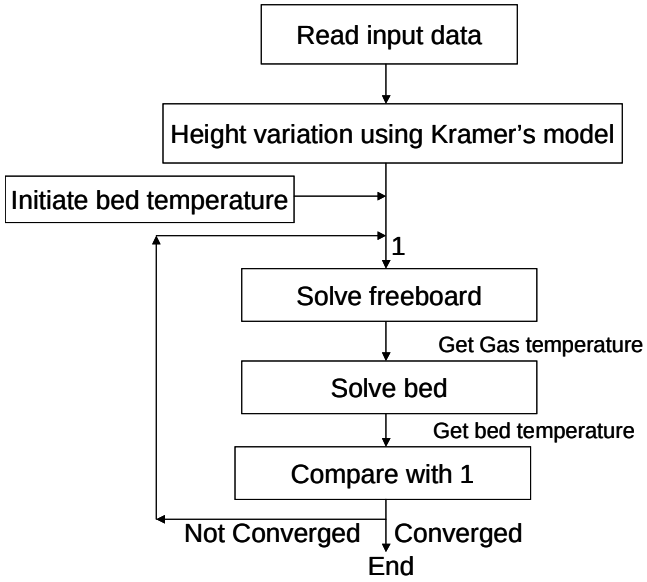

Figure 3.3: Solution Methodology

3.3 Results and Discussion

The computational model described in the previous section was initially used to understand the behavior of rotary cement kilns. Initially the bed model was validated with available

experimental data in published literature. Thereafter, the model was then used to simulate performance of 3 industrial kilns. After that the model was used to understand influence of key design and operating parameters on net energy consumption in kilns. In these simulations, secondary shell around kiln was not considered. The model was thereafter used to examine possibility of using a secondary shell to reduce energy consumption.

3.3.1 Validation of bed model

Watkinson and Brimacombe (1982) have carried out calcination experiments in a laboratory scale rotary kiln and have reported temperature profiles within the kiln. Availability of the experimentally measured temperature profile within the kiln makes this data set particularly useful to evaluate the one-dimensional model developed here. The experiments of Watkinson and Brimacombe (1982) were simulated by providing geometrical and operating conditions of their kiln as input data to the model (as specified in Table 3.3). The measured temperature profile of the free board region was specified as an input instead of solving the freeboard equations. Once the temperature profile for gas phase (in free board region) is known, the two-point boundary value problem reduces to a simple initial value problem and only model equations for bed were solved. The thermal properties of dusty gases i.e. emissivity and thermal conductivity used in the industrial kiln simulations were obtained at an average gas temperature of 1300 K. Gas emissivity for dust free gas was set to 0.1 from the charts reported by Gorog *et al.* (1981).

Table 3.3: Dimensions of kilns and operating conditions of kilns

Sr. No.	Variable	Pilot Kiln
1.	Length, m	5.5
2.	Inner refractory diameter, m	0.406
3.	Outer refractory diameter, m	0.59
4.	Outer shell diameter, m	0.61
5.	Coating thickness, m	-
6.	Speed of rotation, RPM	1.5
7.	Angle of tilt, degrees	1
8.	Solids flow in, kg/sec	0.013
9.	Gas temperature at burner end, K	1600
10.	Gas temperature at solid entry, K	800

Table 3.4: Physical properties used for lime kiln simulations

Sr. No.	Variable	Pilot Kiln
1.	Bed Density, kg/m^3	1680$^{\#}$
2.	Bed Heat capacity, KJ/ kg K	0.8$^{\$}$
3.	Bed emissivity	0.9
4.	Wall emissivity	0.9
5.	Bed Thermal conductivity, W/m K	0.69$^{\#}$
6.	Refractory thermal conductivity, W/m K	0.4$^{\#}$
7.	Gas heat capacity,	$(0.106\ T_G + 1173)^{!}$
8.	Gas Viscosity	$(0.1672\times10^{-5}\sqrt{T_G} - 1.058\times10^{-5})^{!}$

*Perry (1984); $^{\#}$Barr *et al.* (1989); $^{+}$Mastorakos *et al.* (1999); $^{\$}$Martin, (1932)

$^{!}$Guo *et al.* (2003) ;

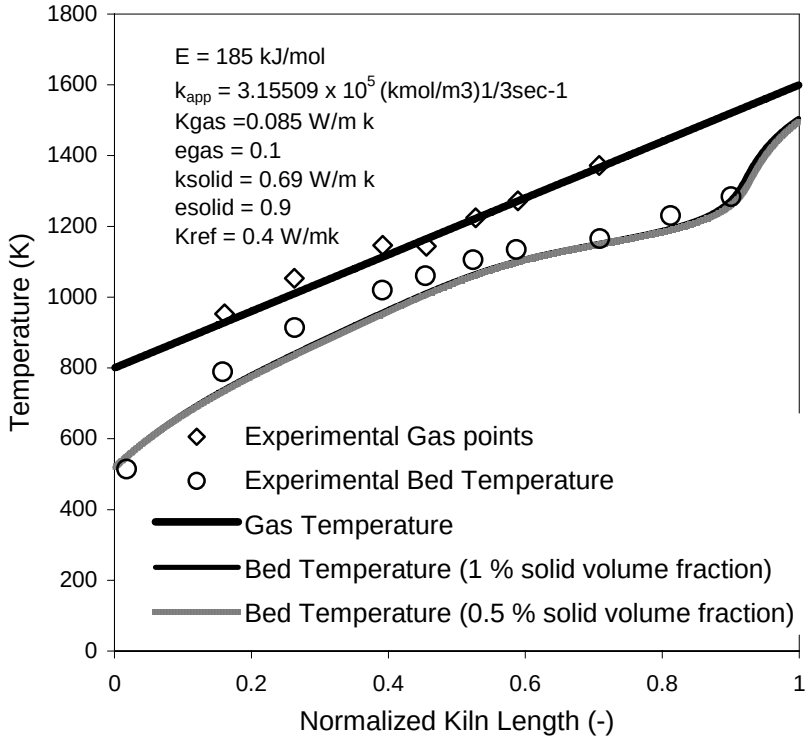

Figure 3.4: Comparison of experimental and simulated results for bed temperature

In this case, there is only one adjustable parameter (since the freeboard temperature profile is known): volume fraction of solids in the freeboard. The value of solids volume fraction was

initially set to 1 %. The kinetic models listed in Table 3.1 were incorporated in the present model to simulate experiments of Watkinson and Brimacombe (1982).

With kinetic parameters reported by Rao *et al.* (1989), the sensitivity of the predicted bed temperature profile was examined for different values of solids volume fraction in freeboard region. These results are shown in Figure 3.4. It can be seen that the predicted temperature profiles are insensitive to the exact values of solids volume fractions within the expected range. Therefore values of solid volume fraction was set to 1 % for rest of the simulations. The model was thus able to simulate the experiments of Watkinson and Brimacombe (1982) reasonably well. The model was then used to simulate performance of industrial cement kilns.

3.3.2 Simulations of rotary cement kilns

Rotary cement kiln operations involve very high temperatures, which restricts sampling of data inside the kiln during the kiln operations. The computational model can be used to gain some insight into complex processes occurring within cement kilns. For this purpose, the model was used to simulate typical industrial cement kilns. Three different industrial kilns were selected for simulations. Details of these three kilns are specified in Table 3.5. It can be seen that the selected kilns cover a reasonable range of kiln dimensions, production capacity and operational parameters like rotational speed, fill ratio and angle of tilt. Appropriate input data for carrying out simulations of industrial cement kilns are however not readily available.

The practical difficulties in sampling inside the industrial kilns restricts for available data only at the pre-heater entrance and clinker cooler exit. The temperature and mass fractions at the kiln inlet are however, required to specify the initial conditions to the model. A direct way to obtain these initial conditions would be actual measurements. In absence of such data, in the present work, the conditions at the kiln entrance were calculated by specifying appropriate degree of calcination occurring in calciner. In order to identify appropriate degree of calcination at the kiln entrance, the over all energy balance on the calciner and kiln was solved for different degrees of calcinations. Knowledge of air temperature at the kiln outlet (at the solids entrance end) then enabled us to select the appropriate value of calcination. The mass fractions and temperature of solids and air entering the kiln are given in Table 3.7. These were used as the initial conditions to the model

Table 3.5: Dimensions of kilns and operating conditions of kilns

Sr. No.	Variable	Industrial Kiln 1	Industrial Kiln 2	Industrial Kiln 3
1.	Length, m	50	60	68
2.	Inner refractory diameter, m	3.4	3.6	4.0
3.	Outer refractory diameter, m	3.8	4	4.4
4.	Outer shell diameter, m	3.85	4.084	4.456
5.	Coating thickness, m	0.13	0.144	0.16
6.	Speed of rotation, RPM	5.5	3.3	3.5
7.	Angle of tilt, degrees	2	3.5	2
8.	Solids flow in, kg/s	38.88	50.78	48.12
9.	Height at solid entry, m	0.46	0.57	0.7
10	Gas Flow rate kg/s	17	18.26	16.72
11.	Gas temperature at burner end, K	1373	1373	1373
12.	Coal Fr, kg/s	1.25	1.33	1.46
13.	Char	0.58	0.55	0.58
14.	Volatiles	0.27	0.35	0.27
15.	Ash Content	0.15	0.1	0.15
16.	Calorific value, kcal/kg coal (kJ/kg coal)	5800 (2.436×10^4)	7000 (2.94×10^4)	5000 (2.1×10^4)
17	Coal Particle size, microns	50	50	50

Table 3.6: Physical properties used for cement kiln simulations

Sr. No.	Variable	Value
1.	Bed Density, kg/m^3	1046
2.	Bed Heat capacity, kJ/ kg K	1.088
3.	Bed emissivity	0.9
4.	Wall emissivity	0.9
5.	Kiln shell emissivity	0.78
6.	Secondary shell emissivity	0.35
7.	Bed Thermal conductivity, W/m K	0.5
8.	Refractory thermal conductivity, W/m K	4.0^
9.	Gas heat capacity (J/kg K)	(0.106 T_G + 1173)
10.	Gas Viscosity (kg/m/s)	$(0.1672\times10^{-5}\sqrt{T_G}-1.058\times10^{-5})$

^ http://www.vrwrefractories.com/cement-industry.html

Table 3.7: Model assumptions/predictions and comparison with industrial data

Sr. No		Industrial Kiln 1 (67 % Calcination in calciner)		Industrial Kiln 2 (60 % Calcination in calciner)		Industrial Kiln 3 (71 % Calcination in calciner)	
		Data	Model	Data	Model	Data	Model
Model inputs at solid entrance							
1.	Mass fraction $CaCO_3$	-	0.340	-	0.398	-	0.305
2.	Mass fraction CaO	-	0.396	-	0.335	-	0.418
3.	Mass fraction SiO_2	-	0.179	-	0.185	-	0.190
4.	Mass fraction Al_2O_3	-	0.0425	-	0.041	-	0.043
5.	Mass fraction Fe_2O_3	-	0.0425	-	0.041	-	0.043
6.	Temperature of solids, K	-	1123	-	1250	-	1025

The simulations of these cement kilns were carried out based on the model discussed in the previous section. The angle of repose for solids was set to 0.71 radians based on experimental data reported by Henein *et al.* (1983) for calcineous materials. The thermal properties of gases i.e. emissivity and thermal conductivity were obtained at an average gas temperature of 1750 K. Gas emissivity for dust free gas was set to 0.4 at conditions prevailing in the kiln from the charts reported by Gorog *et al.* (1983) The convective heat transfer coefficient for calculating heat losses was specified to 30 W/m^2 K based on work of Mastorakos *et al. (1999)* Typical profiles of mass fraction and temperature obtained from simulations for industrial kiln 1 are shown in Figures 3.5a, 3.5b and 3.5c respectively. For all these figures abscissa of 0 denotes the position at which solids enter the kiln and abscissa of 1 indicates the solid exit i.e. the burner end. Figure 3.5a shows the mass fractions of solids in the bed along the kiln length. After the solids enter the kiln, calcination reaction and formation of C_2S take place. This is followed by C_3A and C_4AF formation. Solids start melting after traveling about 75 % of kiln length. The amount of melt starts increasing beyond the point where bed temperature crosses the solidus temperature reaches a maximum and then decreases thereafter. The mass fraction profiles for the freeboard region are shown in Figure 3.5b. It can be seen from this figure that the volatiles concentration in gas phase increases as one move away from the burner end due to coal devolatilization. Thereafter gas phase combustion starts. Hence H_2O concentration in freeboard region increases to about half of the kiln length. Both coal combustion and gas phase combustion gets completed in half a kiln length. CO_2 concentration in the freeboard region near the bed entrance increases due to calcination reaction in the bed region. The predicted temperature profiles of gas, bed walls and coating are shown in Figure 3.5c. Coating was formed around 25 % of kiln length from the solid exit end. The temperature of kiln shell decreases abruptly at the point from which coating formation occurs. This was due to additional resistance to heat transfer due to coating formation. Such sharp dips in shell temperature after coating formation (~200 ^{0}C) have been reported in literature for commercial cement kilns (Markatos and Koyefetis, 1995).

The predicted results thus, agree qualitatively with the previously reported results. The predicted results at the outlet of the kiln were compared quantitatively with the available plant data in Table 3.8. It can be seen that the model was also able to predict the overall performance of the industrial kilns satisfactorily.

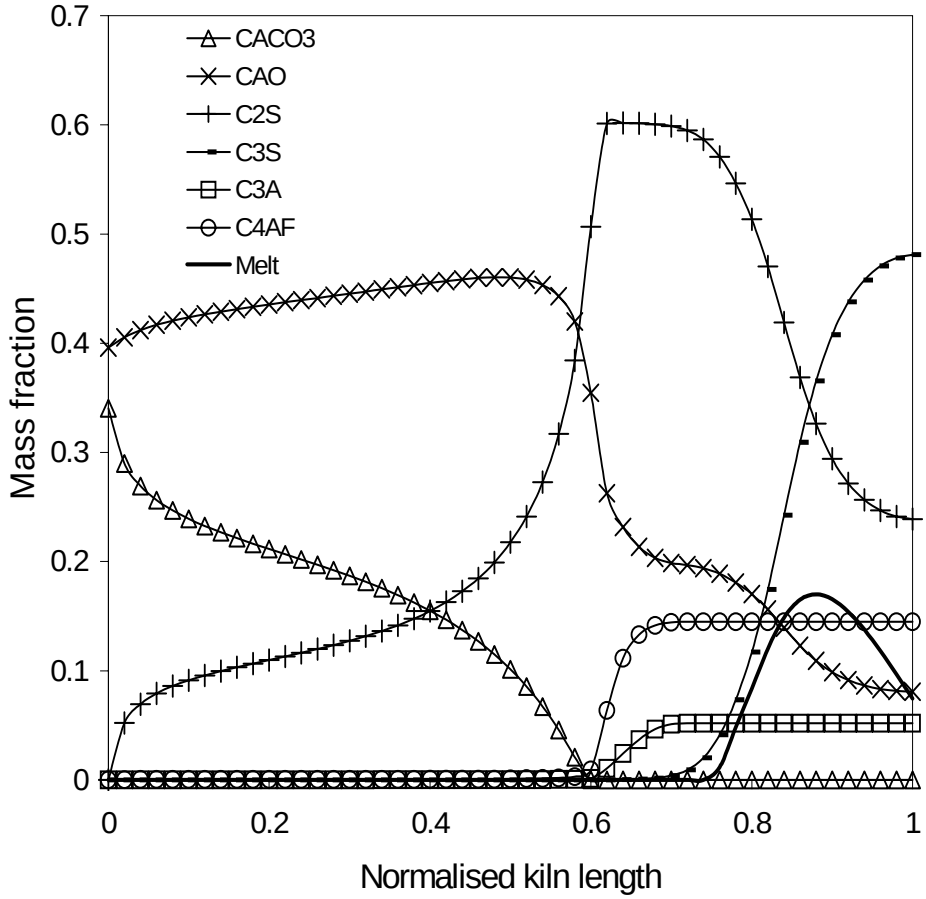

Figure 3.5a: Typical mass fractions in bed region

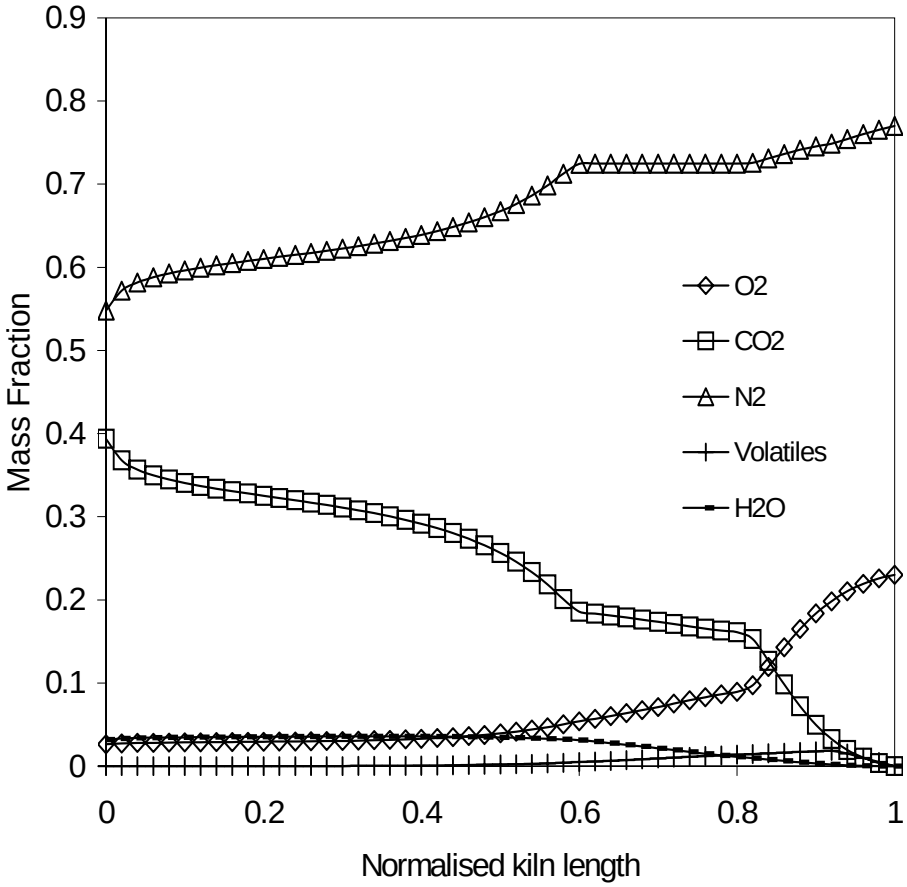

Figure 3.5b: Typical mass fractions in freeboard region

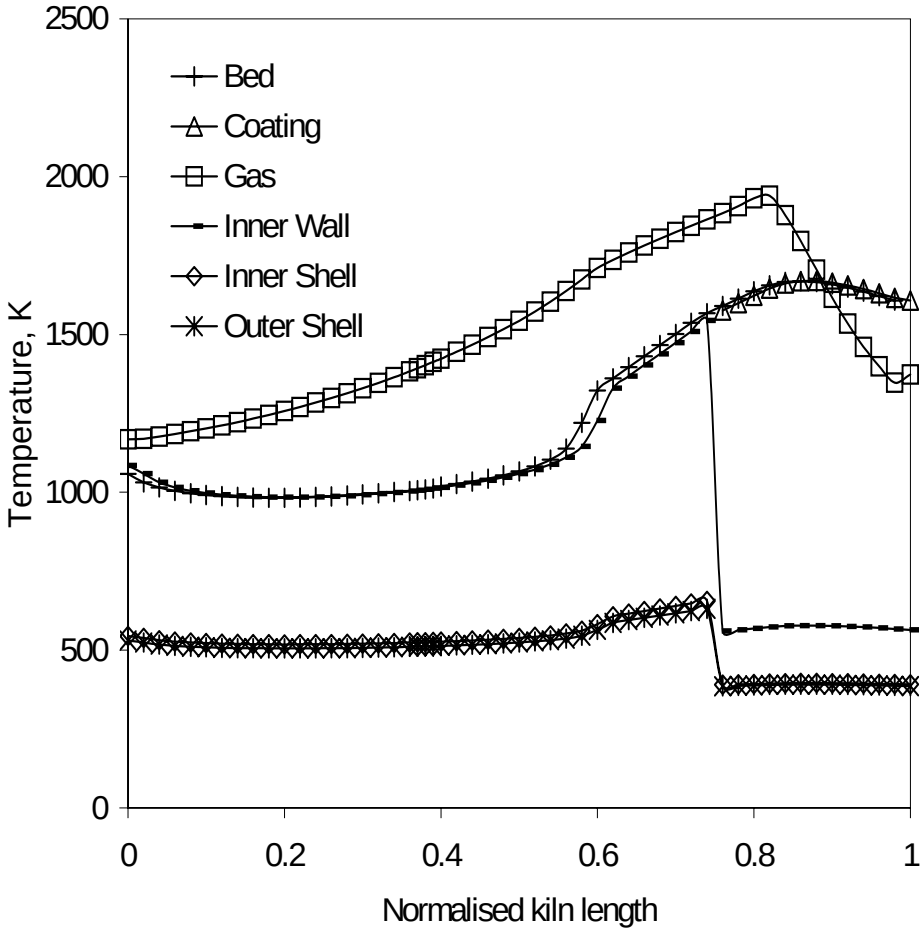

Figure 3.5c: Temperature profiles for industrial kiln1

Table 3.8: Comparison of model equations with industrial data

Sr. No		Industrial Kiln 1 (67 % Calcination in calciner)		Industrial Kiln 2 (60 % Calcination in calciner)		Industrial Kiln 3 (71 % Calcination in calciner)	
Model predictions and industrial data at solids exit		Data	Model	Data	Model	Data	Model
7.	Mass Fraction C_3S	0.483	0.481	0.508	0.487	0.5	0.489
8.	Mass Fraction C_2S	0.239	0.238	0.257	0.277	0.269	0.263
9.	Mass Fraction C_3A	0.051	0.052	0.048	0.052	0.042	0.052
10.	Mass Fraction C_4AF	0.143	0.146	0.152	0.144	0.142	0.147
11.	Mass Fraction CaO	0.084	0.083	0.035	0.04	0.047	0.049
12.	Temperature of solids, K	1673	1608	1673	1636	1573	1600

3.3.3 Influence of key design and operating parameters

The model was then used to understand influence of key design and operating parameters of the rotary cement kiln. Influences of kiln rotational speed and kiln tilt on the predicted outlet composition of C_3S are shown in Figures 3.6a and 3.6b respectively. It can be seen that as the rotational speed increases, the residence time of solids decreases and hence the outlet mass fraction of C_3S decreases. As angle of tilt decreases residence time of solids increases and therefore the outlet mass fraction of C_3S increases. The predictions of model for residence time of solids in the kiln are consistent with published results (Liu and Specht, 2006; Li *et al.*, 2002). Predicted residence time of solids for all these cases are shown in these figures. It should be also noted that the developed model could be used to study the effect of varying different operating conditions simultaneously, in order to find optimum operation condition. For example, the effect of varying kiln tilt and rpm simultaneously on the performance of kiln can be predicted using the developed computational model. The simulated results were used to quantify performance of the rotary cement kilns.

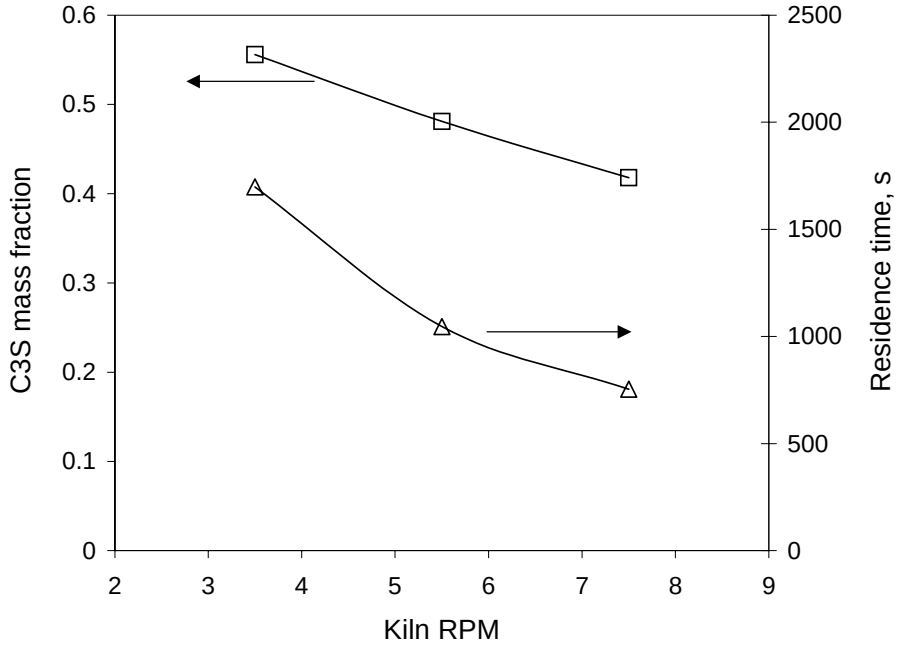

Figure 3.6a: Influence of rotational speed on kiln performance (kiln tilt = 2^0)

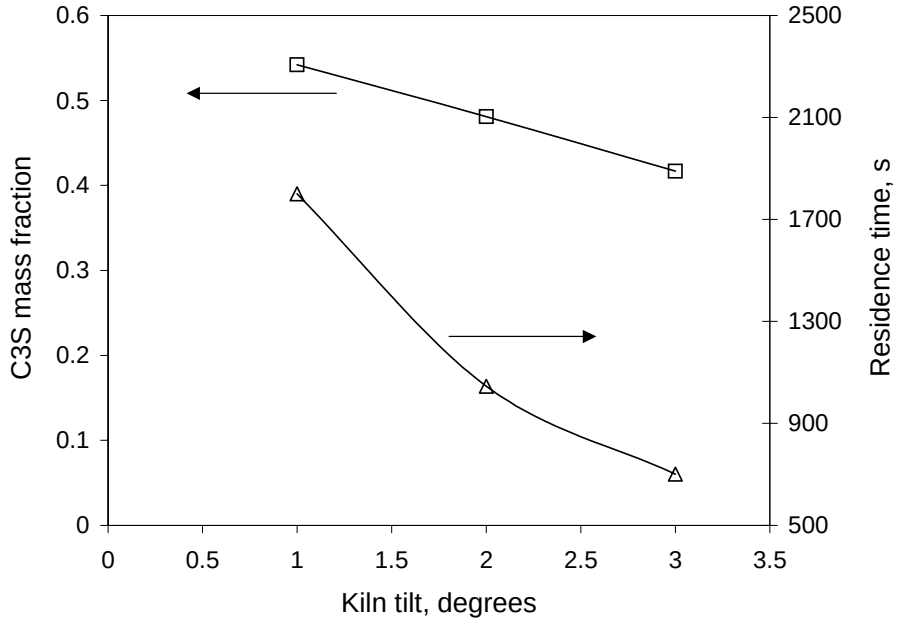

Figure 3.6b: Influence of angle of tilt on kiln performance (kiln rpm = 5.5)

3.3.4 Energy consumption in rotary cement kilns

The kiln performance was characterized in terms of net energy consumption per unit weight of product (clinker coming out of the kiln) for the same (within ± 1%) product composition. The net energy consumption was calculated as (See Figure 3.7):

$$\text{Net energy consumption} = (E_{COAL} + E_{G,IN} + E_{S,IN}) - (E_{G,OUT} + E_{S,OUT}) \quad (3.51)$$

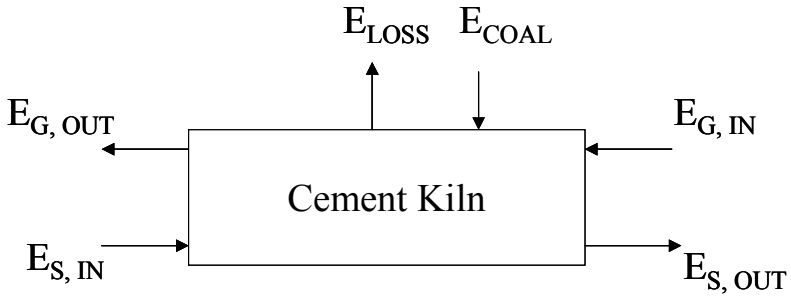

Figure 3.7: Energy consumption in cement kilns

E_{COAL} is the energy given by coal combustion per unit product. Other terms denote energy flow rates (subscripts IN or OUT) for the gas and solid streams (subscripts G or S) per unit weight of product. Influence of mass flow rate of solids on net energy consumptions was studied. For these simulations, mass flow rate of fed air was changed proportional to the solids mass flow rate. The mass flow rate of coal was then adjusted to get the same product composition of solids (within ± 1%) at the kiln outlet. The predicted results in the form of net energy consumption and percentage fill for different solids flow rates are shown in Figure 3.8a. As expected, as solids flow rate increases, the percent fill at kiln entrance increases. It can be seen that the net energy consumption per unit weight of product decreases as solids flow rate increases. This is because the net energy loss from the kiln does not increase proportional to the solids mass flow rate. Thus it is beneficial from the point of view of energy consumption to operate kiln with higher solids flow rate. Other operational concerns like increase in dusting and mixing however need to be considered while identifying maximum solids flow rate for any specific rotary cement kiln. The studies of flow, mixing and heat transfer in transverse plane (for example, Khakhar *et al.,* 1997 and references cited therein) are useful to understand issues related to such operational concerns.

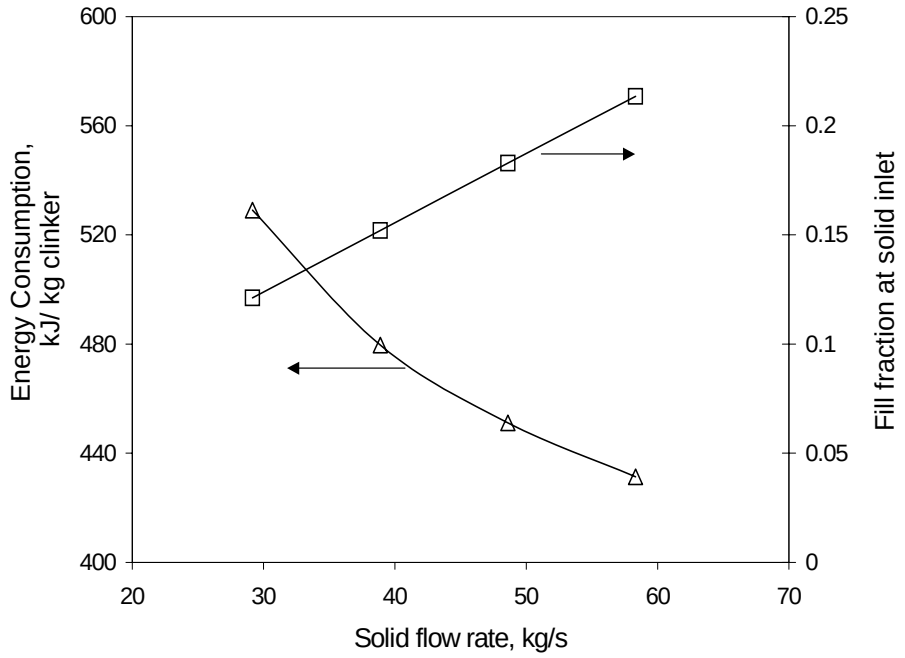

Figure 3.8a: Effect of solid feed rate on net energy consumption in rotary kilns

Influence of kiln rotational speed and extent of excess oxygen over stoichiometric requirement on net energy consumption were also studied. The effect of kiln rotational speed on the performance of kiln is shown in Figure 3.8b. It can be seen that as kiln RPM decreases, the net energy consumption decreases. As the kiln RPM decreases the residence time of solids in the kiln increases. For a fixed outlet composition the energy required to raise temperature of solids to reaction temperature and energy required for clinker reactions is more or less fixed. The heat losses also do not change significantly as RPM is changed. However, since solid spends more time in the kiln resolidification of melt is more in kilns rotated at lower RPM's. Hence overall energy required for solid melting is less in kilns operated at lower RPM. Thus, as long as adequate mixing of solids is taking place, it is beneficial to operate the kiln at lower RPM. The simulations of excess oxygen indicated that (not shown here for the sake of brevity), it is beneficial to operate the kiln with a slight excess of oxygen (~1-4 %). Use of excess oxygen beyond 4 % leads to slight increase in the net energy consumption per kg of clinker. Thus the model can be used for steering the design and operation towards minimizing energy consumption per kg of clinker.

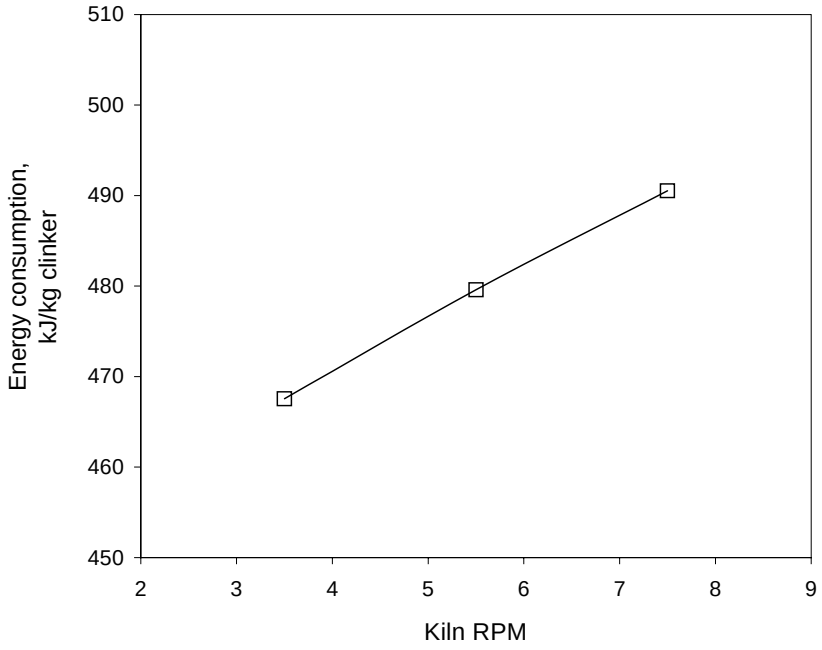

Figure 3.8b: Effect of RPM on net energy consumption in rotary kilns

The computational model developed in this work was also used to explore some unconventional means to reduce energy consumption in kilns. For these simulations freeboard model equations were not solved. Instead a temperature profile was assumed for the gas phase and model equations for bed were solved (See section 3.1). The motivation of this study was to explore for kiln energetics by possibly manipulating temperature profiles in the freeboard region. The shape of the gas profile was assumed to be same as shown in Figure 3.9. This shape seems to be consistent with industrial observations and published results. The position of maximum temperature was varied from 0.2 times kiln length to 0.8 times kiln length. The value of maximum temperature at these positions was adjusted in such a way that solids composition at the kiln outlet is same for all the cases. While carrying out these simulations, the gas inlet temperature was coupled with the solids outlet temperature by assuming a clinker cooling efficiency, η, as:

$$m_G C_{pG}\left(T_{G,in} - 300\right) = \eta\, m_B C_p T_{B,out} \qquad (27)$$

where m is mass flow rate, C_p is heat capacity, η is the cooler efficiency and T is temperature. Subscripts G, B, in and out denotes gas, solids, inlet and outlet respectively. The temperature

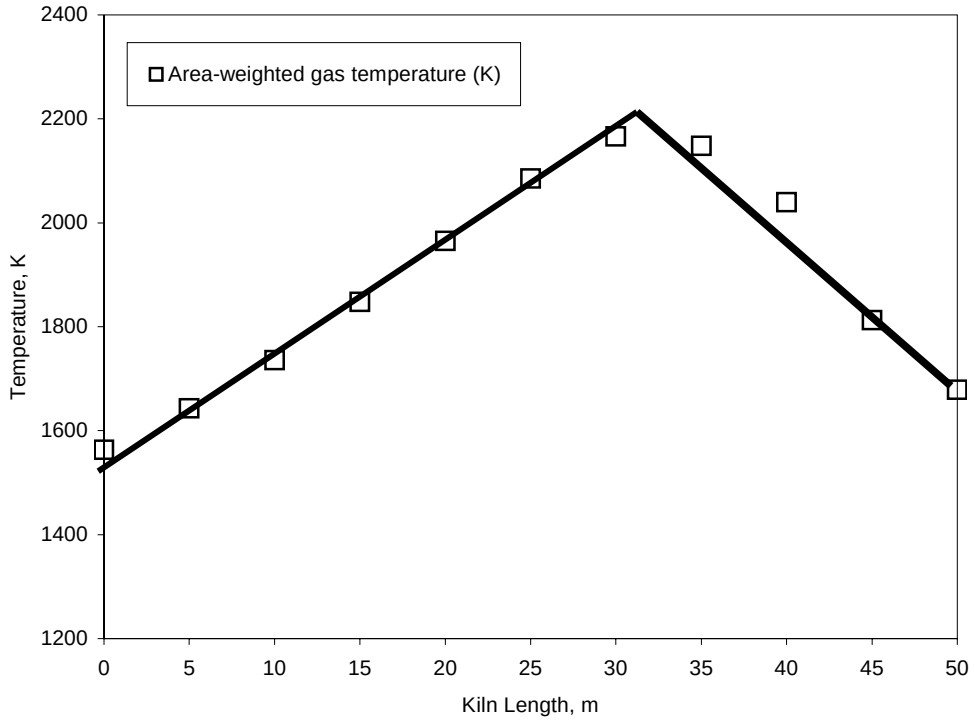

Figure 3.9: Gas temperature profiles in freeboard region

of the gases leaving the kiln from the solid entrance was calculated by solving overall energy balance on the kiln. Following procedure was use to simulate performance of a kiln.

The coal flow rate to the kiln (energy supplied to kiln in the form of coal, E_{coal}) and the maximum flame position were set to specific values. For these simulations the value of E_{coal} was fixed. Assuming the entrance and exit gas temperatures, the magnitude of the maximum flame temperature was adjusted to get same (within ± 1 %) solids composition at the kiln outlet. The inlet gas temperature was recalculated based on overall energy balance and simulations were carried out with this new value of gas inlet temperature. This procedure was continued till the inlet gas temperature did not change by ± 1 % of the previous value. Once inlet gas temperature converged, outlet gas temperature was calculated based on overall energy balance on the kiln. The value of gas outlet temperature was compared with the initially assumed value and the whole procedure was repeated till the exit gas temperature also did not change by ± 1 % of the previous value. Simulations to study effect of changing position of maximum flame temperature were carried out for different values of E_{coal}. The simulated results are discussed in the following.

Typical predicted results for the net energy consumption in the kiln for varying position of maximum flame temperature are shown in Figure 3.10. Corresponding numbers for net energy consumption in kilns and position of coating formation with respect to maximum flame position are tabulated in Table 3.9. As the maximum flame position moves towards the solid inlet, coating formation takes place earlier in the kiln (See Table 3.9). Since coating is formed early in the kiln, heat losses from the kiln are reduced due to additional resistance of coating for heat transfer. The energy required by solids for clinker reactions and melt formation remain more or less same. Therefore, as the maximum flame position moves towards the solid inlet the net energy consumption in the kiln decreases. The computational model and the results presented here will be useful to guide further work on modeling of burner/ free board region and to re-design temperature profiles within the kiln to minimize energy consumption. However, other concerns including possible operational difficulties need to be investigated further in order to identify optimum yet practicable model of operation for rotary cement kiln.

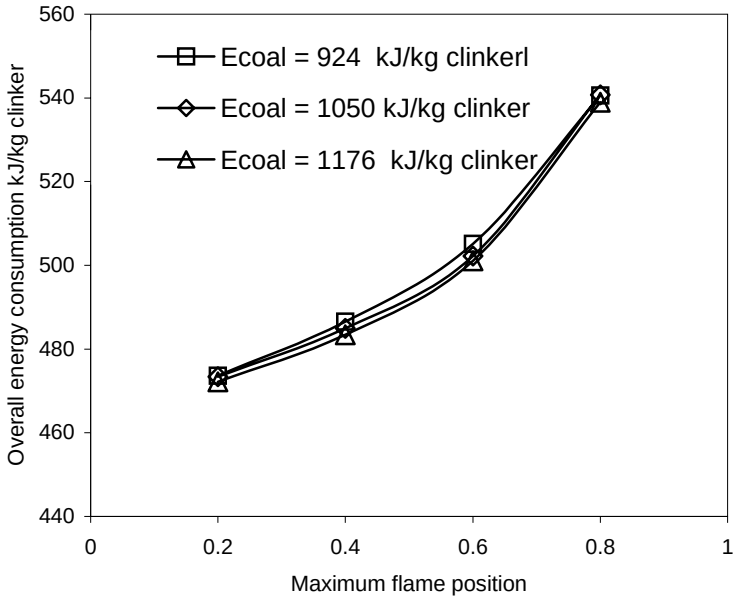

Figure 3.10: Energy consumption in industrial kiln 1 for varying flame position

Table 3.9: Total energy consumption for industrial kiln 1 (kJ/kg clinker)

Maximum Flame Temperature Position	Occurrence of melt in kiln (Normalised from solid end)	Ecoal = 924 kJ/ Kg clinker	Ecoal = 1050 kJ/ kg clinker	Ecoal = 1176 kJ/ kg clinker
0.2	0.52	473.59	473.39	472.15
0.4	0.58	486.52	484.92	483.37
0.6	0.66	505.09	502.19	501.08
0.8	0.77	540.56	540.74	538.94

3.3.5 Use of a secondary shell

Energy savings per kg of clinker by manipulating key parameters as discussed above are possible to a rather limited extent (savings of about ~ 40 kJ/kg of clinker). There is however a significant potential to reduce net energy consumption by using a secondary shell having low surface emissivity and thermal conductivity around the kiln as proposed by Engin and Ari (2005). The secondary shell could be covered with some insulating material to further reduce heat losses. It should however be noted that reduction in losses from the kiln shell would significantly increase temperature of kiln walls. Engin and Ari (2005) have not discussed this issue in their paper. It is therefore essential to devise some way to ensure that the kiln shell temperature does not rise beyond the acceptable limit. In this work, we propose to achieve this by feeding air to the annular space between the kiln shell and the secondary shell. The computational model was used to simulate performance of rotary kilns with secondary shell. Simulations were carried out for the two values of gap between kiln shell and the secondary shell: 0.1 m and 0.2 m. It was observed that the kiln shell temperatures are mainly controlled by the mass flow rate of air. The simulated results of the gap of 0.1 m are shown in Figure 3.11. For these simulations the thickness of secondary shell used was 0.025 m (same as kiln shell), thickness of insulation and thermal conductivity of insulation were set to 0.1 m and 0.05 W/m K respectively (Engin and Ari, 2005)

In absence of a secondary shell, the net energy loss to the surrounding was ~ 150 kJ/kg clinker. With secondary shell and no gaseous stream in annular gap, this loss reduced to ~ 10 kJ/kg clinker. However, at such conditions, the temperature of kiln shell increases beyond 1000 K (see Figure 3.11). Operating cement kilns at such high shell temperatures is not possible. It is therefore essential to reduce the kiln shell temperature by feeding gaseous

stream. As the mass flow rate of air increases, the temperature of kiln shell decreases. It can be seen that the air mass flow rate of about 30 kg/s or more was required to bring the maximum temperature below 650 K. As the mass flow rate of air increases, the extent of energy recovery increases. It is however important to note that though the extent of energy recovered increases with the mass flow rate of air through the gap, the quality (outlet temperature) of the recovered energy decreases (see Figure 3.12). Appropriate balance of extent of recovery and the outlet temperature of hot air stream from the gap needs to strike to enhance the overall performance.

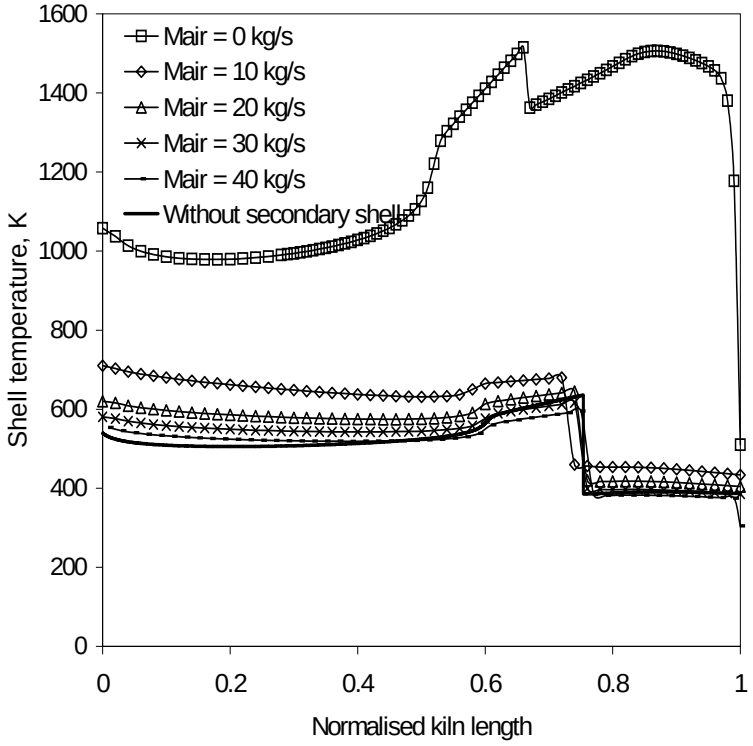

Figure 3.11: Predicted profiles of temperature of kiln shell with secondary shell

If the recovered energy (at temperatures of about 200^0 C) can be utilized within the cement plant (refrigeration, drying of fly ash and so on), the use of secondary shell appears to be promising for reducing net energy consumption.

The models and results presented here can be used to understand the kiln performance and to possibly design appropriate secondary shell to reduce energy consumption. The

computational models can also be used to develop a rotary cement kiln simulator for training and for optimization.

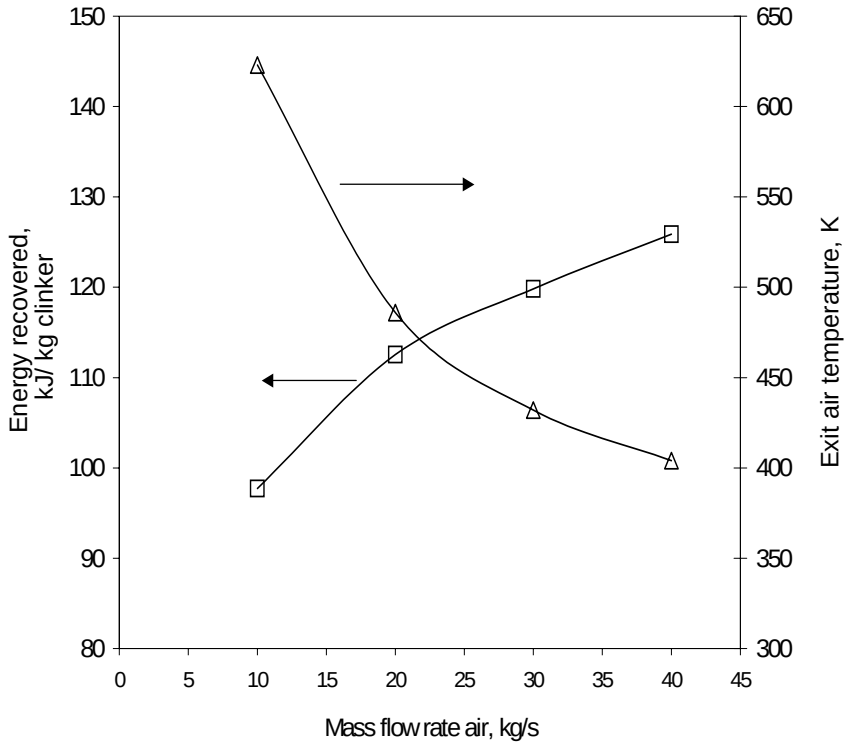

Figure 3.12: Magnitude and quality of recover energy with the secondary shell

3.4 Conclusions

A comprehensive framework based on one-dimensional models was developed to simulate complex processes occurring in rotary cement kilns. Models for simulating reactions and heat transfer in the bed region and coal combustion and heat transfer in the freeboard region were developed. Melting of solids and coating formation within the kiln was accounted. Coal combustion in freeboard region was modeled by considering devolatilisation, gas phase combustion and char reaction.

The model was used to simulate performance of three industrial kilns. The model predictions agreed reasonably with the available plant data. The model was also able to capture influence of key design and operating parameters on kiln performance. The model was used to evaluate possible ways of enhancing performance of rotary cement kilns. The simulations indicated

that the operation of kiln with higher solid loading and lower RPM is favorable from the point of view of energy consumption per kg of clinker. The use of a secondary shell with air stream passing through the gap between the kiln shell and the secondary shell appears to be a promising method to reduce energy consumption in rotary cement kilns. It is possible to recover ~ 80 % of the energy lost to the surroundings (typically 150 kJ/kg clinker) by judicious choice of secondary shell and air flow rate without degrading the quality of recovered energy significantly.

4. Applications of Reaction Engineering based Models to clinker Manufacture

Abstract

This chapter presents an integrated reaction engineering based mathematical model for clinker formation in cement industry. Separate models for pre-heater, calciner, and cooler were initially developed. The model for pre-heater cyclones was formulated by assuming solids and gas to be completely back mixed. The heat transfer coefficient between particle laden gas and walls cyclones was calculated using empirical correlation. The model for calciner was formulated based on Eulerian-Lagrangian approach. The coal particles and raw meal particles were considered as discrete phases and gas phase was assumed to be completely back mixed. Clinker cooler was modeled by assuming solids and gas in plug flow. The heat transfer between solids and air in clinker cooler was predicted via empirical correlations. The individual models were validated wherever possible. The models for pre-heater, calciner, kiln (developed in previous chapter) and cooler were coupled with each other via mass and energy communication through common boundaries to develop a coupled simulator which was solved iteratively. The iterations were continued till the temperature of solids and gases at exit of individual modules converged within error of one percent. The model predictions agree well with the observations and experience from cement industry. Several ways for reducing energy consumption were computationally investigated which provide insights about influence of operating conditions on energetics of cement plant. An easy to use, graphical user interface (GUI) based software called RoCKS (Rotary Cement Kiln Simulator) was developed based on the integrated modules of pre-heater, calciner, kiln and cooler. The integrated model, the developed software RoCKS (for Rotary Cement Kiln Simulator) and results presented here will be useful for enhancing our understanding and for enhancing the performance of clinker manufacturing

Publication based on this work

- ***Kaustubh S. Mujumdar**, Ganesh K.V., Sarita B. Kulkarni and Vivek V. Ranade, "Rotary Cement Kiln Simulator (RoCKS): Integrated Modeling of Pre-heater, Calciner, Kiln and Clinker Cooler", Chemical Engineering Science, 62, 2007, 2590-2607.*

4.1 Introduction

In the previous chapters of this thesis, reaction engineering based computational model for cement kilns was developed. It was shown that such models not only helped in developing better understanding for cement kilns but also provided some useful clues for reducing energy consumption. However, as described in chapter 1, in a clinker manufacturing process, the pre-heater, calciner, kiln and cooler are strongly coupled with each other. The input to rotary kilns in terms of mass fraction and composition can vary if operating conditions in calciner or cooler are varied. Therefore, the utilization of the model developed for the kiln would be rather restricted if it is not coupled with computational models for pre-heater, calciner, and cooler. It is therefore essential to develop an integrated model for pre-heater, calciner, kiln and cooler in order to capture key characteristics of clinker manufacturing and to enable the model to be used as simulation or optimization tool. Such an attempt is made in this chapter. The motivation of the present work was to develop a reliable frame work of reaction engineering based computational model for cement industry and use this model subsequently for possible exploration of performance enhancement. Based on this integrated model a simple graphical user interface based software called RoCKS (Rotary Cement Kiln Simulator) was also developed. The overall organization of this chapter is briefed below.

The key issues that needs to be considered while developing individual models are discussed initially in section 4.2. The computational model and the modeling strategy are thereafter presented in section 4.3. Section 4.4 reports the results of computational simulations of integrated model with respect to key operating parameters. Thereafter the computational model was utilized to gain insights about cement plant energetics via numerical experiments. Key findings of the study are summarized at the end.

4.2 Key Issues and Modeling Approach

Various processes occurring in pre-heater, calciner, kiln and cooler need to be adequately considered while developing computational model for cement plant. Key issues governing the performance of individual units are schematically shown in Figure 4.1. Initially the key issues of individual equipments and review the previous work related to it are discussed to provide background for the model developed in this work.

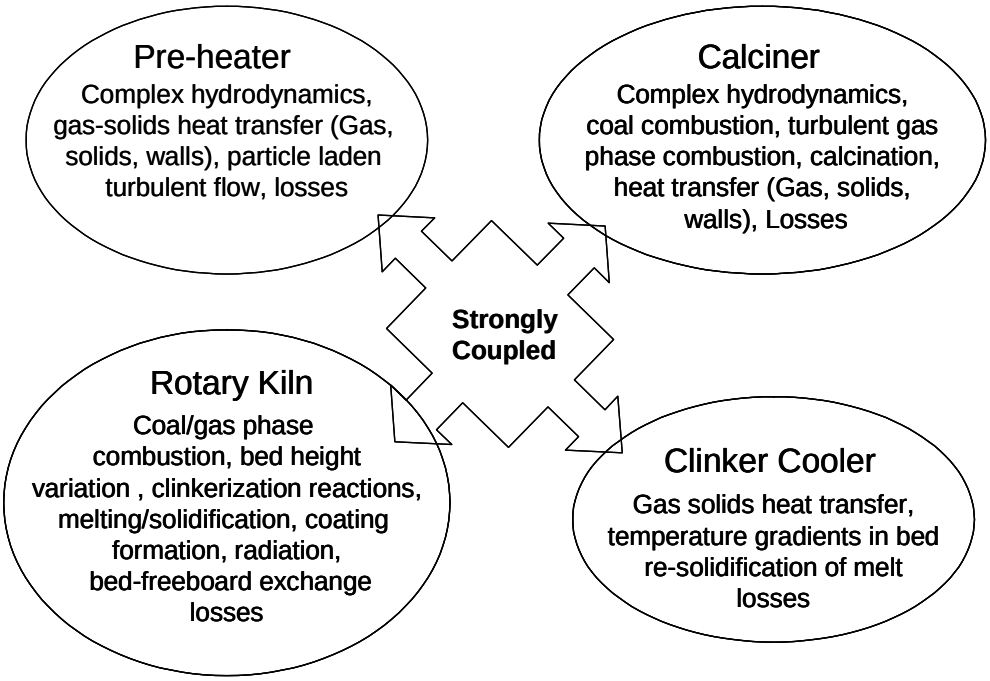

Figure 4.1: Key issues in modeling cement plant

4.2.1 Cyclone preheaters

The calcineous raw meal is passed through a set of pre-heater cyclones (depending on pre-heater assembly) before it is sent to the calciner. In the pre-heater section, the raw meal is pre-heated to around calcination temperature by hot gases coming from the calciner. The operation of cement pre-heater is similar to that of a conventional cyclone. Solids are fed to the cyclone along with the gas coming from the previous pre-heater. Both solid and gas spiral down towards the cyclone bottom where the gas reverses its direction and leaves through the exit duct while the solids leave from the bottom to the next unit. The flow inside the cyclone is characterized by high swirl and turbulent motion. This provides excellent heat transfer between gas and solids. We used computational fluid dynamics (CFD) based model for studying mixing and heat transfer of gas solid flows in cyclones. Our CFD simulations (carried out for typical values of operating conditions as gas flow rate = 60.83 kg/s; solid flow rate = 50 kg/s; inlet gas temperature = 740 K; inlet solid temperature = 500 K; cyclone diameter = 6 m; height of cyclone = 11 m) indicated that the solid and gas temperatures inside the cyclone were quite uniform (in range of 637 K and 644 K) and close to exit temperatures (average temperature of 640 K). Therefore, in this work, each pre-heater cyclone was treated as completely mixed cell for individual phases and was therefore represented by a pair of temperature (one for gas phase and the other for solid phase). The

heat losses from cyclone are controlled by the heat flux across the cyclone walls. Therefore it is essential to predict the heat transfer between particle laden gas and cyclone walls in the pre-heater cyclone. The empirical relation proposed by Gupta and Nag (2000) was used to determine these losses.

4.2.2 Calciner

The operation of calciner is also like a conventional cyclone. The last cyclone in the preheater assembly generally acts as a calciner. Therefore some of the key issues that mathematical model needs to capture in calciners (for example, hydrodynamics and heat transfer between particle laden gas and walls) are essentially same as that in the preheaters. Therefore we assume gas phase to be completely back mixed and empirical correlation to model heat transfer from particle laden gas to cyclone walls. The main difficulty in modeling cyclone calciner is to estimate the residence time of raw meal in the cyclone. Few empirical correlations have been proposed to predict the average residence time of particles in cyclones (Kang *et al.*, 1989; Lede *et al.*, 1987). However all the attempts for prediction of residence time in cyclones were for lab scale cyclones and non of the studies were reported for industrial scale cyclones. Moreover, the proposed empirical correlation works only for their own experimental data and do not work if applied to other system. Due to unavailability of any information for particle residence time in the cyclones as a first approximation this parameter was treated as adjustable parameter in the model. The raw meal residence time in the calciner was adjusted to get the desired degree of calcination the calciner.

Other than this, it is also essential to obtain relevant kinetics for calcination reaction in calciner. Thermal decomposition of limestone calcination is a complex process. Predicting kinetics of calcination reaction has been subject of an extensive research over the years. However, still there is no reliable consensus on the calcination kinetics. It is well established that the overall reaction rate is function of the following three rate processes, 1) heat transfer (to the surface and then to the reaction zone) through the particle 2) mass transfer (both internal and external to the surface) and 3) chemical reaction at the interface of undecomposed particle and product. Relative rates of these three transport processes depend on particle size, particle morphology and operating conditions and varies with varying operating conditions. Hence, a wide discrepancy is observed in the proposed rates for calcination reaction. It was also reported that the proposed models fit adequately their own experimental data. However, when they are applied to other results most of them fail (Khinast

et al., 1996). As shown in Chapter 3 in this thesis, we have compared models proposed by about 18 investigators on available experimental data. The data reported in experiments of Watkinson and Brimacombe (1982) was chosen for this study. Watkinson and Brimacombe (1982) have reported experimental data on calcination of limestone in experimental kiln. The experimental conditions of their experiments were close to industrial operations (bed temperature ~ 1000 to 1300 K) and therefore were used to find calcinations kinetics in this work.

4.2.3 Rotary kiln

The partially calcined raw meal is passed slowly to rotary kiln where the clinkerization reactions occur. In the initial part of the kiln remaining calcination occurs. Other solid-solid and solid –liquid clinkerization reactions take place as solid bed moves towards the burner. Part of the solids melts in the kiln. The melt formation causes an internal coating on kiln refractories. Counter current flow of gas entrains solid particles in the free board region. Such entrainment enhances rates of radiative heat transfer by increasing effective emissivity and conductivity. In a nutshell, the main key issues for modeling rotary cement kilns are estimating residence time of solids in the kiln, cinkerization reaction in bed region, coal combustion in freeboard region, heat transfer between bed freeboard and walls, melting/coating formation around the kiln walls. These issues were discussed in detail in Chapter 3 and therefore are not repeated here.

4.2.4 Clinker cooler

The hot solids from the kiln are discharged on the grate of clinker cooler. As the grate moves with uniform speed along the cooler length, solids lose their heat to cross flow air. A part of air is generally sent to the kiln as secondary air, a part to calciner as tertiary air and part is lost to the surroundings (vent air). The most important key issue in modeling grate coolers is predicting the heat transfer coefficient between hot solids and cross flow air. Unfortunately there is no information on modeling of heat transfer in such cases. In absence of any relevant information we have used heat transfer correlation in packed bed reactors to estimate the heat transfer. Nsofor and Adebiyi (2001) have carried experimental measurements and presented correlation for forced convection gas particle heat transfer coefficient at high temperatures (200 C to 1000 C). Since the temperatures in clinker cooler are in the same range this correlation was used to model heat transfer coefficient between solids and gas. The heat

transfer coefficient was coupled with an efficiency factor which was adjusted to match the temperatures of secondary and tertiary and coming out of cooler.

The key issues for preheater, calciner, kiln and cooler presented in the above section suggests that in order to develop a reliable computational models for cement industry it is required to incorporate all the above-mentioned processes occurring in preheater, calciner, kiln and cooler. Moreover, appropriate algorithms methodologies need to be developed for coupling of individual models. Such an attempt is made here. The motivation of the present work was to predict various processes occurring in preheaters, calciner, kiln and clinker cooler simultaneously in a single framework. The various physical processes considered during development of the model are discussed in the following section.

4.3 Computational Models and Solution Methodology

Individual sub models for pre-heater, calciner, and cooler are discussed in the following section.

4.3.1 Pre-heater model

A schematic of pre-heater unit considered for developing computational model is shown in Figure 4.2. The present framework of computational models was developed for dry process of clinker formation since this process is widely used in cement industry.

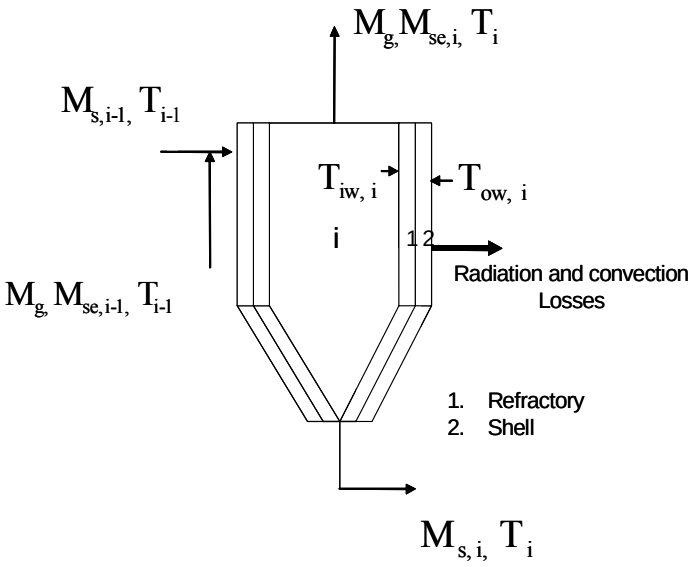

Figure 4.2: Schematic of Pre-heater

For the dry processes, the moisture content is generally present in very small amount [typically ~ 0.5%, see for example Engin and Ari (2005), Peray (1986)]. The energy requirements for removing the moisture from the feed being small (less than 0.5% of the total energy consumption), the feed was considered to be free of moisture in this work. However, the developed framework is quite general and including evaporation of moisture from the feed is straightforward.

In Figure 4.2, $M_{s,}$ is the mass of solids entering the cyclone. M_g is the mass of the air entering the cyclone. M_{se} is the mass of solids entrained from a cyclone. $T_{iw,\,i}$ and $T_{ow,\,i}$ represent the inner and outer wall temperature for the i^{th} cyclone. Each cyclone was assumed to be lined with refractory of thickness t_r

Thus, for any i^{th} cyclone in pre heater assembly following are the inlet streams

1. Solids from the $(i-1)^{th}$ cyclone ($M_{s,\,i-1}$ at temperature T_{i-1}).
2. Solids that are entrained by gas from $(i+1)^{th}$ cyclone ($M_{se,\,i+1}$ at temperature T_{i+1}).
3. Air from $(i+1)^{th}$ cyclone (M_g at temperature T_{i+1}).

The outlet streams for this cyclone are:

1. Solids going out of cyclone ($M_{s,\,i}$ at temperature T_i).
2. Solids that are entrained by gas ($M_{se,i}$ at temperature T_i).
3. Air going out (M_g at temperature T_{i+1}).

The steady state material balance equation for i^{th} cyclone was written as

$$M_{s,i-1} + M_{se,i+1} = M_{s,i} + M_{se,i} \qquad (4.1)$$

$$M_{se,i} = (1-\eta_{m,\,p}) \times M_{s,i} \qquad (4.2)$$

In the above equations $\eta_{m,\,p}$ represents the mass efficiency of the i^{th} cyclone. M represents the mass of the solids (in kg/s) and subscripts s and se represent solids and entrained solids respectively as explained earlier.

The steady state energy balance for the i^{th} cyclone was written as

$$\begin{aligned} M_{s,i-1} \times C_{p,s} \times T_{s,i-1} + M_{se,i+1} \times C_{p,s} \times T_{c,i+1} + M_g \times C_{pg} \times T_{c,i+1} = M_{s,i} \times C_{p,s} \times T_{c,i} + M_{se,i} \times C_{p,s} \times T_{c,i} \\ + M_g \times C_{p,g} \times T_{c,i} + h_{cyc} \times A_{cyi} \times \left[T_{c,i} - T_{iw,i}\right] \end{aligned} \qquad (4.3)$$

In the above equations $C_{p,s}$ and $C_{p,g}$ represents the specific heat of solids and air respectively. Subscript g represents the air and T_c represents the temperature of solids and air in the i^{th} cyclone. h_{cyc} represents the heat transfer coefficient for energy exchange between particle

laden gas and cyclone inner walls. h_{cyc} was evaluated from empirical correlation given by Gupta and Nag., (2000) for heat transfer in cyclones given by

$$\frac{h_{cyc} d_c}{k_g} = 702.818 + 9.0287 \times 10^{-14} u_o \,\mathrm{Re} + 11.1385 \left(\frac{\Delta P}{u^2{}_o}\right) + 4.50398 \times 10^{-5} \left(\frac{\Delta P}{u_o}\right) \mathrm{Re} + R_c$$

Where $$R_c = \sigma F_{p-w} \left(\frac{T^4{}_{iw} - T^4{}_g}{T_{iw} - T_g} \right) \frac{d_c}{k_g} \qquad (4.4)$$

The term $\eta_{h,p}$ is an adjustable parameter (1 in the present simulations) that is provided in the model which can be used to fine tune the model to fit it with industrial data. A_{cyi} (m^2) is the internal surface area of the cyclone. The LHS of Equation (4.3) thus represents the total heat entering the cyclone and RHS represents the heat leaving out of the cyclone. At steady state the energy given to cyclone walls must be same as heat conduction in through refractory and cyclone walls, which is equal to loss from shell walls due to convection and radiation. The energy balance for heat transfer in cyclone cross section was written as:

$$\mathrm{h}_{\mathrm{cyc}} \cdot A_{cyi} \cdot \left[T_{c,i} - T_{iw,i} \right] = \frac{2 \cdot \pi \cdot L \cdot k_r \cdot \left[T_{iw,i} - T_{r,i} \right]}{\ln\left(\frac{\mathrm{r_r}}{\mathrm{r_i}} \right)} \qquad (4.5)$$

$$\frac{2 \cdot \pi \cdot L \cdot k_r \cdot \left[T_{iw,i} - T_{r,i} \right]}{\ln\left(\frac{\mathrm{r_r}}{\mathrm{r_i}} \right)} = \frac{2 \cdot \pi \cdot L \cdot k_{sh} \cdot \left[T_{r,i} - T_{ow,i} \right]}{\ln\left(\frac{\mathrm{r_0}}{\mathrm{r_r}} \right)} \qquad (4.6)$$

$$\frac{2 \cdot \pi \cdot L \cdot k_{sh} \cdot \left[T_{r,i} - T_{ow,i} \right]}{\ln\left(\frac{\mathrm{r_0}}{\mathrm{r_r}} \right)} = \mathrm{h}_{\mathrm{conv}} \cdot A_{cyo} \cdot \left[T_{ow,i} - T_0 \right] + \sigma \cdot \varepsilon_{cy} \cdot A_{cyo} \cdot \left[T_{ow,i}{}^4 - T_0{}^4 \right] \qquad (4.7)$$

In the above equations, $T_{iw,\,i}$ represents the internal wall temperature of the i^{th} cyclone, $T_{r,i}$ represents the temperature of interface of refractory and shell, $T_{ow,\,i}$ represents the temperature of external wall of the i^{th} cyclone and T_0 represents the ambient temperature. L represents the total height the cyclone, k_r represents the thermal conductivity of the refractory and k_s represents the thermal conductivity of cyclone walls. r_0 represents the external diameter, r_r represents the internal diameter of the shell and r_i represents the cyclone internal

diameter. A_{cyo} represents the external surface area of the cyclone. h_{conv} represents the convective heat transfer coefficient of external wall (taken as 30 W/m^2K as presented in Chapter 3), ε_c is the emmissivity of the cyclone outer wall and σ is the Stefan-Boltzman constant for radiative heat transfer.

The above material and energy balances were written for n cyclones. For each cyclone there are 6 equations and 6 unknown variables. Therefore for n cyclones there are $6 \times n$ variables number of variables and $6 \times n$ equations. These set of non linear algebraic equations were solved using Newton-Rapson method to get mass and temperature of solids, gas and walls walls for preheater cyclones

It was essential to test the framework of models developed for pre-heaters at least qualitatively before implementing it in the integrated model. To do this the developed computational model for pre-heater cyclones was used to predict the temperatures and energy losses for two different scenarios. The first test case considered 3 cyclones in pre-heater assembly, while, in the second test case 4 cyclones were considered in the pre-heater assembly. All the cyclones considered in the present study were of identical dimensions (Internal diameter 3 m; External diameter 3.05 m; height 5 m). Calcineous raw meal flow rate to first cyclone was set to 50 kg/s at a temperature of 300 K and air flow rate from the calciner was set to 50 kg/s at temperature of 1100 K. for both the test cases. The flow rates and temperatures of air and raw meal fed to cyclones was obtained from industrial data. The efficiency of each cyclone (i.e. mass collected from cyclone bottom to mass fed) was assumed to be 99.99 % from experimental measurements of Gupta and Nag (2000). Gupta and Nag (2000) have also reported empirical correlation heat transfer coefficient for particle-laden gas in cyclones. This correlation was used to calculate heat transfer coefficient between particle laden gas and cyclone walls. Two pre-heater units comprising four and three cyclones were simulated. The predicted results are shown in Figure 4.3a and 4.3b and are summarized in Table 4.1.

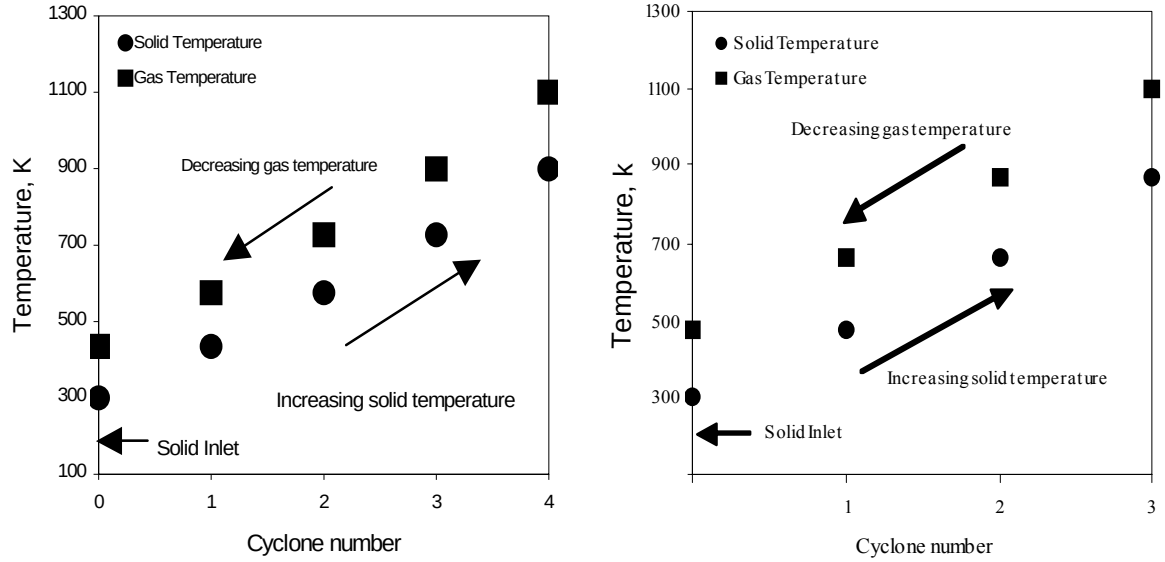

(a) 4 cyclone case (b) 3 cyclone case

Figure 4.3: Predicted results for the pre-heater units

Table 4.1: Predicted cyclone temperatures and loss

	Four Cyclone Case		Three Cyclone Case	
Cyclone	Temperature, K (Solid and gas at exit)	Loss (kW)	Temperature, K (Solid and gas at exit)	Loss (kW)
1	434	283.81	479	383
2	574	606.50	666	833
3	726	992.95	869	1389
4	898	1475.55	-	-

It can be seen from Figure 4.3 and Table 4.1 that with an additional cyclone in the assembly, there is more heat exchange between solids and gas i.e. outlet temperature of solid from the last cyclone increases while outlet gas temperature decreases. Thus, the temperature of solids coming out of pre-heater assembly considering 4 cyclones is more than one considering 3 cyclones, which seems to be reasonable. However, a 3 cyclone assembly has about 25% lower losses due to lower surface area. The model can thus be used to evaluate alternative pre-heater configurations for different pre-heater assemblies.

4.3.2 Calciner model

The mathematical model of calciner was based on a schematic shown in Figure 4.4. The following assumptions were made:

1. Gas phase is completely back mixed.
2. The raw meal and coal particles were treated as discrete phases having uniform particle size. All the particles were assumed to have the same residence time in calciner.

The mass and energy balance equations are presented below.

4.3.2.1 Discrete phase

Coal particles

Mass balance for coal particles in calciner was written as:

$$\frac{dm_{p,c}}{d\theta} = -A_o \cdot f_{v,o} \cdot m_{pc,o} - k_{s1} \cdot e^{\frac{-E_1}{RT_c}_c} A_p \cdot p_{O2}. \qquad (4.8)$$

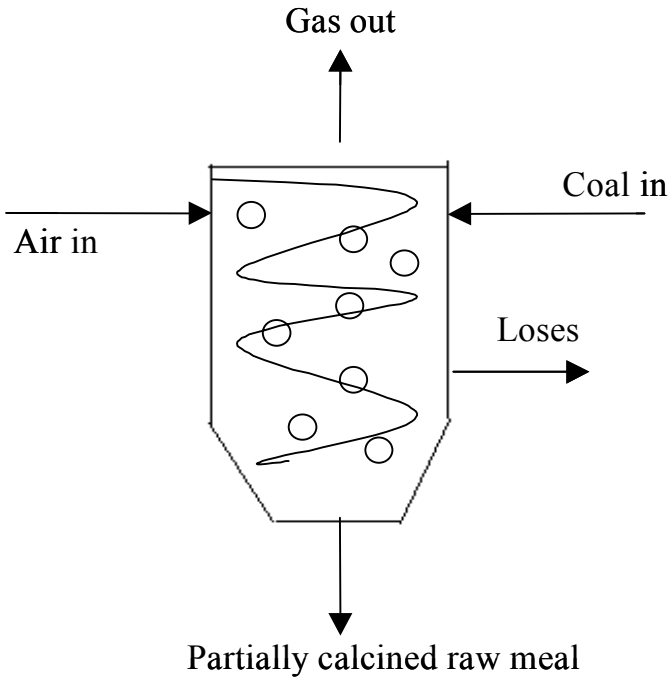

Figure 4.4: Schematic of cyclone calciner

In the above equation, A_0 is the devolatilization constant, $fv_{,0}$ is the initial mass fraction of volatiles in coal particle and the $m_{pc,0}$ is the initial mass of coal particle ,k_{s1} is the rate constant of char (1 kg/m^2-s-kPa, Hamor et al., 1973) , ^cA_p is the available surface area of particle, E_1 is the energy of activation (6.81E4, Hamor et al., 1973) and p_{o2} is the partial pressure of O_2 . θ is time spent by a coal particle in calciner. The first term in the RHS of above equation represents the loss in discrete phase mass due to devolatilization of coal particles and the second term in the RHS of above equation represents the loss in discrete phase due to char reaction

The individual species balance for rate of mass change due to devolatilization is given by,

$$\frac{d(m_{p,v})}{d\theta} = -A_o \cdot f_{v,o} \cdot m_{pc,o} \tag{4.9}$$

Where, $m_{p,v}$ is the mass of volatiles in coal particle.

The individual species balance for rate of mass change due to char combustion is given by

$$\frac{d(m_{p,char})}{d\theta} = -k_{s1} \cdot e^{\frac{-E_1}{RTc}} \cdot {}^cA_p \cdot p_{O2} \tag{4.10}$$

where $m_{p,char}$ is the mass of char.

The energy balance for a coal particle is given by

$$\frac{dm_{p,c}C_{p,c}T_c}{d\theta} = {}^ch_{conv} \cdot {}^cA_p \cdot (T_g - T_c) + \sigma \cdot \varepsilon_c \cdot {}^cA_p \cdot (T_g{}^4 - T_c{}^4) + f_c \cdot \Delta H_{comb} \cdot r_{comb} + C_{p,c}.T_c.\frac{dm_{p,c}}{d\theta} \tag{4.11}$$

In the above equation $C_{p,c}$ is the specific heat of coal and T_C is the coal temperature. Coal was assumed to enter the kiln at 300 K. T_{gout} is the gas temperature. ΔH_{comb} is the heat released due to coal combustion and f_h is the fraction of energy released due to coal combustion, which is absorbed by the particle. This factor was set to 0.3 following the recommendation of Boyd and Kent (1986). The first and second terms in RHS of above equations are the energy absorbed by the coal particle due to convection and radiation from the gas phase during the heat up. The heat transfer coefficient, h_c, is evaluated using the correlation of Ranz and Marshall (1952) as:

$$\frac{h_c d_p}{k_g} = 2 + 0.6(\mathrm{Re})^{0.5}(\mathrm{Pr})^{0.33} \qquad \text{(Re up to } 10^4\text{; Pr>=0.7)} \qquad (4.12)$$

The final term in Equation (4.11) represents the loss of energy from coal particle due to loss of mass.

Raw meal particle

The calcination reaction is given as

$$CaCO_3 \rightarrow CaO + CO_2 \qquad (4.13)$$

The over all mass balance for the raw meal particle is given by,

$$\frac{d^L m_p}{d\tau} = -r_{calc} \cdot \frac{Mw_{co_2}}{Mw_{caco_3}} \qquad (4.14)$$

where

$$r_{calc} = {}^r k_s \cdot \; e^{\frac{-E_2}{RTp}} \cdot 4 \cdot \pi \cdot r_p{}^2 \cdot Mw_{caco_3} \qquad (4.15)$$

where, the ${}^L m_p$, $Mw_{co2,}$ Mw_{caco3} are mass of raw meal particle, molecular weight's of carbon dioxide calcium carbonate respectively is the rate of calcination of calcium carbonate. r_{calc} is the rate of calcination of calcium carbonate, r_p radius of shrinking raw meal particle respectively. The term ${}^r k_s$ is the rate constant of calcination of calcium carbonate of calcination. It has been well established that presence of CO_2 in gas phase inhibits calcination rate (Stanmore and Gilot, 2005). However, the nature of function in which the rate is affected is again a subject of disagreement. In this work we use a simple linear form of relationship to model effect of presence of CO_2 on rate of calcination reaction as

$$r_{calc} = {}^r k_s' \cdot \; e^{\frac{-E_2}{RTp}} \cdot 4 \cdot \pi \cdot r_p{}^2 \cdot Mw_{caco_3} \qquad (4.16)$$

where

$$\begin{aligned} {}^r k_s' &= {}^r k_s && \mathrm{P}_{CO_2} < 10^{-2} P_{eq} \\ {}^r k_s' &= {}^r k_s \left(\frac{\mathrm{P}_{\mathrm{CO}_2} - P_{eq}}{P_{eq}} \right) && 10^{-2} P_{eq} < \mathrm{P}_{CO_2} < P_{eq} \end{aligned} \qquad (4.17)$$

$$\text{and } P_{eq} = 1.826 \times 10^7 e^{(\frac{-19680}{T})} \qquad (4.18)$$

The individual species balances for limestone and calcium oxide are given as,

$$\frac{d\,{}^{L}m_{CaCO3}}{d\tau} = -r_{calc} \tag{4.19}$$

$$\frac{d\,{}^{L}m_{CaO}}{d\tau} = \frac{r_{calc}.Mw_{cao}}{Mw_{CaCO3}} \tag{4.20}$$

The energy balance for the raw meal particle is given as,

$$\frac{d({}^{L}m_{p}C_{p,s}T_{p})}{d\tau} = {}^{L}h_{conv}\cdot{}^{L}A_{p}\cdot(T_{g}-T_{p}) + \sigma\cdot\varepsilon_{L}\cdot{}^{L}A_{p}\cdot(T_{g}{}^{4}-T_{p}{}^{4}) + C_{p,s}T_{p}\frac{d\,{}^{L}m_{p}}{d\tau} \tag{4.21}$$

where, T_p is the temperature of raw meal, ε_L is the emissivity of solid particle, ${}^{L}A_p$ is the area of the raw meal particle and τ is residence time of raw meal particle in the calciner. ${}^{L}h_{conv}$ was estimated as per Equation (4.12)

4.3.2.2 Continuous phase

The over all gas mass balance is given as,

$$\frac{dm_{g}}{dt} = m_{gin} - m_{gout} + [{}^{c}m_{pin} - {}^{c}m_{pout}]\cdot{}^{c}N_{p} + [{}^{L}m_{pin} - {}^{L}m_{pout}]\cdot{}^{L}N_{p} \tag{4.22}$$

where, m_g is the mass of the air, ${}^{c}N_p$ is the number of particles of coal coming in per unit time and ${}^{L}N_p$ is the number of particles of raw meal coming in per unit time. The individual species mass balance for rate of change of mass of oxygen, carbon dioxide, volatile matters and water can be written as:

$$\frac{dy_{o_2}}{dt} = \frac{1}{m_g}(m_{g,in}\cdot y_{o_2in} - m_{g,out}\cdot y_{o_2out} - \frac{[m_{p,c}\cdot y_{c,cin} - m_{p,c}\cdot y_{c,cout}]\cdot{}^{c}N_{p}\cdot Mw_{o_2}}{Mw_{char}} - (\frac{r_{combg}}{Mw_{vol}})\cdot V_{react}\cdot Mw_{o2}\cdot Z_{O2} - y_{o_2}\cdot\frac{dm_{g}}{dt}) \tag{4.23}$$

$$\frac{dy_{CO_2}}{dt} = \frac{1}{m_g}(m_{gin}\cdot y_{CO_2in} - m_{gout}\cdot y_{CO_2out} + \frac{[m_{p,c}\cdot y_{c,cin} - m_{p,c}\cdot y_{c,cout}]\cdot{}^{c}N_{p}\cdot Mw_{CO2}}{Mw_{char}} + [m_{p,Lin} - m_{p,Lout}]\cdot{}^{L}N_{p} + (\frac{r_{combg}}{Mw_{vol}})\cdot V_{react}\cdot Mw_{CO2}\cdot Z_{CO_2} - y_{CO_2}\cdot\frac{dm_{g}}{dt}) \tag{4.24}$$

$$\frac{dy_v}{dt} = \frac{1}{m_g}(m_{g,in} \cdot y_{v,in} - m_{g,out} \cdot y_{v,out} \quad + \quad [m_{p,cin} \cdot y_v - m_{p,cout} \cdot y_v] \cdot {}^{c}N_p$$
$$-(\frac{r_{combg}}{Mw_{vol}}) \cdot V_{react} \cdot Mw_{vol} \cdot Z_{vol} - y_{vol} \cdot \frac{dm_g}{dt}) \qquad (4.25)$$

$$\frac{dy_w}{dt} = \frac{1}{m_g}(m_{gin} \cdot y_{win} - m_{gout} \cdot y_{wout} + (\frac{r_{combg}}{Mw_{vol}}) \cdot V_{react} \cdot Mw_w \cdot Z_{H_2O} - y_w \cdot \frac{dm_g}{dt}) \qquad (4.26)$$

where, y_{o2}, y_{co2}, y_v, y_w are the respective mass fractions of oxygen, carbon dioxide, volatile matters and water. Mw_{O2}, Mw_{CO2} , Mw_{vol} and Mw_w are their respective molecular weights. V_{react} is the volume of reactor. Subscripts in and out represent the inlet and outlet conditions and Z is the stoichiometric coefficient.

The energy balance equation for the gas phase is given as,

$$\frac{dm_g C_{p,g} T_g}{dt} = m_{gin} \cdot C_{p,g} \cdot T_{g,in} - m_{gout} \cdot C_{p,g} \cdot T_g + S_{gcomb} + S_{ccomb} + S_{calc}$$
$$- \mathrm{h}_{cyc} \cdot A_{cyi} \cdot (T_g - T_{iw}) \qquad (4.27)$$

Where,

$$S_{gcomb} = r_{combg} \cdot H_{combg} \cdot V_{react} \qquad (4.27a)$$

$$S_{ccomb} = -\int_0^{\theta_c} ({}^{c}h_{conv} \cdot {}^{c}A_{p0} \cdot (T_{gout} - T_c) + \sigma \cdot \varepsilon_c \cdot {}^{c}A_{p0} \cdot (T_{gout}{}^4 - T_c{}^4) + {}^{c}C_p . T_c \cdot \frac{d\,{}^{c}m_p}{d\theta}$$
$$-(1 - f_c) \cdot H_{comb} \cdot r_{comb}) \cdot d\theta \qquad (4.27b)$$

$$S_{calc} = -\int_0^{\tau_r} (h_{conv} \cdot {}^{L}A_{p0} \cdot (T_{g\,out} - T_L) + \sigma \cdot \varepsilon_L \cdot {}^{L}A_{p0} \cdot (T_{g\,out}{}^4 - T_L{}^4)$$
$$+ {}^{L}C_P T_L \frac{d\,{}^{L}m_p}{d\tau} - r_{calc} \cdot H_{calc}) \cdot d\tau \qquad (4.27.c)$$

In the above equations, S_{gcomb}, S_{ccomb} is the heat source term for gas-phase from volatile combustion and char combustion respectively. S_{calc} is the heat sink term from calcination. H_{combg}, H_{calc} are the enthalpies of volatile combustion and calcination. h_{cyc} is the convective

heat transfer coefficient of the particle laden gas. The steady state equations across the cyclone walls were written same as that of preheaters explained in the previous section to obtain temperature of calciner internal walls, refractory and outer walls .

An iterative method was developed to solve the calciner model equations. The model equations for gas phase were solved assuming steady state. For the first iteration, source terms from discrete phase were assumed to be zero. The temperature and mass of species obtained at calciner exit by solving continuous phase were used in discrete phase equations to get the new source terms from the discrete phase. The sources from the discrete phases were passed to continuous phase to get the new mass and temperature terms for discrete phase. This procedure was continued till the subsequent changes in temperature of gas phase were within ± 0.1 %. Suitable under-relaxation parameters were defined to accelerate convergence. Typically about 20 iterations were required to achieve convergence. The differential equations for discrete phase were solved by modified Gear's method implemented in ODEPACK (Hindmarsh, 1983). The algebraic equations for continuous phase were solved using Newton-Raphson method.

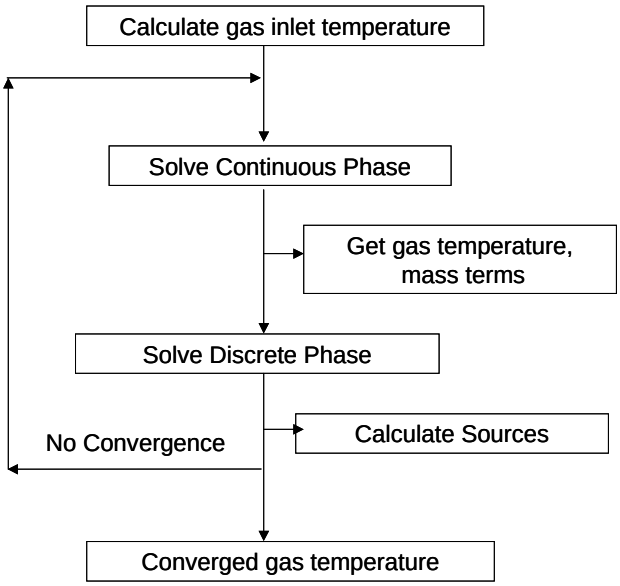

Figure 4.5: Solution Methodology

The computational model of the calciner was then further used to understand influence particle diameters and coal flow rates on calciner performance. Some of these results are discussed in the following. The mathematical model of calciner was evaluated by comparing predicted results with data obtained from ACC. The schematic of the calciner is shown in Figure 4.6 and details of input conditions provided are specified in Table 4.2. The data obtained from ACC unfortunately did not specify the calorific value of coal and actual amount of coal fed to the calciner. From the knowledge of total coal flow rate (which was specified), the coal fed to the calciner was taken to be proportional to the extent of calcination taking place in that calciner. Knowledge of residence time of solids in their calciner was also not available precisely. Simulations were therefore carried out over a range of calorific values of coal (4500 to 5200 kcal/kg coal) and of residence time of raw meal in the calciner (2-20 s). The results obtained from these simulations are shown in Figure 4.7.

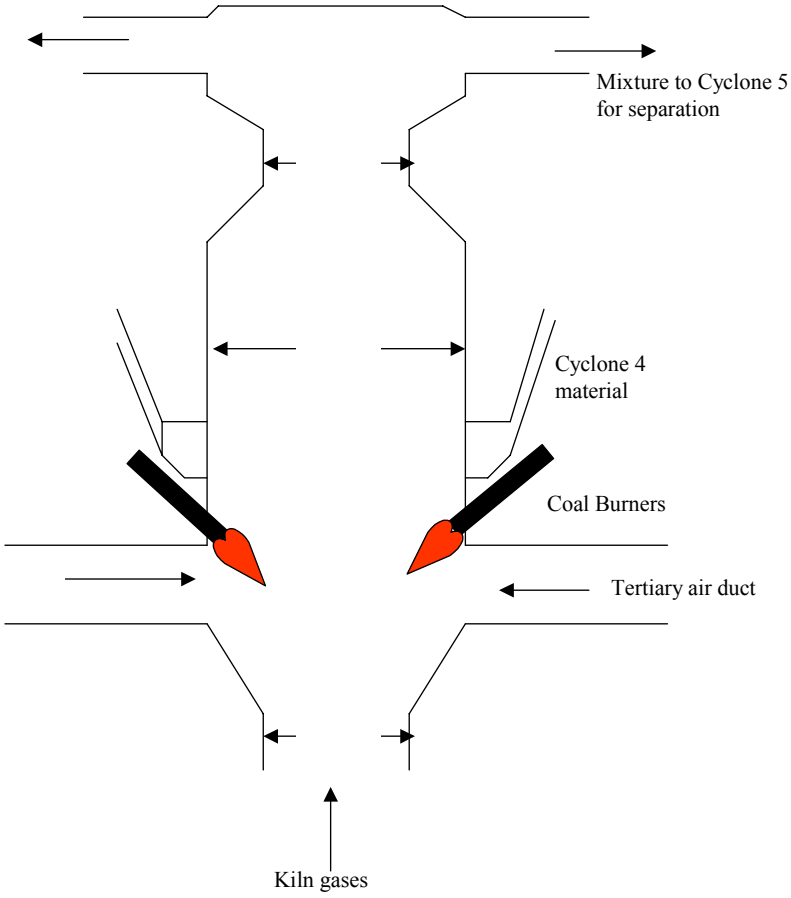

Figure 4.6: Schematic of Kymore line-1 calciner (from Anathraman, 2006, private communications)

Table 4.2: Data specified from Kymore line-1*

Sr. No.	Variable	Inlet	Outlet
1	Tertiary air mass flow rate, kg/s	39.33	-
2	Tertiary air temperature, K	1123	-
3	Kiln air mass flow rate, kg/s	27.33	-
4	Kiln air temperature, K	1293	-
5	Exit air mass flow rate, kg/s	-	79
6	Exit air temperature, K		1168
7	Raw meal mass flow rate, kg/s	63.05	52.5
8	Raw meal temperature, K	1073	1168
9	Coal flow rate, kg/s	5	
10	Mass fraction CaCO3	0.507	0.097
11	Mass fraction CaO	0.177	0.65

* - (52% Calcination of raw meal at Calciner inlet; 92 % Calcination of raw meal at Calciner outlet)

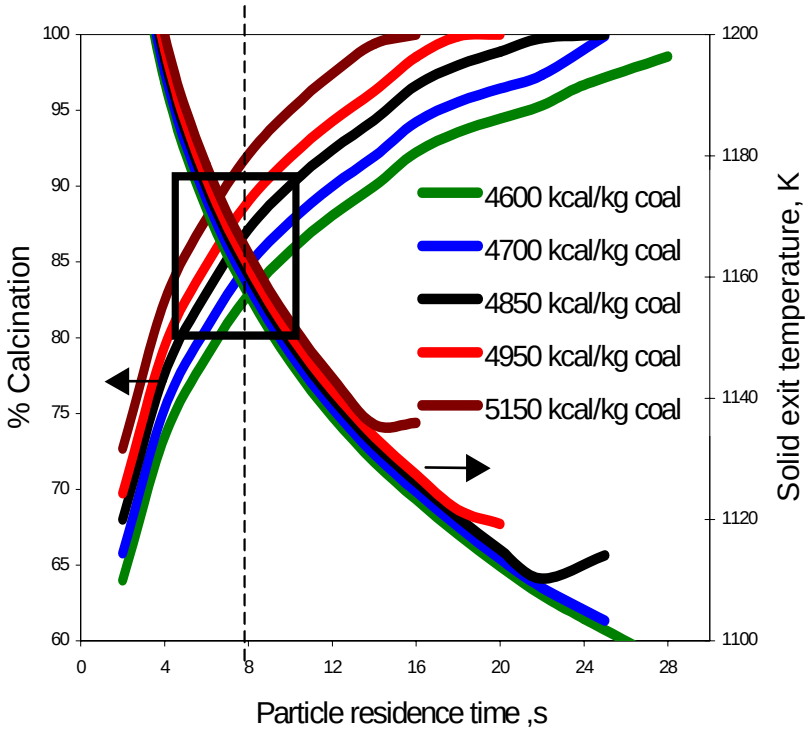

Figure 4.7: Simulation results for various coal calorific values and residence time of solids

The simulation results indicate that for a coal with calorific value of ~ 4500 to 5200 kcal/kg coal, to achieve 80-95 % conversion the raw meal spends about 4-12 sec in the calciner (see window marked in Figure 4.7). This looks quite reasonable. The quantitative comparison of a specific simulation result with industrial data is given in Table 4.3.

Table 4.3: Comparison of model prediction with industrial data at calciner exit

(Calorific value of coal = 4850 kcal/kg coal; Residence time of solids = 8 s)

Sr. No		Model Predictions	Industrial data
1.	Mass Fraction CaCO3	8.09	9.92
2.	Mass Fraction CaO	65.47	63.86
3.	Mass Fraction SiO2	18.62	18.46
4.	Mass Fraction Al2O3	4.47	4.43
5.	Mass Fraction Fe2O3	3.35	3.32
6.	Temperature of solids, K	1160	1158

The model presented in the previous section was used to evaluate the performance of a typical calciner. To test the framework of the developed model, the volume of calciner was taken as 50 m^3. The inlet coal flow rate to the calciner was set to 1 kg/s and raw meal inlet flow rate was set to 35 kg/s. The inlet temperatures of coal and raw meal were taken as 350 K and 1000 K respectively. The gas inlet temperature to the calciner (from kiln exhaust gas and tertiary air from cooler) was set to 1194 K. The inlet conditions to the calciner were reasonable when compared with available data. For the initial simulations we have assumed the residence time of raw meal and coal particles inside the calciner (10 s). The framework is general enough so that mathematical equation to evaluate residence time based on calciner operating conditions can be incorporated later. The kinetic parameters for char combustion, gas phase combustion and calcination reaction were same as used for kiln in chapter 2. With

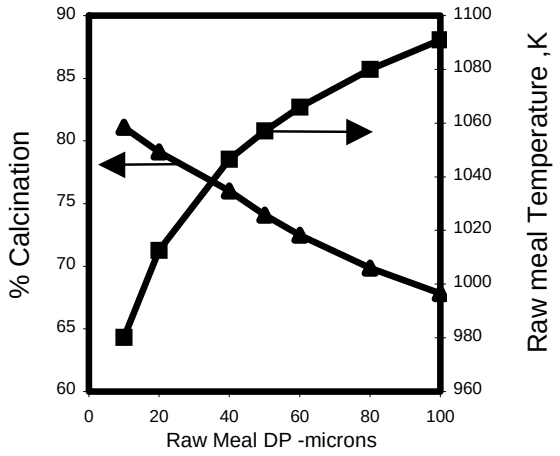

Figure 4.8a: Influence of particle size

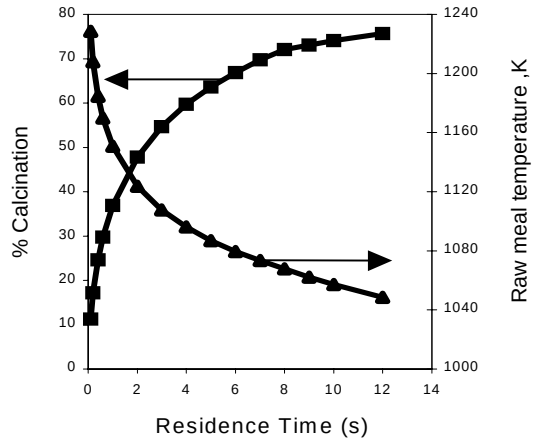

Figure 4.8b: Influence of particle residence time

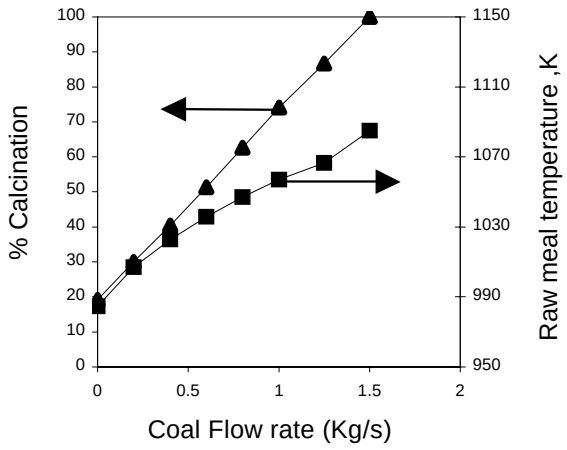

Figure 4.8c: Influence of coal flow rate

Figure 4.8: Predicted performance of a typical calciner

these input and kinetic parameters, the model predicted calcination of 74 %, exit gas temperature of 1057 K, exit solid temperature of 1057 K and losses of about 102 kW (<1 % of total energy input). The above values seem to be reasonable when compared qualitatively with industrial observations.

The influence of variation in inlet raw meal particle diameter on percentage calcination and temperature of raw meal at calciner exit is shown in Figure 4.8a. As expected, it can be seen that with decrease in particle size the percentage of calcination increases. Figure 4.8b shows the predicted influence of particle residence time on the performance of calciner. It can be seen that the extent of calcination increases with increase in particle residence time. The effect of change in coal flow rate on the calciner performance is shown in Figure 4.8c. Thus the computational model developed in this work is useful to simulate behaviour of calciners and to understand influence of key design and operating parameters on its performance. The model needs to be validated by comparing predicted results with industrial data.

4.3.3 Kiln model

The computational model for rotary kiln was developed by coupling bed height model, bed model and freeboard was explained in detail in chapter 3 and will not be discussed here.

4.3.4 Cooler model

The mathematical model of cooler was based on a schematic shown in Figure 4.9. Solids of uniform particle size and constant porosity were assumed to move in a plug flow with constant grate speed v_g in x direction. Air was assumed to enter in a cross flow mode with respect to solids in y direction. The cooler was divided into three sections as can be seen from Figure 4.9. The amount of air fed in each section was distributed proportional to fraction of length of each section. The air coming out of first section was assumed to be sent to the secondary air. The air from the second section was assumed to go to the calciner as tertiary air and air from third section was assumed to be lost to the surrounding as vent air. To get the temperature profiles of solid bed and air, the clinker cooler was divided into n segments along the length of the cooler (L) and m segments along the height of the cooler (H). Mass and energy balances were solved for these segments. Conductive heat transfer was considered for solids in both horizontal and vertical directions. Convective heat transfer coefficient between

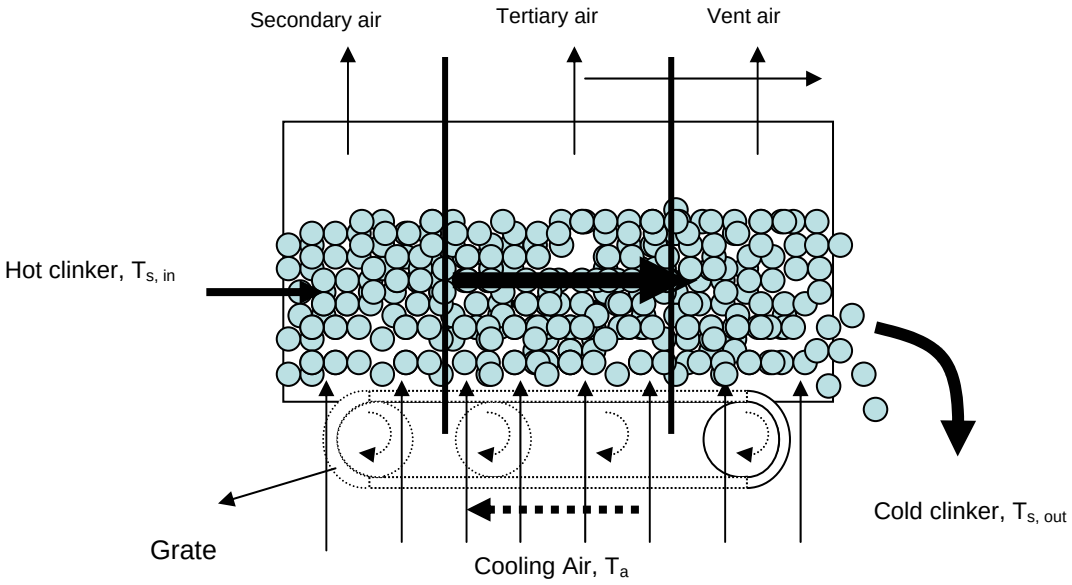

Figure 4.9 Schematic of grate cooler

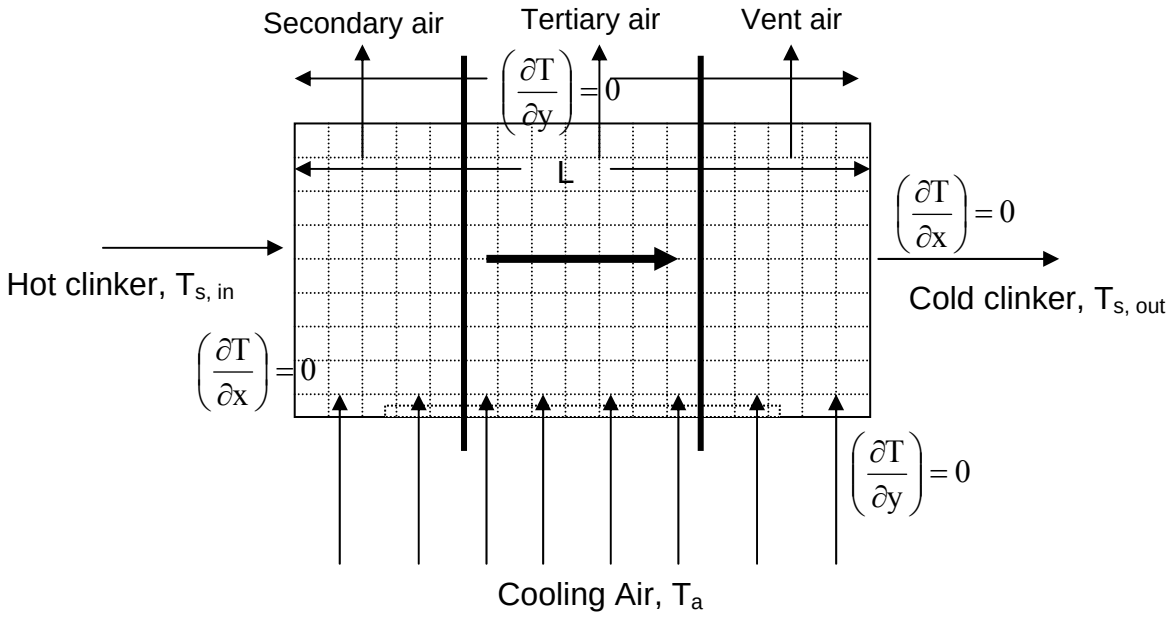

Figure 4.10: Boundary conditions

air and solids was calculated from empirical correlation assuming solids as packed bed. The boundary conditions used in the model are shown in Figure 4.10.

The model equations are presented in the following.

Mass balance for solids can be written as:

$$\frac{dm_{s(i,j)}}{dx} = 0 \tag{4.28}$$

Assuming steady state operation, the energy balance equation can be written as

$$\frac{\partial(\rho^s(1-\varepsilon)u_x^s c_p^s T^s)}{\partial x} + \frac{\partial(\rho^s(1-\varepsilon)u_y^s c_p^s T^s)}{\partial y} = \frac{\partial\left\{(1-\varepsilon)K^s \frac{\partial T^s}{\partial x}\right\}}{\partial x} + \frac{\partial\left\{(1-\varepsilon)K^s \frac{\partial T^s}{\partial y}\right\}}{\partial y} - \bar{a}h^{cv}(T^s - T^a) \tag{4.29}$$

In this equation ρ^s is the cement clinker density, C_p^s is clinker heat capacity, u_x^s is grate speed, and T^s is clinker temperature of solid at any point, K^s is clinker thermal conductivity, $\bar{a}$ is the convection area factor between the clinker and air, h^{cv} is convective heat transfer coefficient between solid clinker and air, T^a is air temperature at any point in the cooler. In Equation (4.29) the first and second terms of the right hand side represent the conduction. The last term in right hand side represents convective heat transfer between the air and solids.

The mass balance for air can be written as:

$$\frac{dm_{a(i,j)}}{dy} = 0 \tag{4.30}$$

Energy balance for air can be written as:

$$\frac{\partial(\rho^a \varepsilon u_x^a c_p^a T^a)}{\partial x} + \frac{\partial(\rho^a \varepsilon u_y^a c_p^a T^a)}{\partial y} = \frac{\partial\left\{K^a \varepsilon \frac{\partial T^a}{\partial x}\right\}}{\partial x} + \frac{\partial\left\{K^a \varepsilon \frac{\partial T^a}{\partial y}\right\}}{\partial y} + \bar{a}h^{cv}(T^s - T^a) \tag{4.31}$$

In this equation ρ^a is the air density, C_p^a is air heat capacity, u_y^a is air inlet speed, and T^a is air temperature at any point, K is air thermal conductivity, $\bar{a}$ is the convection area factor between the clinker and air, T^s is solid temperature at any point in the cooler. In Equation (4.31) the left hand side terms represents the net energy input by the air. First two terms in the right hand side represent the conduction between the air layers and the final term is due to the convection between solids and air. Since the thermal conductivity of the air is very less and

the neighbouring cells are at approximately same temperature so the conductive heat transfer among the air layers will be negligible.

In Equation (4.31) h^{cv} is convective heat transfer coefficient between solid clinkers and air. Developing accurate models for convective heat transfer coefficient between solids and air is most important because the dominating mode of heat transfer in the cooler is convection. The calculations are based on empirically determined heat transfer coefficient for forced convection in packed bed given by (Nsofor and Adebiyi, 2001)

$$Nu = 8.74 + 9.34[6(1-\varepsilon)]^{0.2}\,\mathrm{Re}^{0.2}\,\mathrm{Pr}^{0.33} \qquad (30 < \mathrm{Nu} < 60;\ 50 < \mathrm{Re} < 120) \qquad (4.32)$$

It is important to note that the Reynolds numbers for commercial clinker cooler are significantly higher (Re ~ 1000 to 2000) as compared to experimental conditions of Nsofor and Adebiyi (2001). However, as discussed earlier, there are no other systematic experimental studies reported to predict convective heat transfer coefficients in clinker coolers. The empirical correlation (Equation 4.32) was developed for particle sizes close to one found in industrial clinker coolers and for wide range of temperature conditions as observed in clinker coolers. Fortunately, the empirical correlation seems to be weekly dependent on Reynolds number (Reynolds number is to power 0.2). Therefore possible errors associated with Equation (4.32) are not expected to change the simulation results significantly (predicted Nusselt number is ~ 50 to 60). Hence Equation (4.32) was used to predict gas solid heat transfer in clinker coolers on the present model. All the physical properties are calculated an average temperature of solids and air as $T_f = (T_s + T_a)/2$. The system of algebraic linear equations formulated for above model equations was solved using tri-diagonal matrix algorithm (TDMA).

The model presented in the previous section was used to evaluate the performance of clinker cooler. To test the framework of the developed model, the length of cooler was set to 11 m for all the simulations. The inlet temperatures of air and cement clinker entering the cooler were taken as 300 K and 1625 K respectively (adapted from the data provided by Vikram Cements). Simulation results for grate speed of 0.1 m/s are shown in Figure 4.11 and Figure 4.12. Figure 4.11 shows the temperatures of top, bottom and middle layer of solids along the length of the cooler.

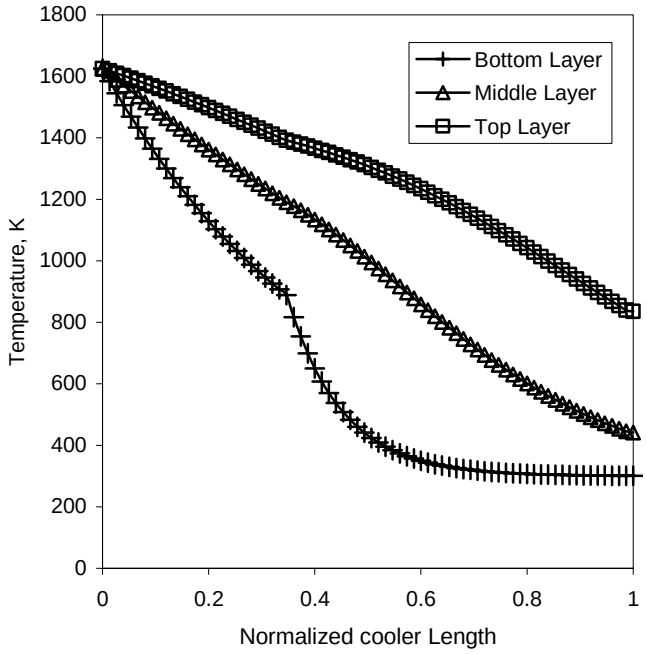

Figure 4.11: Bed temperature along cooler length

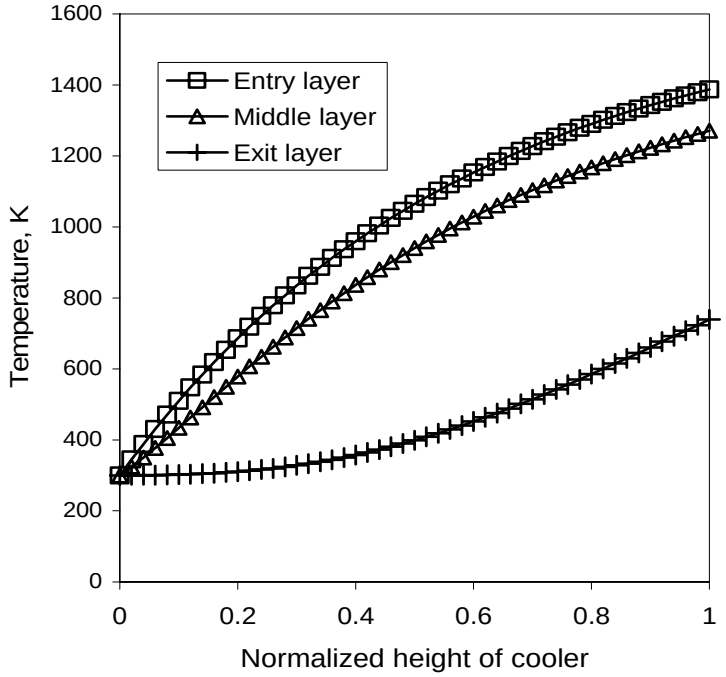

Figure 4.12: Air temperature along cooler height

Figure 4.12 shows the air temperature in the vertical cells at 3 different position viz. near the solids entrance, in the intermediate layer and at the solid exit. As expected, due to a higher

temperature gradient near the solid entrance the air temperature in the initial layers near the solid entrance have higher temperatures. The cooling air is supplied to the clinker cooler in 3 sections at different flow rates. The rate of heat transfer in each section, which is a function of the air flow rate, is different in all the three sections. Therefore the slope of the temperature curve changes at the location where the sections have common intersection. Since the rate of heat transfer is highest in the bottom layer the change of slope is prominent there. Overall, the simulated results seem to be qualitatively reasonable when compared with the published results (Locher, 2002).

The individual models for pre-heater, calciner, kiln and cooler described in the previous section have shown reasonable trends when compared with industrial observations. The individual models were also validated wherever possible. On obtaining a reasonable agreement and confidence, the models for pre-heater, calciner, kiln and cooler were coupled with each other to develop a simulator for the entire system.

4.4 Integrated Model

The individual models were coupled with each other to develop a simulator for the entire system. The schematic of the simulator is shown in Figure 4.13. The required inputs to the simulator are flow rates and composition of (a) raw meal entering the pre-heater (b) air entering the cooler (c) coal entering the calciner and the kiln and (d) the material properties and operating parameters of the individual equipments (for example, kiln RPM, grate speed of cooler).

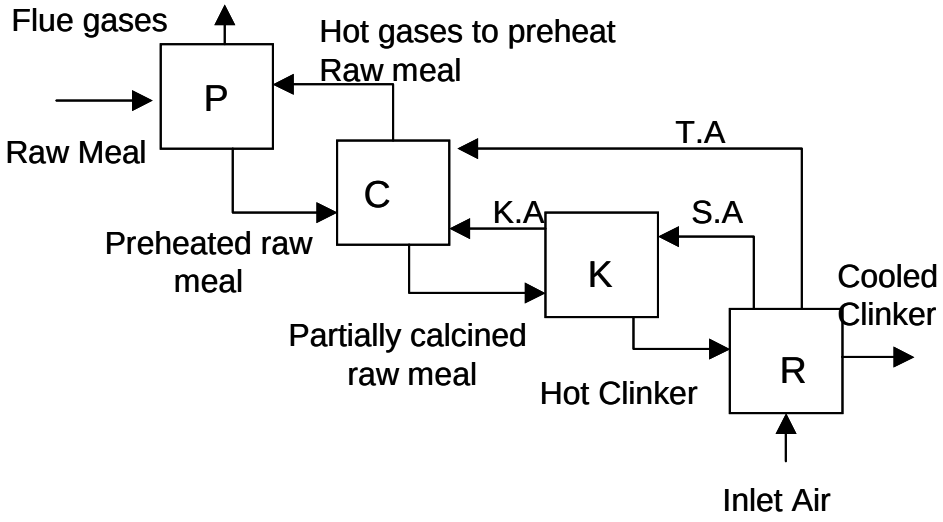

Figure 4.13: Schematic of the simulator

However, to solve the integrated simulator, it is necessary to know the inlet conditions for the calciner (flow rate, mass fractions and temperature of solids and air from pre-heater, kiln and cooler), pre-heater (flow rate and temperature of air from calciner), kiln (flow rate, mass fractions and temperature of secondary air from cooler and partially calcined raw meal from the calciner) and cooler (flow rate and temperature of solids from kiln).

To generate these inputs a pre-processor was developed. The function of pre-processor was two fold. The pre-processor was used to develop good initial guess for the simulator and also to check for any inconsistency of input data. The preprocessor generated the initial guess (for mass flow-rates, composition and temperatures of raw meal and air) for the individual models based on overall material and energy balances. Following parameters were provided to the preprocessor to achieve this:

1. Percentage calcination occurring in the calciner (P).
2. Temperature of secondary air ($T_{g,S}$) and Tertiary air ($T_{g,T}$) leaving the cooler.
3. Temperature of air leaving the kiln ($T_{g,K}$).
4. Temperature of air exiting the pre-heater to the atmosphere ($T_{g,P}$).
5. Temperature of solids exiting the cooler ($T_{s,R}$).
6. Heat losses ($H_{Loss,K}$) and heat of clinkerization reaction in the kiln ($H_{R,K}$).

These values are usually known or can be easily available for any cement plant and can therefore be used to generate good initial guess for faster convergence of solution. The preprocessor solves mass and energy balance equations as discussed in the following. Based on the percentage calcination in the calciner, the mass of CO_2 produced in calciner was calculated as

$$m_{CO2,C} = m_{CaCO3,i} \cdot P \cdot \frac{Mw_{CO2}}{Mw_{CaCO3}} \tag{4.33}$$

where, $m_{CaCO3,i}$ is the total amount of $CaCO_3$ in the inlet raw meal. The mass flow rate of solids entering the kiln was calculated as

$$M_{s,C} = M_{s,P} - m_{CO2,C} \tag{4.34}$$

where, $M_{s,C}$ is the mass flow rate of raw meal leaving the calciner or entering the kiln, $M_{s,\,P}$ is the mass flow rate of the solids entering the pre-heater. The corresponding mass fraction of solids species leaving the calciner or entering kiln were calculated as

$$x_{CaCO3,C} = \frac{m_{CaCO3,i} - m_{CaCO3,i} \cdot P}{M_{s,C}} \qquad x_{CaO,C} = \frac{(m_{CO2,C}) \cdot (Mw_{CaO})}{(M_{s,C}) \cdot (Mw_{CO2})}$$

$$x_{SiO2,\,C} = \frac{m_{SiO2,i}}{M_{s,C}} \qquad x_{Al2O3,\,C} = \frac{m_{Al2O3,i}}{M_{s,C}} \qquad x_{Fe2O3,\,C} = \frac{m_{Fe2O3,i}}{M_{s,C}} \tag{4.35}$$

where x is the mass fraction of the component in the raw meal. The amount of clinker leaving the kiln or entering the cooler $M_{s,K}$ was calculated as

$$M_{s,K} = M_{s,C} - \frac{(M_{s,C}) \cdot x_{CaCO3,C}}{MW_{CaCO3}} \cdot Mw_{CO2} \tag{4.36}$$

Based on overall material balance on kiln, the amount of air leaving the kiln was calculated as

$$M_{g,K} = M_{g,S} + M_{s,C} \cdot x_{CaCO3,C} \cdot \frac{Mw_{CO2}}{Mw_{CaCO3}} + M_{c,K} \cdot y_{c,K} \cdot \frac{Mw_{CO2}}{Mw_{CaCO3}} \tag{4.37}$$

where $M_{g,S}$ is the mass of secondary air entering the kiln, $M_{g,\,K}$ is the air leaving the kiln or entering the calciner, $M_{c,\,K}$ is the amount of coal entering the kiln and $y_{c,k}$ is the mass fraction of char entering the kiln. The amount of air leaving the pre-heater assembly was calculated as

$$M_{g,P} = M_{g,K} + M_{g,T} + m_{CO2,C} + M_{c,c} \cdot y_{c,c} \cdot \frac{Mw_{CO2}}{Mw_{CaCO3}} \tag{4.38}$$

where $M_{g,P}$ is the mass of air entering the pre-heater, $M_{g,T}$ is the mass tertiary air entering the calciner, $m_{CO2,\,c}$ is the CO_2 produced in calciner due to calcination reaction and $M_{c,\,c}$ is the amount of coal entering the calciner and $y_{c,c}$ is the mass fraction of char entering the calciner. The temperature of solids leaving the kiln was calculated as

$$T_{s,K} = \frac{(M_{s,R} \cdot C_{p,s} \cdot T_{s,R} + M_{g,T} \cdot C_{p,g} \cdot T_{g,T} + M_{g,S} \cdot C_{p,g} \cdot T_{g,S}) - (M_{g,in} \cdot C_{p,g} \cdot T_{g,in})}{(M_{s,K} \cdot C_{p,s})} \tag{4.39}$$

In the above Equation $M_{g,in}$ and $T_{g,in,}$ is the mass flow rate and temperature of air entering the cooler and $T_{s,R}$ is the temperature of solids exiting the cooler. The temperate of solids entering the kiln or exiting calciner ($T_{s,C}$) was calculated as

$$T_{s,C} = \frac{(M_{s,K} \cdot C_{p,s} \cdot T_{s,K} + M_{g,K} \cdot C_{p,g} \cdot T_{g,K} + H_{R,K} + H_{Loss,K} - M_{g,S} \cdot C_{p,g} \cdot T_{g,S} - H_{c,K})}{(M_{s,C} \cdot C_{p,s})} \quad (4.40)$$

In the above equation, $H_{C,K}$ is heat released due to coal combustion in kiln, $H_{R,K}$ is heat required for clinker reactions and $H_{Loss,K}$ is the loss from the kiln. The temperature of solids entering the kiln is essentially same as temperature of gases leaving the calciner ($T_{g,C}$). Finally, the temperature of solids entering the calciner or leaving the pre-heater assembly ($T_{s,P}$) was calculated as

$$T_{s,P} = \frac{(M_{s,C} \cdot C_{p,s} \cdot T_{s,C} + M_{g,C} \cdot C_{p,g} \cdot T_{g,C} + H_{calc} - M_{g,K} \cdot C_{p,g} \cdot T_{g,K} - M_{g,T} \cdot C_{p,g} \cdot T_{g,T} - H_{C,C})}{(M_{s,P} \cdot C_{p,s})} \quad (4.41)$$

In the above equation, $H_{C,C}$ is heat released due to coal combustion in the calciner and H_{calc} is the heat required by calcinations reaction. This was easily calculated based on percentage calcination occurring in the calciner. The heat losses in calciner are negligible as compared to total heat supplied to the calciner (<5 % of total energy input) and therefore was not considered in pre-processor calculations. In this way the input conditions (mass, mass fractions and temperature) for pre-heater, calciner, kiln and cooler were calculated using preprocessor. The values calculated by preprocessor were passed as input conditions to the individual models which were then solved iteratively as shown in Figure 4.14.

The iterations were continued till the temperature of solids and gases at exit of individual components were within error of ±1 %. Suitable under relaxation parameters were used. Typically 10-20 iterations were required for solution to converge. The convergence results for two values of under-relaxation parameter are shown in Figure 4.15. An easy to use, graphical user interface (GUI) based software called RoCKS (Rotary Cement Kiln Simulator) was developed based on the integrated modules of pre-heater, calciner, kiln and cooler which is discussed in the nest section

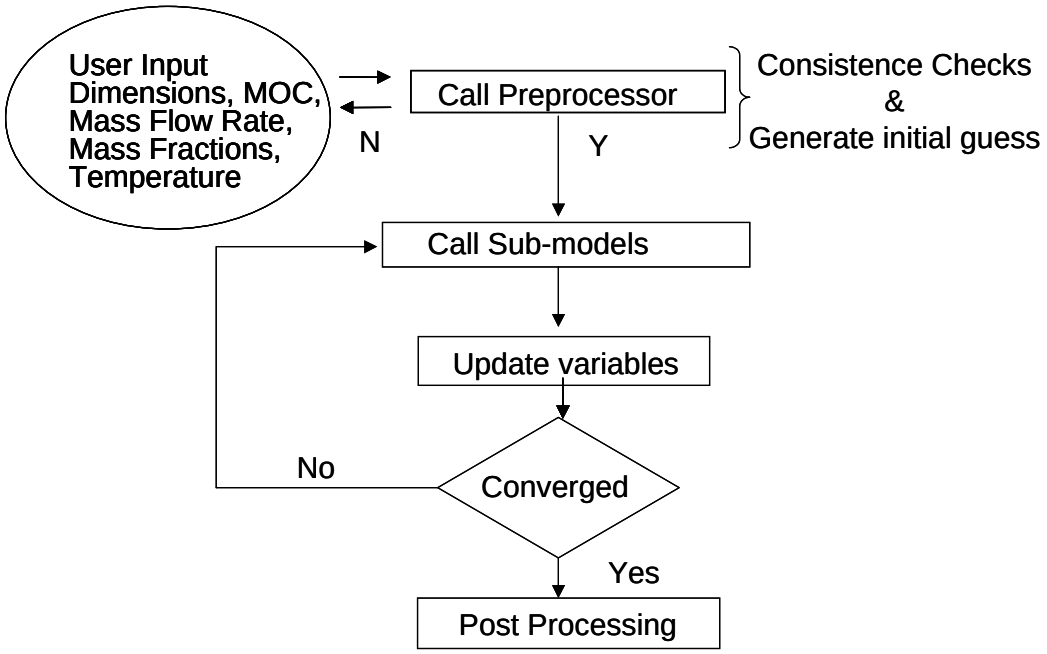

Figure 4.14: Solution Methodology of the simulator

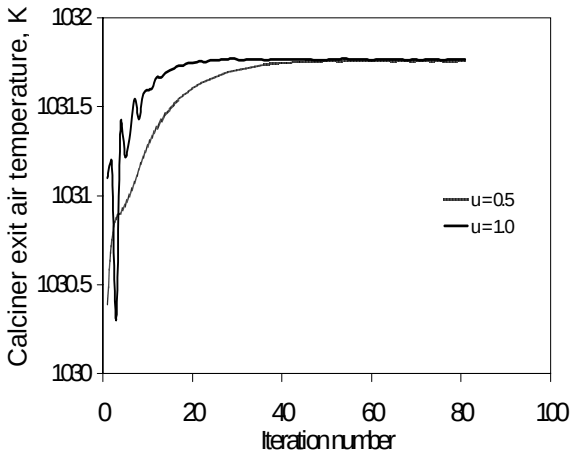

Figure 4.15a: Calciner exit air temperature

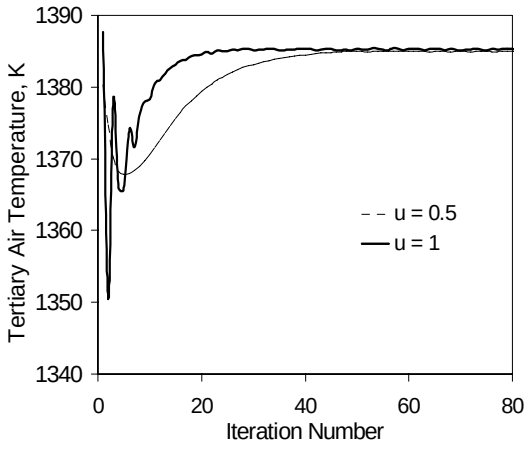

Figure 4.15b: Tertiary air temperature

Figure 4.15: Influence of under-relaxation parameter on convergence behavior (simulations of Vikram cement line I)

4.5 RoCKS (Rotary Cement Kiln Simulator)

The integrated modules of pre-heater, calciner, kiln and cooler were included in RoCKS (**Ro**tary **C**ement **K**iln **S**imulator) software. The FORTRAN programs implementing the solution of integrated simulator were modified to develop dynamically linked libraries (DLL). Two DLL's, one for the preprocessor and second for the main simulator were developed. GUI was developed using Visual Basic (VB) to facilitate use of the models developed in this work. Typical screen shots of RoCKS are shown in figures below.

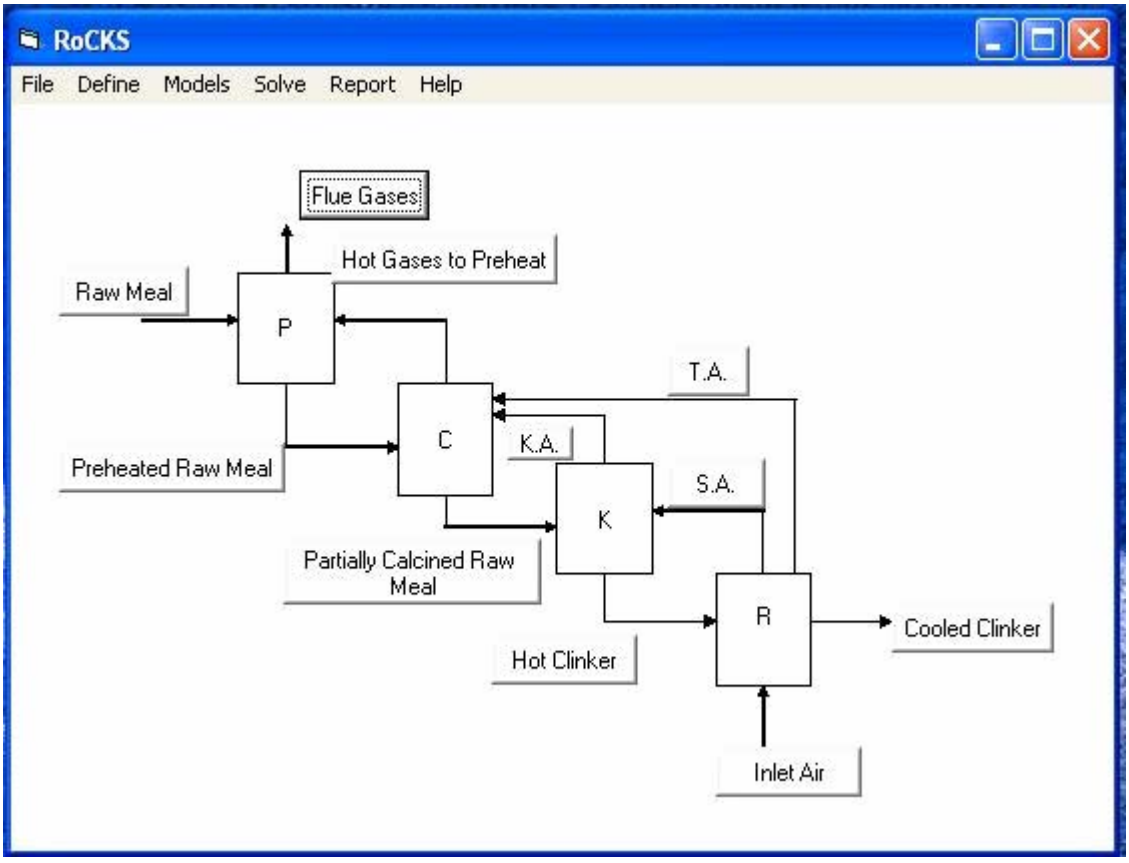

Figure 4.16: Snap shot of Rotary Cement Kiln Simulator (RoCKS) Software.

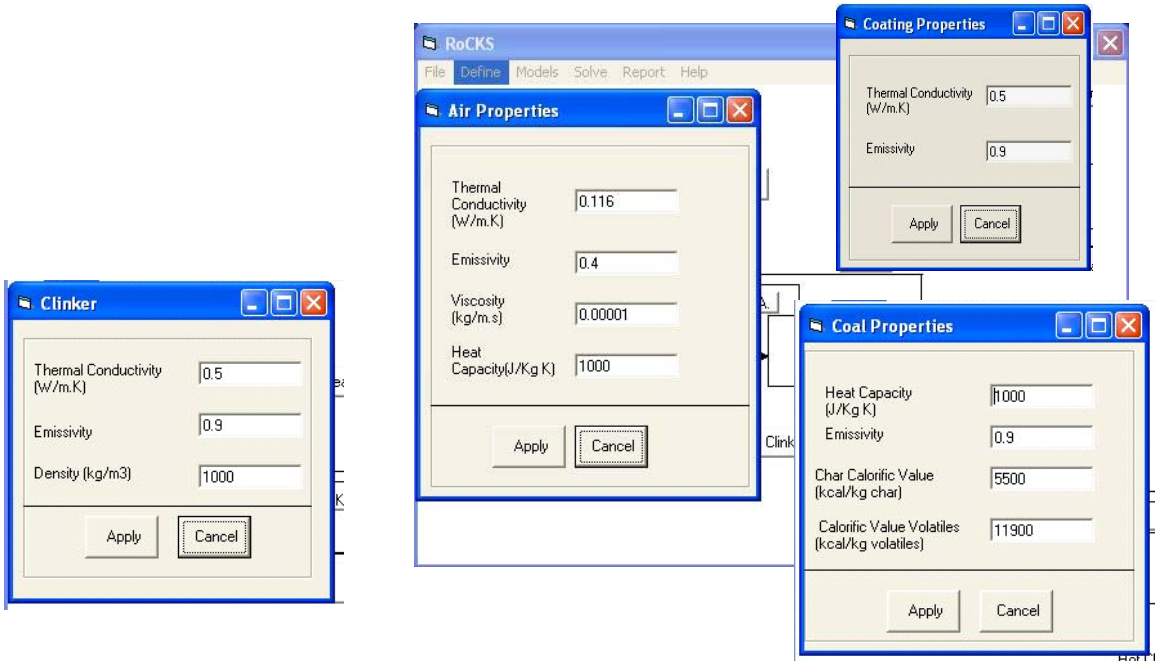

Figure 4.18: Snap shots of internal windows of (RoCKS)

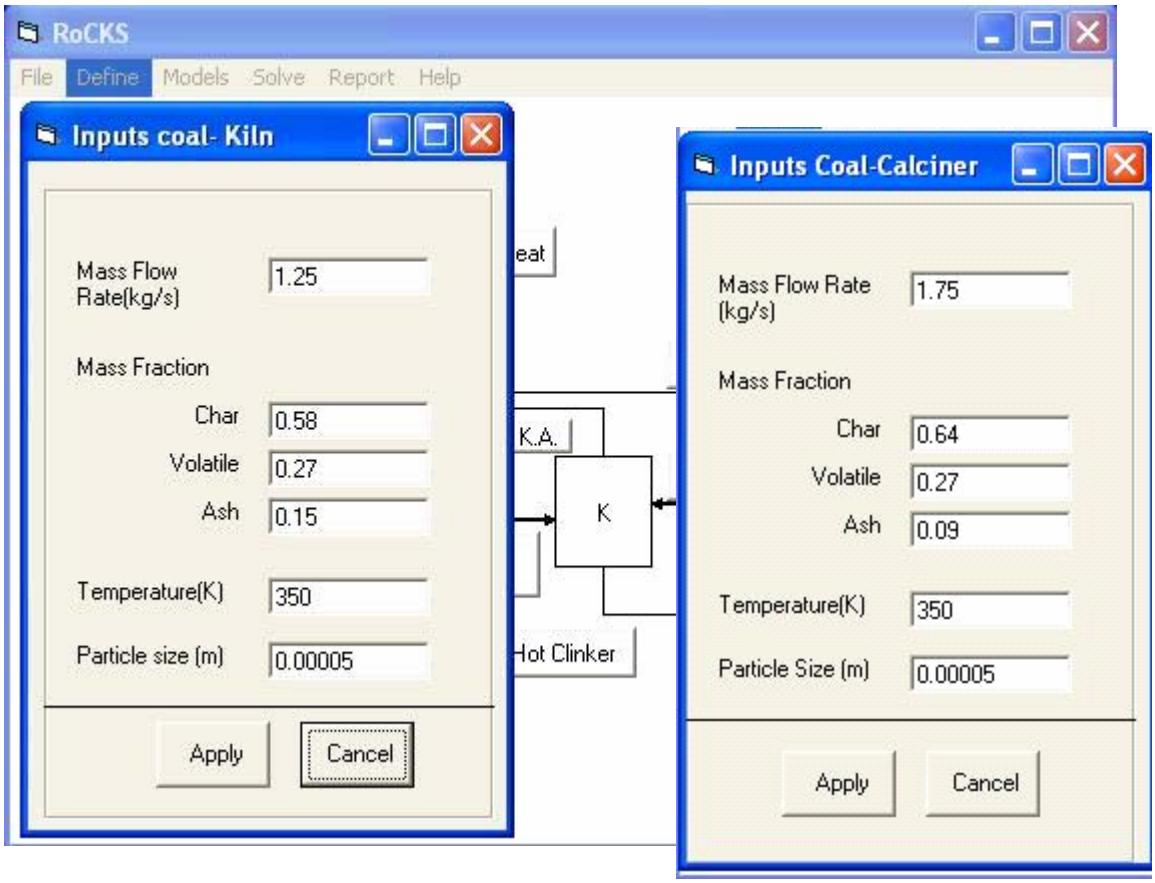

Figure 4.19: Snap shots of Internal windows of (RoCKS)

4.6 Simulation Results

The integrated model (RoCKS) presented in the previous section was used to simulate performances of pre-heater, calciner, rotary kiln and cooler in clinker manufacturing. Based on the available data on rotary kilns (as discussed in Chapter 3) and available information from some of the cement industries, a typical clinker manufacturing configuration was selected as a base case. Some assumptions were made to fill in the gaps in the available data. The details of selected configuration are given in Tables 2a-2c. Though the developed mathematical framework is general enough to accommodate temperature dependent physical properties like heat capacity, at this stage, these properties were treated as constants. The physical properties of solids and air used in this work are specified in Table 3a. Our prior simulations of kiln and calciner indicated that the errors in overall energy consumption associated with the assumption of temperature independent values of specific heat were within 1%. The operation of the base case (described in Tables 2 to 4) was computationally studied to understand the various processes occurring in individual units in clinker formation. On obtaining satisfactory results from the base case, several numerical experiments were performed using the model for understanding interactions among different processes and for possible optimization of clinker manufacturing process.

Table 4.4: The Dimensions of pre-heater unit

PREHEATER UNIT			
S/No	Description	Units	Values
1	No of pre-Heaters		4
2	Height of cylindrical section	m	5
3	Height of conical section	m	3
4	Diameter of Cyclone	m	3
5	Diameter of cone tip	m	1
6	Refractory thickness	m	0.13
7	Shell thickness	m	0.03
8	Inlet duct height	m	1
9	Inlet duct width	m	1
10	Diameter of outlet pipe	m	1

Table 4.5: The Dimensions of kiln

KILN			
S/No	Description	Units	Values
1	Length	m	50
2	Inner Diameter	m	3.4
3	Coating Thickness	m	0.136
4	Refractory Thickness	m	0.2
5	Shell thickness	m	0.025

Table 4.7: The physical properties of solids and air

Description	Air	Raw meal	Coal
Thermal Conductivity, W/m K	0.116	0.5	0.5
Emmisivity	0.4	0.9	0.8
Heat capacity, J/kg K	1000	1000	1000
Viscoscity, kg /m s	1e-05	-	-
Density, kg/m^3	1.3	1500	1000
Char calorific value, J/kg	-	-	5600
Volatile calorific value, J/kg	-	-	11900

Table 4.6: The Dimensions of cooler

COOLER			
S/No	Description	Units	Values
1	Length	m	11
2	Width	m	1

4.6.1 Base case simulation

The predicted results from the simulation of the base case are summarized below. The mass fractions and temperatures of solids and air in pre-heaters, calciner, kiln and cooler obtained from the simulation are plotted in Figure 4.20a and Figure 4.20b respectively. It is important to note that the flow of air is counter current with respect to the flow of solids in the system. The abscissas of Figure 4.20a and Figure 4.20b denote particular equipment in clinker formation as discussed below. Abscissa 1 to 4 corresponds to pre-heater assembly. Abscissas 4 to 5 denote the calciner in the system. Abscissas 5 to 15 denote the rotary kiln and 15-18 denote the cooler section. Figure 4.20a shows a plot of mass fractions in pre-hater, calciner, kiln and cooler (only CaO, C_2S and CO_2 mass fractions are plotted for the sake of brevity). Since there is no reaction occurring in pre-heater section, the composition of CaO and CO_2 in this section do not vary. However, in the pre-heater section the raw meal gets heated from 300 K to 1069 K and hot gases from calciner get cooled (from 1224 K to 539 K) as can be seen from Figure 4.20b.

As the raw meal passes through the calciner, it gets partially calcined. Therefore CaO concentration increases in the calciner section as can be seen from Figure 4.20a. Similarly since CO_2 is formed due to calcination and coal combustion, the mass fraction of CO_2 increases in the calciner. Coal combustion in the calciner accounts for rise in temperature of both solids and gas in the calciner (see Figure 4.20b). Remaining clinkerization reactions occur in kiln. The mass fraction and temperature profiles obtained in kiln (as shown in Figure 4.20a and Figure 4.20b) are similar to previously published results (See Chapter 3; Mastorakos *et al.*, 1999). Since there is no reaction occurring in the cooler, mass fraction of solids in the clinker cooler do not vary. However air entering the cooler gets preheated (from 300 K to 1200 K) and solids get cooled (from 1632 K to 476 K) in the cooler section.

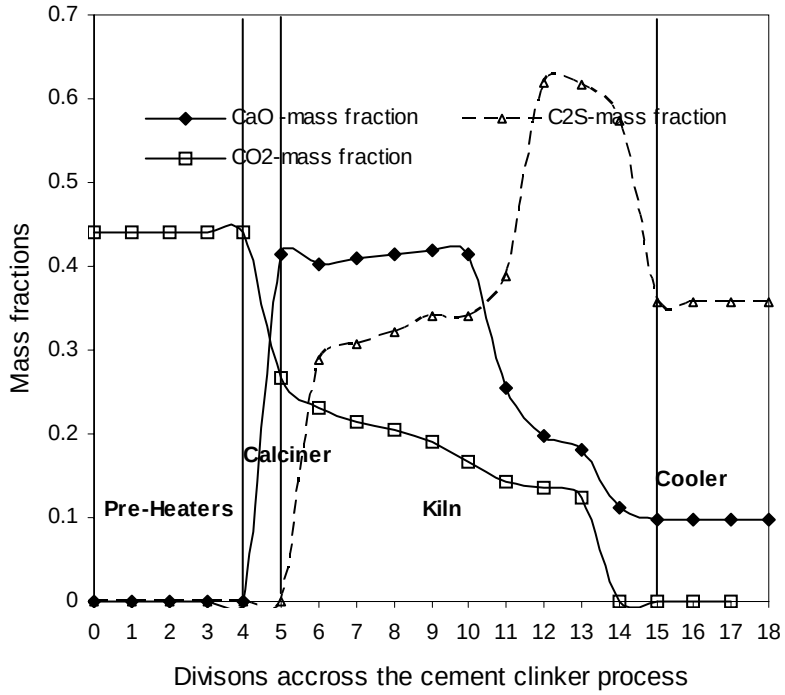

Figure 4.20a: Mass fraction in pre-heaters, calciner, kiln and cooler in a cement clinker process.

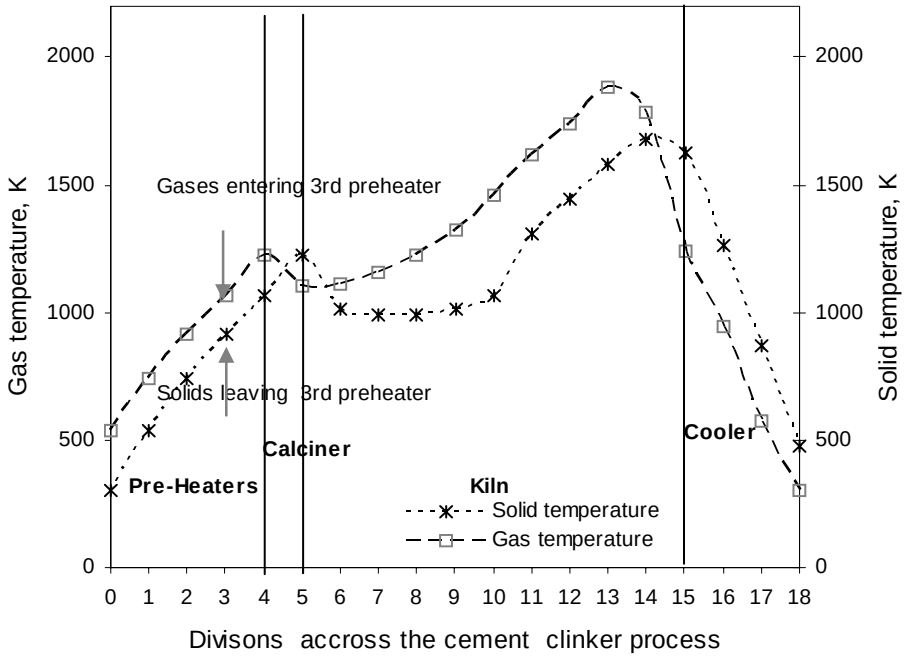

Figure 4.20b: Temperature profile across pre-heaters, calciner, kiln and cooler in a cement clinker process.

The predicted energy requirements of individual processes like clinkerization reactions, losses, melting predicted by the model are listed in Table 4.8. The obtained results are qualitatively similar to previously published results (Engin and Ari, 2005). The performance of the overall system was characterized in terms of net energy consumption per unit weight of product (clinker coming out of the kiln). The net energy consumption (NEC) was calculated as:

$$NEC = (E_{RXN,\,C} + E_{RXN,\,K} + E_{MELT,\,K}) + E_{LOSS} + (E_{G,OUT} + E_{S,OUT} - E_{G,IN} - E_{S,IN}) \qquad (4.42)$$

In the above equation, E_{RXN} denotes the energy required for clinkertization reactions and subscripts c and k denotes the calciner and the kiln respectively. The term $E_{MELT,\,K}$ denotes the energy required for melting in the kiln. E_{LOSS} denotes the summation of energy losses from pre-heater assembly, calciner and kiln. The other terms denote energy flow rates (subscripts IN or OUT) for the gas and solid streams (subscripts G or S) which denote the energy required to raise the sensible heat of the solids. Based on above calculations, the net energy consumption predicted by the integrated simulator, for these operating conditions was 2635 kJ/ kg clinker (630 kcal/ kg clinker) which seems to be reasonable when compared with industrial observations. Overall the integrated simulator was able to predict the clinker manufacturing process in cement industry reasonably well.

Table 4.8: Complete energy balance of the system

S/No	Description	Pre-heater	Calciner	Kiln	Cooler
1	Solid inlet temperature, K	300	1069.2	1214.8	1622.4
2	Mass flow rate , kg	50	50	37.74	32.3
3	Air inlet temperature, K	1214.8	1114.5	1229.9	300
4	Air flow rate, kg/s	60.8	46.7	16.2	45
5	Coal flow rate, kg/s	-	2.15	0.9	-
6	Coal inlet temperature, K	-	350	350	-
7	Heat with solids in, kJ/kg clinker	463.0	1650.2	1415.3	1622.4
8	Heat with air in, kJ/kg clinker	2297.9	1603.6	615.0	416.7
9	Heat with coal in, kJ/kg clinker	-	23.2	9.7	-
10	Combustion of coal, kJ/kg clinker	-	1876.7	747.1	-
11	Heat of reaction, kJ/ kg clinker	-	1384.5	219.0	-
12	Heat of melting, kJ/ kg clinker	-	44.2	-	-
13	Heat of solids leaving, kJ/ kg clinker	1650.2	1415.3	1622.4	463.0
14	Heat of air leaving, kJ/ kg clinker	1014.4	2297.9	1603.6	1415.3
15	Heat of vent air in cooler, kJ/ kg clinker	-	-	-	109.4
16	Heat with ash, kJ/ kg clinker	-	3.22	2.24	-
17	Losses, kJ/ kg clinker	98.9	43.5	140.7	-

4.6.2. Influence of key design and operating parameters on net energy consumption

On obtaining a reasonable agreement, the model was used to explore space of design and operating parameters to understand influence of these parameters on the performance of clinker manufacturing. All these simulations were carried for a fixed product composition (C3S mass fraction 0.48 in the product). This was achieved by altering coal flow rate either to calciner or kiln. This analysis is presented in the section below.

Effect of number of pre-heaters

The effect of changing number of pre-heaters in pre-heater assembly (from 3 to 5) on net energy consumption was studied. For this simulation the coal in the kiln was adjusted to get same product composition at the kiln exit. The results for this simulation are shown in Figure 4.21. It can be seen from Figure 4.21 that as number of pre-heaters in pre-heater assembly increases, solids get pre-heated to a higher temperature before they enter the calciner (see secondary axis in Figure 4.21). Therefore coal requirement for a fixed product composition decreases. Thus the net energy consumption decreases as number of pre-heaters increases. However, the overall capital cost increases by increasing number of pre-heaters in the system. The developed model will be useful to carry out cost to benefit analysis for introducing additional pre-heater in the pre-heater assembly.

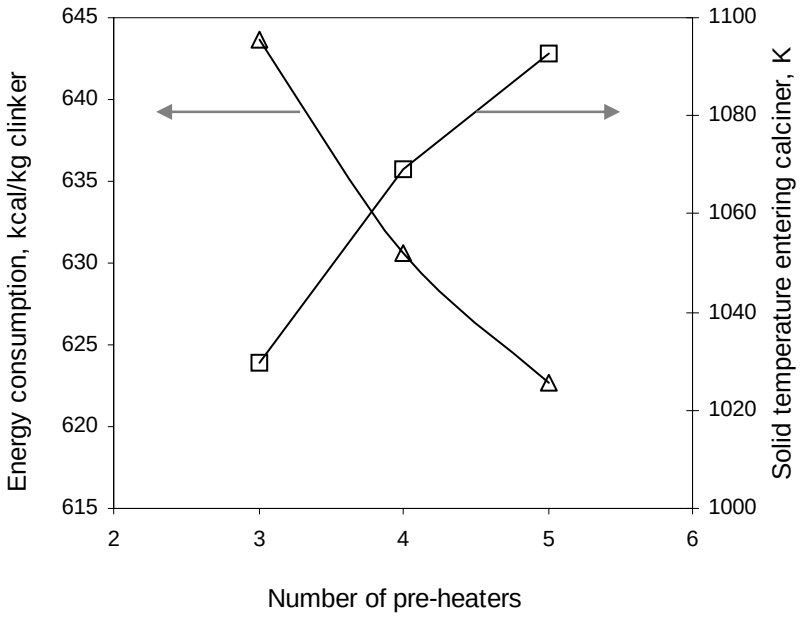

Figure 4.21: Effect of pre-heater number on overall energy consumption

Effect of percentage calcination in the calciner

The pre-calcination of raw meal in calciner is an important process in cement process. The effect of percentage calcination in calciner on net energy consumption was studied. The percentage of calcination in pre-calciner was varied from 50 to 80. To achieve this, the coal feed rate to the calciner and the kiln was altered to get the same clinker composition. The simulation results are shown in Figure 4.22. The net energy consumption is found to decrease till 70 % calcination and then it increases with further increase in percentage of calcination. The secondary axis of Figure 4.22 shows that the kiln exit gas temperature also shows a similar trend. Table 4.9 shows a complete comparison of heat of reaction occurring in kiln and calciner in this process. The heat of reaction in kiln decreases as the percentage calcination increases in calciner. The total heat of reaction in kiln is summation of heat of calcination (endothermic reaction) and heat of clinker formation (exothermic reactions). When calcination occurs pre-dominantly in the pre-calciner (> 70%), the energy requirements for reactions in kiln reduce drastically. This causes increase in kiln flue gas temperature and increase in losses from kiln shell. Therefore the net energy consumption and kiln flue gas temperature increases if more than 70 % calcination occurs in the calciner.

It is also important to note that the variation in net energy consumption appears to be small in nature (< 1%) from results shown in Figure 4.22. However, considering the production capacities of the rotary cement kilns, the overall impact is quite significant. Typically for the cement kiln under study (with production rate of ~ 3000 TPD) within this calcination range, it can be easily shown there is an possibility of energy savings of ~ 1.12 MW. The model and the RoCKS software were thus able to provide valuable clues for determining the optimum percentage calcinations desired for minimizing net energy consumption.

Table 4.9: Heat of reaction in calciner and kiln

S/No	Heat of reaction				
1	CALCINATION, %	50	60	70	80
2	Heat of reaction in calciner, kJ/kg clinker	1038.5	1176.6	1384	1618.5
3	Heat of reaction in kiln, kJ/kg clinker	582.9	433.28	219	-20.28

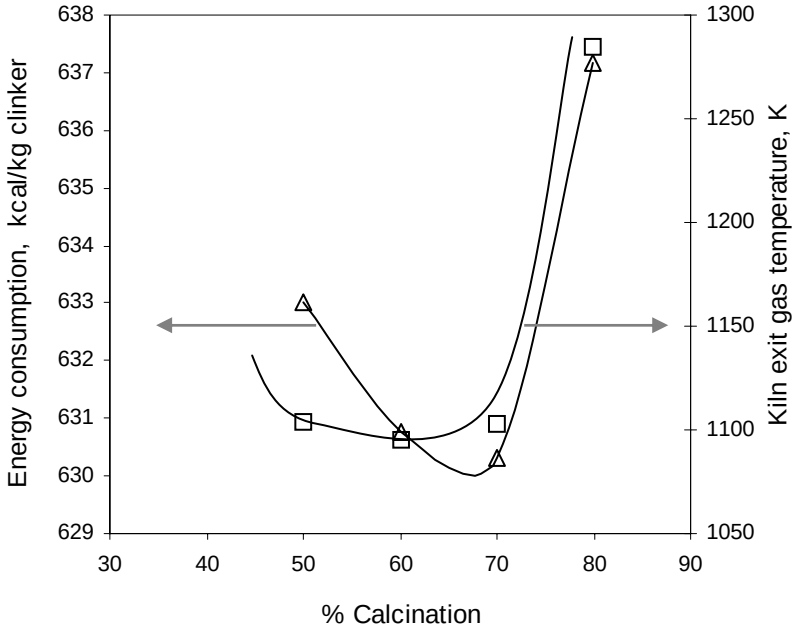

Figure 4.22: Effect of percentage calcination on overall energy consumption

Effect of kiln RPM, kiln tilt and grate speed of clinker cooler

The effect of kiln rotational speed and kiln tilt on the overall performance is shown in Figure 4.23a and 4.23b. For these simulations the coal flow rate to the kiln was varied to maintain constant product composition. It can be seen from Figure 4.23a that as the kiln RPM decreases, the net energy consumption decreases. Changes in kiln RPM changes the bed height and the residence time of solids in the kiln as can be seen from Figure 4.23a and 4.23b (2002.4 s for 3 rpm; 1058.2 s for 5.5 RPM and 703.4 s for 8 rpm). Our simulation results indicate that it seems to be beneficial to operate kilns at lower RPM as long as adequate mixing of solids is occurring. From Figure 4.23b it can be seen that energy consumptions in kilns operated at lower tilt is less as compared to kilns at higher tilt. The grate of clinker cooler is the important parameter that controls the residence time of solids and subsequently the heat exchange between hot solids and counter current air in the cooler. We have studied the influence of varying grate speed on overall energy consumption. The results for these simulations are shown in Figure 4.23c. It can be seen from Figure 4.23 that the net energy consumption increases with increasing grate speed. The increase in grate speed reduces residence time of solids in the cooler. This results in less convective heat transfer between solids and air as clearly indicated by temperature of secondary air plotted in Figure 4.23. Therefore simulation results indicate that it is better to operate grates in the cooler at lower

speed. The simulations presented here provide useful trends of energy consumption as a function of key operating parameters in cement clinker process. This results also gives us a scope to understand the importance of design parameters (kiln tilt) on plant performance and can be very useful to plant engineers.

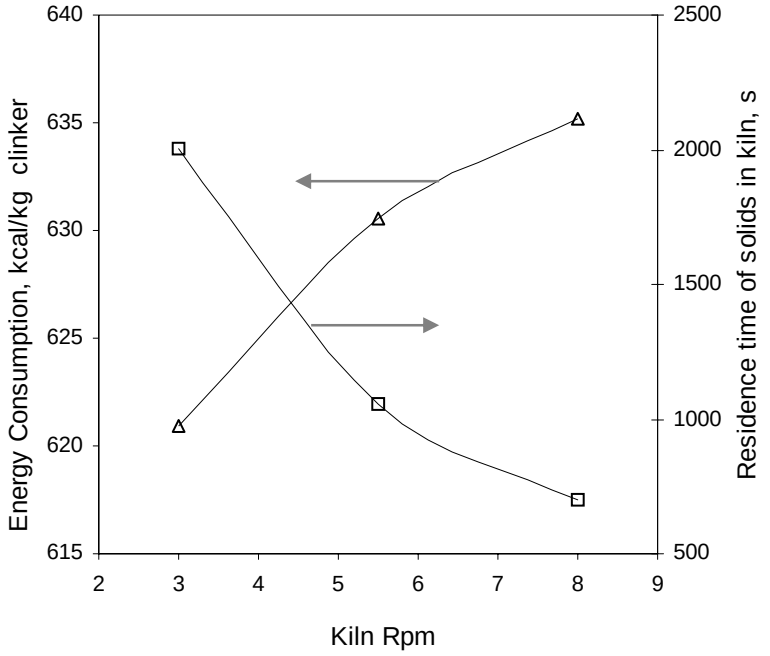

Figure 4.23a: Effect of kiln RPM, on overall energy consumption

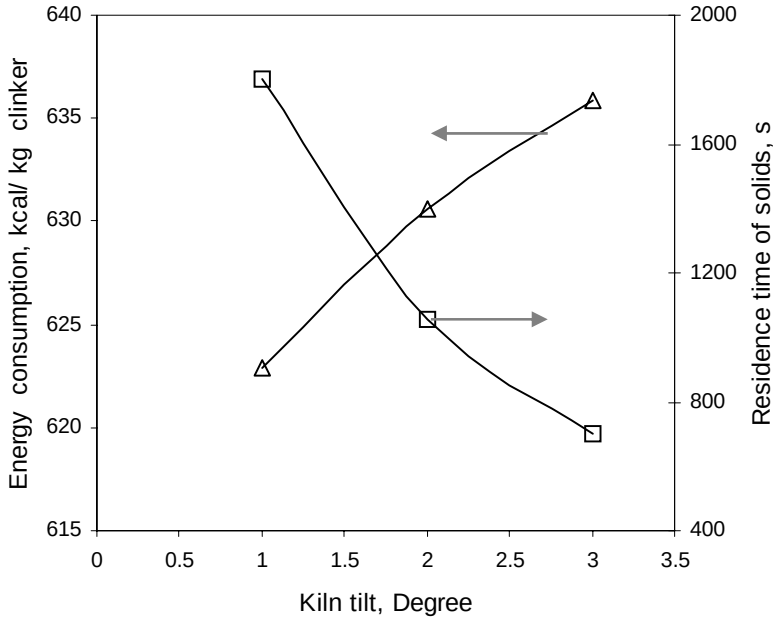

Figure 4.23b: Effect of kiln tilt, on overall energy consumption

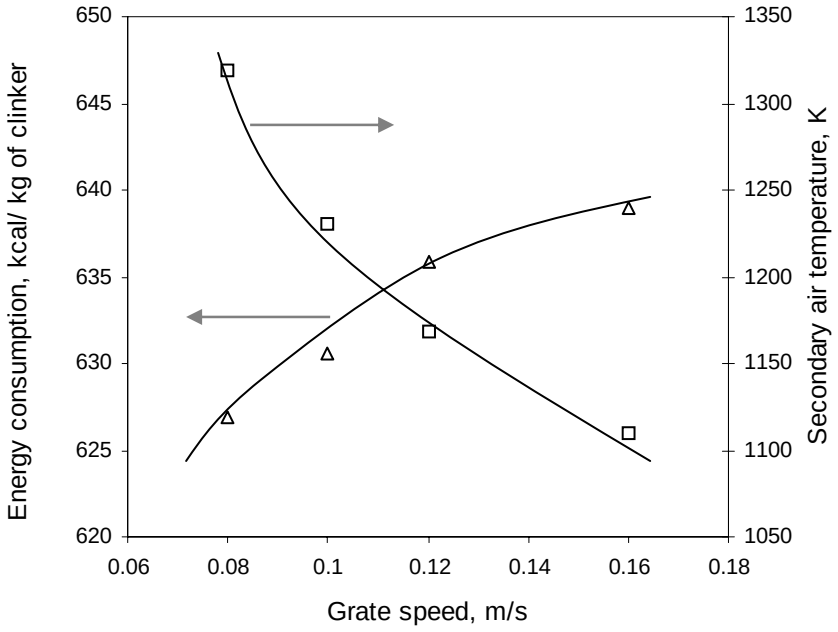

Figure 4.23c: Effect of cooler grate speed, on overall energy consumption

Effect of solid loading

The predicted results in the form of net energy consumption and corresponding overall losses for different solids flow rates are shown in Figure 4.24. It can be seen that the net energy consumption per unit weight of product decreases as solids flow rate increases. The mass flux of the product through the kiln also showed similar trend (Corresponding figures for mass flow rate of 44 kg/s, 47.5 kg/s and 50 kg/s in terms of mass flux are 4.84 kg/m^{2}s, 5.23 kg/m^{2}s and 5.5 kg/m^{2}s respectively). This is because the net energy loss from the entire system decreases as the solid flow rate increases (see Figure 4.24). Thus it is beneficial from the point of view of energy consumption to operate the units with higher solids flow rate. Other operational concerns like increase in dusting and mixing however need to be considered while identifying maximum solids flow rate specifically for cement kilns.

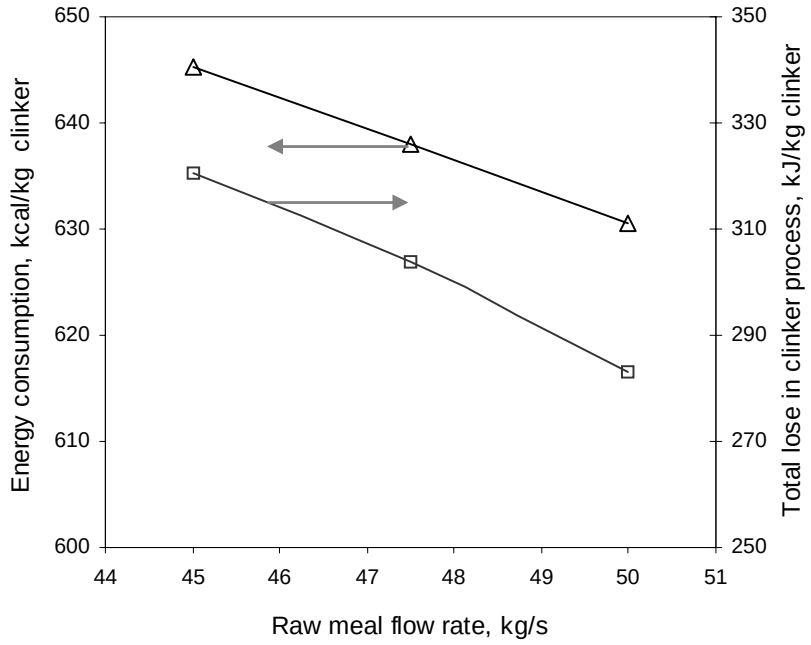

Figure 4.24: Effect of raw meal flow rate, on overall energy consumption

Effect of coal composition

The effect of varying coal composition to the kiln on net energy consumption is shown in Figure 4.25. From Figure 4.25, it can be seen that the overall energy consumption does not change significantly with changing coal composition (ash content 9 %, 15 % and 40 %). For these simulations the coal flow rate to the kiln was adjusted so that same amount of energy is supplied to the kiln. Therefore the insignificant change in overall energy consumption does not seem to be surprising. However, as the coal composition changes, the flame characteristics in the kiln vary. The predicted flame length by the simulator for varying coal composition is shown in Figure 4.25. The flame length was calculated by tracking the region in freeboard where char and volatiles composition in coal go to zero. It can be seen that coal with higher ash content tend to have a longer flame as compared to coal with lower ash content. The flame length is a complicated function of amount of oxygen, amount of char and temperature of gas and particle in the freeboard region. Coals with higher ash content tend consume oxygen at a slower rate and therefore result in longer flames. Such simulations can therefore provide useful information to kiln operators to predict the flame characteristics for wide variety of coal available in the market.

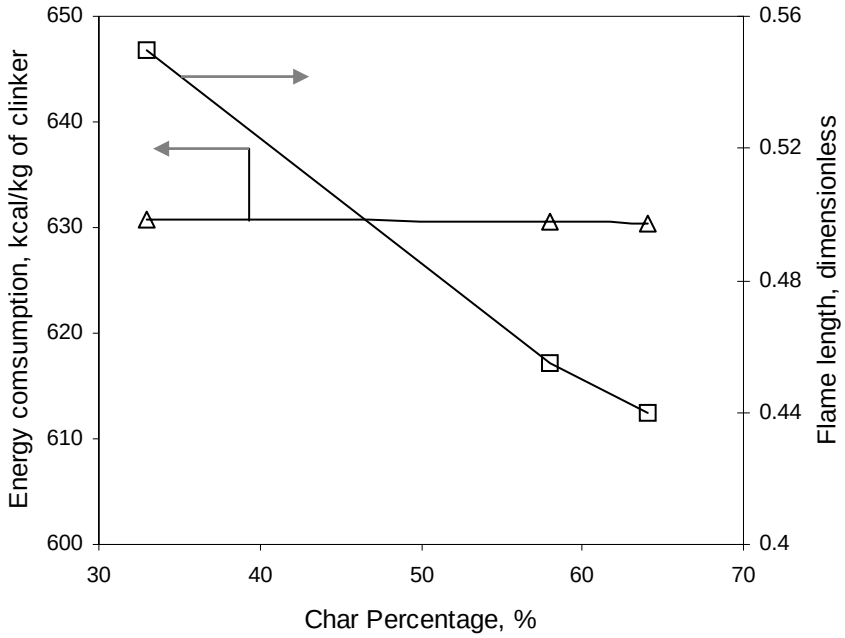

Figure 4.25: Effect of coal composition, on overall energy consumption

Effect of secondary shell

Heat losses to the surrounding from the kiln shell by radiation and convection are a significant source of energy loss in cement kilns and therefore the overall process. These losses can be reduced by using a secondary shell. The idea is to cover the kiln shell with another metallic shell having low surface emissivity and thermal conductivity (Engin and Ari, 2005). However, merely covering kiln shell with metallic shell and insulating it can lead to enormously high shell temperatures. Hence a practical approach to use secondary shell would be to feed air through the interstitial space of shell and secondary shell to recover the energy and still operate kilns under realistic conditions (as discussed in Chapter 3). The developed RoCKS frame work was used to explore the possibility of using such a secondary shell. The losses in kiln reduced from 140 kJ/ kg of clinker to 1.4kJ/ kg of clinker on applying a secondary shell and insulation of dimensions and operating conditions specified in Chapter 3. The net energy consumption reduces from ~ 2635 kJ/ kg clinker to 2493 kJ/ kg clinker (i.e. 630 kcal/ kg clinker to 596 kcal/kg clinker) by using secondary shell and passing air of about 30 kg/s through the interstitial space. If the air coming out of annular space at ~ 496 K can be utilized within the cement plant (refrigeration, drying of fly ash and so on), the use of

secondary shell appears to be promising for reducing net energy consumption in the clinker manufacturing process.

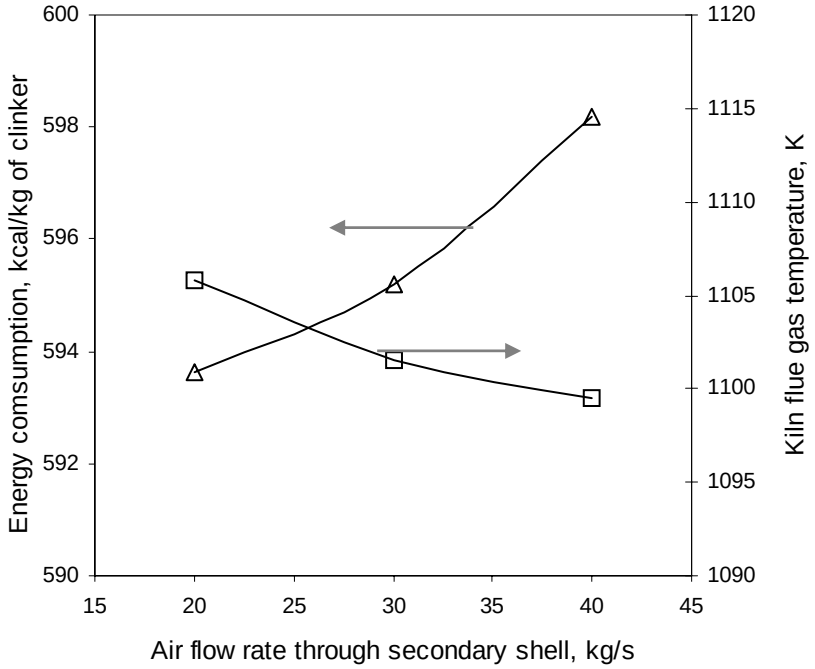

Figure 4.26: Effect of secondary shell, on overall energy consumption

4.6 Conclusions

A comprehensive model was developed to simulate complex processes occurring in pre-heater, calciner, kiln and cooler for clinker formation in cement industry. The models for pre-heater and calciner were developed assuming solids and gas to be completely back mixed. The computational model for the kiln was developed assuming gas and solids as plug flow. The integrated simulator was converted into simple to use GUI based software for cement industry, named as Rotary Cement Kiln Simulator (RoCKS). RoCKS was used to simulate performance of pre-heater, calciner, kiln and cooler for clinker formation. Detailed validation was unfortunately not possible since adequate industrial data could not be obtained. However, the model predictions agreed reasonably with industrial observations. RoCKS was used to understand influence of various design and operating parameters on overall performance. Specific conclusions based on this computational study are:

- Including an additional pre-heater reduces net energy consumption. The developed model can be used to evaluate relative benefits of energy savings by additional pre-heater and required additional capital expenses.

- There is an optimum value for percentage of calcination carried out in calciner with respect to overall energy consumption in clinker manufacture. With the parameters selected in this work, this optimum value of percentage calcination in calciner is about 70.
- The simulation results indicated that operating kiln with higher solid loading, lower RPM, lower tilt and lower grate speed reduces energy consumption per unit production. The upper limit on solid loading (bed height) and lower limits on RPM and tilt (mixing and heat transfer) need to be identified based on other practical issues.
- The use of secondary shell appears to be a promising method to reduce overall energy consumption, if the hot air generates in such secondary shell (~ 200 ^{0} C) can be utilized in some other processes in cement plants.

The model was also able to predict kiln characteristics like maximum flame temperature and overall flame length for coals with different compositions. The models and results presented here will help in developing a better understanding of clinker manufacturing process and may provide clues for possible optimization.

5. Computational Fluid Dynamics based Models for Transverse Section in Rotating Kilns

Abstract

This chapter reports development of CFD models to simulate solids motion and heat transfer in the transverse plane of a rotating kiln. The computational models for flow of solids were developed by following two approaches. Initially a CFD model for simulating gas-solid motion in a transverse plane was attempted based on the Eulerian-Eulerian approach. A pseudo two-dimensional solution domain was considered. Sensitivity of predicted results with respect to various physical parameters like particle size, restitution coefficient, maximum packing limit, frictional viscosity was studied. Emphasis was given to predict the shape of solids in the transverse plane and solids velocities at the surface. Simulated results were compared with the reported experimental data. As an alternative approach, solid motion and heat transfer in rotary cylinder was simulated assuming solids as pseudo-homogeneous fluid. Based on this approach, the computational models were developed to study heat transfer in partially filled rotating cylinders. The numerical simulations were carried out to understand the influence of key operating variables like different solid fills, rotational speeds, source temperatures and bed properties on the temperature gradients in the bed. The models and presented results will be useful to develop more comprehensive, three-dimensional CFD models of rotary cement kilns.

Publications based on this work

- *Vivek V. Ranade and Kaustubh S. Mujumdar, CFD simulations of solid motion in the transverse plane of rotating kilns, Third International Conference on CFD in the Minerals and Process Industries, CSIRO, Melbourne, Australia, 10-12 December 2003.*
- *Kaustubh S. Mujumdar and Vivek V. Ranade, CFD simulations of heat transfer in transverse plane of rotating kilns, CHEMCON- Bhubhaneshwar, 2003.*

5.1 Introduction

The previous chapters reported comprehensive reaction engineering based model for clinker manufacture in cement industry. The reaction engineering based model for rotary cement kilns was developed to gain an overall understanding of the kiln behavior. The phenomenology based kiln model was integrated with computational models for pre-heater, calciner and cooler model to develop a simulator for cement industry, which was named as RoCKS (**R**otary **C**ement **K**iln **S**imulator). The RoCKS was able to capture influence of key design (kiln dimensions) and operating parameters (RPM, solids flow rate, composition, coal flow rate and so on) on overall performance of cement kilns (energy consumption per unit weight of product, production rate per unit volume of kiln and so on). Unfortunately, RoCKS will not able to capture influence of burner design and key operating parameters like ratio of swirl or axial air etc. on performance of cement kilns. Insight into coal combustion and its influence on temperature profiles within the kiln required to be known for variety of coal available in market. In order to ensure the quality of product without jeopardizing the energy efficiency, it is essential to have a tool, which provides an insight and quantitative guidelines for manipulating burner operations. Development of a comprehensive CFD framework which can provide such information for cement kilns was therefore undertaken in this work.

In recent years, CFD based models are being applied to simulate rotary kilns (Mastarokas *et al.*, 1999; Karki *et al.*, 2000). It is possible to simulate coal burner and free board region of rotary kiln fairly accurately using the state of the art CFD models (Mastorakos *et al.*, 1999; Karki *et al.*, 2000). Before we start the development of a comprehensive, three-dimensional CFD model of a rotary kiln, it was thought desirable to understand flow, mixing and heat transfer in a transverse plane of a rotary kiln. One of the objectives of this exercise was to determine and to evolve a rational basis for possible simplifications which may be used with the complete 3D models. The computational models for flow of solids in a transverse plane were developed by following two approaches. Initially flow models using the Eulerian-Eulerian approach were attempted to model solids motion in a transverse section. Sensitivity of various physical parameters like particle size, restitution coefficient, maximum packing limit, frictional viscosity on flow of solids was studied. The predicted results for velocities were compared with available experimental data. The solid motion in transverse section was also modeled assuming solids as pseudo-homogeneous fluid. The computational model based on this approach was extended to study heat transfer in rotating cylinders. In the next section

computational model and subsequent results for solid motion in rotary cylinders are presented. This will be followed by discussion on modeling and simulated results for heat transfer in transverse section of rotary cylinders.

5.2 Motion of solids in transverse section of rotary kilns

Rotating kilns are widely used in the chemical and process industries as mixers, dryers and reactors. The ability of these equipments to handle a large volume of material along with broad particle size distribution makes these equipments very popular and common in process industry. The motion of solids in rotary kilns is extremely complex as the solids simultaneously move forward due to gravity along with enforced rotation due to revolving equipment. The solid motion and mixing in the transverse plane determines the surface renewal rate and hence the rates of bed-freeboard heat and mass transfer, as well as chemical reactions. This was the motivation to develop computational models for simulating the motion of solids in transverse section of rotary kilns. Such models can be coupled with reaction engineering and heat transfer models to develop comprehensive and reliable models for rotary kilns. Also such models can be used to explore possible simplifications which may be used while developing a 3D modeling framework.

Earlier attempts of mathematical modeling to predict solids motion in rolling mode may be classified in three categories [Ding *et al*., (2001)]. The first category is the development of simple models based on geometrical and stochastic analyses, and well-mixed tank theory for example Saeman (1951), Kramers and Crookewit (1952). These models were based on the assumption that particles in a rolling bed move in a circular motion with the rotating kiln, and then fall down from the surface of the bed in a thin layer. The time taken to fall down is small when compared to the time taken by particles to travel up in the bed. The basic model [Saeman (1951)] predicted experimental data well, and the model was further refined to predict axial moment of particles with different bed fills, taking into account the time for particles to fall down the surface of the bed. The second category is discrete particle models based on Lagrangian approach [Walton and Braun (1993), Cleary *et al*., (1998)]. The third category models are based on the Eulerian approach, which assumes solids behave as continuum and flow properties like solids concentration and velocities are continuous

function of position. [Perron an Bui (1990), Ferron and Singh (1991), Boateng and Barr (1996)].

In rotary kilns the dispersed phase has a high volume fraction, generally greater than 10 %. Since it will be computationally demanding to use the discrete particle models, the solid motion was modeled using the Eulerian-Eulerian approach i.e. treating both solids and gas as continuous phases. In this approach we develop mass, momentum and energy balances and associated constitutive equations based on volume averaging. The constitutive equations for granular flows however are not well established. Boateng and Barr (1996) developed a model, which employed boundary layer approach in deriving governing equations. They presented their integro-differential set of equations, which contained granular temperature term. Recently Ding *et al*. (2001) developed a more sophisticated model considering a quasi-static contribution, which becomes important at low rotational speed. This term was not considered in Boateng's model. The above-mentioned models use a polynomial function for the velocity profile in the active layer to get the solution to the integro-differential equations. This velocity profile is mostly obtained from experiments. The models assume surface of solids to be flat, which is not really the case especially near the walls. Most of the work was carried out at low to medium rotational speeds. Further, these models are restricted to the rolling mode of operating regime. More generalized models need to be developed which may account for different particle sizes, shapes and properties at higher rotational speeds.

Recent advances in understanding of granular flows, numerical techniques and computing resources may make computational fluid dynamics (CFD) based modeling a better approach to simulate transverse motion of solids in rotating kilns. Appropriate models to represent interphase coupling and frictional viscosity are needed. If such models are developed, these models will not require velocity profile from experiments and could be used to make 'a priori' predictions. These models could also be extended further to understand flow in other regimes as well. CFD based simulations of flow in a typical transverse section of rotating kilns, rotating at different speeds carried out initially are shown in Figure 5.1. It can be seen that the simulations qualitatively captured the different flow regimes in rotating kiln for varying rpm (The regimes for corresponding rpm is mentioned in legend in Figure 5.1).

These initial simulations have given encouragement to develop and to use CFD based models to predict flow in the transverse section.

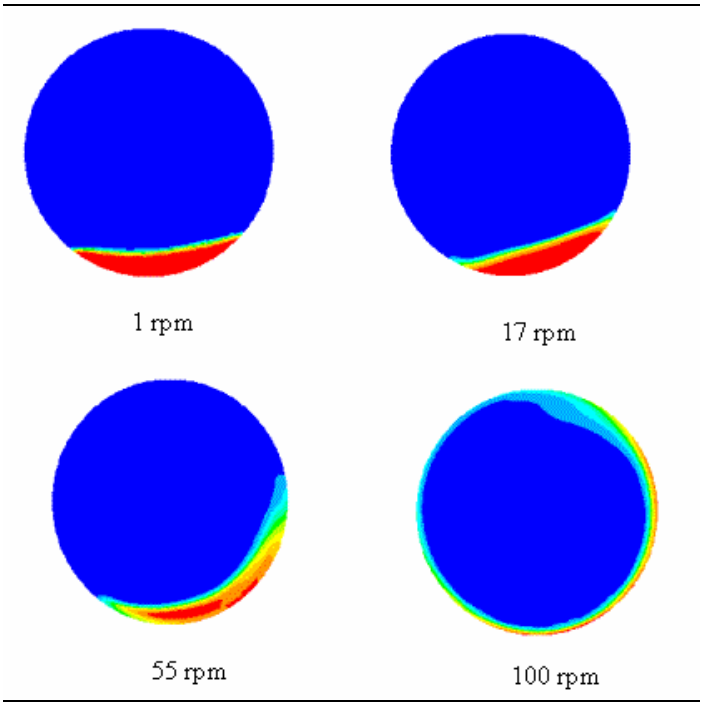

Figure 5.1: CFD simulations of different regimes in rotary kilns

(1 rpm: Slipping; 17 rpm: rolling; 55 rpm: Cascading; 100 rpm: Centrifuging)

In this chapter, we report development of a CFD based models to simulate solids flow in a kiln operating in a rolling mode. Several numerical experiments were carried out to study effect of various physical parameters like density of solids, particle size, restitution coefficient, angle of internal friction, maximum packing limit, etc on the flow. Numerical simulations were compared with the available experimental data. The model and results will be useful for understanding complex flow in the transverse plane of rotary kilns.

5.2.1 Model description

The Eulerian-Eulerian approach was used for the two phases in which both solid and gases were treated as continuum.

The continuity equation for each phase is given by

$$\frac{\partial(\alpha_k \rho_k)}{\partial t} + \nabla \cdot (\alpha_k \rho_k U_k) = 0 \tag{5.1}$$

The momentum balance for each phase is written as

$$\frac{\partial(\alpha_k \rho_k U_k)}{\partial t} + \nabla \cdot (\alpha_k \rho_k U_k U_k) = -\alpha_k \nabla p - \nabla \cdot (\alpha_k \tau_k) + \alpha_k \rho_k g + F_k + F_g \tag{5.2}$$

Where, α_k represents the volume fraction of each phase, ρ_k is the density of k^{th} phase. U_k is the velocity of k^{th} phase. P is a mean pressure shared by all the phases present in the system. There is no inter-phase mass transfer. The mass balance Equation (5.1) therefore, does not have any source term on the right hand side. Left hand side of Equation (5.2) represents the rate of change of momentum for k^{th} phase. The right hand side represents pressure forces, drag, gravitational acceleration, average shear stresses and inter-phase momentum exchange. The term F_k represents the drag interaction between the two phases. The drag force interaction between the two phases however was found to have a negligible influence on the flow of solids. Hence all the simulations were carried out without drag interaction between the two phases.

The equation describing solids flow, [Equation (5.2)] has a shear stress term in which, appropriate stress terms needs to be incorporated. Frictional and collisional interactions may govern this term [Boateng (1998)]. However, in case of rotary kilns, the particles interact with each other largely through enduring frictional contact between multiple neighbors and to a lesser extent through collisions. These frictional interactions indeed play a very important role in dense phase gas-solid flows. Particulate stresses are developed in such dense flows by frictional interactions between particles at points of sustained contact. It has been shown that frictional stresses play a critical role in maintaining stable operations of dense solid flows [Srivastsva and Sunderesan (2002)]. Recently Shrivastava and Sunderesan (2003) have presented a frictional-kinetic rhoelogical model for dense assemblies of solids in gas solid flows. They have modeled frictional stress model as proposed by Schaeffer (1987) and modified it to account for strain rate fluctuations. Schaeffer (1987) assumed that granular material is non-cohesive and that it follows a rigid-plastic rhoelogical model given by:

$$\alpha_s \bar{\tau}_s = -p_F \bar{I} + A(p_F, \alpha) \frac{S}{\sqrt{S:S}} \tag{5.3}$$

where

$$p_F = \frac{\sigma^f_{s,xx} + \sigma^f_{s,yy} + \sigma^f_{s,zz}}{3}$$
$$S = \frac{1}{2}\left(\nabla U + (\nabla U)^T\right) - \frac{1}{3}(\nabla \cdot U) I \tag{5.4}$$

and A is a function to be specified. A variety of models have been described for A(p_F , α) in the soil and granular mechanics literature. This model was modified this frictional-kinetic model and presented a model for strain rate fluctuations as (Shrivasta and Sunderesan (2003):

$$\alpha_s \bar{\tau}_s = -p_F \bar{I} + A(p_F, \alpha) \frac{S}{\sqrt{S:S} + T/d^2} \tag{5.5}$$

Simulated results obtained with these models are discussed in the following sections.

5.2.2 Geometry, grid and solver

All the numerical simulations were carried out on a cylindrical geometry with a 400 mm diameter and 3.5 mm in length. Symmetry boundary conditions were specified to the sidewalls of the cylinder. The mesh for this geometry generated using commercial grid generation software (GAMBIT of Fluent Inc.) is shown in Figure 5.2.

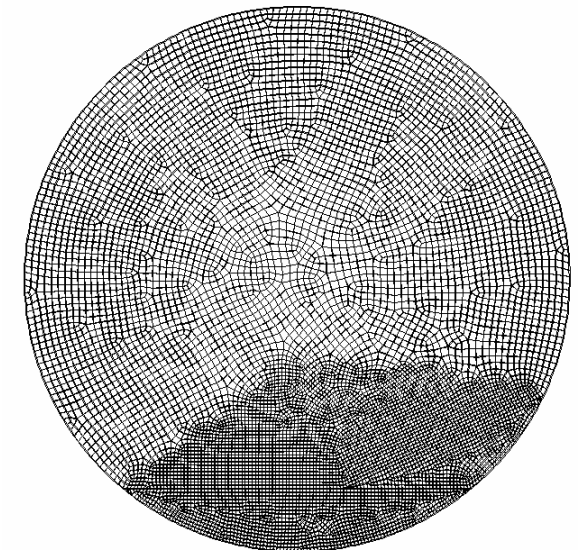

Figure 5.2: Computational grid used for simulations

The grid was refined in the lower section of cylinder where gradients are expected to be steeper. The simulations were carried out in commercial CFD code FLUENT 6.0.12. Simulations were carried out with time step of 0.0005 s and carried out until the surface velocity of the solids reached a steady state.

In the next section we outline results of a sensitivity study of various physical parameters like density of solids, maximum packing limit, restitution coefficient, particle diameter, angle of internal friction, frictional viscosity on the solids flow. Numerical simulations were also carried out for different frictional viscosity models. In all the numerical simulations carried out emphasis was given to two factors:

1. Shape of the solids in transverse section.
2. Velocity of the solids at the surface. (Tangential velocity at that point)

Ding *et al*. (2001) have reported experimental data on the flow of solids in the transverse direction in rotating drums for the rolling mode of operation. A sample of these results is shown in Figure 5.3. Their experimental data was used to evaluate the CFD model developed here.

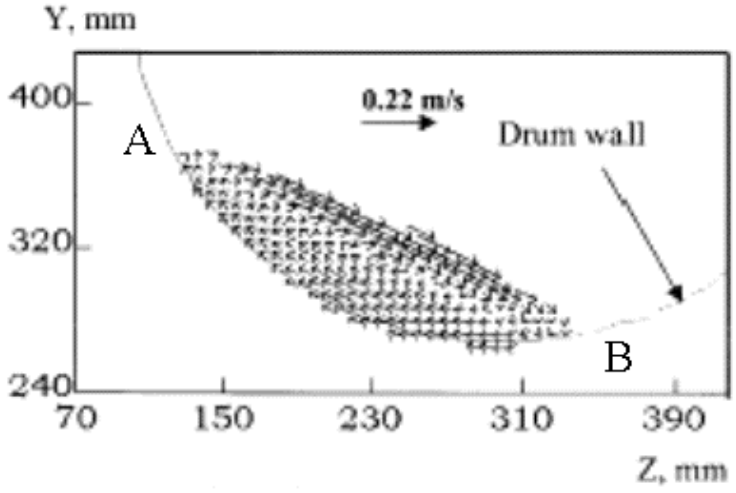

Figure 5.3: Experimental results of Ding *et al*. (2001)

5.2.3 Numerical experiments and results

The nature of solids flow in rotary kilns can change significantly with particle characteristics. It is indeed desirable to have tools to make ‘a priori’ estimates of the effects of different key parameters on the generated flow in a kiln. To quantify the influence of different parameters,

detailed sensitivity studies were carried out using the CFD model. For all the numerical experiments presented here experimental conditions of Ding et al., (2001) were used (1.7 rpm; 12 % solids fill). Initially, effect of particle diameter and restitution coefficient on flow was studied. However, for a dense bed of solids, as found in a kiln, frictional interactions are expected to be more important than these parameters. Influence of key parameters governing the frictional interactions, namely, maximum packing limit of solids (0.6), angle of internal friction (30^o) and frictional viscosity (Equation 5.3) was computationally studied (values in parenthesis denote base values at which numerical simulations were carried out). The simulations and their results are presented below.

Effect of particle diameter

Particle diameter sensitivity was studied by considering three sets of particles with diameters 1 mm, 1.5 mm and 2 mm. Other parameters like density, restitution coefficient between solids maximum packing limit were kept constant. Simulation results are shown in Figure 5.4.

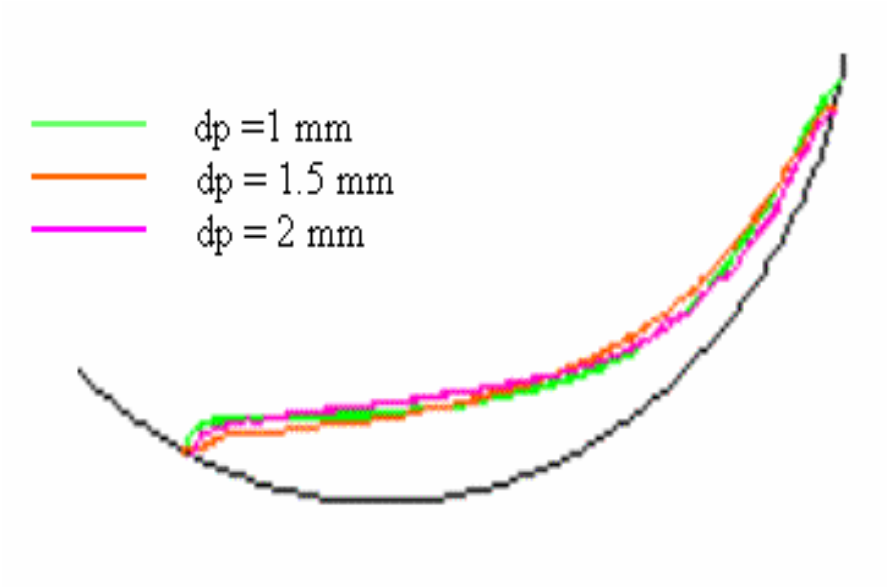

Figure 5.4: Effect of particle diameter on flow on shape

From Figure 5.4, it can be clearly seen that effect of change in particle diameter on the shape of solid bed in transverse section is insignificant. The surface velocities however were found to be dependent on particle diameter as can be seen from Figure 5.5. It may be noted that the velocities shown in Figure 5.5 are for the iso-surface of solids volume fraction of 0.5. Small changes in the shape of the surface and inherent numerical issues involved at the sharp interface might have caused the differences in the results predicted for these three particle sizes. The x-axis is the chord length of the free surface of solids (chord AB in Figure 5.3). In the figure at some points the velocity becomes negative which means that solids have changed their direction in that region.

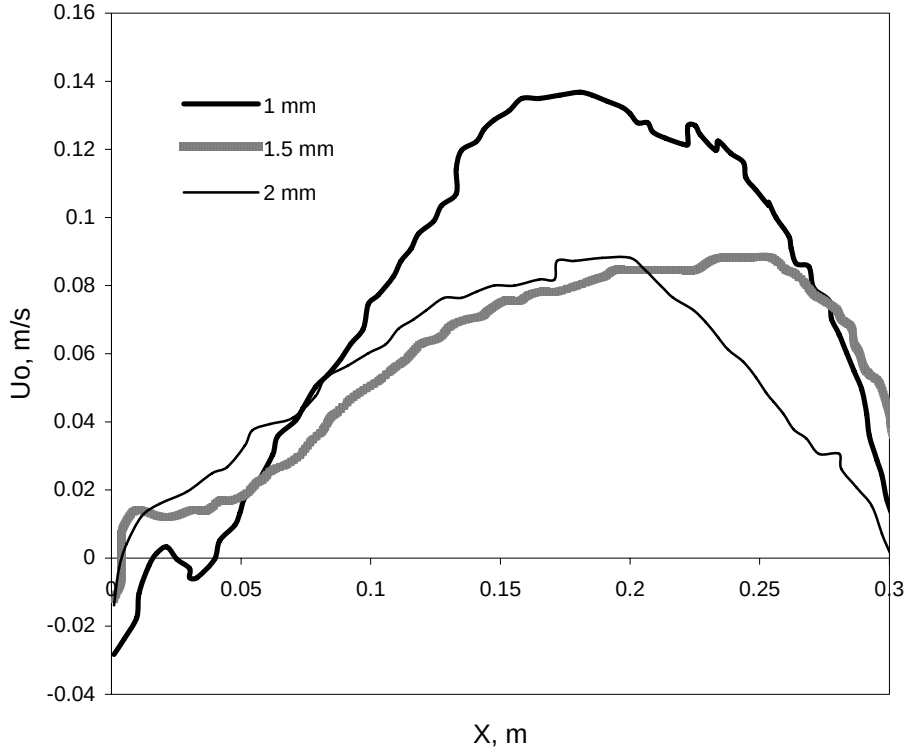

Figure 5.5: Effect of particle diameter on surface velocities of solids

Effect of restitution coefficient

Three values of restitution coefficients 0.8, 0.9 and 0.95 were used to study influence of restitution coefficient on flow of solids. The simulated results are shown in Figure 5.6. It can be seen that within the considered range the influence of restitution coefficient on shape of the solid bed in the kiln seems to be more or less same.

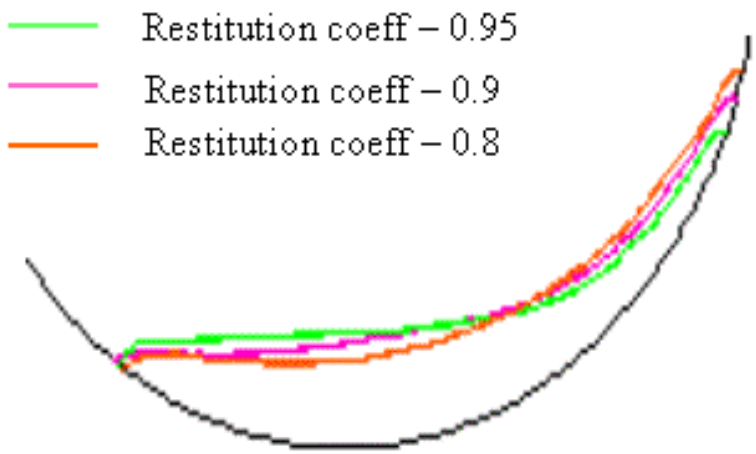

Figure 5.6: Effect of restitution coefficient on the flow

Effect of maximum packing limit on flow

Maximum packing limit of 0.6 and 0.4 were used to see the effect of the solids packing on the resulting flow. Results obtained are shown in Figure 5.7.

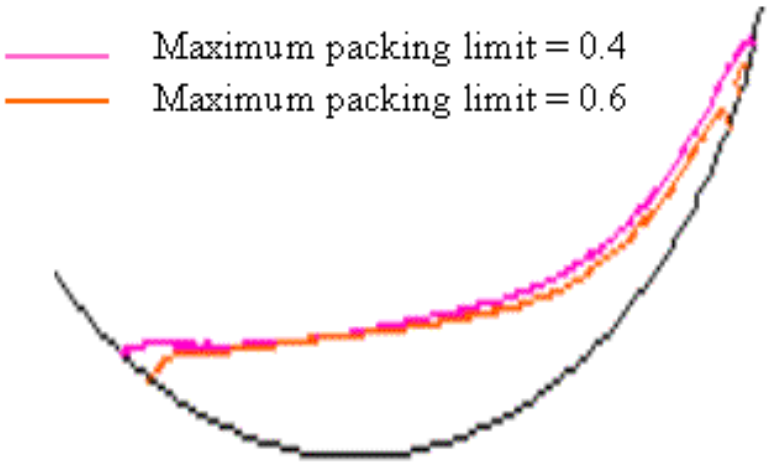

Figure 5.7: Effect of maximum packing limit on flow

From Figure 5.7 it can be seen that although there is not much of effect on the shape of the solids flow, loosely packed solids tends to move upwards in the rotating kiln.

Effect of angle of internal friction

The numerical experiments were carried out using three values of angle of internal friction 3^o, 30^o and 60^o. Since frictional interactions are expected to be high in flow of solids in rotary kilns (which will also be discussed in the next section), the effect of angle of friction was studied on a much wider range. Figure 5.8 shows results of shape of solids obtained for different angle of internal friction. From Figure 5.8, it can be seen that angle of internal friction has a significant effect on flow of solids in terms of shape. Similar effect was found on surface velocities. The effect of angle of internal friction on solids flow is complex ands needs to be understood in further detail. However, it can be concluded at this point that friction indeed plays an important role in the flow of the solids in rotating kilns

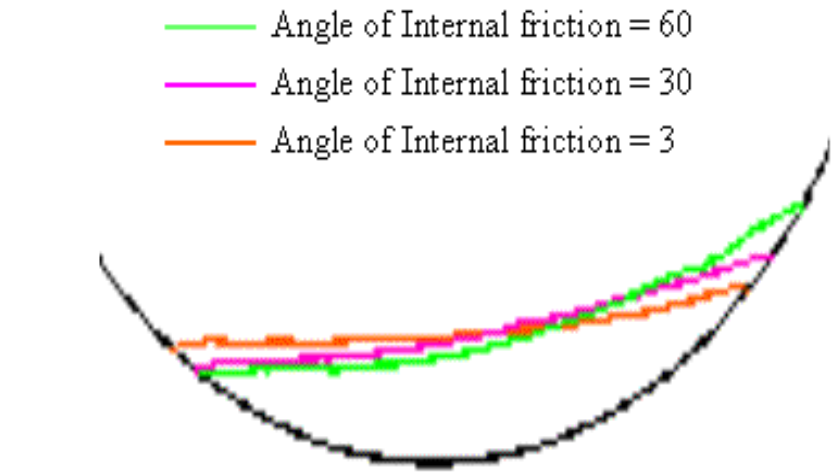

Figure 5.8: Effect of angle of internal friction of shape

Effect of frictional viscosity

Initially simulations were carried out using constant frictional viscosity values of 10, 25 and 100 Pa-s. The results obtained are presented in Figure 5.9 and Figure 5.10.

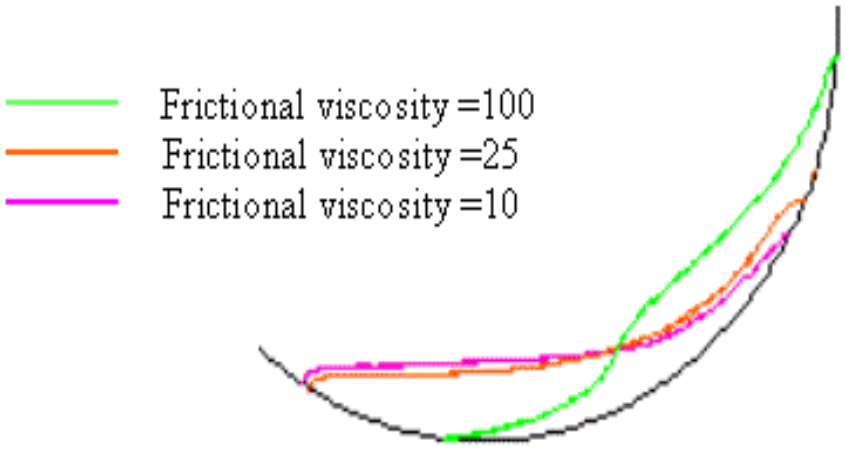

Figure 5.9: Effect of frictional viscosity on shape.

From Figure 5.9, it can be seen that frictional viscosity indeed significantly affects the shape of solids in the transverse plane. The shape of solids is widely different at frictional viscosity of 100 Pa-s than that at frictional viscosity of 10 Pa-s. The predicted surface velocities of solids were compared with each other in Figure 10. Experimental data of Ding *et al*. (2001) is also shown in Figure 5.10 to provide a reference. The physical properties of the solids, operating conditions used in these simulations were the same as those reported by Ding *et al*. (2001). It can be seen from Figure 5.10 that there is a significant difference in the surface velocities for different frictional viscosities. Although, frictional viscosity in the range of about 10 Pa-s gives a better agreement with the experimental data as compared to the other values, around this value of viscosity the shape of solids in the transverse section did not match with the experimentally reported shape (see Figure 5.3). For frictional viscosity of 100 Pa-s, the shape seems to be satisfactory but the surface velocities did not match with the reported values. These initial simulations clearly indicates that further work on modeling frictional viscosity is needed to predict the flow with adequate accuracy.

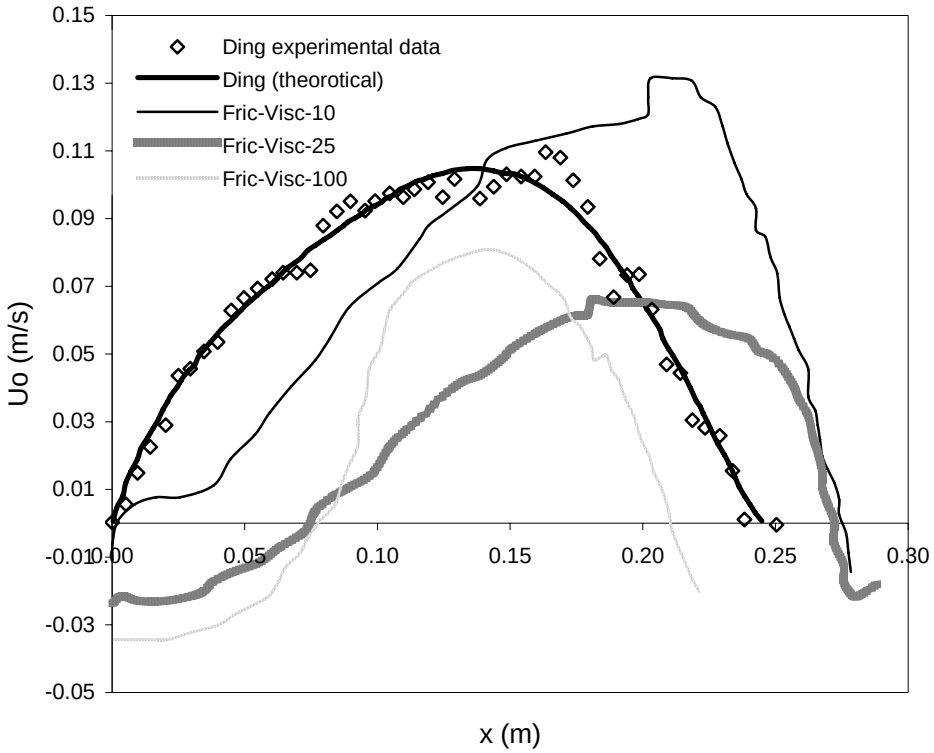

Figure 5.10: Effect of frictional viscosity on surface velocities

Frictional viscosity models

Simulations were carried out using frictional viscosity models proposed by Schaeffer (1987) and Shrivastava and Sundaresan (2003). The simulation results are shown in Figure 5.11.

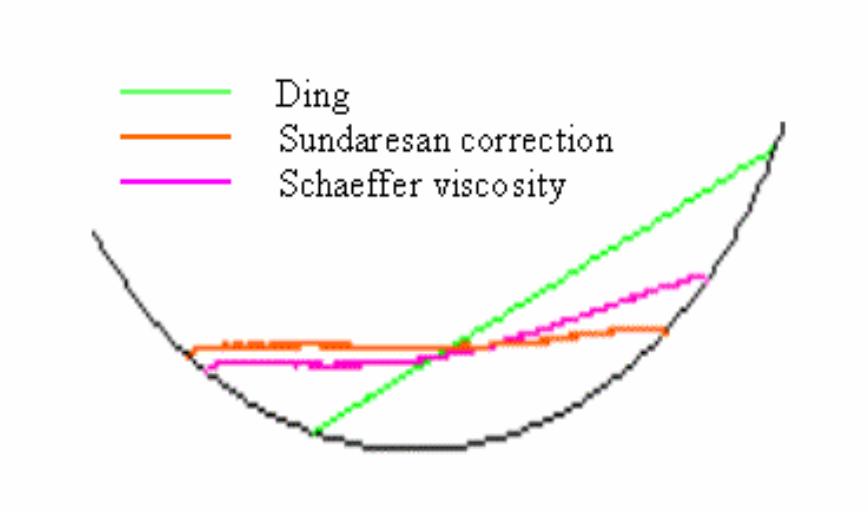

Figure 5.11: Effect of frictional viscosity on shape

From Figure 5.11 it can be seen that using frictional viscosity proposed by Schaeffer (1987) and Shrivastava and Sundaresan (2003), the predicted shape of the solids did not match with the experimentally observed shape. The angle of repose obtained by simulations is about 8^o which further deteriorates as solids move down the surface, where as the experimentally obtained angle of repose is about 25^o.

Comparison of solids velocity at the surface is shown in Figure 5.12. Close examination of Figures 5.11 and 5.12 indicates that prediction of the shape of solids bed in the kiln and prediction of surface velocity of solids are intimately linked with each other. It can be seen that, in the top portion of the solids bed, where angle made by the predicted bed surface is closer to that observed in the experiments, the predicted velocities are in good agreement with the experimental data. In the bottom portion, the predicted shape of bed is too flat compared to that observed in the experiments. Consequently, the predicted velocities are much smaller than the experimentally observed values. The right prediction of the shape of the solids bed is crucial for better predictions of solids motion in the kiln.

The velocity profiles obtained in the interior of the bed using Schaeffer viscosity model is shown in Figure 5.13a. Although the surface velocities could not be captured well by the described computational models the prediction of interior velocities was not bad.

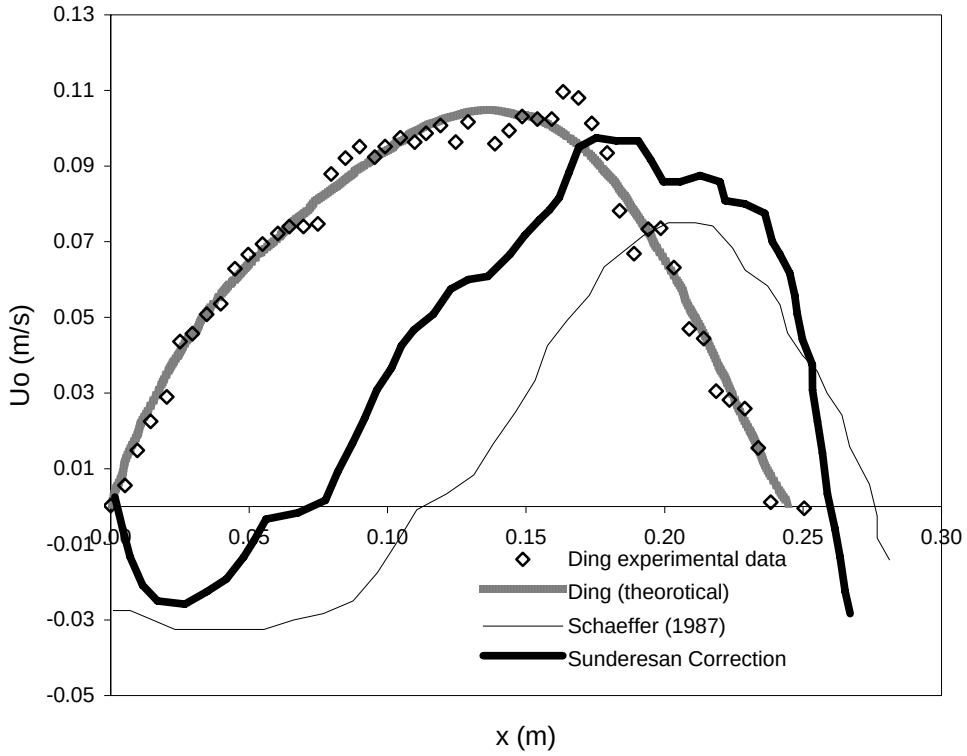

Figure 5.12: Comparison of surface velocities for frictional viscosity models

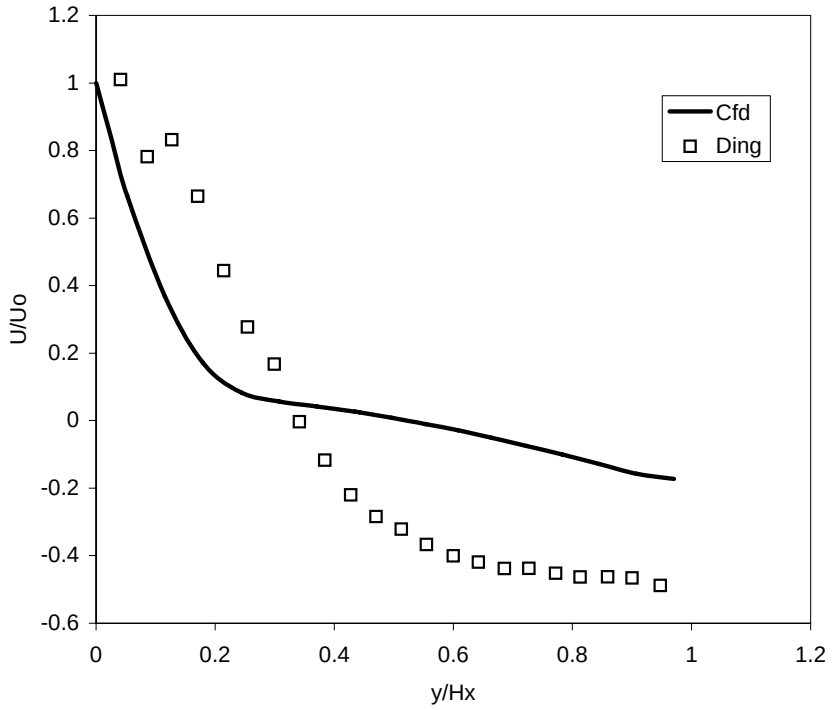

Figure 5.13a: Comparison of bed interior velocities predicted by Schaeffer's model

Solids as pseudo fluids

The previous section of the chapter discussed about modeling solid motion in transverse section of rotary kiln using different frictional viscosity models. However, these simulations were not very successful from the point of quantitative prediction of velocity profiles in the bed. Computational models were also developed by assuming solids as pseudo-homogeneous fluid to predict motion of solids in transverse plane. Simulations were carried for the identical geometry and operating conditions for rotary kiln as described in previous section (Ding *et al*., 2001).

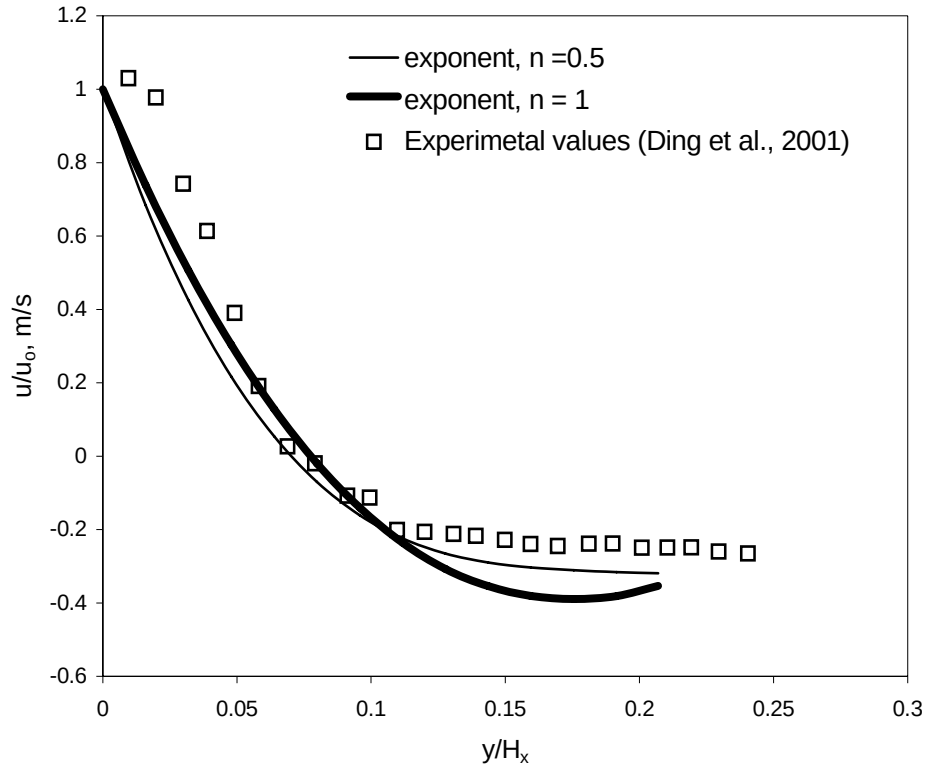

Figure 5.13b: Comparison of bed interior velocities assuming solids as pseudo fluids

For these simulations however, solids were assumed as fluids with constant viscosity and power law viscosity. The results obtained from these simulations were qualitatively similar to those obtained in the previous section. The velocities obtained at the bed surface did not match qualitatively with experimental results. A typical comparison of simulated values of velocities in the bed interior for one of the case assuming power law viscosity (n = 0.5 and n = 1 i.e. constant viscosity) is shown in Figure 5.13b. These results seem to be comparable with results obtained for Schaffer's frictional viscosity models (see Figure 5.13a). It can also

be seen from these simulation that the differences in predictions of velocities considering power law viscosity and constant viscosity for fluids were insignificant. Considering the relatively similar performance of model developed in this work (based on the Eulerian-Eulerian approach) and the pseudo-homogeneous approach, the latter approach was used to study heat transfer in transverse section of rotary kilns.

5.3 Heat transfer in transverse section of rotary kilns

The heat transfer in rotary kilns is very important as determines its overall performance in terms of product quality and uniformity. The temperature gradients, if present in radial direction can directly affect the kiln performance in terms of product uniformity. Hence it is essential to develop a model which can predict heat transfer (for a set of operating conditions) in transverse section of rotating kilns. Therefore, a 2D model was developed to study temperature gradients in transverse section of bed. This section reports the development of CFD models to simulate heat transfer in the transverse plane of a rotating kiln. In these simulations solids were treated as pseudo homogeneous fluids as described earlier. The idea was to check if CFD models are able to predict temperature gradients in bed reasonably well by assuming solids as pseudo-homogeneous fluid. Numerical simulations were carried out to see the influence of key operating variables like different solid fills, rotational speeds, source temperatures and bed properties on the temperature gradients in the transverse plane. A fictitious heat source was assumed in the central region of the cylinder to provide heat to the solid bed. Heat transfer occurs by all possible modes i.e. conduction, convection and radiation. The bed of solids receives heat from the free board gases by radiation and convection. Along with this, the bed receives heat from kiln walls by radiation and by conduction. Also, there is convective and radiative heat transfer between the free board gas and kiln internal walls. One needs take into account all the above mentioned modes of heat transfer in the model for accurate prediction of temperature gradients in the transverse plane.

5.3.1 Model description

In this work a pseudo-2D model was formulated using the CFD framework to study the heat transfer. The cylinder geometry and grid used for numerical simulations is explained in the next section. A fictitious heat source at constant temperature is assumed in the central region of the cylinder to provide heat to the solids bed. The heat given by this source to the bed is analogous to the heat given by the flame in the rotary kilns.

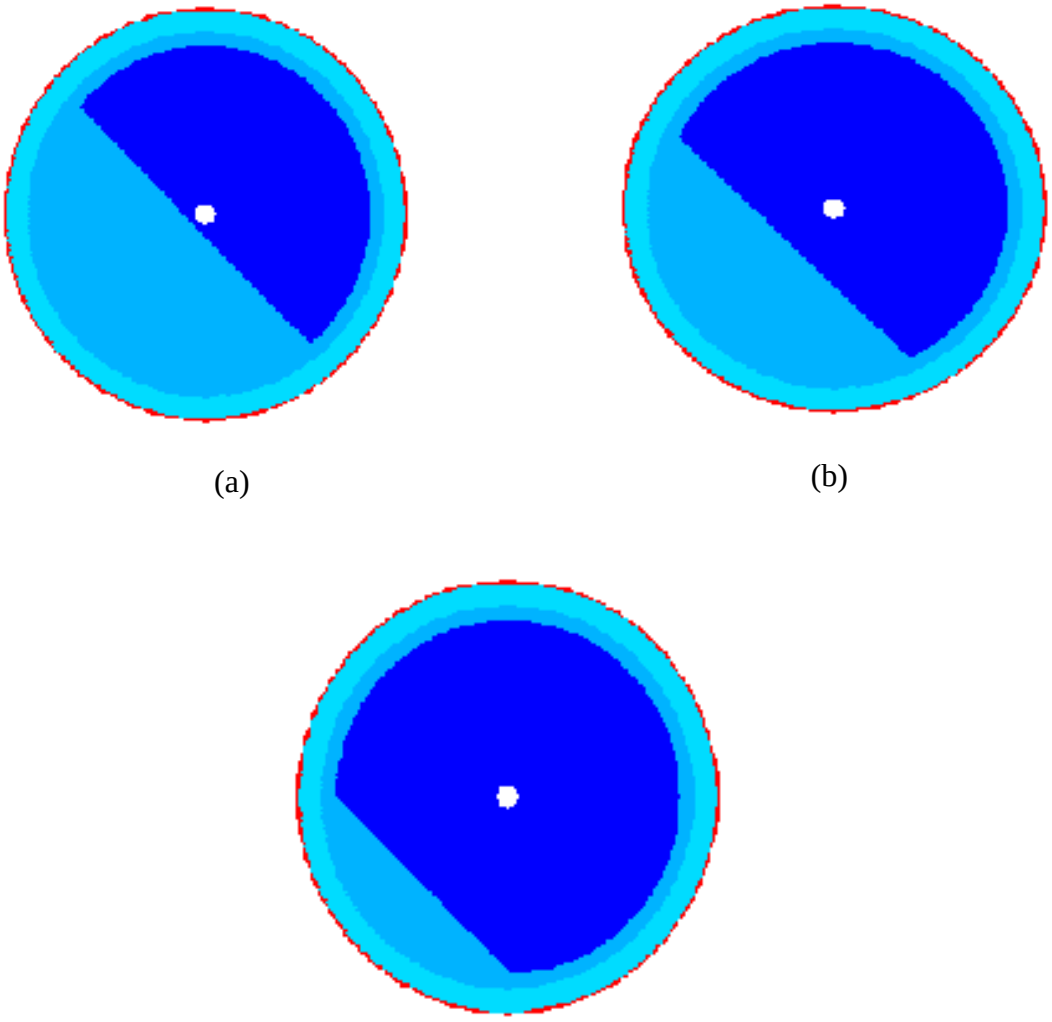

(a) (b)

(c)

Figure 5.14a: Different solid fill for simulation study

The density of solid bed is assumed to be constant along with material properties. In this work, we have assumed solids to be pseudo homogeneous fluids with constant viscosity. Chemical reactions are not considered at this stage. But, the overall framework is such that they can be incorporated at a later stage. The cylinder outer wall is given rotational boundary condition and heat loss through outer wall is modeled using convection and radiation. The sidewalls of cylinder are given symmetric boundary conditions to reduce required computations. Ambient temperature is assumed to be 300 K and convective heat transfer

coefficient is considered to be about 25 W/m^2 K. Mass, momentum and energy conservation equations are given below.

Bed region

Mass conservation equation:

$$\frac{\partial \rho}{\partial t} + \nabla \cdot (\rho u) = 0$$

Momentum conservation equation:

$$\frac{\partial (\rho u)}{\partial t} + \nabla \cdot (\rho u u) = -\nabla p - \nabla \cdot \sigma + \rho g$$

Energy conservation equation:

$$\rho C_p \frac{\partial T}{\partial t} + \rho C_p u \cdot \nabla T = \nabla \cdot (k \nabla T) + \sum_{i=1}^{N_c} R_i (-\Delta H_{r,i})$$

Free board region

The mass and momentum conservation equations remain same with appropriate changes in material and their properties. The energy conservation equation with required changes is given below

Energy conservation equation

$$\frac{\delta (\rho E)}{\delta t} + \nabla \cdot (v(\rho E + p)) = \nabla \cdot (k_{eff} \nabla T - \Sigma h_j J_j + (\tau_{eff} \cdot v)) + S_h$$

The first three terms on the right hand side of the equation represent heat transfer due to conduction, species diffusion and viscous dissipation respectively. S_h represents the heat source due to chemical reactions or other volumetric heat sources. Here in this case the fictitious heat source is the heat source to the solids. Radiation is modeled using the simple P-1 model. This is the simplest case of more general P-N model, which is based on the expansion of the radiation intensity into an orthogonal series of spherical harmonics.

A two dimensional geometry for the cylinder is considered in this study. The cylinder interior contains solid bed with three layers of solids viz. coating, refractory and steel shell (R_{in}= 3.14 m, $R_{in,\ refr}$= 3.4 m, $R_{in,\ sh}$= 3.8 m, $R_{out,\ sh}$= 3.85 m). Numerical simulations are carried out at

three different heights (h ≈ R, h = 2R/3, h = R/3, a, b and c in Figure 5.14a respectively) with various rotational speeds, source temperatures and properties of bed material. The mesh for this geometry generated using commercial grid generation software (GAMBIT of Fluent Inc.) is shown in Figure 5.14b. The simulations are carried out in commercial CFD code FLUENT 6.0.12. Steady state simulations were carried out till the heat flux given by the source and outer wall (steel shell) of cylinder is same.

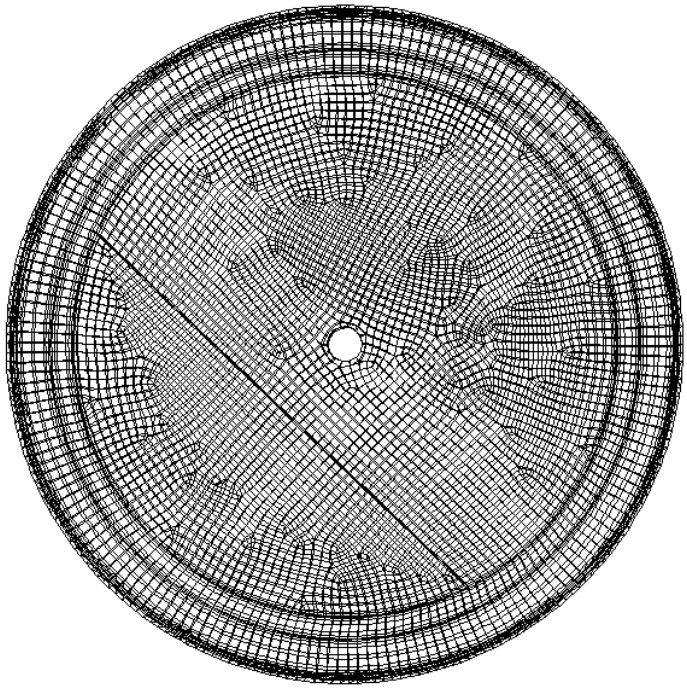

Figure 5.14b: Sample of grid used for simulation

5.3.2 Numerical experiments and results

Several numerical experiments were performed to see the influence of important operating variables like different solid fills, varying rotational speeds, source temperatures and bed properties on the temperature gradients in the solids bed. In all the numerical experiments, the source is given a fixed temperature for a particular set of experiments. Initial attention was focused to analyze the temperature gradients in bed (assumed as pseudo fluid) by variation in operating parameters like solids fill, rotational speed and source temperature. Radiation is expected to have a significant effect on the heat transfer. Hence, in the next set of simulations

influence of absorption coefficient of the freeboard gas on temperature gradients is studied. Finally thermal conductivity of solids is changed to see the effect on the heat transfer.

Effect of bed height and rotational speed

The solids fill in rotary kilns has a significant effect on heat transfer in transverse section. Higher solids fills will tend to have higher temperature gradients and require more energy requirements. Lower solids fill not only results in lower production capacity but also may have an impact on life of refractories and kiln shell. We consider in our study three different solid fills, as shown in Figure 5.13. The numerical simulations are carried out for 2 different rotational speeds 1 rpm and 5.5 rpm and stationary cylinder as well. The source temperature is kept at 1700 K. Such high temperatures are often encountered in rotary kilns. The results for these 9 numerical experiments are shown in Table 5.1.

Table 5.1: Influence of different solid fills

	Stationary	1RPM	5.5 RPM
High Height	3	2.4	0.5
Medium Height	2.4	0.6	0.4
Low Height	0.2	0.1	0.3

Figure 5.15 shows contours of temperature in the bed for different solids fill (column 1 of Table 5.1) when bed is not given any rotation. Table 5.1 gives quantitative estimation of temperature gradients with in the bed. The gradients in the bed are higher in cases of stationary bed as there is no mixing of the solids. The gradients reduce when the cylinder is given rotation as mixing is enhances. The temperature gradients in the solid bed increases as the height of the bed increases, which is as expected.

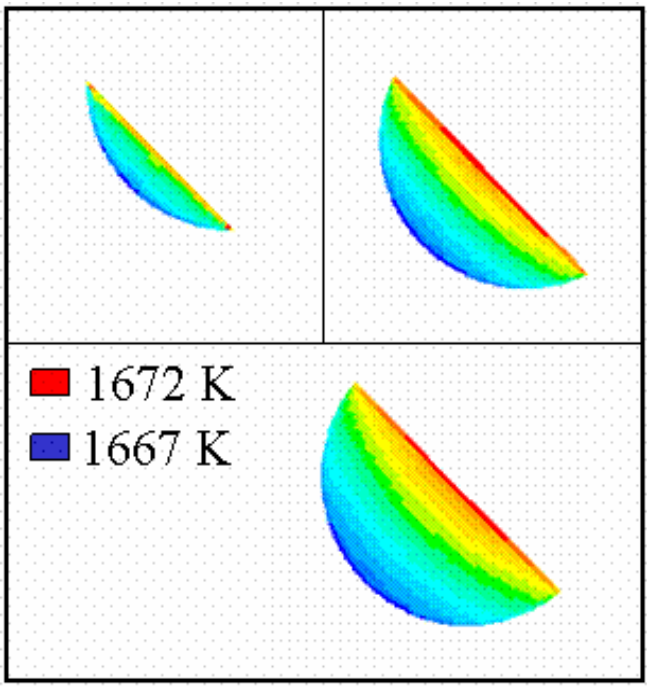

Figure 5.15: Contour plots of temperature for different solids fill

Effect of source temperature

It can be seen from above analysis that the temperature gradients are quite small (only a difference of 3 K for even 50 % solids fill). The reason for this could be that the source temperature being at very high temperature. The temperature in kiln varies along the kiln length for industrial kilns and hence it is necessary to analyze results at lower source temperatures as well. Therefore, 2 simulations are carried out in order to see the effect of source temperature on heat transfer. Three source temperatures considered here are tabulated below along with the results. For the above runs, the kiln is not given any rotation and simulations are carried on high solids fill ($h \approx R$) is considered as it is expected to give largest temperature gradients. As can be seen from the table, the temperature gradients rise with decreasing the source temperature. Also, as the source temperature decreases the overall heat the bed will receive will decrease. Hence the average temperature of bed will decrease if source temperature decreases. This is what we get from our simulations as well.

Table 5.2: Influence of source temperature

	High height (stationary)	
Source Temperature	Temperature Range (K)	ΔT_{MAX} (K)
1700 K	1666– 1669	3
1350 K	1300 – 1306	6
1000 K	917 – 930.	13

Effect of rotational speed

The effect of rotational speed on the gradients is already mentioned. We can appreciate its role better in case of lower source temperatures. Two runs are carried out at lower source temperature for rotational speeds of 1 rpm and 5.5 rpm. The results for these runs are tabulated below.

Table 5.3: Influence of rotational speed

	High height	
RPM	Temperature Range (K)	ΔT_{MAX} (K)
Stationary	917 – 930	13
1 rpm	924- 927	3
5.5 rpm	924-924.5	0.5

From the results it can be seen that the temperature gradients slowly vanish as the rotational speed increases. Interesting thing to note is that even at 1 rpm, temperature gradients decrease significantly as compared to stationary case. This is also found in other simulations. This probably means, even for small rotation speeds uniform temperature is achieved in the transverse section of the kiln.

Effect of radiation absorption coefficient

From the literature, it is seen that radiation has a significant contribution to heat transfer in transverse plane than convection and conduction. The effect of radiation on total heat transfer

could be verified by manipulating absorption coefficient of the freeboard gas. The absorption coefficient of the freeboard gas, which is assumed to be 0.7, is reduced to 0.07 in a couple of steps. Although this seems to be a bit unrealistic, this will clearly state the roll of radiation in the heat transfer. The results for these runs are tabulated below. From the above runs, the dominant role of radiation is displayed for heat transfer in rotary kilns (Compare run 3 in Table 2 and run 3 in Table 5.4). It can be seen that as absorption coefficient decreases the heat received by the bed due to radiation decreases. The result of this is the overall bed temperature reduces significantly (by about 150 K).

Table 5.4: Influence of Radiation

High height (stationary)		
Source Temperature	Temperature Range (K)	ΔT_{MAX} (K)
1700 K (absorption coeff = 0.7)	1666– 1669	3
1700 K (absorption coeff = 0.07)	1565 -1596	31.
1000 K(absorption coeff = 0.07)	727.6 –826.5	98.9

Effect of effective thermal conductivity

Finally the effect of the change in clinker properties is considered. The clinker thermal conductivity is increased from 0.5 to 200 W/m K. This physically would simply mean that the mixing in bed is very good. The effect of using higher thermal conductivity is thus same as that of giving rotation to the rotary kiln. The idea behind this is to check if effective thermal conductivity could be used instead of giving rotational boundary condition to the shell to reduce the computational requirements. Following is the comparison of the results for true clinker thermal conductivity and enhanced clinker thermal conductivity with no rotation given to the kiln.

Table 5.6: Effect of effective thermal conductivity

	High height (stationary)	
Thermal conductivity of clinker	Temperature Range (K)	ΔT_{MAX} (K)
0.5 W/ m K	1566 - 1597	31
200 W / m K	1609 - 1621	12

The drastic increase in thermal conductivity of clinker has resulted in less temperature gradient as expected. However, the temperature gradients almost fade out when rotation boundary condition is specified. Hence a more quantitative relation between the rotational speed and effective thermal conductivity needs to be developed. The effective thermal conductivity should also be implemented carefully as the overall bed temperature increases when effective thermal conductivity is used instead of rotational boundary condition.

5.4 Conclusions

Computational models for modeling motions of solids and heat transfer in transverse section of rotating cylinders were developed in this study. Following are the conclusions of the present work.

- A detailed sensitivity study of various physical parameters like diameter of solids, restitution coefficient, maximum packing limit, angle of internal friction, frictional viscosity revealed that frictional viscosity has the most significant influence on flow of solids in transverse plane.
- Solid flow was simulated using a constant frictional viscosity initially and then by using models proposed by Schaeffer (1987) and Shrivastava and Sundaresan (2003) with the CFD models. However, the simulation results did not agree with the experimental results quantitatively. Use of simpler models like pseudo-homogeneous assumption for the solids phase were found to give results similar to those with much more complicated models. Further work is needed to accurately

model motion of the solids in bed of rotating kilns. In absence of this, all the subsequent cement kiln simulations were carried out by treating solids as pseudo homogeneous phase.

- Numerical study carried out considering solids as pseudo fluids predicted reasonable trends for temperature gradients in bed of rotating kilns at least qualitatively. Further work is required in order to have quantitative validation in this respect.

6. Computational Fluid Dynamics based model for Rotary Cement Kilns

Abstract

In this chapter, we report a comprehensive computational fluid dynamics (CFD) based model to capture key transport processes in rotary cement kilns. Separate but coupled computational models were developed for the bed and the freeboard regions of the rotary kiln. The complex swirling air flow produced by kiln burners, coal combustion, gas phase combustion of volatile matter and radiative heat transfer in free board region were modeled. The clinkerization reactions in the bed region were modeled assuming solids as pseudo fluids. Coating formation in cement kilns (for both bed and freeboard regions) was considered. Appropriate source and sink terms were developed to model transfer of CO_2 from the bed to the freeboard region due to calcination reaction in the bed region. The developed bed and freeboard models were coupled by mass and energy communication through common interface. These coupled computational models were able to predict the available data from industrial kilns and previously published results quite satisfactorily. The computational models were also able to predict the intricacies of burning zone of rotary cement kilns for changing burner operational parameters like axial to swirl ratio and oxygen enrichment. The developed approach, computational models and simulation results will not only help in developing better understanding of cement kilns but also provide quantitative information about influence of burner design and other design parameters on kiln performance.

Publication based on this work

- *Kaustubh S. Mujumdar and Vivek V. Ranade, "CFD Modeling of rotary cement kilns" accepted for publication in Asia Pacific Journal of Chemical Engineering*
- *Vivek V. Ranade and Kaustubh S. Mujumdar, March 2006, "Gain an insight into coal fired cement kilns using CFD", The Chemical Engineer, UK*

6.1 Introduction

This chapter discusses development of comprehensive CFD model for rotary cement kilns. As discussed earlier, the developed 1D model (in Chapter 3) cannot adequately capture influence of burner design and key operating parameters like ratio of swirl to axial air, oxygen enrichment, etc. on flame characteristics and performance of cement kilns. The knowledge of influence of these parameters on coal combustion, flame characteristics and temperature profiles within the kiln is essential to ensure optimum performance of kilns. Computational fluid dynamics (CFD) framework offers promise of becoming such a tool. Development of a comprehensive CFD framework which can provide an insight and quantitative guidelines for burner design and optimization for cement kilns was therefore undertaken in this work. The complexity and co-existence of a wide range of spatio-temporal scales and processes in rotary cement kilns demand different and unconventional approaches for developing CFD models. Some attempts of developing CFD models for rotary cement kilns have been made (for example, Kolyfetis and Markatos, 1996; Karki *et al.*, 2000). These models were limited only to predict the overall behavior of cement kilns. These models did not consider some of important processes like coating formation or modeling clinkerization reactions. This chapter reports the development of CFD models, which adequately accounts for most of the relevant processes occurring in cement kilns and provides a tool to predict the influence of burner design and operational parameters on the overall performance.

In the next section of the chapter, we discuss the computational model in detail. Previously published CFD models were critically reviewed before presenting the approach and model developed in this work. A solution methodology and simulated results are discussed thereafter. The computational model was then used to understand influence of various burner operating parameters on the kiln performance. Key conclusions based on this work are discussed at the end.

6.2 Computational Model

Cement kilns are complex systems which involve occurrence of several simultaneous processes in both bed and freeboard region. It is therefore essential to first identify key issues and use appropriate methodology to develop tractable computational models for rotary cement kilns. The main key issues which need to be considered while developing comprehensive model for cement kilns are flow, heat transfer and reactions occurring in bed

and freeboard region. These issues are discussed in detail chapter 2 and will not be repeated in this chapter. It is important to note that most of the previously published CFD models do not consider these key issues during model development as is discussed below.

6.2.1 CFD models for cement kilns

Due to complexity of physics involved, occurrence of multiple phases with large number of reactions in bed/freeboard regions, very few CFD models have been published for rotary cement kilns (Kolyfetis and Markatos, 1996; Mastorakos *et al.,* 1999; Karki *et al.,* 2000). Most of these computational models do not account the main key issues simultaneously in a single framework as discussed in Chapter 2. Mastorakos *et al.* (1999) developed a CFD based model for cement kilns, which included combustion, radiative heat transfer, conduction in the bed/ walls and chemical reactions. The bed and freeboard models were thus treated as separate domains and coupling between them is handled explicitly. However, the geometry of kiln was assumed to be axisymmetric in this work and therefore the boundary conditions were applied only in an approximate manner. Moreover, Mastorakos *et al.* (1999) assumed coating formation throughout the kiln length. Karki *et al.* (2000) developed a 3D CFD based model for simulating simultaneous combustion and heat transfer in cement kilns. Karki *et al.* (2000) have used an effective thermal conductivity to define degree mixing in bed region, developing a single computational model for simulating cement kilns. Different values of effective thermal conductivities at different locations in the kiln were used. However, there are no proper guidelines to choose proper effective thermal conductivity and the values used are based on experience. Moreover, Karki *et al.* (2000) have focused on fluid dynamics and heat transfer and did not model clinkerization reactions. The model predictions thus gave only qualitative agreement with industrial observations reasonable for global quantities of interest. Kolyfetis and Markatos (1996) also focused on coal combustion and heat transfer in freeboard region and did not account clinker reactions. Also, Kolyfetis and Markatos (1996) did not consider any coating formation in their computational model. The above discussion clearly indicates that CFD based models presented earlier for cement kilns are more or less approximate and not rigorous models. A comprehensive model for cement kilns should account for simultaneous flow, heat transfer and reactions occurring in rotary cement kilns.

It is also important to note that along with physical issues that needs to be captured, there are numerical issues involved in cement kiln modeling. The free board region of the kiln in

which combustion of coal takes place and the bed region of the kiln where clinkerization reactions take place are strongly coupled with each other. However, the characteristic time and space scales of free board region and bed region are significantly different. The typical velocities of gas phase in the free board region is about 10 m/s while typical velocities of solid particles in the bed region is of the order of a typically about 0.05 m/s. In addition to the time scales of the free board and bed region, actual chemical reactions occur at the scale of the particles, which is much smaller than length scale of a kiln. Considering these vastly different characteristic time and length scales of processes, building a single computational fluid dynamics (CFD) based model with an objective of capturing all the relevant space and time scales might fail it can become computationally extremely expensive. Earlier, Spang (1972) has also reported convergence difficulties while solving flow, heat transfer and reactions in the freeboard and the bed region simultaneously. Therefore in the present work, we develop separate but coupled models for the bed and the freeboard regions. The strategy was to simulate different regions with similar time scales separately and then couple them by mass and energy communication via common boundaries. The methodology adopted will be explained in detail in the next section. Before that we discuss the individual model equations for bed and freeboard in the following.

6.2.2 Bed model

Several solid-solid and liquid-solid reactions occur in the bed region of rotary cement kilns. The five major reactions considered by most of the researchers are given in Table 1. It can be seen that these reactions involve components like $CaCO_3$, CaO, C_2S, C_3S, C_3A and C_4AF. While formation of some of the minor phases viz. $C_{12}A_7$, C_2AS, CS, C_3S_2, CS_2, CF, C_2F etc. have been reported (Hewlett, 1998), they are generally present in insignificant amount and hence are usually neglected for modeling purposes (Spang 1972; Mastorakos *et al.*,1999). We also consider only five major reactions occurring in cement kilns during clinker formation (as given in Table 6.1) in the present study. One of the important issues in modeling these reactions is the availability of the relevant kinetics. In Chapter 2 of the thesis, we have critically analyzed the modeling of clinkerization reactions in cement kilns. The kinetic parameters used in this work for clinker formation reactions were shown to work reasonably well for 3 different industrial kilns covering wide range of operational conditions. Therefore, these parameters were used to model kinetics in the present work

Table 6.1: Reactions, kinetics and heat of reactions (Refer Table 3.2, Chapter 3)

	Reaction	k_0	E (kJ/mol)	ΔH (kJ/mol)
Bed				
1.	$CaCO_3 = CaO + CO_2$	1.18×10^3 (kmol/m^2-s)	185	179.4
2.	$2CaO + SiO_2 = C_2S$	1.0×10^7 (m^3/kg-s)	240	-127.6
3.	$C_2S + CaO = C_3S$	1.0×10^9 (m^3/kg-s)	420	16.0
4.	$3CaO + Al_2O_3 = C_3A$	1.0×10^8 (m^3/kg-s)	310	21.8
5.	$4CaO + Al_2O_3 + Fe_2O_4 = C_4AF$	1.0×10^8 (m^6/kg^2-s)	330	-41.3

In our one-dimensional model of rotary cement kiln, the height variation of bed along the kiln length was modeled using Kramer's model (See for example, Chapter 3 of the thesis). The same bed height profile can in principle be included in the CFD model. However, since the focus was on understanding flame characteristics, the bed height variation along the kiln was ignored in the present work to simplify the grid generation.

The motion of solids in rotating cylinder exhibits complex motion and various flow regimes. Attempts have been made to simulate motion of solids in transverse section of rotating cylinders as discussed in Chapter 2. The state of the art CFD models developed in Chapter 5 did not capture the details of solids motion accurately. These preliminary studies on simulations of motion of solids in transverse plane of rotating cylinder however, indicated that the flow generated in transverse section of kiln might be approximated by treating solids as pseudo homogeneous fluids. The constant viscosity as well as power law viscosity model was evaluated. Based on these studies, in this work we have treated solids as pseudo homogeneous fluids with constant viscosity (2 kg/m-s).

Another important aspect of cement kilns is the formation of coating which has significant influence on shell temperature profile and heat transfer. Formation of coating in cement kilns is a complex function of liquid formation in bed, flow/reactions occurring in bed and freeboard regions, kiln RPM and energy exchange between bed and freeboard. The phenomenon of coating formation in cement kilns is not yet well understood. In the reaction engineering based model developed in Chapter 3, the location of coating formation was calculated as a part of the solution of model equations. Nevertheless, such an approach is

difficult to use with the CFD framework since it will involve dynamic meshing. The model predictions for three industrial kilns with varying operating conditions and dimensions presented in Chapter 3, showed that, the coating formation occurred only after half of the kiln length from solids entry. This also seems to be consistent with shell temperature measurements reported by Kolyfetis and Markatos (1996). However there is no data/model which gives inputs regarding beginning of coating formation in cement kilns. In absence of any information, the location of coating formation was assumed to be formed at 50 % of kiln length from the feed end.

It was essential to formulate appropriate boundary conditions for the kiln walls to estimate the heat losses through the kiln shell. The outer wall of the kiln was given a rotational boundary condition (5.5 RPM, see Table 3) and heat loss through the shell was modeled using convection and radiation. Ambient temperature was assumed to be 300 K. The convective heat transfer coefficient was considered to be 30 W/m^2 K as suggested by Mastorakos *et al.* (1999) for industrial cement kilns. Mass, momentum and energy conservation equations for the bed region are given below.

Mass conservation equation:

$$\frac{\partial \rho}{\partial t} + \nabla \cdot (\rho u) = S_{m,b} \tag{6.1}$$

Momentum conservation equation:

$$\frac{\partial (\rho u)}{\partial t} + \nabla \cdot (\rho u u) = -\nabla p - \nabla \cdot \sigma + \rho g \tag{6.2}$$

Energy conservation equation:

$$\frac{\partial (\rho E)}{\partial t} + \nabla \cdot (u(\rho E + p)) = \nabla \cdot (k_{eff} \nabla T - \Sigma h_j J_j + (\tau_{eff} u)) + S_{e,b} \tag{6.3}$$

Species conservation equation:

$$\frac{\partial (\rho Y_i)}{\partial t} + \nabla \cdot (\rho u Y_i) = \nabla \cdot (\rho D_i \nabla Y_i) + R_i \tag{6.4}$$

In the above equations u is velocity, ρ is density, T is temperature and Y_i is mass fraction of species, i. D_i is the diffusion coefficient of species i. The rate of reaction R_i was based on simple Arrhenius law with activity coefficients and Energy of activation given in Table 6.1. $S_{m,\,b}$ and $S_{e,\,b}$ are the volumetric mass sink term (kg/m^3-s) and volumetric heat sink term

(W/m^3) respectively due to loss of CO_2 due to calcination reaction occurring the bed. The calculation of these terms is discussed later in this section. The equations were solved for steady state so that time differentials in all the equations were zero.

6.2.3 Free board model

A computational model based on Eulerian-Lagrangian approach was developed to simulate a pulverized coal burner in a cement kiln. Since the volume fraction of coal particles in the freeboard region is not expected to go beyond 10 %, the motion and burning of coal particles was modeled using the Lagrangian approach (Ranade, 2002). The standard k-ε model was seen to predict the gas phase turbulence for freeboard region of cement kilns quite satisfactorily and therefore was used in this work (Mastorakos *et al.*, 1999; Karki *et al*, 2000). Gas phase combustion was modeled using finite rate chemistry. Radiation was modeled using the P-1 approach. The reason for choosing these models are discussed in the individual sub sections later. The model equations for the continuous (Eulerian frame) and for the dispersed particles (Lagrangian frame) are given below.

Continuous phase:

Mass conservation equation:

$$\frac{\partial \rho}{\partial t} + \nabla \cdot (\rho v) = S_{m,\text{comb}} + S_{m,\text{calc}} \qquad (6.5)$$

where, $S_{m,\text{comb}}$ (kg/m^3s) is the mass added to the continuous phase from dispersed phase (i.e. due to devolatilization, char reaction) due to coal combustion in freeboard region and $S_{m,calc}$ (kg/ m^3s) is the mass added due to CO_2 addition from bed due to calcination reaction.

Momentum Conservation:

$$\frac{\partial (\rho v)}{\partial t} + \nabla \cdot (\rho v v) = -\nabla p + \nabla \cdot (\tau) + \rho g + F \qquad (6.6)$$

where, p is the static pressure, τ is the stress tensor, ρg is the gravitational force and F is the external body force that arises due to interaction of the dispersed phase and other model dependent source terms.

Energy Equation:

$$\frac{\partial (\rho E)}{\partial t} + \nabla \cdot (v(\rho E + p)) = \nabla \cdot (k_{eff} \nabla T - \Sigma h_j J_j + (\tau_{eff} v)) + S_{e,calc} + S_{e,comb} \qquad (6.7)$$

The first three terms on the right hand side of the equation represent heat transfer due to conduction, species diffusion and viscous dissipation respectively. $S_{e,comb}$ represents the heat source due to char combustion and $S_{e,calc}$ is the heat source due to CO_2 addition from bed due to calcination reaction.

Discrete phase:

The motion of the coal particles was simulated using the Lagrangian frame of reference by solving the following equations

$$\frac{du_p}{dt} = F_D(u - u_p) + \frac{g_x(\rho_p - \rho)}{\rho_p} + F_x \qquad (6.8)$$

where u_P is a particle velocity and u is a continuous phase velocity. The additional force F_x includes the forces on the particles that arise due to rotation of the reference frame. $F_D(u-u_p)$ is the drag force per unit mass of the particle. The present computational model assumes coal particles to be comprised of char, volatiles and ash. The computational models for coal devolatilization, gas phase mixing and combustion used in Chapter 3 were shown to predict the performance of three different kilns with different coal composition and calorific values quite reasonably. Therefore, the same models were used in the present work. The coal particle first gets heated by absorbing energy from the gas. The energy is received by convection and radiation. Due to heat up the coal particle starts devolatilization. Some approaches use correlations of volatile yield with particle temperature or define devolatilization rates using single or two step Arrehenius schemes (Karki *et al.,* 2000). The present model assumes a constant rate devolatilization for coal combustion (Pillai, 1981). The devolatilization constant recommended as 12.0 for coal combustion (Pillai, 1981) was used in the simulations. The coal particle density was assumed to decrease in proportion to the volatiles released in the gas phase (Heidenreich *et al.,* 1999). On devolatilization, gas phase combustion occurs. The investigations of coal devolatilization have given rise to a number of models for volatiles and kinetics of their gas phase combustion (see for example, Li *et al.,* 2003). In many cases, assumption of a generalized single global step reaction of volatile fuel (and assumption of CH_4 as volatile matter in coal) have reproduced temperature profiles for gas in freeboard region reasonably well for commercial coal combustors (Li *et al.*, 2003; Guo *et al.*, 2003; Chen *et al.*, 2001a; Chen *et al.*, 2001b). In Chapter 3, it was shown that simulation of three different industrial cement kilns fed with coal of different physical

compositions also lends an indirect justification for using the assumption of single step gas phase combustion reaction. Hence we have used a global single step reaction of volatile fuel to model gas phase combustion in this work as:

$$CH_4 + 2O_2 \rightarrow CO_2 + 2H_2O \quad (6.9)$$

However, the framework developed is general enough that more complicated volatile combustion reactions can be included as required. The kinetics and heat of reaction for the assumed gas phase reaction are given in Table 6.1. It should be noted that the characteristic reaction time scales at temperatures prevailing in kilns (>1500 K) is less than 1 ms. Therefore, at such high temperatures, the reaction will be limited by turbulent mixing rather than reaction kinetics. Two approaches i.e. generalized finite rate formulation [eddy breakup (EBU) model] and mixture fraction/PDF formation are used generally to model mixing limited turbulent gas phase combustion (Eaton *et al.,* 1999). The main advantage of EBU combustion model of Magnussen–Hjertager (1976) lies in its simplicity and robustness for wide range of operating conditions. Hence it is widely used for predicting gas phase combustion in coal combustors (Karki *et al*, 2000, Guo *et al.,* 2003; Li *et al.,* 2003 and references cited there in) and therefore was used in this work. This model compares the kinetic rate and the turbulence mixing rate and selects the lower rate for further calculations as:

$$R_{combg} = \min (R_{S,\,EBU}, R_{S,\,Arr}) \quad (6.10)$$

where

$$R_{S,EBU} = C_R \rho \frac{k}{\varepsilon} \min(y_{F,} \frac{y_{ox}}{b}),$$
$$R_{S,Arr} = B_s \rho^2 y_F y_{OX} \exp(-\frac{E_s}{RT}) \quad (6.11)$$

y_F is the mass fraction of the fuel and y_{OX} is the mass fraction of oxygen. The values for Arrhenius kinetic constants B_S and E_S are specified in Table 1. C_R is a parameter of the eddy breakup (EBU) turbulent combustion model, which is usually set to 4. Char combustion was modeled using diffusion limited surface reaction model derived from model of Baum and Street (1971). This model is extensively used for modeling char combustion in coal-fired furnaces (Williams *et al.,* 2002) and is therefore used in the present work. The model assumes that the surface reaction proceeds at a rate determined by the diffusion of the gaseous oxidant to the surface of the particle ignoring the kinetic contribution to the surface reaction rate.

Radiation modeling:

The radiation was modeled using the P-1 radiation model. The P1 radiation model is recommended to use when the optical thickness aL >1, where 'a' is the absorption coefficient of gas and L is the characteristic length of the system (Fluent 6.2 user manual). For the operating conditions prevailing in the cement kilns, the optical thickness is generally > 1 (~ 1.2 to 1.8 for kiln under study) and therefore P1 model was used to model radiation in the present work. P1 model is the simplest case of more general P-N model, which is based on the expansion of the radiation intensity into an orthogonal series of spherical harmonics. When only four terms in the series are used, the radiation heat flux is given by:

$$q_r = -\Gamma \nabla G \tag{6.12}$$

$$\text{where, } \Gamma = \frac{1}{3(a+\sigma_s) - C\sigma_s} \tag{6.13}$$

in which G is the incident radiation, a is the absorption coefficient, σ_s is the scattering coefficient, C is the linear anisotropic phase function coefficient

From the transport equation of G and combining the above equation, we get,

$$-\nabla q_r = aG - 4a\sigma T^4 \tag{6.14}$$

When the effect of the coal particles in the P-1 radiation model is included, the incident radiation is written as,

$$-\nabla q_r = (a + a_p)G - 4\pi\left(\frac{a\sigma T^4}{\pi} + E_p\right) \tag{6.15}$$

where, a_p is the equivalent absorption coefficient and E_p is the equivalent emission of the particles. The local absorption coefficient for the gas-particle mixture was calculated using the following expression (Boyd and Kent, 1986; Karki *et al.*, 2000)

$$a = 0.32 + 0.28\, e^{\frac{-T_g}{1135}} \tag{6.16}$$

where T is the temperature in Kelvin. In the vicinity of the burner region, the absorption coefficient was augmented by 0.4 m^{-1} to account for soot (Boyd and Kent, 1986; Karki *et al.*, 2000). A constant value of 0.13 m^{-1} was used for isotropic scattering coefficient (Boyd and Kent, 1986; Karki *et al.*, 2000).

6.2.4 Mass transfer from bed to freeboard

As calcination reaction takes place in the bed region, CO_2 is released from bed to the freeboard region. The release of CO_2 from bed to freeboard was modeled in each region individually. For the bed region volumetric sink terms for mass (kg/m^3 s) and energy (W/m^3) were applied to each cell through user defined functions (UDF'S) as

$$S_{m,b} = - R_{CO2} \quad (6.17)$$

Where R_{CO2} is rate of CO_2 produced in each cell and $S_{m,b}$ (kg/m^3 s) is the volumetric mass sink in each cell (in Equation 1). The mass sink in each cell was thus calculated proportional to amount of CO_2 produced due to calcination reaction. The corresponding heat sink in each cell was calculated as

$$S_{e,b} = -R_{CO2} \times C_{P,\,CO2} \times (T_{CO2,\,avg} - T_{Base}) \quad (6.18)$$

Where $S_{e,\,b}$ (W/m^3) is the volumetric heat sink in each cell (see Equation 6.3). As a first approximation we use an average temperature of bed in calcination region (i.e. $T_{CO2,\,avg}$ = 1000 K) to evaluate the heat sink from the bed. This mass and sink were passed as source to the freeboard region as described below.

In this model, we implemented the transfer of CO_2 from the bed to the freeboard as a function of axial position. It is possible to transfer CO_2 lost from the bed to the freeboard at every cell interfaces appearing on the bed-freeboard boundary (cell to cell coupling or 2D coupling). CO2 transfer from bed to freeboard can also implemented in the CFD model by averaging over the chord of the bed at every axial position (1D coupling as done in Chapter 3). Since the difference in the results predicted with the 1D and 2D coupling was not significant (as will be discussed later) we used 1D coupling for mass transfer from bed to freeboard. From the bed run the averaged loss of mass at different axial locations was calculated. From this information mass flux F_z (kg/m^2 s) at different axial locations could be calculated. The mass source was passed to freeboard region as

$$S_{m,calc} = \int_0^L F_z(z)/V \, dA \quad (6.19)$$

where $S_{m,\,calc}$ (kg/ m^{3}s) is the mass source of CO_2 to the freeboard, F_z (z) is the mass flux profile obtained along the kiln length, V is the volume of cell and dA is the cross sectional area through which CO2 enters the freeboard region. Corresponding heat source term was

written for freeboard model to account for heat accompanied by CO_2 from the bed was written as

$$S_{e,calc} = \int_0^L (F_z(z)/V) \times C_{P,CO2} \times (T_{CO2,avg} - 298.0)\ dA \qquad (6.20)$$

where $S_{e,fb}$ (W) is the heat source due to CO_2 entering the freeboard region and $T_{CO2,avg}$ is the average temperature of CO_2 as discussed previously. With these model equations, we now discuss the methodology adopted to simulate rotary cement kiln.

6.2.5 Methodology adopted

Though separate computational models were used for the bed and the free board region, the computational grid was generated for the whole kiln. Different components and the generated grid are shown in Figure 6.1.

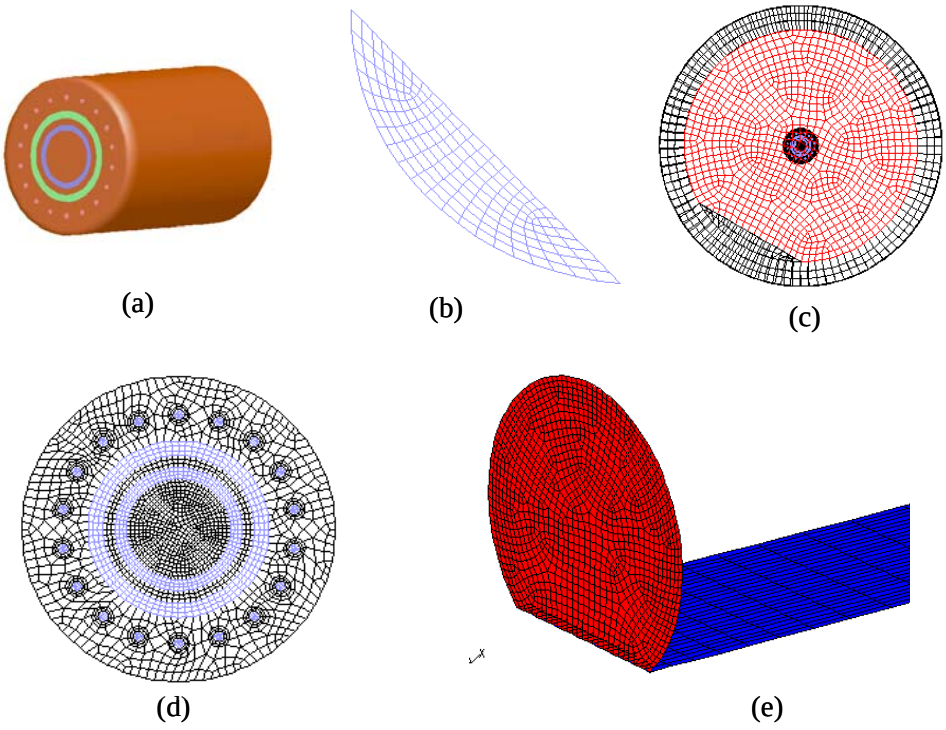

Figure 6.1: Computational grid

a: kiln burner,12 axial air ports, coal air inlet (blue), swirl air inlet (green);
b: bed region grid; c: cross sectional view of kiln (kiln internal diameter: 3.14m)
d: Burner grid; e: freeboard region grid

The computational grid for the bed, free board and shell region was extracted from this single computational grid. The commercial grid generation code GAMBIT 2.0 was used to model the geometry and to generate a computational grid for the entire kiln. All the simulations were carried out using commercial FLUENT 6.2.9 solver. The overall methodology is shown schematically in Figure 6.2 and explained below

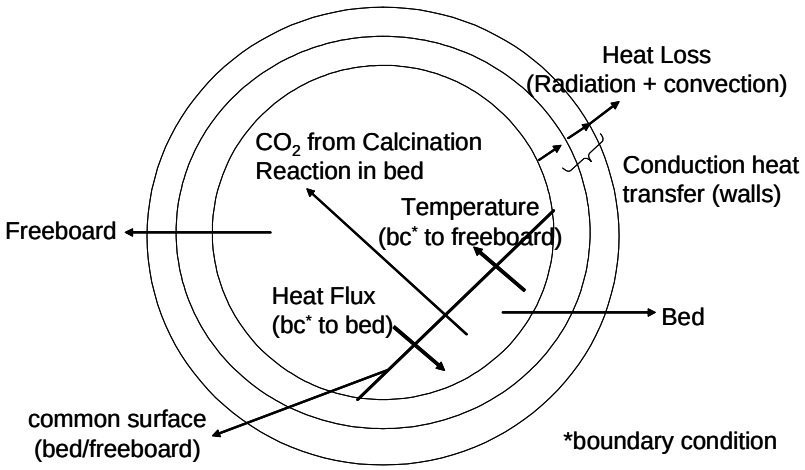

Figure 6.2: Coupling methodology

The bed model was first simulated independently. A pseudo-homogeneous approximation was used to simulate the motion of solids in the bed region. In the first phase, a constant viscosity was specified for the bed material as discussed earlier. Simulation of the bed region was initiated by assuming a heat flux at the bed-free board common interface (considered as wall for these simulations). The bed flow and the reactions occurring were solved simultaneously to get the temperature profile for the common interface between the free board and bed regions. The predicted bed temperature was then used to initiate simulations of the free board region. Combustion of coal particles in the free board region was modelled using the Eulerian-Lagrangian approach. The free board was then simulated using temperature profile from the bed run to get the heat flux profile for the common interface. This heat flux was then passed as boundary condition to simulate the bed region again. This process was continued till the temperature and the heat flux through the interface did not changed with further iterations. For the initial simulations 1d coupling was initiated. Thereafter some simulations were also carried with 2d coupling between freeboard and bed. This is discussed later in results and discussion section. Exchange of CO_2 from bed to

freeboard due to calcination was accounted by proper source/sink terms. Suitable under-relaxation factors were identified for faster convergence of coupled solution.

6.3 Results and Discussion

The computational model described in the previous section was used to understand the details of burning zone and overall behavior of rotary cement kilns. A hexahedral grid of 18,100 (~ 12 nodes in radial direction and 150 nodes in axial direction) and 5,85,000 cells (~ 35 nodes in radial direction and 150 nodes in axial direction) was used to simulate bed and freeboard regions of kiln respectively. Care was taken to resolve grid near the burner region finer in order to capture swirl laden high velocity flows produced by the kiln burner. Grids of similar magnitude are found to be adequate for cement kiln simulations [See Mastarokos *et al.* (1999) and references cited there in]. The mass, momentum and energy balance equations were discretized using first order discritization scheme. During individual simulations of bed and freeboard the temperatures at different locations were monitored. The individual runs for bed and freeboard were simulated till the temperatures at these locations did not changed by an error of 0.1 %. Typically one bed run required CPU time of ~ 5 hrs and freeboard required CPU time of ~ 20 hrs to convergence with this grid on a dual processor machine of 2 Ghz processor speed and 2GB memory. Before presenting the simulation results we initially present results for coupling of bed and freeboard region in the following.

6.3.1 Coupling of bed and freeboard region

The computational model was used to simulate typical industrial kiln whose dimensions and operating conditions are specified in Table 6.3 (See Chapter 3). The properties of gas and solids used for these simulations are specified in Table 6.2. The bed and freeboard regions of kiln were simulated separately and communicated via mass and energy communication through common interface. To accelerate the convergence, typically for first few iterations 1d coupling was done. For this 1d coupling the temperature and heat fluxes were averaged radially at each axial location and were passed to freeboard and bed runs respectively (See section 6.2.3). An under relaxation of 0.5 was used in these simulations. The iterative procedure was carried till the temperature and heat flux of common interface did not changed further with in an error of ± 1%. Once 1d coupling was converged 2d coupling was initiated. For these simulations coupling the heat flux and temperature values between common interface of bed and freeboard were not averaged in radial direction. A cell to cell

correspondence of temperature and heat flux at common interface was carried. Since 1d runs were already converged, an under relaxation of 1 was used in 2d coupling for faster convergence. The iterations with 2d coupling were carried till the bed temperature in the kiln did not changed further within an error of ± 0.1%. Typically 10 iterations of 1d coupling and 3 iterations for 2d coupling were required for complete convergence.

Table 6.2: Physical properties used in simulations

Sr. No.	Variable	Value
1.	Bed Density, kg/m^3	1046$^+$
2.	Bed Heat capacity, kJ/ kg K	1.088$^\$$
3.	Bed Thermal conductivity, W/m K	0.5*
4.	Gas heat capacity (J/kg K)	$(0.106\ T_G + 1173)$ $^!$
5.	Gas Viscosity (kg/m/s)	$(0.1672\times10^{-5}\sqrt{T_G} - 1.058\times10^{-5})^!$

*Perry (1984); $^+$Karki *et al.* (2000); $^\$$ Spang (1972); $^!$Guo *et al.* (2003) ; $^\wedge$

Table 6.3: Dimensions and operating condition of kiln

Sr. No.	Variable	Industrial Kiln
1.	Length, m	50
2.	Inner refractory diameter, m	3.4
3.	Coating thickness, m	0.13
4.	Speed of rotation, RPM	5.5
5.	Solids flow in, kg/s	38.88
6.	Height at solid entry, m	0.46
7.	Secondary air	13.469 kg/s; 1373K
8.	Axial air	1.17926 kg/s; 313 K
9.	Coal air	0.943 kg/s; 328 K
8.	Swirl air	0.5266 kg/s; 313 K
10.	Coal Fr, kg/s	1.25
11.	Char	0.64
12.	Volatiles	0.27
13.	Ash Content	0.09
14.	Calorific value, kcal/kg coal	6200
15	Coal Particle size, microns	100

However, it was observed that difference in predicted results of converged 1d coupled simulations and 2d coupled simulations were insignificant. Typical results are shown in Figure 6.3. Figure 6.3a and Figure 6.3b shows the comparison of temperature contours for converged 1d and 2d coupled simulations (The numerical values are not shown in any of contour plots to maintain secrecy of industrial data). The predictions for area weighted average temperature of the gas in freeboard region are shown in Figure 6.3c. It can be seen from Figure 6.3c the difference in averaged predictions is also insignificant. Moreover, the percentage error in total amount of heat flux given to bed by the two methods is less than ~ 0.5 %. Therefore, all simulations were carried using a 1d coupling methodology. This not only saves CPU time of approximately ~ 20 % but also avoid convergence problems of bed/freeboard coupling simulations (for example, a bed/freeboard coupling simulation with direct 2d coupling has significant convergence problems).

Figure 6.3a: Temperature contours in central x plane (1D Coupled)

Figure 6.3b: Temperature contours in central x plane (2D Coupled)

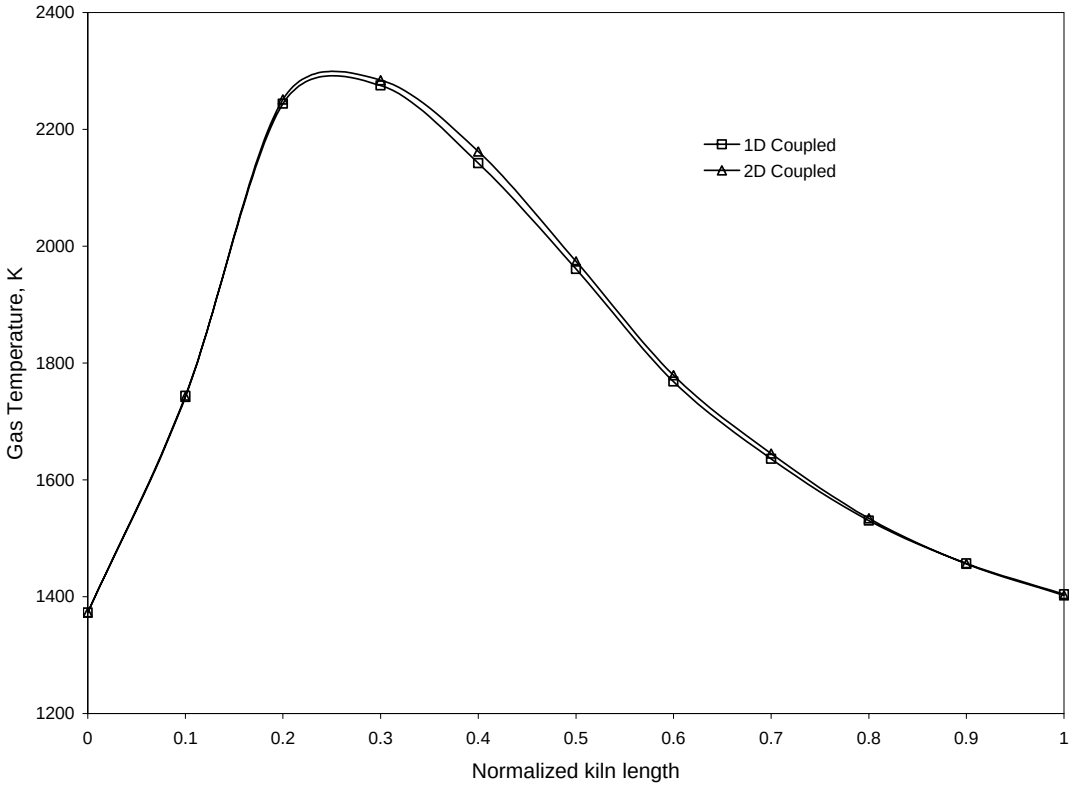

Figure 6.3c: Comparison of area weighted averaged freeboard gas temperature

6.3.2 Simulations of rotary cement kilns

The converged simulations of bed and freeboard model were analyzed to gain insights into flame characteristics and three-dimensional flow, temperature and composition distribution with the kiln. Unfortunately there were no temperature and composition measurements available inside the kiln. Hence the model predictions were initially compared with available data at the kiln exit. The predicted results were also compared with those predicted by one dimensional model presented in Chapter 3. A comparison of bed and freeboard temperature predicted by the present CFD model (temperature predictions in central x-plane) and the 1d model for the same kiln with same operating conditions are shown in Figure 6.4a and Figure 6.4b. A deviation in temperature predictions by CFD and 1d model, as can be seen from these figures, could be due to difference in assumption of internal coating formation in both the models. This is explained later in this section. The predicted mass fraction profiles of C_3S and C_4AF along the kiln length by CFD and 1d model are shown in Figures 6.4c and 6.4d. These results seem to be reasonable.

The temperature distribution of kiln wall controls the net loss to the environment which is one of the major contributors in the net energy consumption in the kiln. Therefore it is essential to predict the shell temperatures accurately. The comparison of shell temperatures predicted by the two models is shown in Figure 6.5a. It is important to note that CFD model was able to predict the temperature dip (~ 200 ^{0} C) as observed in industrial data (see Figure 6.5b). This was due to additional resistance to heat transfer due to coating formation. Such dips in shells temperatures have not been presented in previously published CFD models due to inconsistent modeling of coating formation (Kolyfetis and Markatos, 1996; Mastorakos *et al.*, 1999). The quantitative difference in temperature predictions of the two models could be due to difference in location of coating formation assumed/predicted by CFD and 1d model respectively. 1d model was able to predict the coating formation based on operating conditions (coating was predicted to be formed around 25 % of kiln length from the solid exit end). However, in CFD approach, due to a prior meshing requirement, one has to assume coating length in kiln before the simulations (coating formation was assumed be to formed around 50 % of kiln length from solid exit in the present work).

The quantitative comparison of the temperature and clinker composition predicted by the model with the industrial data and 1d model is given in Table 6.4. In general, the presented

CFD model was able to predict the overall behaviour of kiln reasonably when compared with industrial observations and published results.

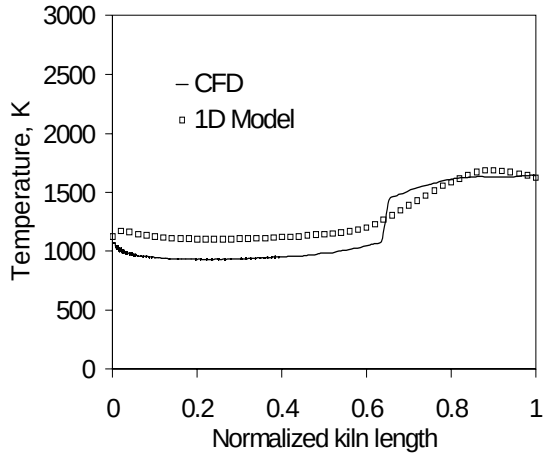

Figure 6.4a: Comparison of bed temperature with results presented in Chapter 3

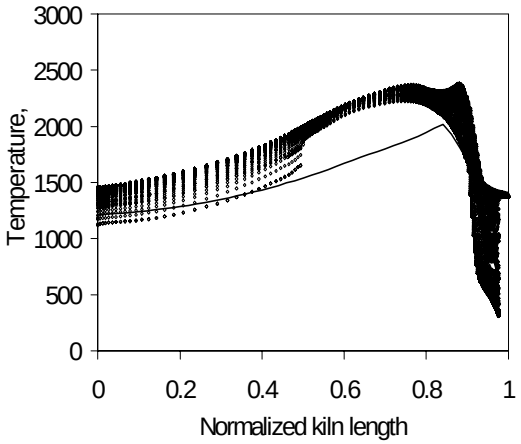

Figure 6.4b: Comparison of freeboard temperature results presented in Chapter 3

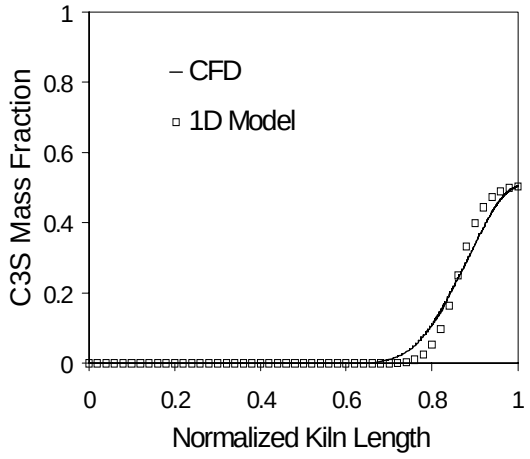

Figure 6.4c: Comparison of clinker composition (C3S) results presented in Chapter 3

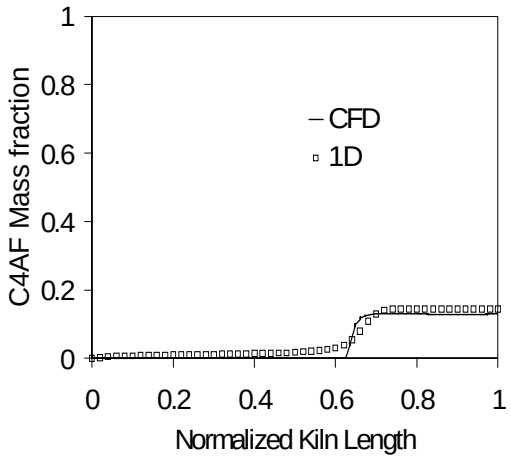

Figure 6.4d: Comparison of clinker composition (C4AF) with results presented in Chapter 3

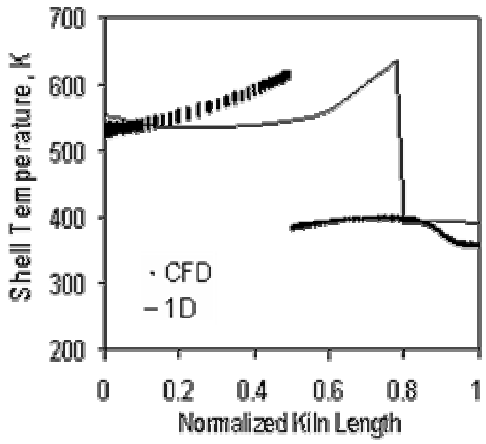

(6.5a) Predictions by computational model
Abscissa 1 corresponds to burner location

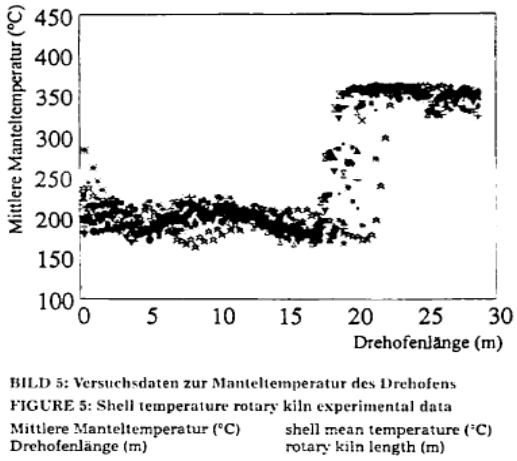

BILD 5: Versuchsdaten zur Manteltemperatur des Drehofens
FIGURE 5: Shell temperature rotary kiln experimental data
Mittlere Manteltemperatur (°C) shell mean temperature (°C)
Drehofenlänge (m) rotary kiln length (m)

(6.5b) Reported shell temperature measurements from industrial kiln (Kolyfetis and Markatos, 1996) Kiln Length: 75 m, Inner diameter: 4.35 m
Abscissa 0 corresponds to burner location

Figure 6.5: Comparison of shell temperatures with published literature

Table 6.4: Comparison of model predictions with industrial data

Sr. No.	Variable	Industrial data	CFD	1D (See, Table 3.8 Chapter 3)
1.	Mass Fraction C_3S	0.483	0.506	0.481
2.	Mass Fraction C_2S	0.239	0.225	0.238
3.	Mass Fraction C_3A	0.051	0.052	0.052
4.	Mass Fraction C_4AF	0.143	0.129	0.146
5.	Mass Fraction CaO	0.084	0.087	0.083
6.	Temperature of solids, K	1673	1632	1608

On obtaining reasonable agreement with industrial observations and previously published results the CFD model was used to understand intricacies of burning zone of cement kilns which cannot be predicted by 1D model. Typical predictions of the CFD model for coal devolatilization, char burn out and CO_2 mass fractions in the central plane of freeboard region are shown in Figure 6.6. Information regarding location of release of volatiles in freeboard region [See Figure 6.6a], char burn out [See Figure 6.6b] in the radial direction can be obtained from such simulations. Such simulations can help to identify various zones of coal combustion. The possibility of coal particles hitting the walls or bed due to improper burner design or operating conditions can be figured out from such simulations. Figure 6.6c shows CO_2 mass fraction is central plane of freeboard regions. The CO_2 mass fraction is higher near the solid entrance due to calcinations reaction. Such information can be useful to identify calcinations region in rotary kilns. Figure 6.6d represents the temperature contours in the central plane of freeboard region. The Possibility of temperature zones beyond acceptable limits due to tilting of flame and possible damages to the refractory can be examined using such results. If the simulations indicate that the flame characteristics are not optimum, the CFD model can be used to understand influence of various burner operating protocols on flame characteristics. The figures predicted by developed model for temperature and mass fraction predictions for coal and air in freeboard region seem to be reasonable when compared with industrial observations. Thus the developed model was not only able to predict the behavior of cement kilns as predicted by previously published results but also able to provide information regarding burning zone intricacies quite satisfactorily.

Figure 6.6a: Coal devolatilisation, kg/s (■ = 1.52 x 10-5; ■ = 0)

Figure 6.6b: Char burn out, kg/s (■ = 1.24 x 10-4; ■ = 0)

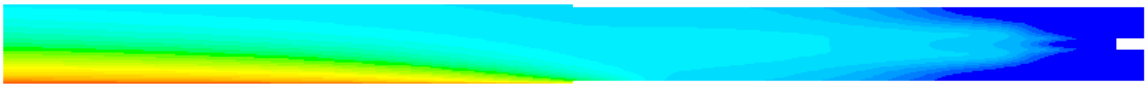

Figure 6.6c: CO_2 mass fraction (■ = 1.0; ■ = 0)

Figure 6.6d: Temperature contours in central vertical plane of freeboard region, K

6.3.3 Effect of burner operational parameters on the kiln performance

On obtaining satisfactory predictions from the model, numerical experiments were carried using the model to investigate influence of burner operational parameters on the kiln behavior. The burner of cement kilns forms one of the most important components of the entire system which controls the flame characteristics in the freeboard region and subsequently the performance. Predetermined quantities of primary air and secondary air are passed through the burners along with swirl air and fuel to get the desired flame characteristics. For industrial cement kilns, typically primary air is passed through burner as high momentum jets (~ 200-250 m/s) along with relatively slow secondary air (~ 15-20 m/s) The swirl air passed through the burner opens the primary jet and influences the rate of entrainment of secondary air in the primary air. The relationship between jet momentum and the swirl/secondary component of air has significant effect on flame length and heat transfer in cement kilns (Mullinger, 1984). It is observed that kilns with low jet momentum suffer from poor air/fuel mixing and long flames leading to more fuel consumption (Mullinger, 1984). The developed computational model was used to analyse the effect of variation of axial/swirl ratio through the burner (consequently effect of axial jet) on the flame characteristics in freeboard region and corresponding effect on clinker composition.

The base case simulation (explained in Section 6.3.3) was carried out at an axial to swirl ratio of 2 with a very high primary jet velocity (~ 245 m/s). To predict the freeboard region temperature profiles at low momentum jets, the ratio of axial to swirl air was reduced from 2 to 1 (with axial velocity of reduced to ~ 100 m/s). The consequent change in the temperatures due to reduced axial jet momentum in central plane of freeboard region is shown in Figure 6.7a and Figure 6.7b. As the primary air jet momentum was reduced the flame (shown by temperature contours) tends to become larger (see Figure 6.8b). Consequently for low axial jet simulation C_3S composition decreased to 0.45 from 0.5 by reducing axial to swirl ratio from 2 to 1. Both these results seem to be in reasonable agreement with previous results for cement kiln coal burners (Mullinger, 1984). The reduction in axial velocity and consequent increase in swirl component causes expansion of primary jet (i.e. enhanced jet entrainment, see Figure 6.8a and Figure 6.8b) which is also in agreement with published results (Frassoldati *et al.*, 2005). Moreover, the temperature profiles obtained in freeboard region (see Figure 6.8a and Figure 6.8b) for different axial/swirl ratios seems to be reasonable at least qualitatively when compared with published results for burners operated with different fuels (Huang and Yang, 2005). Thus, the developed computational model was able to capture

influence of ratio of swirl or axial air on the flame characteristics and the performance of cement kilns.

Figure 6.7a: Temperature contours in central vertical plane of freeboard region, K

Figure 6.7b: Temperature contours in central vertical plane of freeboard region, K

The computational model was also analyzed to predict the temperature profiles in freeboard region of the kiln for different burner operational parameters. For example, influence of changing inlet coal particle size, coal flow rate, ash content of coal at same energy input (by changing coal flow rate) and oxygen enrichment of the primary air on temperature profiles in the kiln is shown in Figure 6.8a. It can be seen that, at the same levels of energy input by coal, the temperatures are more or less similar (no significant influence of particle size or ash content) except with oxygen-enriched air. As expected, decreasing the coal flow rate from 1.5 to 1 kg/s decreases the overall energy supplied to the kiln and therefore freeboard temperature decreases. With coal particle containing more ash, the position of maximum temperature shifts slightly away from the burner. When oxygen enriched air was used, significant increase in the predicted maximum temperature was observed. This is because of enhanced combustion rates due to availability of more oxygen due to oxygen enriched air. The comparison of predicted mass fraction of volatiles for this case with the base case is shown in Figure 6.8b. It can be seen that with enriched oxygen, the rate of consumption of volatiles is significantly higher as expected. Thus the model can provide guidelines for ensuring the

desired flame size and position for different coal grades either by manipulating coal particle size, swirl to axial air ratio or possible use of oxygen enrichment of primary air.

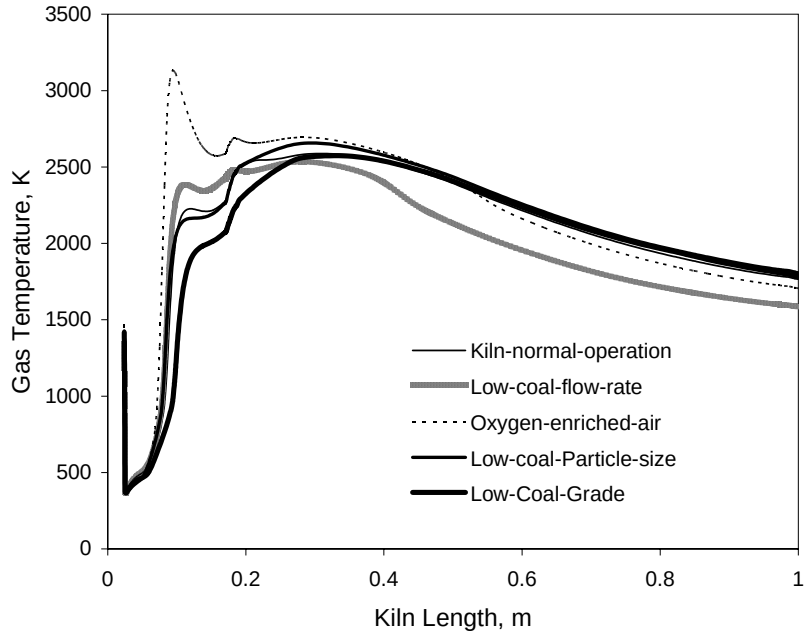

Figure 6.8a: Predicted gas temperature profiles
(kiln center line; Abscissa 0 is burner end)

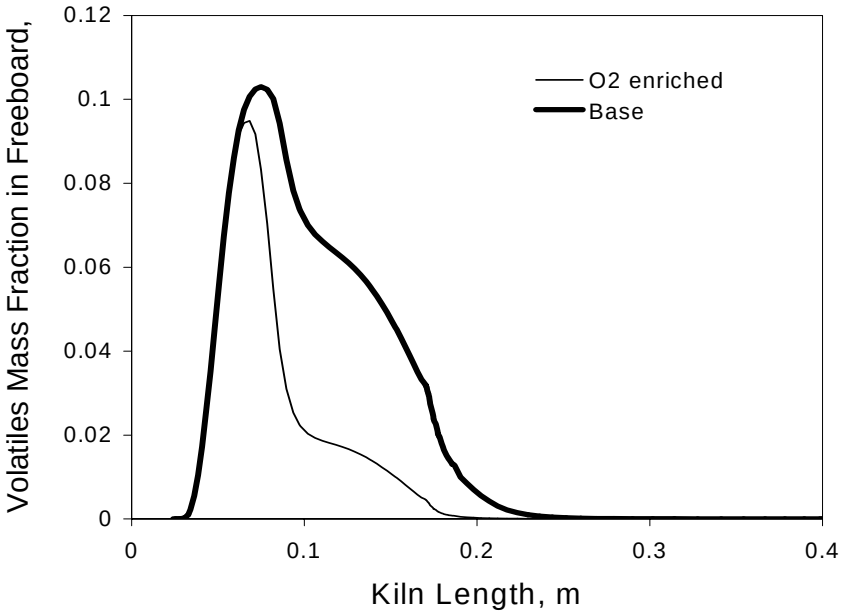

Figure 6.8a: Predicted profiles for volatile mass fraction
(kiln center line; Abscissa 0 is burner end)

Further work on modelling of melting and using better constitutive equations for solids phase is in progress and may enhance the utility of models and framework developed in this work.

6.4 Conclusions

A comprehensive framework of computational fluid dynamics based model was developed to simulate coal combustion, radiation and clinkerization reactions occurring in rotary cement kilns. Due to significantly different physical time scales, separate but coupled models were developed for bed and freeboard regions of cement kilns. The Eulerian-Lagrangian based model was developed for combustion of pulverized coal in the free board region of kilns. The radiation was modelled using a P-1 radiation model. The solid-solid reactions in the bed region were simulated using a pseudo-homogeneous model. The bed and the free board region models were coupled together by mass and energy communication though common boundaries. Some specific conclusions drawn from the present study are

- The presented coupling methodology to solve model equations representing processes occurring in rotary cement kiln worked well and can be extended to other similar complex reactors. It was observed that averaged coupling methodology (i.e. 1d coupling) saves computational resources compared to the cell to cell coupling methodology (i.e. 2d coupling) without jeopardizing accuracy of predicted results.
- The developed CFD model was able to predict the performance of cement kiln in terms of the data at the exit of industrial kilns quite satisfactorily.
- The predicted results indicate that reducing burner primary jet velocities produce longer flames in freeboard region and consequently increase energy requirements of rotary cement kilns.

Overall the developed model and presented results will help in providing developing better understanding of freeboard region and providing some clues for better burner operations.

7. Conclusions

In the present work, framework of realistic computational models was developed for clinker manufacture in cement industry. The computational models were developed using conventional reaction engineering approach and computational fluid dynamics based approach. A software viz., Rotary Cement Kiln Simulator (RoCKS), was also developed to capture influence of key design (kiln dimensions) and operating parameters (RPM, solids flow rate, composition, coal flow rate and so on) on overall performance of cement kilns. Key aspects of the developed models and scope of future work is discussed below.

1. Reaction engineering based model for rotary cement kilns

A model based on one-dimensional framework was developed to simulate rotary cement kilns, considering most of the underlying physics for the first time. Models for simulating reactions and heat transfer in the bed region and coal combustion and heat transfer in the freeboard region were developed based on a segregated approach. Melting of solids and coating formation within the kiln was accounted. Coal combustion in freeboard region was modeled by considering devolatilisation, gas phase combustion and char reaction. The model was used to simulate performance of three industrial kilns having wide range of operating conditions. The model predictions agreed reasonably with the available plant data for all the three kilns. The model was also able to predict influence of key design and operating parameters like kiln tilt, kiln RPM on the overall kiln performance. The model was also used to propose and to evaluate a practical solution of using a secondary shell to reduce energy consumption in rotary cement kilns. Specific results obtained from model simulations are briefed below:

- The simulations indicated that the operation of kiln with higher solid loading and lower RPM is favourable from the point of view of energy consumption per kg of clinker. Other operational concerns like increase in dusting and mixing however need to be considered while identifying maximum solids flow rate or optimum RPM for any specific rotary cement kiln.
- The use of a secondary shell with air stream passing through the gap between the kiln shell and the secondary shell appears to be a promising method to reduce

energy consumption in rotary cement kilns. It is possible to recover ~ 80 % of the energy lost to the surroundings (typically 150 kJ/kg clinker) by judicious choice of secondary shell and air flow rate without degrading the quality of recovered energy significantly.

2. RoCKS (Rotary cement kiln simulator): An Integrated reaction engineering model for pre-heater, calciner, kiln and cooler in clinker manufacture

A comprehensive reaction engineering model was developed to simulate complex processes occurring in clinker formation in cement industry. The models for pre-heater and calciner were developed assuming solids and gas to be completely back mixed. The computational model for the kiln was developed assuming gas and solids as plug flow. The integrated simulator was converted into simple to use GUI based software for cement industry, named as Rotary Cement Kiln Simulator (RoCKS). RoCKS was used to simulate performance of pre-heater, calciner, kiln and cooler for clinker formation. These results were satisfactory when compared with available plant data and industrial observations. Specific conclusions based on this model are:

- Including an additional pre-heater reduces net energy consumption. The developed model can be used to evaluate relative benefits of energy savings by additional pre-heater and required additional capital expenses.
- There is an optimum value for percentage of calcination carried out in calciner with respect to overall energy consumption in clinker manufacture. With the parameters selected in this work, this optimum value of percentage calcination in calciner is about 70.
- The simulation results indicated that operating kiln with higher solid loading, lower RPM, lower tilt and lower grate speed reduces energy consumption per unit production. The upper limit on solid loading (bed height) and lower limits on RPM and tilt (mixing and heat transfer) need to be identified based on other practical issues.

3. CFD model for rotary cement kilns

A comprehensive framework of computational fluid dynamics based model was developed to simulate transport processes in rotary cement kilns. Initially CFD models were developed for predicting solids motion in transverse section of rotary kilns. These models illustrated that use of simpler models like pseudo-homogeneous assumption for the solids phase were found to give results similar to those as predicted by more complicated models. The solids in the bed region of cement kilns were therefore simulated using a pseudo-homogeneous assumption. The Eulerian-Lagrangian based model was developed for combustion of pulverized coal in the free board region of kilns. The radiation was modelled using a P-1 radiation model. The bed and the free board region models were solved separately and coupled together via mass and energy transfer though common boundaries. Specific conclusions drawn from this study are:

- The developed coupling methodology is an efficient way for modeling rotary cement kilns which involves physical processes having significantly different time scales. Coupling of bed and freeboard regions for cement kilns using averaged coupling (i.e. 1d coupling) seems to be a better choice over cell to cell (i.e. 2d coupling) since the former not only saves computational time by ~ 20 % but also avoids convergence difficulties.
- The developed CFD model was able to predict the performance of cement kiln in terms of the data at the exit of industrial kilns and published literature quite satisfactorily.
- The predicted results indicate that reducing burner primary jet velocities produce longer flames in freeboard region and consequently increase energy requirements of rotary cement kilns.

On the whole, the developed models and presented results will be helpful for developing better understanding and for realizing performance enhancements for clinker manufacturing in cement industry.

4. Scope for future work

- Developing accurate frictional viscosity models for flow of solids in transverse plane of the kiln is essential to make this framework more comprehensive
- The effect of particle size distribution is neglected in the scope of this work. Incorporating size distribution of raw meal particles would be the next milestone in further development of this framework.
- Incorporating population balance models to capture size of particles due to agglomeration after melting of solids is another aspect which can be added in the present framework of cement kiln models.
- The internal conduction inside clinker particles is not considered while developing computational model for grate coolers. The present framework can be extended by developing a more comprehensive and computationally intense model for clinker cooler considering the internal gradients in the particles in clinker cooler.

References

Barr, P. V., Brimacombe, J. K. and Watkinson, A. P., 1989, “A heat transfer model for the rotary kiln- I. Pilot kiln trials”, Met. Trans B., 20B. 391-402.

Boateng, A. A., 1998, “Boundary layer modelling of granular flow in the transverse plane of a partially filled rotating cylinder”, International Journal of Multiphase Flow, 24, 499-521.

Boateng, A. A. and Barr, P. V., 1997, “Granular flow behaviour in the transverse plane of a partially filled rotating cylinder”, Journal of Fluid Mechanics, 330, 233-249.

Boateng, A. A. and Barr, P. V., 1996, “A thermal model for the rotary kiln including heat transfer within the bed”, International Journal of Heat and Mass Transfer, 39, 2131-2147.

Borgwardt, R. H., 1985, “Calcination kinetics and surface area of dispersed limestone particles”, AIChE Journal, 31, 103

Beretka, J. and Brown, T., 1983, “Effect of particle size on the kinetics of the reaction between Magnesium and Aluminium Oxide”, J. Amer. Cerm. Soc., 66, 383-388.

Boyd, R. K. and Kent, J. H., 1986, “Three-dimensional furnace computer modeling”. 21st Symp. (Int.) Combust., [Proc.], 265.

Chen, C., Horio, M. and Kojima, T., 2001a, “Use of numerical modeling in the design and scale up of entrained flow coal gasifiers”, Fuel, 80, 1513-1523

Chen, K.S., Hsu, W.T., Lin, Y.C., Ho, Y.T. and Wu, C.H., 2001b, “Combustion Modeling and Performance Evaluation in a full-scale rotary kiln incinerator”, J. Air & Waste Manage. Assoc., 51, 885-894

Chern, J. and Hayhurst, A.N., 2004, “Does a large coal particle in a hot fluidized bed lose its volatile content according to shrinking core model ?” Comb and Flame, 139, 208-221.

Cleary, P. W., Metcalfe, G. and Liffman, K., 1998, “How well do discrete element granular flow models capture the essentials of mixing processes?” Applied Mathematical Modelling, 22, 995-1008.

Dhanjal, S.K., Barr, P.V. and Watkinson, A.P., 2004, “The rotary kiln: An investigation of bed heat transfer in transverse plane”, Met. And Mat. Trans B, 35B, 1059-.

Ding, Y. L., Seville, J. P. K., Forster, R. and Parker, D. J., 2001, “Solids motion in rolling mode rotating drums operated at low to medium rotational speeds”, Chemical Engineering Science, 56, 1769-1780

Duchesne, C., Thibault, J. and Bazin, C., 1996, “Modelling of the solids transportation within an industrial rotary dryer: A simple model”, Industrial Engineering Chemistry Research, 35, 2334-2341.

Djuric, M. and Ranogajec J., 2002, “Mathematical modeling in cement technology”, in - Advances in Cement Technology: Chemistry, Manufacture and Testing, 2nd ed. Editor - S.N. Ghosh, New Delhi, Tech Books International, India

Eaton, A.M., Smoot, L.D., Hill, S.C., and Eatough, C.N., 1999, “Components, formulations, solutions, evaluation, and application of comprehensive combustion models” Prog. Energy Comb. Sci., 25, 387-436.

Engin, T. and Ari, V., 2005, “Energy auditing and recovery for dry type cement rotary kiln systems–A case study”, Energy Conversion and Management, Volume 46, Issue 4, 551-562

Friedman, S.J. and Marshall, W.R., 1949, “Studies in rotary drying, Part- I, Hold up and dusting”, Chem. Engg. Prog., 45(8), 482.

Ferron, J. and Singh, D., 1991, “Rotary kiln transport processes”, A.I.Ch.E. Journal, 37, 747-758.

Frassoldati, A, Frigerioa, S., Colombob, E., Inzolib, F. and Faravelli, T, 2005, "Determination of NO_x emissions from strong swirling confined flames with an integrated CFD-based procedure", Chemical Engineering Science, 60, 2851-2869.

Garcya-Labiano, F., Abad, L.F. de Diego, Gayan, P. and Adanez, J., 2002, "Calcination of calcium-based sorbents at pressure in a broad range of CO2 concentrations", Chem. Eng. Sci., 57, 2381– 2393.

Gang, L, Rongxian, L. and Zhou, L., 2000, "Numerical simulation of gas particle flows with different swirl numbers in a swirl burner" Tsinghua Science And Technology, Vol 5, No 1, 96-99.

Gorog, J. P., Brimacombe, J. K. and Adams, T. N., 1981, "Radiative heat transfer in rotary kilns", Met. Trans B, 12B, 55-69.

Gorog, J. P., Brimacombe, J. K. and Adams, T. N., 1983, "Heat transfer from flames in a rotary kiln", Met. Trans B, 14B, 411-424.

Guo, Y.C., Chan, C.K. and Lau, K.S., 2003, "Numerical studies of pulverized coal combustion in a tubular coal combustor with slanted oxygen jet", Fuel, 82, 893–907

Gupta, A.V.S.S.K.S. and Nag, P.K., 2000, "Prediction of heat transfer coefficient in the cyclone separator of a CFB", Int. J. Energy Res. 24, 1064-1079.

Hamor, R.J., Smith, I.W. and Tyler, R.J., 1973, "Kinetics of combustion of pulverised brown coal char between 630 and 2200 K", Combust. Flame 21, 153.

Hao, Y. J. and Tanaka, T., 1990, "Analysis of solid-solid reaction controlled by unideirectional diffusion", Int. Chem. Eng. (English Trans.), 30, 244-253.

Hewlett, P.C., 1998, Lea's Chemistry of Cement and Concrete, Arnold, London.

Heidenreich, C.A., Yan, H.M. and Zhang D.K., 1999, “Mathematical modelling of pyrolysis of large coal particles—estimation of kinetic parameters for methane evolution”, Fuel, 78, 557–566

Heinen, H., Brimacombe, J. K. and Watkinson, A. P., 1983, “Experimental studies of transverse bed motion in rotary kilns”, Meteorological Transactions B, 14B, 191-205.

Hills, A.W.D., 1968, “The mechanism of the thermal decomposition of calcium carbonate”, Chem. Eng. Sci., 23, 297-320

Hindmarsh, A.C., 1983, ODEPACK, a systematized collection of ODE solvers. In: Stepleman, R.S., et al. (Eds.), Scienti.c Computing. North-Holland, Amsterdam, 1983. IMACS Transactions on Scientific Computation 1, 55–64.

Hottel, H.C., 1967, Radiative heat transfer, 1st Edition, New York: McGraw-Hill.

Huang, Y. and Yang, V., 2005, “Effect of swirl on combustion dynamics in a lean-premixed swirl-stabilized combustor”, Proceedings of the Combustion Institute, 30, 1775–1782

Ingraham, T. and Marier P., 1963, “Kinetic studies on the thermal decomposition of calcium carbonate,” Canadian Journal of Chemical Engineering, 63, 170–173.

Irfan, A. and Dogu, G., 2001, “Calcination kinetics of high purity limestones”, Chemical Engineering Journal, 83, 131-137.

Johansen, V., 1973, “Model for the reaction between particles and portland cement clinker,” J. Amer. Cerm. Soc., 56(9), 450–454.

Kang, S.K., Kwon, T.W. and Kim, S.D., 1989, “Hydrodynamic characteristics of cyclone Reactors”, Powder Technology 58,211-220.

Karki, K.C., Patankar, S.V. and Grant, J., 2000, “Simulation of fluid flow, combustion and heat transfer in a coal-fired cement kiln”, FACT-Vol 23/ HTD-Vol. 367, Combustion, Fire and Computational Modeling of Industrial Combustion Systems, ASME.

Khakhar, D. V., McCarthy, J. J., Sninbrot, T. and Ottino J. M., 1997, “Transverse flow and mixing of granular material in a rotating cylinder”, Phys. Fluids, 9(1), 31-43.

Khinast, J., Krammer, G.F., Brunner, C. and Staudinger, G., 1996, “Decomposition of limestone: the influence of CO2 and particle size on the reaction rate”, Chem. Eng. Sci., 51, 623–634.

Khraisha, Y.H. and Dugwell, D. R., 1992, “Coal combustion and limestone calcination in a suspension reactor”, Chem. Eng. Sci., 47, 993–1006.

Kolyfetis, E. and Markatos. N. C.,1996, “Aerodynamics and coal – Flame modeling in burning zone of cement rotary kilns, part 2. , ZKG International, 49, 326-334

Kramers, H. and Croockewit, P., 1952, “The passage of granular solids through inclined rotary kilns”, Chemical Engineering Science, 1, 259–265.

Lebas, E., Hanrot, F., Ablitzer, D. and Houzelot, J.L., 1995, “Experimental study of residence time, particle movement and bed depth profile in rotary kilns”, Can J. Chem. Engg., 73, 173-180.

Lede, J., Li, H.Z., Soulalignac, F. and Villermaux, J., 1987, “Measurment of solid particle residence time in cyclone reactor: A comparison of four methods”, Chem. Eng. Process, 22, 215-222.

Lee, J., Keener, T.C., Knoderera, M. and Khang, S., 1993, “Thermal decomposition of limestone in a large scale thermogravimetric analyzer”, Thermochemica Acta, 213, 223-240.

Li, Z.Q., Wei, F. and Y. Jin, 2003, “Numerical simulation of pulverized coal combustion and NO formation”, Chemical Engineering Science, 58, 5161 – 5171

Li, S.Q., Yan, J.H., Li, R.D., Chi, Y. and Cen K.F., 2002, “Axial transport and residence time of MSW in rotary kilns, Part – I. Experimental”, Powder Technology, 126, 217-227

Li, K.W., 1974, “Entrainment in rotary cylinders”, AIChE J., 20(5), 1031-1034.

Liu, X. Y. and Specht, E., 2006, “Mean residence time and hold up of solids in rotary kilns”, Chemical Engineering Science, 61, 5176-5181

Locher, G., 2002, “Mathematical models for the cement clinker burning process, Part 3: Rotary Kiln”, ZKG International, 55 (3), 68-80.

Lu, J., Huang, L., Hu, Z. and Wang, S., 2004, “Simulation of gas-solid, two-phase flow, coal combustion and raw meal calcination in a pre-calciner”, ZKG International, 57(2) 55-63.

Martin, G., 1932, Cement engineering and thermodynamics applied to the cement rotary kiln. The Technical Press, London.

Martins, M.A., Oliveira, L.S. and Franca, A.S., 2001, “Modeling and simulation of petroleum coke calcination in rotary kilns”, Fuel, 80, 1611-1622.

Martins, M, A., Oliveira, L, S. and Franca, A.S., 2002, “Modeling and simulation of Limestone calcinations in rotary kilns”, ZKG International. 55(4), 76-87.

Marias, F., 2003, “A model of a rotary kiln incinerator including processes occurring within the solid and gaseous phase”, Computer and Chemical Engineering, 27, 813-825.

Mastorakos, E., Massias, A., Tsakiroglou, C.D., Goussis D.A. and Burganos V.N., 1999, “CFD predictions for cement kiln including flame modeling, heat transfer and clinker chemistry”, Applied Mathematical Modelling, 23, 55-76.

Magnussen, B.F and Hjertager, B. H., 1976, “On mathematical modeling of turbulent combustion with special emphasis on soot formation and combustion”, 16th symposium(International) on Combustion, 719-729.

Megalos, N.P., Smith, N.L. and Zhang, Z.L., 2001, “The potential for low NOx from a precessing jet burner of coal”, Combustion and Flame 124:50–64

Mullinger, P.J., 1984, “Burner design for coal fired cement kilns”, World Cement,348-353.

Nsofor, E. C. and Adebiyi, G. A., 2001, “Measurements of the gas-particle convective heat transfer coefficient in a packed bed for high-temperature energy storage”, Experimental Thermal and Fluid Sciences, Vol. 24, No. 1-2, 1-9.

Parker, D. J., Dijkstra, A. E., Martin, T. W. and Seville, J. P. K., 1997, “Positron emission particle tracking studies of spherical particle motion in rotating drums”, Chemical Engineering Science, 52, 2011-2022.

Perron, J. and Bui, R. T., 1990, “Rotary cylinders: solid transport prediction by dimensional and rheological analysis”, Canadian Journal of Chemical Engineering, 68, 61-68.

Peray, K. E., 1986, Rotary Cement kilns, 2nd Edition, Chemical Publishing Co. Ltd., NY.

Perry, R.H., 1984, Perry’s Chemical Engineers’ Handbook, 6th Edition, Don Green, Mc-Graw Hill, New York.

Pillai, K. K., 1981, “The Influence of Coal Type on Devolatilization and Combustion in Fluidized Beds.” J. Inst. Energy, 142.

Quirrenbach, F.J., 1960, Allg. Warmetch, (9), 271-276

Richman, M. W. and Oyediran, A. A. 1992, “Grain size reduction in granular fows of spheres: the e!ects of critical impact energy”, .Journal of Applied Mechanics, 59, 17-22.

Ranade, V.V., 2002, Computational Flow Modeling for Chemical Reactor Engineering, Academic Press, London.

Rao, T.R., Gunn, D.J. and Bowen, J.H., 1989, “Kinetics of calcium carbonate decomposition”, Chem. Eng. Res. Des., 67, 38-47.

Ranz, W.E. and Marshall, Jr, 1952, “Evaporation from Drops, Part I. Chem. Eng. Prog., 48(3):141-146.

Saeman, W. C., 1951, “Passage of solids through rotary kilns”, Chemical Engineering Progress, 47, 508-514.

Satterfield, C.H. and Feakes, F., 1959, “Kinetics of the thermal decomposition of calcium carbonate”, AIChE J., 5, 115-122.

Schaeffer, D. J., 1987, “Instability in the evolution equations describing incompressible granular flow”, J. Differ. Equa., 66, 19– 50.

Selcuk, N., Batu, A. and Ayranci, I., 2002, “Performance of method of lines solution of discrete ordinates method in the freeboard of a bubbling fluidized bed combustor”, Journal of Quantitative Spectroscopy and Radiative Transfer, 73, 503–516

Sherritt, R. G., Chaouki, J., Mehrotra A.K. and Behie, L. A., 2003, “Axial dispersion in the three-dimensional mixing of particles in a rotating drum reactor”, Chemical Engineering Science, 58(2), 401-415.

Shrivastava, A. and Sundaresan, S., 2002, “Role of wall friction in fluidization and standpipe flow”, Powder Technology, 124, 45-54.

Shrivastava, A. and Sundaresan, S., 2003, “Analysis of a frictional-kinetic model for gas particle flow”, Powder Technology, 129, 72-85.

Smith, I.W., 1971, “Kinetics of combustion of size graded pulverized fuels in temperature range of 1200 -2270 K”, Combustion and Flame, 17(3), 303-314

Spang, H. A., 1972, “A dynamic model of a cement kiln”, Automatica, 8, 309-323.

Spurling, R.J., Davidson, J.F. and Scott D.M., 2001, “The transient response of granular flows in an inclined rotating cylinder”, Trans IchemE, 79, 51-61.

Solomon, P.R., Hamblen D.G., Carangelo, R.M., Serio M.A. and Deshpande G.V., “Very rapid coal pyrolysis”, Fuel, 65, 182-194.

Stanmore, B.R. and Gilot, P., 2005, “Review—calcination and carbonation of limestone during thermal cycling for CO2 sequestration”, Fuel Processing Technology, 86,1707– 1743

Syamlal, M, Rogers, W. and O' Brien T. J., (1993). MFIX Documentation: Volume 1, Theory Guide. National Technical Information Service, Springfield, VA..DOE/METC-9411004, NTIS/DE9400087.

Thunman, H. and Leckner, B., 2002, “ Thermal conductivity of wood – models for different stages of combustion”, Biomass and Bioenergy, 23, 47-54.

Tscheng, S. H. and Watkinson, A. P., 1979, “Convective heat transfer on rotary kilns”, Can. J. Chem. Engg., 57, 433-443.

Van der Lans, R.P., Glarborg, P. and Dam-Johansen, K., 1999, “Influence of process parameters on nitrogen oxide formation in pulverized coal burners”, Prog. Energy Comb. Sci., 23, 349-377.

Walton, O. R. and Braun, R. L., 1993, “Simulation of rotary-drum and repose tests for frictional spheres and rigid sphere clusters”, Proceedings of Joint DOE/NSP Workshop on Flow of Particulates and Fluids.

Watkinson, A. P. and Brimacombe, J. K., 1982, “Limestone calcination in a rotary kiln”, Met. Trans. B, 13B, 369-378

Williams, A., Backreedy, R., Habib, R., Jones, J.M. and Pourkashanian, M., 2002, “Modeling coal combustion: the current position”, Fuel, 81, 605-618

Vahl, L. and Kingma, W.G., 1952, “Transport of solids through horizontal rotary cylinders”, Chem. Eng. Sci., 1, 253.

Young, B.C. and Smith, I.W., 1989, “The combustion of Loy Yang Brown coal char”, Combustion and Flame, 76, 29-35.

Journal Publications

1. Mujumdar, K.S., Arora, A., and Ranade, V.V., Modeling of Rotary Cement Kilns: Applications to Reduction in Energy Consumption. Ind. Eng. Chem. Res., **45,** (7), 2315 -2330, 2006.
2. Kaustubh S. Mujumdar and Vivek V. Ranade, Simulation of Rotary Cement Kilns Using a One-dimensional Model", Chemical Engineering Research and Design, **84,** 165-177, 2006.
3. **Kaustubh S. Mujumdar**, Ganesh K.V., Sarita B. Kulkarni and Vivek V. Ranade, "Rotary Cement Kiln Simulator (RoCKS): Integrated Modeling of Pre-heater, Calciner, Kiln and Clinker Cooler", Chemical Engineering Science, **62,** 2007, 2590-2607.
4. Mujumdar, K.S. and Ranade V.V. A CFD tour of a cement kiln. Chemical Engineer (London), 777, 39-41, 2006
5. Kaustubh S. Mujumdar and Vivek V. Ranade, "CFD Modeling of rotary cement kilns" accepted for publication in Asia Pacific Journal of Chemical Engineering

Conference/Poster presentations

6. Sumedh Warudkar, V.Ganesh Kumar, Kaustubh S. Mujumdar and Vivek V. Ranade, A Phenomenolgy based model for cement calciners, presented at CHEMCON-Delhi, 2005
5. Kaustubh S. Mujumdar and Vivek V. Ranade, CFD modeling of rotary cement kilns: Influence of Characteristics of Coal Combustion on Clinker Composition, presented at CFD FOR CRE IV-Italy, 2004.
6. Amit Arora, Kaustubh Mujumdar and Vivek V. Ranade, A one-dimensional model for Rotary cement kilns, Presented at Chemcon-Mumbai, 2004 **(Received Best Paper Presentation award)**
7. Kaustubh S. Mujumdar and Vivek V. Ranade, Coupling of CFD models with different time scales - A case study of rotary cement kiln, FLUENT UGM for India and South East Asia, Pune, 2003 **(Received Best Technical Paper Award)**
8. Vivek V. Ranade and Kaustubh S. Mujumdar, CFD simulations of solid motion in the transverse plane of rotating kilns, Third International Conference on CFD in the Minerals and Process Industries, CSIRO, Melbourne, Australia, 10-12 December 2003.
9. Kaustubh S. Mujumdar and Vivek V. Ranade, CFD simulations of heat transfer in transverse plane of rotating kilns, CHEMCON- Bhubhaneshwar, 2003.
10. Vivek V. Ranade, Kaustubh S. Mujumdar, S. Bandopadhyay and Devaki Ravi Kumar, Modeling of Rotary Cement Kiln, ISPSEC, I.I.T, Bombay, 2003
11. Kaustubh S. Mujumdar and Vivek V. Ranade, Modeling of Rotary Cement Kilns, CHEMCON-Hyderabad, 2002

Acknowledgments

There are many people whom I owe acknowledgement and who have helped me in several ways during my doctorate degree. I would like to thank my advisor Prof. Anurag Mehra for his constant support throughout my work. Interactions with him during the thesis work and particularly during his course "Reaction Engineering in Dispersed Phase System" was combination of real fun plus deep knowledge building about Chemical Engineering. I am also thankful to my RPC members Prof. A.K. Suresh and Prof. D.V. Khakhar for their valuable suggestions during the RPC meetings.

I am highly indebted to Dr. V.V. Ranade, my supervisor at National Chemical Laboratory (NCL), Pune. Working with him was one of the most fortunate things that have happened in my life. I could not have imagined having a better advisor and mentor for my PhD, and without his knowledge, perceptiveness and approach to crack problems I would never have finished in time. With very high standards of quality work set by him in our group at NCL, Pune I would like to repeat my colleague Dr. Vivek Buwa's words "I hope this work at least partly satisfies his expectations."

There are several friends whom I would like to acknowledge whom I met during my stay at our group Industrial Flow Modeling Group (IFMG) at NCL, Pune. I would like to acknowledge my seniors Vivek, Gunjal and Khopkar who helped me in several things other than technical stuff. Special thanks to one of my colleague Ranjeet for helping me several times during my work. Interacting with Ranjeet has always helped me in getting some new idea to tackle a problem. Also I would like to thank him for sitting with me and helping me out in debugging some of my FORTAN codes several times. I would also like to thank my other colleagues Mohan and Ajay for their constant help in some or the other way. I would also like to thank several other friends Naren, Sarita, Dev, Madhavi, Latif, Ganapathy, Prakash, Abhijit, Amit, Yogesh, Madhav, Subbu, Rashmi, Puneet, Surendra, Himanshu, Manan, Gaurav Gupta for making my stay at IFMG very pleasant. I would also like to thank Sandip Talwalkar from IIT, Bombay who has been a constant source of help during my visits at IITB.

I would specially like to thank three of my colleagues Amit Arora, Sumedh and Ganesh who worked with me during my stay at IFMG. I would like acknowledge all the three for their enthusiasm, promptness towards work and the awareness of time frame for completing the undertaken work in time.

I would like to acknowledge CSIR, India for providing the financial support during my research work.

I would also like to say thanks to my entire family particularly to my mom and my dad and most importantly to my wife Namrata for standing by me at all times, may be good or bad. I would also like to thank God for blessing me and my wife with our baby kid “Ananya” who has added some of very sweet memories that have happened during my Ph.D.

Kaustubh S. Mujumdar